

DEVELOPMENT AND IMPLEMENTATION OF PHOTO-NUCLEAR  
CROSS-SECTION DATA FOR MUTUALLY COUPLED  
NEUTRON-PHOTON TRANSPORT CALCULATIONS IN THE  
MONTE CARLO N PARTICLES (MCNP) RADIATION TRANSPORT CODE

by

MORGAN C. WHITE

A DISSERTATION SUBMITTED TO THE GRADUATE SCHOOL  
OF THE UNIVERSITY OF FLORIDA IN PARTIAL FULFILLMENT  
OF THE REQUIREMENTS FOR THE DEGREE OF  
DOCTOR OF PHILOSOPHY

UNIVERSITY OF FLORIDA

2000

Copyright 2000

by

Margaret C. White

Don't panic!

You don't *have* to buy now!

## ACKNOWLEDGMENTS

As with any long-term project, there are a myriad of people who deserve thanks for their contributions to this work. I would like to try to thank as many of you by name as possible and sincerely apologize if I miss anyone who should have been included. This has been a long hard stretch of my life, but it was also well spent thanks to your support and care.

The first words of thanks must go to my mentor and friend, Steven Arghavan. As chairman of both my masters and doctoral research committees, he has guided me through my opening steps into a new world. Personally, he has been an inspiration. I know few people of as fine character and spirit.

To my committee members, my sincere appreciation for your time and presence as we have progressed down this path. Without your encouragement and support, this work would never have been possible. I would like to thank Deborah Ellis, Frank Berra and Wolfgang Tross for their patience with an engineer trying to understand the medical physics world. Fred Fiedrich for his guidance in the world of computer simulations and Robert Huxthorne for his unique perspective. A special thanks to Drs. Bob Letko, Stephen Finkle and Mark Chadwick. Their contributions to helping me understand the use of nuclear data for Monte Carlo simulations turned this work into a fulfilling project of which I am truly proud.

There have been too many people with whom I have had useful discussions for me to be able to remember, much less list, them all, but I would like to acknowledge

from left. Thanks to Emily Hagler, Larry Coss, Ken Adams, Chris Werner, Tim Barth, Dirk Fred, Jack Conley, James Campbell, Jody Silverstein, Jeff Freerick, Art Farnes, Henry Lieberman, John Hendricka and Gregg McKenney for the many discussions and laughs on the Miami Cello-mat! Thanks to Edwin Cherry, John Donawick, Tim Solberg, Jim Saunders, Paul Delano and David Rogers for the discussions on medical physics and simulating medical electron accelerators. Thanks to Sam Friesen and Bill Vermorel for their assistance with the use of the PSLA facility at LP. Thanks to Jane Park, Thomas Lee and Jinyang Kim for their assistance in performing the ionization experiments around the Phillips MFA.

I would also like to acknowledge the support of those people who have been there for the day-to-day grind at both the University of Florida and the Los Alamos National Laboratory. Thanks to Erik Brice, John Mendelsohn, Christine Kelly and Ann Wigg for their assistance in making life easier. Thanks to Ed Dugan, Ben Stark, Alexander Hersh and Tom Sack for their encouragement and support.

I would also like to acknowledge several sources of monetary support. First, thanks to the U.S. Department of Energy. In one way or another, the DOE has paid for my time at graduate school. First, through a four-year National Superscience Fellowship and more recently as a graduate research assistant at LANL. I also need to thank two other resources. The project for the Accelerator Production of Tritium sponsored the creation of photomicro data here at LANL. This was in part due to the diligent and thoughtful efforts of Laura Werner. Many thanks. Also thanks to the Advanced Computing Laboratory at LANL. Many of the calculations presented here were performed using spare CPU cycles from the Blue Mountain supercomputer.

Finally, I want to thank my family. To my mother and father, you have been the most wonderful parents one could have. You taught me the power of imagination and persistence. To my brother, many thanks for motivating me to always look at things from a different perspective. And at last, thanks to my wife thank for her patience, encouragement and love. I love you all.

## TABLE OF CONTENTS

	(page)
<b>ACKNOWLEDGMENTS</b>	iv
<b>ABSTRACT</b>	v
<b>CHAPTERS</b>	
<b>1 INTRODUCTION</b>	<b>1</b>
<b>2 BACKGROUND</b>	<b>3</b>
Introduction	3
Physics of Photoelectron Interactions	4
Experimental Photoelectron Data	12
Previous Photoelectron Studies	14
Current Developments	17
<b>3 IMPLEMENTATION: COUPLING PHOTOELECTRIC PHYSICS INTO MCNPX</b>	<b>18</b>
Introduction to Trilete Monte Carlo Radiation Transport	18
Data Storage	26
Data Processing	31
Coupling Photoelectric Physics into MCNP	36
Future Work	50
<b>4 VERIFICATION AND VALIDATION</b>	<b>74</b>
Introduction to Verification and Validation	74
Verification	87
Comparison to Theoretical Yields	89
Comparison to Measured Yields	92
Conclusions from Verification and Validation	114

3. APPLICATION: SIMULATION OF A MEDICAL ELECTRON ACCELERATOR .....	118
Introduction .....	118
Validating the Simulation .....	119
Implementation .....	124
4. SUMMARY AND CONCLUSIONS .....	130
APPENDICES	
A. PHOTOGRAPHIC ACT TABLE FORMAT .....	200
B. MDPMT PROCESSING CODE .....	237
C. PHOTOGRAPHIC PATCH FILE .....	405
D. MISCELLANEOUS DATA FROM VALIDATION STUDIES .....	448
E. MISCELLANEOUS DATA FROM APPLICATION STUDIES .....	460
REFERENCES .....	529
BIOGRAPHICAL SKETCH .....	539



*Journal of Dissertation Presented to the Graduate School  
of the University of Florida in Partial Fulfillment of the  
Requirements for the Degree Doctor of Philosophy*

**DEVELOPMENT AND IMPLEMENTATION OF PHOTONUCLEAR  
CROSS SECTION DATA FOR MUTUALLY COUPLED  
NEUTRON-PHOTON TRANSPORT CALCULATIONS IN THE  
MONTE CARLO-N-PARTICLE (MCNP) RADIATION TRANSPORT CODE**

By

Margie C. Weiss

May 2008

Chairman: Steven Archambault

Major Department: Nuclear and Radiological Engineering

The fundamental motivation for the research presented in this dissertation was the need to development a more accurate predictive method for characterization of mixed radiation fields around nuclear electron accelerators (PEAs). Specifically, a model is developed for calculation of neutrons and other particle production from photonuclear reactions and incorporated in the Monte Carlo N-Particle (MCNP) radiation transport code. This enhancement of the capability within the MCNP-code provides for the more accurate treatment of the mixed radiation fields.

The Nuclear Theory and Applications group of the Los Alamos National Laboratory has recently provided first-of-its-kind evaluated photonuclear data for a select group of isotopes. These data provide the reaction probabilities as functions of incident photon energy with angular and energy distribution information for all reaction products

The availability of these data is the cornerstone of the new methodology for state-of-the-art neutrally coupled plasma-neutron transport simulations.

The descriptive methods details of the model development and implementation necessary to run the new photoneutron data within MCNP simulations. A new data format has been developed to include tabular photoneutron data. Data are processed from the Evaluated Nuclear Data Project (ENDF) to the new data file. A Compact ENDF (CENDF) format using a standard processing code. MCNP modifications have been completed to enable Monte Carlo sampling of photoneutron reactions. Note that both neutrons and gamma production are included in the present model.

The new capability has been subjected to extensive verification and validation (V&V) testing. Verification testing has established the expected basic functionality. Two validation projects were undertaken. First, comparisons were made to benchmark data from literature. These calculations demonstrate the accuracy of the new data and transport routines is better than 20 percent. Second, the ability to calculate neutron dose due to the neutron environment around a MHA is shown. An uncertainty of a factor of three in the MHA calculations is shown to be due to uncertainties in the primary modeling. It is believed that the methodology is sound and that good agreement between simulations and experiment has been demonstrated.

## CHAPTER I INTRODUCTION

At the beginning of this work, several of the graduate students and faculty from both the Molecular and Biophysical Engineering Department and the Department of Radiation Oncology at the University of Florida had begun an extensive exploration of the evidence to recommend around typical radiotherapy equipment. The goals in mind were more accurate measurement and evaluation of their radiation environments. During the course of these early studies, it was observed that the evaluation of photoacoustic interactions had not entered the systematic treatment that electron, photoacoustic and neutron interactions receive in the generally available radiation transport codes. This presented a good opportunity for a doctoral project and the work you read today is the final result.

The stated course of action was to determine what tools were available for the task of modeling photoacoustic interactions. It was quickly determined that the single greatest obstacle to performing photoacoustic calculations was the lack of complete double-differential cross sections describing the neutron-neutron system as well as the secondary particle electron spectra from the reactions. Complete, evaluated nuclear cross section data are the fundamental keys to performing high-accuracy Monte Carlo radiation transport simulations. As a result of the lack of such data the course proposed at the beginning of this work was to evaluate the best of what was available by developing a method for using experimental photoacoustic data to create interaction probabilities and

radiant modeling to compute neutron spectra. Thus, using this data, a working assistance would be implemented for more widely general production of the neutron flux at the vicinity of high-energy medical electron accelerators (HMLAs).

The importance of the maintenance of the neutron field around HMLAs is a long-standing subject of debate. It has been known since early in the development of high-energy electron accelerators that they create neutrons as a by-product. The term by-product in most medical neutron use typically refers to a contaminant, not an asset. Even HMLAs have become the mechanism of this radiotherapy-contaminant: the production of neutrons from these machines is a significant concern. In the use of HMLAs for radiotherapy, the desire is to maximize the dose caused by the neutron dose to the patient and neutron-flaring the secondary delivery of a dose of photon dose to most cancerous growths.

The most intense investigation of the neutron production and transport around HMLAs was during the 1970's and early 1980's when the electron energies used in medical treatments began to climb above the threshold for significant photonuclear production. The two most noteworthy publications on this subject date from that time. In 1979, the National Bureau of Standards held a conference devoted to examining the production of neutrons from HMLAs [4]. Several years later, in 1984, the National Council on Radiation Protection and Measurements (NCRP) released a report [1] documenting their recommendations for screening risks associated with the production and transport of neutrons within a HMLA treatment room. However, despite a wealth of studies produced before, during and since these seminal works, the systematic treatment of the situation

of photo-neutron production has not been addressed, hence the following motivation for the current work.

It should be noted that this work has been generated from the perspective of nuclear and radiological engineering, not necessarily that of medical physics. To recognize this difference, the goal of this work is clearly mentioned. This work seeks to provide a systematic treatment of photo-neutron production as a part of the simulation of electron accelerators. It is its applied objective in the sense that the end product is a tool capable of simulating the production and transport of neutrons around a MHA and quantifying the uncertainty. The final product may then be used by future researchers to conduct efforts in this field aimed at understanding, evaluating and reducing neutron contamination around electron accelerators.

Early in this work, it was decided that the Monte Carlo N-Particle (MCNP) neutron transport code [1] would be used as the base for the development of a simulation code including photo-neutron production. This choice was made for a number of reasons. First and foremost, it was desired to build upon an well established code in order to take advantage of existing validated algorithms. In addition, the author was already familiar with the use of MCNP for transport simulations.

MCNP provided the starting point for starting an effort to integrate photo-neutron physics into a neutron transport code. It already included the algorithms and data necessary for modeling electron, photo-neutron and neutron transport. More than that, it has been the product of hundreds of man-years of development dating back to the very origination of the Monte Carlo neutron transport method [4]. This development work has been verified and validated through the efforts of thousands of scientists with deep

of problems. Specifically, MCNP includes both an electron-photon and a neutron transport package, each of which have a well-established history of use. In fact, as will be discussed in the following chapter, MCNP had already been used for simple, unscripted simulation of photoelectron production and subsequent neutron transport. Therefore, all that remained was to formalize the coupling between the two transport packages and provide verification and validation of the new functionality.

However, the combination of a large code in a daunting task. MCNP is 60,000 lines of highly interdependent, extremely terse Fortran77 code. When it was first developed, the formal rules of software management had not yet been conceived. Therefore, after considering using the code, the author approached the X-6 group at the Los Alamos National Laboratory (LANL) who maintain the MCNP code and its related data, about the possibility of a collaboration to pursue this work. The acceptance this idea received was much more than expected.

For the author, this work entailed the saying about being in the right place at the right time. As discussed above, the primary obstacle to accurate simulation of photoelectron interactions has been the lack of complete, validated data necessary for single Monte Carlo sampling. Not only were the staff at LANL interested in pursuing a collaboration, they were willing to enroll the author onsite with access to the MCNP development team and, more importantly, access to first-of-a-kind validated photoelectron data. The full significance of this will be discussed in the following chapter.

The remainder of this discussion is composed of four main chapters and the conclusions. The next chapter provides a basic understanding of the mechanics of

phenomena physics and the data and models available to describe them. While there is not an abundance of experimental data or validated nuclear models, it is important to discuss what is available. In particular, the addition of the newly available evaluated phenomenological data is discussed. As part of this chapter, previous phenomenological studies will be compared to evaluate how the available data have determined the *likelihood* of conclusions being possible.

The third chapter begins the original work presented here for consideration. It opens with a brief discussion on the first step needed to perform a Monte Carlo simulation. From there it progresses through the development of the necessary formats for storing the data, how evaluated data are incorporated into these formats and, finally, how the data are actually used within the transport code. This chapter is the core of the work presented. The development discussed here met and moved the original goal of providing a systematic treatment of phenomenological production.

With the new ability to perform fully coupled phenomenological calculations, the next step was to attempt the uncertainty in the use of the simulation with the current evaluated data. The fourth chapter presents the strategy of uncertainty and validation as methods to assess how well the newly developed simulation capability is able to calculate nuclear production from high-energy electron incident on materials for which evaluated data exist. It presents two sets of yield measurements based on the literature and does comparisons to the current calculations. Conclusions about the uncertainty in the new capability are drawn from these comparisons.

As the original motivation for this work was the more accurate simulation of medical electron accelerators, the fifth chapter presents an initial assessment of use of the

acceleration currently at use at Space Coast Center at the University of Florida. The difficulties in modeling such facilities are discussed and an estimate is made about the compression involved based on experimental observations made around the MFA during this work. The final chapter summarizes the developments and conclusions of this work.



## CHAPTER 2 BACKGROUND

### Introduction

The single greatest obstacle to accurate simulations of photoelectron interactions within the context of Monte Carlo solutions (transport) lies both in the lack of evaluated, complete data. The use of probabilities to sample interactions rates and resultant products is the key defining feature of Monte Carlo transport. This can be done either through nuclear models or by tabular data. Evaluated tabular data contain the most accurate description of the data available as determined by an evaluator based on judgement of the experimental measurements and nuclear modeling available. For tabular data, complete indicates that in addition to reaction rates, important resultant products are given with energy and angular emission spectra as a function of incident particle energy.

Evaluated data are based on the best judgement of a data evaluator. This small field of researchers has in-depth knowledge of both the experimental data and the nuclear models available to describe nuclear reactions for an incident particle on a given target nucleus. Both experimental data and nuclear models are required for this process. Experimental measurements are the best description of physical reality as they demonstrate measured fact. However, experimental measurements are difficult to obtain and cover some the full spectrum of interest. Nuclear models are complete descriptions of interactions based on theory. Both are subject to error. Therefore, the evaluator must use

experience and judgment to avoid history and experience into the best available description of the data.

For transport calculations, it is necessary to have complete descriptions of the interactions. Current theories describe the interaction probability for a particle traversing a material as a function of the incident particle's energy. Empirical spectra describe the energy and angle of the secondary particles resulting from an interaction event if one occurred. It is in the evaluation of this second set of information that nuclear models are needed. They can provide well-specified complete descriptions of the empirical spectra.

Evaluated, complete nuclear data are generally considered the most accurate description of the interactions available. Until very recently such data have not existed for photoneutron interactions. As will be discussed in the section of this chapter entitled Current Developments, several groups of evaluations, both in the United States and internationally, have recently provided such data. Before discussing the newly available data, it is worth stepping back and taking a brief look at the physics of photoneutron interactions and the history of the experimental data and calculation models describing them.

First it is necessary to clarify the use of the term data. "Data" is a word shared word and it must be placed in context for it to be truly meaningful. Within the body of this work, the phrase "experimental data" refers to measurements made under laboratory conditions. "Theoretical data" refers to values computed using some form of an analytical model based equally on theory or guided by, but not directly taken from, experimental data. The term "evaluated data" has been described above. "Tabular data" indicate values listed at discrete points in the phase space. "Functional data" are

theoretical, experimental or calculated data considered to be correct. To confirm the same, data often fall into more than one category.

### Physics of Photo-nuclear Interactions

It is important to spend a few moments discussing the physics behind photo-nuclear reactions in order to provide a context for describing the information contained within the evaluated data. The descriptions presented here is not intended to be a comprehensive explanation of the nuclear physics underlying this phenomena. Rather it is intended to be an illustrative description presenting the basic concepts and providing useful references for further details.

A photo-nuclear interaction begins with the absorption of a photon by a nucleus. There are many mechanisms by which this can occur. The data currently available from nuclear energy ranges up to 150 MeV incident photon energy. The value of 150 MeV was chosen as this energy is just below the threshold for the production of pions and the subsequent need for much more complicated nuclear modeling. Below 150 MeV, the primary mechanisms for photo-nuclears are the existence of either the giant dipole resonance or a quasi-deuteron nucleon pair. A conceptual illustration of these processes is given in Figure 1-1.

The giant dipole resonance (GDR) absorption mechanism can be conceptualized as the electric-magnetic wave, the photon, interacting with the dipole moment of the nucleus as a whole. This results in a collective excitation of the nucleus. It is the most intense process by which photons interact with the nucleus. It occurs with highest probability when the wavelength of the photon is comparable to the size of the nucleus. However, this resonance is peaked with a width of only a few MeV. For deformed

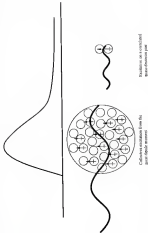


Figure 3-1. Schematic representation of the quasi-dipole resonances and quasi-dipole resonant scattering.

model, a double peak is seen due to the variation of the nuclear radius. Outside of the peak region, the GDR mechanisms are negligible. A more complete description of the process, and of nuclear physics in general, can be found in the text by Bohr and Mottelson [5].

The giant dipole (GD) absorption mechanism can be conceptualized as the electric dipole moment increasing with the dipole moment of a correlated neutron-proton pair. In this case, the neutron-proton pair can be thought of as a spin-aligned having a dipole moment with which the photon can interact. This mechanism is not as intense as the GDR but it provides a significant background cross section over all nuclear photon energies. The seminal work describing this process was published by Lenzinger [6,7]. Recent efforts to model this process includes the work of Chudakov et al. [8].

Once the photon has been absorbed by the nucleus, one or more secondary particle emissions can occur. The secondary particles typically emitted for the energy range below 180 MeV are neutrons, protons, deuterons, tritons, helium-3 or alpha, or a combination thereof. Any emission process that does not leave the residual nucleus in the ground state will also produce secondary gamma-ray emission. The photoneutron threshold for the production of a given secondary particle is governed by the separation energy of that particle. Pre-equilibrium and equilibrium emissions are responsible for most of the secondary particles emitted by photon absorption over the energy range under discussion though direct particle emission is possible.

Pre-equilibrium emission can be conceptualized as a particle within the nucleus that receives a large amount of energy from the absorption mechanism and escapes the binding forces of the nucleus after a fraction of a very few interactions with other nucle-

Typically this occurs from QD-absorption of the photon where the incident energy is initially split between the neutron-proton pair. Particles created by this process tend to be characterized by higher momentum-energy and forward-peaked angular distributions. Several references are available on the ground neutron-proton after photoabsorption (9-11).

Equilibrium-reactions can be conceptualized as particle resonances. Typically the process occurs after the available energy has been generally dissipated among the nucleons. In the classical sense, particles tend out of the nucleus as they penetrate the surface potential barrier. The kinetic energy-system contributions from Coulomb potential for charged particles and effects of angular momentum conservation. It should be noted that the heavy elements, compression-reactions are started preferentially as they are not subject to the Coulomb barrier. Particles created by this process tend to be characterized by isotropic angular emission and anisotropic energy spectra. The same references (9-11) apply to the pre-equilibrium-reactions.

For all of the neutron reactions discussed thus far, the nucleus will most probably be left in an excited state. It will subsequently relax to the ground state by the emission of one or more gamma-rays. The gamma-ray energies follow the well known patterns for relaxation. The only reactions which do not produce gamma-rays are direct reactions where the photon is absorbed and all available energy is transferred to a single neutron particle leaving the nucleus in the ground state.

Reactions at higher energies, greater than 150 MeV, require more complete descriptions of the underlying nuclear physics. The delta-mechanism and other absorption mechanisms become significant and the amount of energy involved in the reaction

provides the opportunity for the production of more fundamental particles, e.g. pions. While beyond the scope of the current work, descriptions of the physics involved can be found in the paper by Pines et al. [14].

The study of photoneutron physics has been important for two communities, nuclear physics and health physics. Obviously, the current work approaches the subject from the viewpoint of the second community. As such, the descriptions above have tried to convey a general picture of the mechanisms governing photoneutron interactions. To bring this into the overall picture of photon transport, the probability that a photon will undergo a photoneutron interaction is not much less, and typically much less than, even percent of the total photon interaction probability. However, that mechanism can provide a source of neutron production, specifically neutrons, that constitute a significant health physics risk.

### Experimental Photoneutron Data

Experimental measurements provide the fundamental values describing interaction probabilities, e.g. reaction cross sections, and the subsequent yield and spectra of secondary particles. Unfortunately, there are relatively few accurate measurements of the photoneutron reaction cross sections in comparison to the measurements that have been made for neutron reactions. The vast majority of the available experimental data are the result of unfolding measurements made by bombarding with neutrons. These data suffer from extremely large uncertainties due to the unfolding process and are not generally accurate enough to be used on their own as a basis for evaluated data. The cross section measurements using tagged bombarding or photon sources from multiple positron annihilations are generally considered to be highly accurate. However,

relatively few measurements of this type have been made. Further, available neutron data, these measurements typically do not include photoneutron secondary-neutron spectra. For the purposes of data that are available, several compilations similar to the *Nuclear Data Book* [13] exist.

The first compilation listing of experimental data was produced by Fuller working at the National Bureau of Standards (NBS) and is generally known as the *Photoneutron Data Series* [14,15]. This compilation includes references to all known publications of experimental data at that time. Dattich and Berman published two editions of the *Photoneutron Atlas* [16,17]. These compilations contain only measurements made with photons produced from the in-flight annihilation of positrons in target materials. The most recent compilation of photoneutron data has been carried out by Vlachos et al. [18]. These are the primary references for locating the available experimental photoneutron data.

As most of the references in these publications contain the measured data in the form of plots, it is worth mentioning two further resources. Dattich and Berman created an electronic tabulation of the more useful measurements. This tabulation is available from the authors. The EXFOR database [19] maintained by the National Nuclear Data Center provides tabular listings of many, but not all, of the reported measurements. Vlachos et al. have tried to update the EXFOR database with the data from their compilation but it still contains only a small percentage of the reported data.

### **Previous Photoneutron Studies**

This section provides a brief description of some of the known studies that have measured photoneutron interactions for various reactions. It is not a comprehensive review



of the available literature but rather provides examples of the typical work performed in past. It is described here in order to provide a context by which to show how the current work has advanced the previously model's capabilities.

One of the first studies in this field was the work of Alexander et al. [20-22] carried out at the Oak Ridge National Laboratory in the late 1960's. These calculations were performed using an early nuclear-escape model to estimate the neutron yield and spectra from 150 MeV electron incident on selected materials. This work was carried out in part to help select the target material for use as a photo-neutron source in the Oak Ridge Electron Linear Accelerator Facility (ORRELAF). Subsequent work by this group included extending their code, known as FICA, to handle higher-energy electron photons [23,24]. Similar studies have been performed by Bacon et al. [25] and Kass et al. [26].

The FLUKA [12], MARIE [27] and CHIM [28] codes provide Monte-Carlo sampling of photo-neutron interactions in the medium- to high-energy regime. These codes compute the interaction probabilities and secondary particle emission spectra immediately during the transport process from nuclear models. Recent work on the FLUKA neutron transport code is particularly noteworthy in that it was expanded for to experimental data to extend its applicability to the ORE (low-energy) region.

These codes are all alike in the sense that they suffer from inaccuracies inherent in estimating the photo-neutron spectra. While there are systematic trends in the photo-neutron data, there can be significant discrepancies for some isotopes that nuclear theoretical nuclear models are required for resolution. These discrepancies are most noticeable at lower energies (especially around the ORE peak), and for lighter isotopes. However, these codes are primarily used for intermediate- to high energy (>100%

of MeV to TeV) particle-accelerator modeling and around the intermediate energies in the models at low energies and at all geometries. It should be evident that transport based primarily on neutral models has the advantage that neutrons can be computed on any target material and neutron distributions are available for all secondary particles.

Many studies involving an accurate assessment of neutron production from photons in the low-energy region have used different methodology. The photon flux in a given geometry can be calculated either by analytical theory or by an electron-photon transport code. This flux can then be folded with an experimental photo-neutron cross section to estimate the neutron production. Neutron energy and angle spectra are obtained and the neutron source “manufactured” in this manner may undergo further transport. Examples of studies using this method include works by Simmons [25–33], McCall et al. [34], Madhukrishna et al. [35], Agnew et al. [33–36], Gellerauer [37], Lee et al. [38] and Chabwick et al. [39]. These studies have focused on examining the health physics effects of neutrons produced from low-energy electron accelerators. The use of this method for that purpose is difficult due to the intermediate size accuracy in coupling the geometries and significant error is possible if done inappropriately.

There are many difficulties in using experimental data as an uncoupled neutron source. Experimental data must be broad covering the relevant reactions, energies and energy range of interest to the simulation. Where such data do not exist, extrapolation should be used but introduced as unknown source of error. Experimental data describing neutron spectra do not generally exist. Therefore, neutron spectra must be extracted using nuclear modeling or other techniques. The simple models that have been used as just an accurate fluxes distributions allow do not fully represent the true neutron spectra.

Simulations using this technology are typically run at a series of sequential steps. First, the plasma flux is used to estimate the neutron production. Next can be introduced at this step by the inadequacies in the description of the plasma flux, the experimental plasma-neutron cross-section data and the fitting method used to estimate the neutron source. The neutron source is then given energy and angular distributions and subsequent neutron transport is performed. Next can be introduced at this step by the inadequacies in the spatial description of the coupled neutron source and in the energy and angular distributions and their appropriate components in the source neutrons. Lastly, the statistical correlation to estimate the uncertainty in the calculation are lost because the transport is not fully coupled. The works referenced in the previous paragraph have attempted to solve one or more of these problems. The current work seeks to address all of these problems.

### Current Developments

The greatest obstacle to Monte Carlo simulation of fully-coupled plasma-neutron transport using tabular data has recently been overcome. Several projects at the Los Alamos National Laboratory (LANL) have discovered the need to account for photo-neutron interactions in accelerator environments. Therefore, the Nuclear Theory and Applications Group (T-2) of the Theoretical Division was commissioned by the Accelerator Simulation of Fusion (ASF) project to perform a number of photo-neutron evaluations as part of the LA158 data library [36]. These evaluations were carried using the GNASH nuclear model code [37] as guided by experimental data. The library produced neutron cross-sections evaluated data for neutron capture-reactions, and photon (for photo-neutron reactions) for the energy range up to 150 MeV. For a limited set of

samples, evaluated data were created in association with the MCNPX code to significantly advance the state of the art in Monte Carlo neutron transport.

To benchmark for a moment, the Monte Carlo-X Particle (MCNPX) neutron transport code [43] has the goal of being the most versatile simulation code for neutron-photon-electron-reaction transport available. It seeks to accomplish this goal by the use of nuclear-evaluated data. Interestingly, these same data define the scope of MCNPX's applicability. MCNPX [44] has the goal to extend the region of applicability of MCNP to those particles and energies previously treated high-energy neutrons. It seeks to accomplish this goal by incorporating nuclear evaluated data where available and supplementing the tabular data with nuclear models where necessary. Both of these codes stress the incorporation of photochemical reactions to enable the coupled simulation of photon-optics-transport problems. This work presents the development and implementation of the newly available evaluated photochemical data for that purpose.

The research community at LANL is not the only group which has recognized the need to provided evaluated photochemical data. It is interesting to note that the International Atomic Energy Agency (IAEA) has created a Coordinated Research Project (CRP) entitled "Compilation and Evaluation of Photochemical Data for Applications" [45]. A library containing photochemical evaluations of 100 isotopes, including some of those produced by TIE at LANL, will be released in 2000 together with documentation in an IAEA report [46]. This library stands as a valuable nuclear data to performance evaluation situations where photochemical reactions are of interest.

## CHAPTER 3 IMPLEMENTATION: COUPLING PHOTONUCLEAR PHYSICS INTO MCNPX

### Introduction to Transport Monte Carlo Radiation Transport

Monte Carlo radiation transport as defined within the scope of the Monte Carlo N-Particle (MCNP) code is the transport of radiation through a geometry by random sampling of nuclear interaction probabilities. MCNPX is built upon the same foundation but excludes the restrictions to use nuclear models to generate interaction probabilities if nuclear data do not exist. The focus of this chapter is to show the steps necessary to provide user-supplied nuclear photoreaction data within MCNP(X). MCNP(X) is used throughout this chapter as reference to both MCNP and MCNPX. A general familiarity with either of these codes is assumed in the following discussion.

Many steps are necessary to implement photoreaction physics within the MCNP(X) code. First the photoreaction data must be available in a format that can be used in a transport code. Traditionally, the energy cross-section data stored as Evaluated Nuclear Data Files (ENDF) must be processed into A Compact ENDF (ACE) table suitable for Monte Carlo sampling of interaction probabilities. This processing is typically necessary to transform data structures into more easily sampled forms.

Once the data are available in an appropriate ACE format, they must be loaded into the code structures used by the collision routines. This involves defining a user interface to specify which data tables are to be used, extending the `isr` routine to store the new data and integrating new algorithms to sample photoreaction collisions.

Parameters must be made within these steps to ensure that existing capabilities, particularly within work connectivity and that auxiliary tables include relevant information about the sampling of photochemical interactions.

The sections of this chapter provide the detailed step-by-step account of the steps taken by this work. Key concepts and algorithms are explained along with the estimate details, e.g. the names of the internal MCHP variables containing the table codes. The level of information included is equal to the estimates. That is not the details necessary such that upon reading the actual coding, the value of specific code is obvious. This will facilitate the maintenance and alteration of the code. It is necessary to document these details here because the MCHP coding style (that was inherited for this work) dictates that some code with internal comments should be used. Between this philosophy and the sheer complexity of the coding solutions, it is often difficult to follow what ought to be simple solutions.

## Data Storage

### Photochemical Kinetic Photochemical Data

Data storage was the first major issue addressed by this work. The MCHP radiation transport code was derived originally from the fact that it was capable of anisotropy and photon transport. It later became *A* Particle when electron transport was added. MCHPFC extends further the latter moving beyond the name. Currently only photochemical interactions have been treated as pure photochemical absorption, elastic scattering, anisotropy scattering and gas production. (Note that the name implies the triplet production is included in gas production and treated identically.) The MCHP(X)-ACE files containing time-step descriptions are tabulated as cross sections by element.

Photomachar interactions, indeed all nuclear interactions, are dependent on the specific target nucleus. This means the first problem – how/for to archive data, photomachar data should be collected and used by concept, not by element.

As for separate storage and use of photomachar and photomachar data is considered unworkable (by some), several additional arguments are made to explain why that should be. Photomachar and photomachar data-references are not typically from the same source. Most experiments, theoretical and evaluation experiments in providing data for use in the other set/sets. Compilation of the data are generally separate. Photomachar data are usually updated in a complete, consistent library for all elements. Photomachar data are expected to follow the path of reaction data where updates occur for individual isotopes as they become available. If they were stored by element, it would be necessary to create more ACE data set every time either was updated.

For those reasons and more, photomachar data is stored and accessed separately from photomachar data. This philosophy reserves the necessity of determining how to use elemental and isotope data in the same storage table and generally provides for easier management and access of the different ACE data sets. However, it also necessitates the creation of a new class of ACE table to contain the photomachar data for use in

MCNP(X)

### Standard ACE Tables

The nuclear data tables used by MCNP(X) are known by the acronym ACE. The acronym stands for *A* Compact ENDF. The Evaluated Nuclear Data File (ENDF) is a collection of formats for storing data and procedures for creating and compiling that data.

[44] It is the de facto international standard for storing nuclear data and is maintained by the National Nuclear Data Center (<http://www.nndc.bnl.gov/nndc/>) of the Brookhaven National Laboratory. The ACE table format contains the data in a form more suitable for random sampling by a transport code.

There are currently eight classes of ACE data tables created by MCNP: continuous-energy neutron ' $\nu$ ', discrete-neutron spectrum ' $\nu$ ', neutron fluency ' $\gamma$ ' ( $S(\nu, E)$  thermal ' $\nu$ '), continuous-energy photon ' $\gamma$ ', continuous-energy electron ' $e^-$ ', multigroup neutron ' $n$ ' and multigroup photon ' $\gamma$ ' tables. MCNPX extends this to new classes with continuous-energy proton ' $p$ ' tables. Plutonium-like tables will now add a new class of data to MCNP(X). As this new data describes the microscopic nuclear interactions, the plutonium-like format depends heavily on the continuous-energy neutron and proton table formats. Therefore it is useful to examine how the continuous-energy format has evolved for storing nuclear interaction data.

ACE tables use a system of parameter distributions to access data stored in a one-dimensional array. Table 3-1 shows the standard structure for an ACE table. As originally conceived, the XXX array stores all parameters, the XXX array stores all locations and the XXX array contains the actual data. In a library file, instead of tabular data has its own header with NCE and PCE entries and its own XXX array. In the MCNP(X) executable code, a single XXX array contains all tabular data necessary for the simulation and NCE/PCE are two-dimensional arrays (by array entry with file index).

For describing a single isotopic nuclide and related particle type, a fixed NCE/PCE array can be a reasonable solution. The original neutron data table used only five parameters and required location for  $\lambda$  data. Photon production data were added later by duplicating



Table 3.1: Standard ACE table description

Reference	Laser Address		Contents	Format (Columns: Standard)
	Reference	Address		
1		10N	ZAXIS, Atomic Weight Temperature, flow, frequency	A16, B17, C18, D19, A10
2		10N+1	Channel	A10
3-6		10N+2 - 10N+5	Subtotal data currently stored (000 with zero, or from 0001)	A01, F01.03 per line
7-8		10N+6 - 10N+7	25.500121 - 100	A023 per line
9-12		10N+8 - 10N+11	25.500121 - 1.100	A023 per line
13-14		10N+12 - 10N+13	25.500121 - 0.000	A023.03 per line

key elements (parameters and locators for secondary neutrons etc) to reference photon production data. This required three new parameters and eight new locators. Two additional locators for neutron data were also added to items the table which exists for use by MCMP4B (3, Appendix F). More recently, delayed neutron data added yet another parameter and four new locators [44].

MCMP4B expands the capabilities of MCMP to include tracking light ions as well as other particles of interest to high-energy particle accelerators [42]. Whereas MCMP only expects to transport secondary photons and neutrons, MCMP4B transports all light particles. To do this, the data blocks needed to be expanded to include emission information for an arbitrary number of new secondary particles. Currently, these new neutron-collision include, as appropriate, secondary neutrons data for protons, deuterons, tritons, helium 3 and alpha particles as well as for neutrons and photon data. This placed a burden on the various continuous-energy tables that could not be solved by using the traditional NXS/XXS format code. It was solved by mapping the type and introducing the IXS group.

The DCS array was introduced into the system to store energy fluxes in order to account for secondary charged particle cascade information [H1, 49]. Unlike HCS and DCS that are fixed in length, the DCS array is stored within the XCS array and can be expanded to include entries for as many sets of secondary particle information as needed. In the expanded version table, the DCS array is used to locate the neutron and photon production data and the DCS array for all other secondary particles. Proton tables were adapted in two places as well. The photonuclear data table takes the same logical step and references all secondary cascade information through the DCS array.

### Photonuclear Class 'u' ACE Table

Photonuclear interactions describe photon-induced nuclear processes. The projected final state of a given photonuclear data table make use of the same EXODUS format and procedures as neutron and proton data. This implies that the same concepts used in ACE tables to store other particle data should be used for the photonuclear table such that the existing storage and mapping algorithms can be used for all types of nuclear interactions. However, the existing neutron/proton table has become extremely overloaded. Therefore, photonuclear tables have logically reorganized the data to significantly simplify access.

The photonuclear format has been modified from the existing neutron/proton format to store all secondary particle production in a self-contained manner. However, the table still relies heavily on the sub-formats established for neutron and proton data. The remainder of this section focuses on presenting the key concepts for the photonuclear class 'u' ACE table format. That description is supplemented by Appendix A that includes the full details of all appropriate data structures, how they are stored, what user

stacking can be performed and recommendations as to use of specific sub-formats for photomicro data.

The NXS entry card contains only those parameters that apply to the table as a whole. The NXS parameters are presented in Table 3-2. The first entry is the length of the XRD array. This entry is mandatory for all ACE tables such that they may be manipulated as a generic database. The second entry contains a target identifier and is mandatory for those ACE tables where it is applicable. The next three entries contain the only three global parameters needed for transport: the number of ranges in the main array (n4), the number of cross sections included in the table and the number of secondary particles for which response data are included.

Secondary particle information consists of parameters and locations. The parameter NPICOL (in conjunction with NTRPE) can now be used to determine the memory requirement to store the DS array elements. The DS array has twelve entries in this format version. The parameter NPICOL is the number of secondary particles.

Table 3-2: Description of the NXS Array elements of a photomicro type 'N' ACE format.

Entry	Parameter	Typed Numeric Acronym
NXS(1)	LEN	Length of the XRD Data Block
NXS(2)	ZA	Integer coefficient number of the target isotope $ZA = Z \times 1000 + A$
NXS(3)	NIS	Number of energy ranges in the main array (n4)
NXS(4)	NTR	Number of reaction cross sections
NXS(5)	NTRPE	Number of secondary particle types with reaction information
NXS(6)	NPICOL	Number of parameter entries in the DS array 1 of 12 DS entries in the current format (NPICOL=1)
NXS(7)	NPICOL	Number of entries in DS array per secondary particle The current table format includes 12 DS entries
NXS(8-11)		Unused DS with value zero
NXS(12)	TVN	Table Format Version TVN = 1 for the current table format

parameters at the start of each DSI entry. There are two parameters in this format version. All other DSI entry entries are assumed to be locations and are subject to updates as data are moved within memory as the MCNP(X) executable is run-time.

The table format version parameter (TVF) is the first attempt at documenting each table type format as it is produced. This marks photomuclear format number one. If it is changed later (e.g. expanded to hold a new sub-format, the table format version would be updated at the time to indicate what information may be within the table. This also introduces a mechanism whereby backwards compatibility can be maintained without rapidly evolving the exact table structure.

Similar to the DSI entry, the DSF entry has also been refined to contain only those locations that are general to the table. The DSF entry entries are presented in Table 3-3. The first five entries for this table are located for reaction data that traditionally has been accessed through the pre-defined DSI entry. As the overall number of DSI entries

Table 3-3: Description of the DSF entry structure in a photomuclear type "D" ACB format.

Entry	Location	Object to entry of
DSF(1)	DSF	Macroscopic $\mu_{eff}$
DSF(2)	TOT	Total cross-section data
DSF(3)	MRN	Total non-photo-neutron-section data
DSF(4)	PSA	Photo-neutron-section data
DSF(5)	TOTV	Total scattering cross-section data
DSF(6)	MTX	MT reaction numbers
DSF(7)	QTX	Q-value reaction energy data
DSF(8)	LSRX	Cross-section locations (adjacent to DSI)
DSF(9)	MS	Primary location for cross-section data
DSF(10)	DSAS	First word of DSI entry
DSF(11)	DSB	First word of DSI block
DSF(12,13)		Unused (fill with zeros)

has been reduced, it is left that understanding the ESE location was unnecessary. Therefore, each set of reaction data is associated through its own location.

By isolating the first location, ESE, as the value as the XSE entry for the main energy grid. The four other reaction data sets that have traditionally been associated through this entry were have individual locations. The total cross-section is now located by second entry, TOT. The energy and total cross-section data are the fundamental values necessary for computing the distance to collision during photon transport.

The elastic cross-section is now located by the fourth entry, ELE. The elastic cross-section for photons interacting with the nucleus is negligible in comparison to other photo-nuclear reactions. The evaluated data files are not required to include it. Therefore since that location has isolated the elastic cross-section entries, if the elastic cross-section is not included in the original evaluation, no location is set to zero, no values are made in the XSE block and the elastic scattering of photons on the nucleus is ignored during the transport process.

The absorption cross-section has typically been included for the purpose of heating. For shielding problems, it is sometimes useful to consider capture explicitly. In this type of evaluation, only non-capture reactions are considered at the collision rate and the particle weight is updated accordingly. This heating technique means that a neutron or photon always leaves the collision site. This is the default treatment for both neutron and photo-nuclear interactions.

Photo-nuclear absorption almost always produces a secondary gamma ray. Only photo-nuclear processes involving a transition directly to the ground state of the nucleus do not. Additionally, the secondary particle of interest from the photo-nuclear interaction

is nearly, if even, a plateau. Therefore, the explicit energy-leaking technique is not needed and the absorption cross section has been replaced by the non-elastic cross section.

The non-elastic cross section is located by the third entry, *NEN*. This change has the benefit that when the elastic cross section is not present, the non-elastic cross section is identical to the total cross section. Therefore, the location can be set to make the same data, thereby reducing storage needs.

The total heating numbers are located by the fifth entry, *TEN*. Energy deposited in units of neutrons per fission is stored in *NENSTOX* and the heating numbers for that purpose. The total heating number is an average of the average amount of energy the fissioning particle deposits locally at the collision site. There are numerous assumptions involved in calculating this value (see Appendix A for a more complete description). As it is difficult to compute and extracted by this work, this number is given a zero value to indicate that no data are currently available. When the ability to produce clean  $^{235}\text{U}$  ACE values migrates into the SNOT nuclear data processing code, it will be possible to compute the heating numbers.

The next four locations provide information about the reaction cross sections. The sixth location in the index is the reaction-type listing. These are the RYT reaction-type numbers as defined on the ENDF format manual [45]. The LQR number is the index to the array of Q-values corresponding to each reaction. The LSG and SQ locations index the locations of the cross-section inputs.

The DEIA location is an index to the DSI entry. As described above, the DSI array contains the parameters and locations for all secondary-reaction information. The meanings of the DSI entry values are described below. The DSI location is a

conversion. The data value in ACE table can be limited in any order desired, so long as the locations are appropriately updated. However, for the value of *array*, the data should be limited to the index corresponding to their appearance in the table description. If this is done, the DSI location is the first word of the DSI block of secondary/particle information located within the DSI array.

The DSI array should be thought of as a two-dimensional array containing a set of parameters and locations for each secondary/particle. There are  $NTYPE(3) - 1$   $NTYPE(3)$  secondary/particle reaction descriptions in the DSI block. The DSI array entries are listed for the 36 secondary periods in Table 3-4. Two parameters are necessary for each set of reaction data. The secondary particle type is identified by the parameter *IPT* as described in Table 3-3. The number of reactions that produce the secondary particle is given by parameter *NREP*.

Table 3-4 Description of the DSI Array elements in a photomatrix-type 'u' ACE format.

Index	Parameter	Field number description
DSI(1,3)	<i>IPT(3)</i>	Particle IPT number
DSI(2,3)	<i>NREP(3)</i>	Number of RDT reactions producing this particle
<i>array</i>	<i>Location</i>	DSI(3-array, 3)
DSI(3,3)	<i>PCH(3)</i>	Total particle production cross-section data
DSI(4,3)	<i>PCH(4)</i>	Particle average fission number data
DSI(5,3)	<i>MTSF(3)</i>	Particle production MT reaction weights
DSI(6,3)	<i>TY(3,3)</i>	Reaction coordinate system data
DSI(7,3)	<i>YPR(3,3)</i>	Reaction yield locations (relative to XREP)
DSI(8,3)	<i>REPR(3)</i>	Primary location for reaction yield data
DSI(9,3)	<i>LSRNG(3,3)</i>	Reaction regular distribution locations (relative to XREP)
DSI(10,3)	<i>LSRNG(4)</i>	Primary location for regular distribution data
DSI(11,3)	<i>LSRNGP(3)</i>	Reaction energy distribution locations (relative to XREP)
DSI(12,3)	<i>LSRNGP(4)</i>	Primary location for energy distribution data

Table 3-5: Associations of particles with their spatial and IPT index number as defined in HENP(3)

Particle Name	Spatial	IPT
neutron	1	1
photon	2	2
electron	3	3
positron	4	3
deuteron	5	14
triton	6	15
helium_3	7	16
alpha	8	18

There are two locations that have been designated to be necessary for locating secondary-neutron data. The location and parameters are kept separate: parameters first, within the CES array such that the locations can be updated or discarded within the Setup and Storage system before. As mentioned above, a full description of the locating number concept is found in Appendix A. Locating numbers are not used by this work and thus all PHN locations have been set to zero until no further values are given.

The locations PLS, MTRF, LSGP, SGCP and the parameter MTRP are used to determine the secondary particle production. The production cross sections for the secondary particle is located by the array PLS. The materials which contribute to the production of the particle are located by the array MTRF. The yield data for each material are retrieved in the SGCP block as located by the LSGP array address. This is a change from the previous table layout which overlaid the TYRP materials across yield data as well as the material coordinate system. The TYRP array address designates the reaction coordinate system. The material distributions are stored in the ANDP and DLWP blocks as located by the address in the LAND and LDW/P arrays. The full details



of the neutron formats are complex. In order to avoid claiming that there were more than is already the case, they have been included in Appendix A.

### **Data Processing**

As discussed in the previous section, evaluated data are available in the ENDF format. It is therefore necessary to have a data processing code capable of transferring the ENDF formatted data into the appropriate ACE format. This has traditionally been done by the NJOY code [9]. However, in this case as a recent project to develop the new table format, it was preferable to write a stand-alone processing code that was easily changed in order to explore different formatting options.

The MCNPX data processing code was developed to process data stored in the ENDF format into the ACE class 'a' placeholder format described above and in Appendix A. As this was a developmental tool whose capability will be enhanced by the NJOY code, it was not necessary to implement full functionality for all possible ENDF formats. Instead, MCNPX is focused on the data that were currently available. This section will discuss how the data were processed and what formats were used. The full source code for MCNPX is given in Appendix B.

For the purposes of this work only data from the LA150 Group produced at the Los Alamos National Laboratory have been used for verification. Some preliminary data have been made available from the other institutions involved in the International Atomic Energy Agency (IAEA) Coordinated Research Program (CRP). However, the IAEA data were provided on the condition that they were to be used for testing purposes only. Therefore, some functionality has been implemented in the MCNPX processing code for the IAEA data which was not necessary for this work but looked to long term goals.

ACCPNT works by loading the ENDF data into memory and then creating the corresponding sections in the ACE format. The ENDF format contains sub-sections needed for the ACE table in the "file". Each section of the ENDF format is known as a file and given a file type code (MF), e.g. file MF 1. ACCPNT was implemented with a limited understanding of the format of files as demanded below.

File MF 1 contains general information about the data set. The target identifier ZA is the atomic number, atom 1000 plus the mass number ZA, the atomic weight value (AWG) and the temperature are taken directly from the corresponding entries. ZA is also used to create the table identifier ZATD by adding an ID. The library number plus the table identifier 't', for instance a photonuclear table, are reflective the table ID. The library number is a unique two digit number chosen at the processing time. All ACE tables also include the data processed.

With preliminary data read, the first step in building the table is to form a unified energy grid. The photonuclear data processed to-date have contained relatively low on the order of tens to hundreds, energy grid points. The energy points are obtained as a super-set of the energy grids from each of the reaction cross sections. The value must be adjusted from eV, in ENDF, to MeV, in ACE. All reaction cross sections are found in ENDF File MF 3 and are given as energy/area-section pairs. Parameters which describe thresholds are checked to ensure that the cross-section values start at zero, if necessary adding the zero point. Because there are no few points in these files, as compared to various neutron data sets, that the constant rate of thousands of energy points, forming of the energy grid is not required.

There may be additional energy points contained within polynomials. Yields are stored in file MF 1 of the EXDF format. These energy points are added to the main energy grid of points. The addition of these points allows the verification process to exactly match resonant species. With this done, the total number of energy points, global NEX parameter NEX, is now fixed as well as the dimensions for array EDE.

The fusion ELS and TDS are currently set to zero. None of the calculated data provided to date have included the charge cross section. As discussed in the previous section, TDS is a complicated value which was not needed for this study. Algorithms exist in NOD to compute the total and partial fusion reactions and it was felt unnecessary to duplicate this capability within EXDFE.

The cross-section data are obtained next. Each reactor's cross-section is taken from the MF 2 values and stored in the MD block as located by the LMD offsets. The corresponding MF number and Q-values are stored in the MTR and LQR arrays, respectively. The number of reactions is stored in the parameter NTR. The total cross section is computed from the appropriate particles and checked against the values from the EXDF MF 1 total cross section. The verified computed totals are then stored in the TDE array. As no charge cross sections are present, the NOD fusion is set equal to the zero value in TDE.

Secondary particle reaction data can be specified by either of two methods in the original EXDF convention. The first method described here is not recommended but still allowed. For reactions which produce neutrons, the MF 4 and MF 5 give the angular distribution and energy distributions, respectively, as a function of incident particle energy. MF 3 energy distributions are useful for representing neutron photoneutron

reactions, e.g. fission reactions. Currently, MCNP7 can process MF 3 lines 1, 2, 3 and 11. The corresponding MF 4 angular distribution must be isotropic. The neutron yields for fission reactions from file MF 3. All other yield data for reactions specified by the method are implicitly given by the reaction type, e.g. reaction MT 10 implies two neutron neutrons. The data from these three files are merged appropriately into the neutron secondary particle information. To date only JAEA does have used this format. It is highly recommended that all fissionable reactions be described by the following method so all secondary particles, not just neutrons, can be included.

Secondary-particle reaction spectra may also be described in the ENDF file MF 8 format. ENDF file MF 8 contains raw values describing each reaction with appropriate subroutines for every product from that reaction. MCNP7 loops over each file MF 8 section and extracts the appropriate secondary particle spectrum data into the ACB table. Currently MCNP7 extracts spectrum data for secondary neutrons, photons, protons, deuterons, tritons, helium-3 ions, and alphas. This set of particles represents what exists in an alpha-particle in the fissionable that can be transported by MCNFX. Obviously, MCNP7 is limited to the transport of secondary neutrons and photons. This processing methodology has the caveat assumption that all other reaction products are stopped at the collision site without producing any further secondary particles of interest.

MCNP7 currently processes LAW 1 combined energy-angle distributions from file MF 8. The yield for each particle is taken directly from the energy/yield pairs given and the data are stored in the SDEF block as located by the corresponding LDEF value. Likewise, the left number for the production reaction and the coordinate system for the emitted particle are stored in the MTYP and TYLP arrays, respectively.

The LAND 1 regular option presents a tabular-energy distribution with Legendre coefficients describing angular dependence. MCNP only processes isotropic distributions and they are stored as tabular-energy distributions, ACE Energy Law 4, in DUMP with the corresponding effect is LOURP. The isotropic regular distribution is selected by a zero value in the LANDF entry and no action is the ANDF block.

The LAND 2 regular option specifies a tabular-energy distribution with Eddington regular symmetries. This anisotropic distribution is stored with the appropriate LOURP effect in the DUMP block as ACE Energy Law 44. The corresponding LANDF entry is given the value negative one to indicate the presence of the correlated energy-angle distribution and no action are made in the ANDF block. The Eddington slope parameter, designated  $\kappa$ , is computed according to Chudakov's criterion [11] of Eddington's original formulation [26,27] to maintain the related normalization of the photon.

The LA150 photo-neutron evaluation (2) use the ENDF format (114-LAW 1) LAND 2. As the LA150 evaluated data are used exclusively in this study, processing of the LAW1 LAND 2 format functions exclusively tested. This is a tedious procedure done either by hand or by script to ensure that the ACE data match the original ENDF data. The other options discussed were implemented to process data provided by the OMA CRP and their processing has not been checked with the same rigor. All ENDF evaluation distribution formats not specifically mentioned are not supported.

At this stage the ACE table is almost complete. The photo-neutron cross sections and the associated yields for each secondary particle are used to compute the total particle production cross section that is stored in the F08 entry. The number of reactions

producing the particle  $n$  stored in the parameter NTRP. The particle history-number keyword, PHN, is given a value of zero to indicate no history numbers are included. The final processing verifies the values for the headers, sums the total number of NDS entries in the NDS parameter LNS and prints the final table in an ASCII file.

With the appropriate additions to the MCNP(X) user-section directory file `XXXX`, the data are now ready for use in a simulation. At the time the simulations in this study were performed, the LA190 library contained evaluated photonuclear data for the following isotopes:  $^{27}\text{Al}$ ,  $^{40}\text{Ca}$ ,  $^{56}\text{Fe}$ ,  $^{63}\text{Cu}$ ,  $^{90}\text{Zr}$ ,  $^{100}\text{Mo}$ ,  $^{180}\text{W}$ ,  $^{208}\text{Pb}$ ,  $^{209}\text{Bi}$  and  $^{238}\text{Pu}$ . The evaluated data were processed into the ACE photonuclear format using the MCNPCT code as described here. The collection was given the ID file as earlier testing had been done using library numbers 04 and 05.

## Coupling Photonuclear Physics into MCNP(X)

### Introduction

The work presented here describes a prototype code based on MCNP4B2 [3]. MCNP was chosen as the base code for the reasons described earlier. This section describes the modifications that were made to MCNP4B2 to produce the photonuclear-capable-prototype code designated MCNP4BPM. Once verification was complete, these changes were frozen and the final version described here was used for all subsequent calculations presented in this work. Where standard MCNP capabilities are discussed, see the users guide [1] if further explanations are necessary.

The MCNP code package is maintained by the X-5 group of the Los Alamos National Laboratory. A project homepage is maintained and can be accessed through the X domain homepage (<http://www.xdr.lanl.gov/>). The code package is distributed by a

persons and companies within the U.S. by the Radiation Safety Information

Computational Center (<http://www.rssc.com> and [www.rssc.com](http://www.rssc.com)). Foreign distribution

handled by the Nuclear Energy Agency (NEA) in Paris, France. Changes to this guide are

to be made via patch files as documented in the next guide [3, p. C-4]. Appendix C of

this document contains the patch file corresponding to the changes described here.

Before breaking into the gory details of the changes, a few comments will be  
 spot-pervading as warnings. There were four major tasks necessary to implement  
 photoacoustic interaction into MCNP: (1) the user interface needed to be modified to  
 allow specification of photoacoustic tables for a given material; (2) the nuclear data  
 sampling routines needed modification to appropriately handle particles other than  
 neutrons; (3) the photon collision routines needed to be updated to include sampling  
 photoacoustic cross-section; and (4) the file routines needed to be updated to include reading  
 photoacoustic tables and printing necessary information about photoacoustic interactions.

The specification of materials is done in a very standard manner within MCNP.  
 Several words define the final interface for photoacoustic. First, the standard interface  
 must be kept. However, it was designed with the concept of one table type for each  
 particle type. Further, it means there is always a table available for each component of  
 the material.

The intent of the specification of photoacoustic tables was to keep the standard  
 interface as is and suggest it to work similarly for specifications of the new tables. That  
 is, the components of the material are defined by the material card. Component ZAID  
 names can be specified directly in the entry or indirectly through the ZA with a default of

more specified theory (e.g. Neutrons, electrons, photons) and photonuclear table (ZAGDs or theory) than of acceptable.

However, the interface has also been augmented to include an escape routine for photonuclear tables. Specifically, because more complete escape data will likely be available for various isotopes, the best description of the material should be given in the material card by routine table. The new routine card allows the escape to be changed for any shell of the material composition. This provides for use of the best neutron and photonuclear table data for a material. It should be considered at some point in the future to allow material specifications by routine particle in MCNP(X).

The neutron data sampling routines were originally written for neutron reaction, neutron emission interactions. They were later updated to include photon reactions. Recent interest, including the current work, needed to expand the tables to handle neutron photon capture or emission and the subsequent emission of any particle type. The set of updates that presented is described only briefly below. It is now commonly known as the ACE modifications and has been implemented [32,33] in the current versions of both MCNPX and hMCNP [34].

The revision of the photon collision routine to include photo-nuclear interactions is the key objective of this work. These routines have been updated to include use of the photonuclear cross sections, in addition to the photo-nuclear, for the sampling of distance-to-next collision. At a photon collision site, either neutral or charged collision can occur (based photonuclear-collision subroutines that a contribution from photonuclear interaction in secondary/particle production is to be obtained at every photon collision). In either



new secondary particles are sampled from the evaluated tabular data and made available for further transport.

There are no unexpected changes in the file input/output. A post/MCNP user will be able to fully utilize the new capability based on their previous experience using the code. As mentioned before, the standard material interface will work unchanged. All tables are loaded from standardized ACE libraries specified through user XCORR directory file. The few new interface options available are simple to use when necessary and are not required. All tables and necessary information include the effects of photoatomic sub-materials as presented in standard MCNP output tables. Thus, the savings were realized using the capability immediately and became an aspect user familiar with all the versions over time.

### Setup and Storage

**Material specification.** The first task necessary to use the photoatomic data within MCNP was to implement user options to specify where data is read and to store that data appropriately. It was determined that the external specifications to load photoatomic data should be as similar to what was currently done as possible. However, some variations have also been made.

As present with material two sets of isotopes and atomic fractions associated with it. For example, the material description for an element might be given by the MCNP input card `mat 71000 17` or by `mat 71185 3 80812 71140 0 100000`, both of which indicate that material one is a natural mixture. The first specifies elemental isotopes directly and the second specifies the constituent isotopes by their atomic fractions. Since photoatomic data is stored by element, either card could be

used to specify which tables, or in the example table, should be used. However, neutron data is stored by isotope, with a few exceptions, such that the neutron description in the main summary represents the control. Photoneutron tables are also stored by isotope and therefore more accurately described by isotope tables.

Unfortunately, very few photoneutron evaluations were available for this study from when the IAEA library is made available, not all isotopes will have an evaluated data file. Some provision is necessary to allow the user to specify the best photoneutron data available without compromising the fidelity of the representation by other tables, in particular neutron tables. Therefore, a photoneutron isotope summary card has been implemented.

To overcome this problem, reactor's internal input card describing actual isotopes. The best description for neutron isotope is given by the internal card "n.1 74182 0.243 74183 0.243 74184 0.3047 74184 0.2813". Hence, for this description is incomplete, isotope  $^{238}\text{U}$  with a natural atomic fraction of 0.9927 is not included in the description because a neutron table is not available. MCNP will compensate for this by re-normalizing the sum of the other atom fractions to one. However, photoneutron data are currently available only for  $^{238}\text{U}$ . Following the logic of drop what is unavailable and re-normalize the significant contributions by other isotopes for neutron isotope would be almost simply because of the lack of photoneutron table for the remaining isotopes. The driver for the test representation for both neutron and photoneutron interactions in the internal requires a new capability to internal input specification.

**Photonuclear escape cross-section (MPN)** The photonuclear escape cross-section, designated MPN, has been implemented to allow submission of photonuclear data. Specifically, for the example above the photonuclear escape cross-section "mpn" TC184 TC204 TC184 TC184" used in conjunction with the material specification card from the previous paragraph would provide the best data for all particles transported through the material. MCNP6/MPN would use photonuclear data for elemental regions, the user available cross-sections for the major targeted isotopes and the  $^{238}\text{U}$  data table for all photonuclear collisions.

There are several restrictions on the use of the photonuclear escape cross-section. It must be used in conjunction with a material specification card, i.e. M1 with MPN1 describes material use. The escape card must come after the corresponding material specification card in the standard MCNP input deck. There must be one entry on the MPN card corresponding to each ZAID entry on the M1 card. Entries on the MPN card must correspond to a ZA for which a photonuclear table exists or be zero-to indicate no photonuclear interactions should be considered for that portion of the isotopes.

The photonuclear escape card has been implemented as a new input card. The number of cards for use in the input was increased by one by increasing the value of parameter in the deck `jp`. The new card, `comppn`, was included in the deck `libtbl` with the option to allow only integer entries. (The set of `libtbl` type in this chapter includes material subroutines in the MCNP system code. Likewise, table type regulates the names of variables within those subroutines.)

This capability requires an entry to give a different ZA for photonuclear interactions than the default for the material. The M1 card stores ZA/element fraction pairs

in the range *low* and *high*, respectively. The user can assign memory for the array as a storage location in the dynamically-allocated common-blocks. They are both set to length *one*, the number of integer/fraction pairs for the specific problem, at runtime.

No processing was necessary for the MPM card during the first reading of the input deck. Therefore the routines *newmfi*, *readfi* and *addmfi* update the card. Several processing routines are necessary during the final reading of the input deck. When the MPM card is first encountered, the routine *newmfi* checks to ensure that photodesorption physics is turned on in the simulation. If photodesorption physics is on, it then checks to ensure that a material card has already been read describing the material. If either of these conditions are not met, the MPM card is ignored and a warning message is printed.

Each entry for the card is checked and stored individually. From the card initialization set in deck *initset*, the entries are automatically checked to ensure that they are integer numbers. The routine *checkfi* returns the entries to ensure that a valid ZA, in the range 00001 to 99999, or zero has been entered. A fatal error is issued for invalid ZA entries. The routine *addmfi* then stores each entry in array *low* to correspond to the appropriate M card entry. Finally, the routine *addmfi* checks to ensure that the number of entries on the MPM card corresponds to the number of entries on the M card. If they do not match, all material values are reset to the material default and a warning message is printed ending the card was ignored. If the update override has been successful a warning is printed for each update override. It is the responsibility of the user to ensure that appropriate substitutions have been made.

**Table ID specification:** MCMF allows the user to specify the data table ID to be used for each material by several methods. The first method is to describe materials by

complex EAIDs. For example, natural copper can be described by the material specification card "60 21043 60c 0 4313 21045 60c 0 3033". The "60c" is the table identifier, ID, indicating the natural-copper "c" tables should come from the JENDL4b library. JENDL4b tables having the same-library number 60. Photoneutron tables can be specified in an analogous manner. The table identifier "60c" can be used to specify the library, with 60 appropriately replaced, denoting a lead for photoneutron tables.

The second method to specify a data table for an isotope is to use the defaults as defined in the XSDEF library file. The XSDEF file includes the lookup table used to determine what data tables are available in each library. Thus table identifier (ID) has been specified, the first match to EA for each class of table will be used. For example, if the XSDEF file contains entries for JENDL 4b and JENDL 60c as that order and the 60 code enters the EA 20640 without an ID as a pre-set truncating criterion, the JENDL 4b table will be used for neutron influences as that material as it was seen first. Thus, the order of the EAID entries in the XSDEF file can be used to determine which tables are used as a provision. This is the reason the default XSDEF file distributed with the MCNP code is revised such that the recommended tables appear first.

**Default LIB specifier** The default library used for a table class can be specified using a material option entry on the material specification card. The MCNP, three material options are available to do this. They are the PLIB, FLIB and ELIB options corresponding to the neutron, photoneutron and electron default library specifiers, respectively. The names of the material options are stored in the variable `library` in the character common block, `afchdgn` as initialized by deck `initlib`.

To illustrate the use of the default library specifier, consider the IM card 'IM 21003 0 4517 24000 450 0.3000 0.010-0.00 0.010-0.01p'. Any combination of material options can be used as needed but they only apply to that IM card. The order of precedence for selecting a ZAIR is the ZAIR on the entry card, the ZA from the entry with the ID from the default library specifier or the first appropriate match to the ZA in the XSDIR file. In our example, the electron, photoelectron and electron tables are selected using the specified XSDIR file as follows. The electron tables 21003.00 and 21003.00p are used, the first from the ZA and FLIB library specifier and the second specified directly by ZAIR. The photoelectron table 21000.01p is used, selected by the ZA, shortened to elemental X and FLIB library specifier. The electron table 21000.04p is used, selected as the first appropriate electron table listed in the XSDIR file.

The original option FOLIO has been added so that the user can specify the photometric default library that is wanted to be used as a reference source. This was done by renumbering the number of optional options in block (and adding the string constant 'units' to the variable name corresponding to block **UNIT**).

To make use of the FNUJF material option, consider the example in card "c1 21043 0 4317 21043 0 3533 pos.10-03a" with the corresponding MPF card "type1 21043 21043". The example card specifies that  $^{44}\text{Ca}$  should be used in place of  $^{40}\text{Ca}$  for photoelectron cross-sections in the second instance of the material. The FNUJF default library specifies indicates all photoelectron widths should come from the LAMM exclusive 3 electron-atom data library, with library number 05. Thus, the

2000) this table would be needed to link material names for handling photo-nuclear collisions

**Table selection and storage** - The portion of the coding that controls this table selection and storage required extensive changes to enable loading a new class of table. The storage allocation process was completely rewritten. The specific changes are documented here

The original version of code responsible for determining the storage needs for the cross-section data made primitive, complicated algorithms. It contained dependencies that assumed one table type per particle type attached to each material constituent, i.e. only neutrons, photo-nuclei and electron tables. (That is not strictly true as thermal tables represent the entire data set and are stored separately but that is handled as a separate optional exception.) As implemented, the algorithm was not amenable to selective request photo-nuclear table request as distinct from photo-nuclear table. The algorithm's complexity derived from a convoluted process whereby it determined the number of duplicate tables required in order to reduce the memory allocated for use in table header and storage arrays. This was an unnecessarily complex process for relatively minor savings in total memory needs.

The sections of code that made material specification made was heavily revised. Several new arrays were introduced to reduce the existing data pointers. The array for has been described above. To enhance the array for neutrons the material request being for the purpose of simulating photo-nuclear collisions increasing the array one which contains the default request being for all other non-photo-nuclear reaction constituents of the material.

All dynamically allocated memory in MCHP is placed in a single long array, `data`, and referenced by offset. This creates a confusing situation because all dynamically allocated arrays are actually the same array, through either the Fortran77 equivalence or pointer statement. To illustrate, this module has the array `pxs`, `pxoff` located in the `data` array, contains locations that `pxs` indexes into the other arrays also located in the `data` array. Therefore, all arrays must be referenced by their `pxs` position, e.g. `pxs(px)`, that contain the index of the first word of the corresponding array.

In the description of the table format in a previous section above, `NXS`, `DO` and `DS` are shown as one and two-dimensional arrays. In use within the code, arrays `pxs`, `pxs` and `pxs` group up additional dimensions corresponding to these table index, variable `pxs`. Each table has a unique index assigned by its index within the array `pxs`. Thus, to find the fifth element of the `NXS` array for the fourth table is found at the location `pxs(table+5,4)`. Similarly, the third element of the `DO` array for the second emission particle is the fifth table is found at the location `pxs(table+5,2,3)`.

There are numerous variables and arrays associated with the table selection and storage. The array `len` has dimensions of the number of materials specified as the material code by the number of particles available for transport, i.e. `mat` by `type`. It contains the weights, physical and self electron table indices for each combination of all materials in the current simulation. The array `len` has dimensions `mat` and contains the photoabsorption table indices. Arrays `mat` and `len` have dimensions `material` `type` and contain the `EA` algorithm for the electron-photoabsorption/electron and photon `len` material constants, respectively. The tables are selected using these `EA`, from either array `mat` or `len`, and then `ID`, from either the directly specified `ID` or array `len` or the



default specifier located in other way *data* file. The arrays *acc\_low* and *acc\_high* are the arrays corresponding to each of the axes within *cc* file simulation. The arrays *acc\_low*, *acc\_high* and *acc* have been added to the appropriate common blocks to mirror the arrays *acc\_low*, *acc\_high* and *acc*, respectively. The parameters *maxacc* and *maxn* are added to the deck as to indicate the maximum number of secondary particles per table and the maximum number of DDX array entries, 8 and 12, respectively.

A number of other new variables are also necessary to the task at hand. The variable *isps* is added to the first common block *beam* to hold the flag indicating whether photoneuclear physics is on or off. The array *psd* is added to the block, *dynmically-allocated common block data* to contain the lowest photoneuclear threshold energy for each material. The variable *isps* is added to the task common block *taskcom* to hold the total photoneuclear cross-section value for the current photon *is* or its corresponding energy for each task transporting particles. The variable *isps* is added to the variable common block *varcom* for use in printing on cross-sections. The variable *hsc* has been added to the character common block *cc* block *cc* to contain the string *whypagm*<sup>17</sup> listing the choices of *cc* file in their default order.

Several scoring variables have been enlarged to contain new values. The arrays *psd* and *psdc* contain the weight values by particle type for the overall geometry tables for the problems as a whole and the individual tasks, respectively. Their dimensions have been increased by one, from 16 to 17, to cover photoabsorption and photo-production information by particle. The array *psd* is the mapping from particle interaction type, *isps*, to the appropriate storage location in the array *psd*. Its dimension has also been increased by one to account for photoabsorption termination of the photon. The array

probabilities from information for each particle type for each cell. The databases have been constructed as text by rows, from 12 to 24, to store photoabsorption and photoionization production for photons as well as photoabsorption for other particles. The array *prob* stores interaction activity information by table, currently only photoabsorb and neutrons, for each cell. The databases have been expanded to include space for photoabsorb tables, first index from 1 to 3, as well as new entries, second index from 0 to 4, for the additional photoabsorb interaction.

Now that the key variables are known, the initialization algorithms can be described. MCNP starts a problem by reading the default input file "inp". It makes two passes through the cards in this file. The terms card derives from the days of punch cards and is simply a single line of input. The first pass sets up the storage necessary to process the input and stores a few key user input parameters. The second pass stores the remaining user input values.

Since photoabsorb interactions is a new capability to MCNPQ, it was decided that during the time it is a beta test capability the user should have to turn on photoabsorb physics. This was done in large part so that the existing regression test suite could be used without change. The default way eventually be changed to have photoabsorb physics on such that the best available transport algorithms are used unless the user turns them off. The fourth entry on the PHYS F card is set to flag the use of photoabsorb physics. It is read on the first pass through the input file and stored in the variable *apn*. Any non zero integer number will indicate that photoabsorb physics is to be used during the current transport simulation. Any positive integer indicates neutron

photoreaction influences are to be computed. Any negative integer indicates forward photoreaction influences are to be computed.

During the first pass several key parameters are determined about the materials specified. The number of materials specified in the input deck is stored in variable `nmater` as incremented by routine `nmater1`. The number of isotopologue fraction pairs specified on a material card is stored in variable `isop` as incremented for each entry in the routine `nmater1`. The number of pairs for the material is then used to update several other variables in the routine `nmater1`. The total number of pairs over all material cards is stored in variable `ntot`. The maximum number of pairs for any material is stored in variable `maxmat`. The variable `apc` sets the storage for the array `pauc` and is incremented by the number of pairs times the number of cards containing the material. Thermal reaction tables, which come in low energy (starting data to compute reaction rates), are handled by the MT card. The variable `mt` contains the total number of thermal table entries for all MT cards as updated by routine `mttbl1`.

As the data flow goes through the input file, the storage requirements are computed in the routine `hsize` and written for the table headers as well as other dynamically allocated variables. The error checking takes a simple approach to allocating space for table headers. In routine `hsize`, just after the call to `pauc1` that read the input file the array file for the first time, do the following. Count the number of particles that are to be transported as the previous containing one table set is needed per particle. If photons are transported and electrons are not, increment the count because no electron table set is needed for the dark input branching ratios. If photons are being transported and photochemical physics is on, increment the count to indicate that two sets of tables are

needed for photos. Remember that the variable *tbls* contains the total number of compositions (fraction pair for all materials). The maximum number of tables needed for the problem can be computed by multiplying *tbls* times the table size needed and then adding one to account for the formal tables. This value is stored in variable *maxtbl* which is then used in *tblsize* to allow it to range for table freedom.

The set of routines described above has simplified the original coding. It seems that any composition-fraction pair will need a set of tables and every formal table requested is different. The original logic in these routines changed to account for tables that were used by more than one material and remove the storage allocated for duplication. This represents a small memory savings in comparison to the amount of coding and work needed. It therefore has been eliminated from the current coding.

Once the memory layout has allocated the dynamic memory, variables are initialized as necessary and the second pass of the input file is made. The arrays *tbls* and *tblsize* are initialized to the default table type for each particle for each material; "P" for particles, "F" for photostones, "C" for clays and "G" for glauconites. The array *tblsize* is initialized to parameter *tblsize*, the largest value allowed by the system. All other arrays of interest to materials are initialized with zero values.

The second pass through the input file checks and stores the remaining user input. In the original program, material cards are checked to ensure they are used by either a cell or a fully multiplex. The *tblsize* is updated otherwise and a warning is printed. The number of materials after discarding those not used is stored in variable *matcnt*. The notes, i.e. description from the M card deck, of each material is stored in the array *mat* in the order they are seen.

The system checks against each item on the material schedule if it pertains to the system status to be moved. User input default Money operations are examined to ensure that the table type is suitable and that the corresponding periods of being transported. Material movement functions are checked to ensure they are non-zero and reflect all items in all weight fractions. Warnings for final cost messages are printed as appropriate.

The master continually stores the user input values from the input deck in the correct memory locations. The ZAD entries are split apart. The ZA is stored as entries for and for. The MPN card, which must follow the corresponding M card, can then overwrite the ZA values in the entry for. The material movement functions are stored as *array for*. Positive values are cost fractions. Negative values are weight fractions that are changed to mass fractions in the master routine. A user input default material library operation is stored appropriately to either *array for* or for.

The master checks that values final-costs exists and completes the storage of material references. If any ZAD entry does not have a corresponding fraction, a final-cost is moved. Otherwise, the number of pairs for the material is stored in *array for* and locations for the material entries are stored in *array for*. Warnings are printed to ensure the use of the photomicroscopy controls has been used.

The master staff determines the actual cross-section tables to be loaded. The *array for* contains a coded list of all cross-section tables to be loaded. The first version of the master staff adds the neutron, photomicroscopy and electron tables requested to this list. The *array for* is updated with the table index into *array of* to associate each table for each periods type with the appropriate material statements. A new version of code adds

the placeholder tables requested and presents a similar option for the entry list. The thermal tables are also added to entry list and entry lists used to associate them with the appropriate material.

The order of precedence for the table ID is determined by the algorithm in routine **sort**. The exact ZADD is requested if specified in the material entry. The ZA and default ID are requested otherwise. The default ID can be from a material option in which case it can include a library number. Otherwise, the input is for the first table of the appropriate type in the XSDIR file.

The list of requested tables in entry list is then sorted and checked for duplicates. The list is sorted by default table order and then alpha-ascending by ZA to facilitate finding and locating the tables. Duplicate entries are removed from the list. Warnings are issued in this case for any duplicate entries, e.g. ZADD 29664.00a and 29663.00a. The table index entry list, desc and loc are updated to maintain correspondence to the appropriate material entry.

The entry list is passed to routine **locate** that determines the tables available for use. The available cross-section tables are listed either on XS cards in the input deck or in the default XSDIR file. The XS card or XSDIR entry provides basic information about the cross-section table including its location under computer file system. The ZADD entries are checked first against the XS cards and then against the XSDIR entries. The first exact match, i.e. correct ZA and table type, is kept as candidate exact match or not found. The information from either the exact match or the exact match, if found, is stored in the entry list. Exact matches are not used for fully specified ZADDs. For example, if

only 20481-416 was found and not 20481-416 was requested, the new table would never read.

All array of tables should now be searched with every available location information. As the process may have introduced duplicate entries for matches in partially unspecified tables, they are removed. Every attempt is made to read a table, the condition is stopped and an error message is printed. The transport process cannot be run if any error occurs while it is running. Remember that the photomicroscope outputs every output as table to read in which case no table is needed. This completes the input file processing.

The cross-section tables are loaded by the routine read and its subroutines. All cross-section tables are loaded, processed and stored individually except for electron tables. Electron tables are a special case. The electron data tables are loaded but not processed all at once. The raw photomicroscope tables are handled individually just as all other normal tables.

The routine getmat is called to process each collected table. After finding the location of the next table in the appropriate library file, it calls the routine read to read the data into memory. The routine read first checks to make sure that the table header matches the table requested. It then stores the XES and DES names in the corresponding array and all other entries in the use array. Then in the routine getmat, the jcr location values are updated to become values and the names are array. If appropriate, the DES entries are then extracted from the use array and stored in the appropriate use array. The location on line are updated in a manner similar to jcr. If appropriate, data that are not

needed in the current transport simulation are extracted from the run array upon appropriate updating of locations.

To this point only one data table has been stored in the run array at any time. During the transport process all data tables are stored consecutively in the run array. Therefore, all locations are updated one more time to point to where the data will be during the simulation. The table is then written to the file "runqps" and the next table is generated. When all tables have been generated, the array run, now with all the tables stored in order, is loaded back into memory from the file runqps. This completes the setup and storage phase.

It is worth noting here that this coding has been subject to extensive review in addition to what was needed for this work. The MCNPX code has recently been updated with the capability to load evaluated proton data to enable reliable sampling of neutron events. The coding to do this corresponds to the description above except without an output controls card. This coding has been implemented in MCNPX and was reviewed upon its first issue. The process was documented [20] and the coding has been at use in MCNPX with no bugs reported to date.

### Physics Implementation

In the tabular data regime, MCNPXQ implements a statistical Monte Carlo method to simulate individual transport. This means that the details of any one history do not necessarily represent physical reality. It is only when the details of many histories are accumulated and averaged as a run that average values corresponding to physically meaningful quantities can be determined. This has a significant impact on the data needed to perform the simulation as well as on how the simulation is conducted.



The ACE algorithm makes various approximations and the average reaction probabilities of the secondary particles. For most evaluated data, the worst average approximation is that if a reaction produces two neutrons from a  $(\alpha,2n)$  reaction, the neutron energy spectrum is the average considering both neutrons together, not separately. In a real collision, the amount of energy the first neutron takes away determines the energy available for the emission of the second neutron. In a statistical long term process, this averaged neutron spectrum is used to sample both neutrons. It is therefore possible to sample reactions in which energy is not conserved for the collision. However, given that enough collisions are sampled, the average statistical parameters for the secondary particles are correct.

Statistical averaging also requires considerably less memory than data free sampling data. As current statistical tables require as much as two megabytes of storage per table, routinely using complete data is prohibitively expensive. A complete table would need to include appropriate distributions for every second, third, etc. neutron particle and would exponentially increase the storage requirements.

The algorithm for material Monte Carlo sampling is simple and straightforward. During the transport process, the distance to the next event is used along with the direction of flight to move particles through a material geometry. If the particle is in a material, the distance to collision is one of the possible next events. The distance to collision is sampled using a random number and the probability of the particle colliding with an atom in the material. The probability of collision is known as the total macroscopic cross section and is typically given as sums of atomic cross sections. The macroscopic cross section at the start density times the total macroscopic cross section

for all materials involving an incident-particle type is a given material. The macroscopic cross sections are tabulated as a function of the incident-particle-energy in the *ACTS* tables.

As the neutron history tracks a photon through a medium, it first calls the neutron *photon* to compute the total macroscopic cross sections for the current energy of the current material. Previous to that work, the neutron *photon* returned only the total photoatomic cross sections. The value of the total photoatomic cross sections is stored in variable *sum*. The logic to compute the photoatomic total cross sections is left unimplemented. However, a user test to realize *photon* decides to use a photoatomic physics as an aid if no valid the neutron *photon*.

The neutron *photon* has been added to compute the total photoatomic macroscopic cross sections. It summarizes the total photoatomic cross sections in the variable *sum*. This variable is initialized to zero upon entering the routine. If the incident energy is below the photoatomic threshold as stored in array *photo* material, the routine is done. Otherwise, the total cross sections for each range in the material is summarized in *range*. Additionally, as each cross section is found, the current-energy, the index and effect of the current energy in the cross energy *pool* and the value of the cross sections for the *range* are stored in the array *list* and *val*. This is done such that these values are available immediately if the next request exceeds the current energy.

Once back in neutron *photon*, the total photoatomic cross sections for the material is added to the total photoatomic cross sections and stored in *sum* just before returning to neutron history. The neutron history uses this value to compute the total macroscopic cross sections. variable *sum*, the cross density, *sum* variable *sum*. The current effect

value is known as the mean free path and stored in variable `g1`. The distance-to-collision stored in variable `rng1` is then generated from the well known Monte Carlo sampling formula. (For general information on the Monte Carlo method for simulating random transport, see the reference by Carter and Chabot [34].) This is an important step in achieving a more correct photon simulation as the use of only the photoelectron cross section can overestimate the distance-to-collision by up to seven percent for photon energies in the giant dipole resonance region and otherwise distorts the photon collision distribution.

If the user event is a photon collision, the routine `collide` is called to handle the interaction. Similar to the treatment of nuclear particles, photouclear interactions are treated in a separate subroutine. If photouclear physics is on and the photon is above the photouclear threshold energy, the routine `collide` is called at the beginning of `collide` to handle a possible photouclear event.

Photouclear events are very in comparison to photoelectron events. For this reason, it is useful to have a method to turn the sampling. The variable `open`, set by the user in the fourth entry on the PHYS-P card, controls the turning method. If the value is a positive integer, photouclear events occur at their natural frequency. That is, sample a random number from zero-to one and if it is less than the ratio of the total photouclear cross section to the total cross section, the collision is a photouclear event. If not, account for not sampling a photouclear event, return to the routine `collide` and sample a photoelectron event at the correct distance.

Setting `open` to a photouclear collision. If the user has set the variable `open` to a negative integer, the photon is split. Two particles each of reduced weight (a measure of

these interactions) are created. One is forced to undergo photouclear absorption and the other is passed back to the nuclear validity for normal photouclear sampling. The weight is adjusted by the probability of each type of event, photouclear or photoatomic. Specifically, the weight of the photon that undergoes forced photouclear coupling is scaled by the ratio of the photouclear cross section to the total cross section. The weight of the photon that undergoes photoatomic coupling is the original photon weight minus the portion that underwent photouclear absorption.

For other natural or forced photouclear collisions, it is necessary to update the secondary information. If it is a natural sampled photouclear collision, the secondary energy  $sec\_en$  and  $sec\_id$  are updated to indicate the photon was terminated by a photouclear absorption. If it is a forced collision, the numerics are updated to account for the weight and energy loss, but do not indicate absorption as the original photon with the remaining weight continues on its path.

Once it has been decided that all or part of the nuclear photon will undergo a photouclear collision, the target isotopes must be chosen. A random number is sampled and a target isotope is chosen based on the ratio of its partial cross section to the total cross section. This is done by accumulating the cumulative probability that the reaction occurred for each isotope in the material in turn until reaching the randomly sampled probability. After the target isotope is chosen, the  $sec\_en$  is updated to indicate a collision using that isotope's table.

Based on the target isotope and the incident photon energy, a production cross section can be calculated for each secondary particle of interest. The ratio of the secondary particle-production cross section to the total cross section for that isotope is

stored in variable  $j_0$  and represents the average number of particles produced expected. An integer number of particles available for sampling can be obtained by adding a random number from zero to one to the average value  $j_0$  and taking the integer, floor, value. The number is stored in variable  $np$ . Again, notice that because this is statistical Monte Carlo, the average number of particles created is preserved only over large numbers of iterations.

Because heavy photonuclear particle production can cause considerable variations in weight, it is desirable to have a method to control the situation particle's weight. The weight windows present a reasonable method for achieving this. Weight windows are user input values that control the value of particle weight in an energy region in a spatial region. If the particle is above the weight-window limit, the weight is reduced by splitting it among several identical particles such that the new particles fill the window. If the particle is below the weight-window limit, Russian roulette is played and particles which survive have their weight increased to a value within the window. The splitting or roulette of particle is limited to a maximum value for any given step.

If only one energy group exists for the particle at interest at its current position, the weight window control can be applied before sampling the emission parameters. Specifically, the opportunities to be sampled are split or reduced appropriately. This is advantageous for two reasons. First, it prevents sampling particles that do not undergo further transport, thus saving CPU time. Second, it splits particles of high weight before sampling emission parameters. This generally provides better statistics faster in terms of the number phase-space is sampled per collision. Otherwise, if more than one

energy group exists for the weight window, the volume can only be applied after the particle is sampled and its energy is known. This is done as described below.

A loop over the target number of particles to be created is used to select appropriate neutron parameters. Similar to the selection of target isotopes, a production reaction is randomly sampled from those available. Once the reaction is picked, the energy and scattering angle are sampled using the modified ACE sampling routines and entered in the laboratory system. The current value of time in laboratory time units does not account for the phase momentum. The routine makes then updates the current particle's direction of flight. Note that this is a *stochastic* method that randomly samples the reactions producing the neutron particles, e.g. if two reactions are available, one may be from a (p,n) and the second from a (p,2n) reaction.

Updates to the ACE sampling routines were needed for four different effects. The delayed neutron capability implemented by Chris Weaver [23] needed to sample neutron emission spectra from a new location in the data 'v' table. The upcoming release of a new ACE continuous-energy neutron library took from the latest release of the ENDF/B-VI evaluated data library will use correlated isotope energy-angle spectra. The coding to implement Energy Loss E1, correlated isotope energy/isotope angular distribution, and Angular Loss L1, isotope angular distributions, were written by Bob Latta of X-5 at LANL. The ACE sampling routines have only been used for neutron sources, emitted neutron photon reactions. Sampling for emitted photons and positrons with subsequent creation of all light particles required creating neutron dependencies within data sources and updating source algorithms. The effort to use positron tables at MCNP5 and the effort to use photonuclear tables at both MCNP and MCNP5 required these changes.

In order to avoid multiple implementations, most of source code was needed implementing the necessary changes. The integration of these changes was coordinated within the scope of this work. The implementations and testing of the updated ACRI routines, done in cooperation with Larry Cox of the MCNP-development team and Cindy Hughes of the MCNP-Development team, is documented in two internal memoranda [11,12]. The details of the modifications are left to these documents.

Once the secondary particles are born sampled, several updates must be made. The arrays `part`, `psid` and `pswt` are updated to reflect the particle system. Particles below their respective energy cutoff are killed. The neutron distance and weight are calculated continuously to detect sphere and point detectors. The particle weight is checked against the rules for the weight windows, if in a region with energy dependent weight windows, and adjusted as described above. Finally, assuming no other have been encountered, the particle is looked for further transport by the scoring history.

### Tallys, Scoring and Other Capabilities

The major MCNP capabilities are all fully functional with the version of secondary particles from photoabsorption interactions as implemented in the present work. Contributions to detector systems and point detectors are calculated as appropriate. Created particles are transported using the standard routines. The weight window scheme is used to control particle weights. The modified MCNP will work without change. Only a few auxiliary functions are necessary to transport neutrons to be integrated.

Summary table information is the last important topic to cover. Robert Martin Carlo can be dangerous if used as a black box. It is possible to force the random walk to skip large areas of importance within a problem such that the answer produced does not

reflect physical reality. In order to avoid this, MCNP provides the user a number of summary tables to assist in the understanding of the details of the simulation. The example summary tables discussed below are located at the end of the chapter.

All MCNP simulations print a general problem summary. This is a set of tables by particle type that present statistics and basic information for material, physical and variance reduction events. Photonuclear adds three new events to the standard MCNP tables: photonuclear absorption of photons, emission of photoelectrons and creation of photo-neutrons. MCNPN will include similar entries for photoproduction of other light particles. Examples of the expanded summary tables for neutrons and photons are shown in Table 3.1.4 and Table 3.1.5, respectively.

Implementing the new entries for the problem summary tables was straightforward. The user just is used to hold the values for these tables. It has been expanded and updated as described above. The routine **summary** actually prints the table to the output file. New headings were added to this routine for the new table entries. The tables are printed via a loop over each set of entries for each particle type. This loop was appropriately updated to include printing of the new entries. The summary information, such as average time to event has also been updated.

Often more insight into the problem is needed than the general problem summary provides. There are three optional print tables that provide more detailed information. This information is provided by **ctrl** in each case. This allows the input user to understand the flow of events within the simulation and hopefully determine if so many or many is under sampled or appropriately biased.







Thus, Table 1.26 provides gross-cell activity by particle. It contains information about the population of particles and their average weight, energy and mean free path. No changes were necessary to the methodology for this print table. The values are updated using information that is consistent with the new photouclear capability.

Thus, Table 1.26 provides a detailed weight balance for each cell by particle type. It is split into three parts: external, resonance-absorption and physical events. The original version of this table printed sub-events listed horizontally across the page and cells listed vertically down the page. The complexity of the event list in 132-column width and could not be expanded to include photouclear events without exceeding the release limitations. Therefore, when the new photouclear events were added, the format was retained such that events are listed vertically down the page and cells are listed horizontally across the page. A maximum of four cells are printed across the page before the process is repeated. A sub-total for each-event type is included as, well as a total over all cells. Table 3-4 and Table 3-5 show examples of the new format for the neutron and photon weight balance tables, respectively.

The change in format for Table 1.26 required that the print sequence be revised to print the information stated as described above. During the revision, the coding was reorganized as its own routine, **tbl 26**, called as needed by routine **tbltbl**. It is implemented as a simple series of print statements. For each event, it first prints the header and then the individual-cell values out as a line across the page. The 132-column limit corresponds to a maximum of four cells across the page. New pages are generated as needed and headers are printed each time. The dimension for storage array **gwt** has been increased by one to provide storage for the calculations of the total over-all cells

1020-1211: *Revised 1992 from the original Volume 1020 (1992)*

Location	Year	Population	Area (km²)	Population Density (per km²)	Notes
London	1801	1,013,015	1,361	744	First census of the United Kingdom
	1851	2,369,793	1,361	1,741	Second census of the United Kingdom
	1901	4,535,000	1,361	3,328	Third census of the United Kingdom
	1951	8,251,000	1,361	6,062	Fourth census of the United Kingdom
	2001	7,530,000	1,361	5,532	Fifth census of the United Kingdom
	2011	8,961,000	1,361	6,584	Sixth census of the United Kingdom
	2021	9,042,000	1,361	6,636	Seventh census of the United Kingdom
	2031	9,500,000	1,361	6,980	Projected population for 2031
	2041	9,700,000	1,361	7,127	Projected population for 2041
	2051	9,800,000	1,361	7,200	Projected population for 2051
New York City	1790	33,000	580	57	First census of New York City
	1800	41,000	580	71	Second census of New York City
	1810	54,000	580	93	Third census of New York City
	1820	69,000	580	119	Fourth census of New York City
	1830	94,000	580	162	Fifth census of New York City
	1840	123,000	580	212	Sixth census of New York City
	1850	167,000	580	288	Seventh census of New York City
	1860	221,000	580	381	Eighth census of New York City
	1870	286,000	580	493	Ninth census of New York City
	1880	369,000	580	636	Tenth census of New York City
Tokyo	1868	1,000,000	1,500	667	First census of Tokyo
	1878	1,500,000	1,500	1,000	Second census of Tokyo
	1888	2,000,000	1,500	1,333	Third census of Tokyo
	1898	2,500,000	1,500	1,667	Fourth census of Tokyo
	1908	3,000,000	1,500	2,000	Fifth census of Tokyo
	1918	3,500,000	1,500	2,333	Sixth census of Tokyo
	1928	4,000,000	1,500	2,667	Seventh census of Tokyo
	1938	4,500,000	1,500	3,000	Eighth census of Tokyo
	1948	5,000,000	1,500	3,333	Ninth census of Tokyo
	1958	5,500,000	1,500	3,667	Tenth census of Tokyo
Sydney	1788	10,000	1,500	6.7	First census of Sydney
	1808	20,000	1,500	13.3	Second census of Sydney
	1828	30,000	1,500	20.0	Third census of Sydney
	1848	40,000	1,500	26.7	Fourth census of Sydney
	1868	50,000	1,500	33.3	Fifth census of Sydney
	1888	60,000	1,500	40.0	Sixth census of Sydney
	1908	70,000	1,500	46.7	Seventh census of Sydney
	1928	80,000	1,500	53.3	Eighth census of Sydney
	1948	90,000	1,500	60.0	Ninth census of Sydney
	1968	1,000,000	1,500	666.7	Tenth census of Sydney



The total area cell width is recalculated in the table is printed and is printed just after the last cell. This procedure is done for each particle type being transported. It has been verified that the values of the array *path* have not been corrupted and that the new point sequence appropriately places the neutron.

Print Table 1-40 provides details of particle interactions by nuclei for each cell. Two tables previously provided information by nuclei cell-cell for neutron and photoatomic interactions. A new table provides similar information for photoatomic interactions. Table 3-10, Table 3-11 and Table 3-12 show examples of the format for each type of interaction.

For neutron reactions, the production of photons due to neutron interactions was previously listed in the photoatomic summary table. The photon statistics include the total number of tracks produced as well as the average weight and energy of the photons produced. The new location of these values in the neutron nuclei summary is highlighted in Table 3-10. The removal of the information from the photoatomic summary is shown in Table 3-11.

The information provided in Print Table 1-40 for collisions sampled using photoatomic tables is similar to that provided for neutron tables. The nucleus and its mass fraction for the cell in question are listed first. The total number of collisions and the average weight per collision are listed next. The number of tracks and the average weight and energy of the secondary particles produced are given for both photoatomic and photoatomic. Tracks by nuclei are also included.

The changes necessary to implement the revised Print Table 1-40 were extensive. The array *path* was expanded in dimension from two to three to allow for a new table type.







Table 5-11 Example page from the phonemic activity by grade when first (Table 1-4)

Upper elementary activity of first (Table 1-4) by grade when first (Table 1-4)									
Grade	Activity	Grade	Activity	Grade	Activity	Grade	Activity	Grade	Activity
1	1st grade	2	2nd grade	3	3rd grade	4	4th grade	5	5th grade
6	6th grade	7	7th grade	8	8th grade	9	9th grade	10	10th grade
11	11th grade	12	12th grade	13	13th grade	14	14th grade	15	15th grade
16	16th grade	17	17th grade	18	18th grade	19	19th grade	20	20th grade
21	21st grade	22	22nd grade	23	23rd grade	24	24th grade	25	25th grade
26	26th grade	27	27th grade	28	28th grade	29	29th grade	30	30th grade
31	31st grade	32	32nd grade	33	33rd grade	34	34th grade	35	35th grade
36	36th grade	37	37th grade	38	38th grade	39	39th grade	40	40th grade
41	41st grade	42	42nd grade	43	43rd grade	44	44th grade	45	45th grade
46	46th grade	47	47th grade	48	48th grade	49	49th grade	50	50th grade
51	51st grade	52	52nd grade	53	53rd grade	54	54th grade	55	55th grade
56	56th grade	57	57th grade	58	58th grade	59	59th grade	60	60th grade
61	61st grade	62	62nd grade	63	63rd grade	64	64th grade	65	65th grade
66	66th grade	67	67th grade	68	68th grade	69	69th grade	70	70th grade
71	71st grade	72	72nd grade	73	73rd grade	74	74th grade	75	75th grade
76	76th grade	77	77th grade	78	78th grade	79	79th grade	80	80th grade
81	81st grade	82	82nd grade	83	83rd grade	84	84th grade	85	85th grade
86	86th grade	87	87th grade	88	88th grade	89	89th grade	90	90th grade
91	91st grade	92	92nd grade	93	93rd grade	94	94th grade	95	95th grade
96	96th grade	97	97th grade	98	98th grade	99	99th grade	100	100th grade

and from not in right location for additional information. The expansion for additional information allowed the photon production from neutron collisions that is far removed back into the system table listing. The new listing for photonuclear collisions is updated in the system **table** to account for the number of collisions and their weight as well as the constant weight and average energy of photons and neutrons produced.

Similar to the system **table**, a new system was written for Print Table 140. The system **table** now calls routine **tbl140** to print the matrix security information. Again, a sample, brain-force solution was implemented to print the necessary information. It follows the same format as in the original Print Table 140 though it has been condensed in width to allow for the additional information as described above. The values for the values for these output tables have been checked to verify they have not been corrupted by the restoration. The new values have been checked by hand.

### Future Work

The next step in this effort is to implement the prototype code into the MCNPX code for release to a broader community. It is believed that this is the best solution to begin using the new photonuclear physics capability. Over the last three years, these users have helped guide the evolution of the MCNPX code by testing new capabilities and suggesting future directions. As the best features necessary to implement the photonuclear physics capability are finalized, the acceptance of this community should ensure that the final product is long-lived and user-friendly.

There are a few areas of known concern in the current coding. The LA010 photonuclear data make use of only one reaction cross section with secondary particle production based on appropriate yields and emission spectra given by La010b.

systematic. The errors and warnings in the prototype have been verified to ensure they would catch problems with the LA150 data but further checks are needed to verify they will catch all generic data errors. Similarly, the coupling systems have been verified to currently read the LA150 data, but further checks are needed to verify that other processed data will work correctly. Last, MCNP and MCNPX are riddled with hidden dependencies. It is expected that further error testing will produce several more glitches.

The current coupling of photomultiplier data using Energy Loss 44 is based on the original formulas by Kolbich [56,57]. Chubach has proposed [11] that the reduced measurement of the photon particle incident on the heavy target is more reliably coupled to account for multi-step compound decay. A new Energy Loss including this modification needs to be proposed to the Cross Section Evaluation Working Group (CSEWG), the group which controls the ENDF format.

MCNP(3) provides many auxiliary functions as add-ons to its mainframe capabilities. Some of these features, such as event log printing, have updated to include photomultiplier information. However, several others, including but are not limited to the tally multiplex card, cross section plotting and post file writing, have not been updated. For that work, time is scarce was not necessary. As time permits, they will be added into future implementations.

## CHAPTER 4 VERIFICATION AND VALIDATION

### **Introduction to Verification and Validation**

In today's scientific world, the computer has become an essential tool. However, the use of the computer is still an evolving subject. An entire field of study has devoted itself to software quality assurance. The cornerstones of software quality assurance are verification and validation. As this work is in large part a software codes project, it is desirable to address the questions of verification and validation here.

Verification in the context of software quality assurance is the process of ensuring the desirability of the software. It can also be thought of as looking for subtle holes in the garbage or eggs, garbage not problem. The issue is how to ensure that the functionality of the coding performs in the manner expected and does so for all valid cases. A brief summary of the verification of the present work is presented in the next section. The larger problem of ensuring that the results are not garbage is the domain of validation, and the primary focus of this chapter.

The quest of validation in the context of software quality assurance is to prove that the coding and data in question perform with reliable results in the region of interest. For the purposes of this work, the region of interest is the production of neutrinos from bremsstrahlung photons in the energy range up through several tens of MeV. As the ability to use tubular photomultiplier tubes within MCP has not been generally available

lation, the relation's results discussed here provide the basis for estimating the general uncertainty for the data new-capacity as a whole.

For the purpose of this work, the ideal relations benchmark should include the production of photons via bremsstrahlung radiation and the subsequent production of neutrinos from these photons. Additionally, such a benchmark should contain as few systematic complications as possible and must document enough of the setup and analysis to indicate that a fair comparison to any simulation is being obtained. The literature has been searched for such benchmarks with numerous results.

There is a dearth of experimental data available in the area of photon-lepton physics. Of the published results, few are suitable for use as benchmarks. Many early experiments measured the photoneutrino cross section of materials with bremsstrahlung photons. The raw data of neutrinos observed for a specific experimental configuration would be an ideal benchmark. However, the raw data is typically "unbinned" and represented as a set of mean values. The experimental data then presented is unusable as a benchmark as the unbining method is not documented and typically a poor quality cross section measurement is compared to those obtained with mono-energetic photons.

There are numerous other measurements in the literature that would be useful but come from complicated systems that are not well documented. Measurements that are based on poorly documented systems cannot be used as benchmarks because too many assumptions must be made in the simulation model. For a measurement to be useful as a benchmark, it must contain a description of the experimental setup that thoroughly documents every significant parameter.

Two studies have been chosen from the available literature for the purposes of validation of the work presented in this dissertation. Swenson [34, 32] tested differential photon fluxes calculated from analytical shower theory with measured cross sections to obtain neutron yields from electrons incident on some realistic slab geometry. Barber and George [34] reported absolute measurements of neutrons produced per electron incident on several materials.

The results presented by Swenson are not from experimental measurements. However, they are useful for a number of reasons. The Barber and George experiment was the only work found in literature containing the details necessary to be classified as experimental benchmark data. As a second study was desired for comparison, the work of Swenson was chosen. That this study was chosen was not an arbitrary decision. The original motivation for this work was the assessment of the neutron field in a medical accelerator room. The defining work in this area is ICRP Report 19 [2]. Swenson participated as a consultant to the task force which wrote this report. The methodology used to calculate theoretical neutron yields is recommended in the report to calculate the neutron source production values as well known.

Swenson utilizes analytical shower theory and experimental cross section measurements to obtain an expected neutron yield released by electrons incident on a material. The accuracy of the neutron yield calculated is highly sensitive to the accuracy of the cross-section measurements used. However, in the absence of the experimental data measurement, this is a useful way to calculate neutron yields.

The Barber and George results are experimental and they are considered as benchmark/benchmark data. As such benchmark data are not, great pains have been taken here

to explain how the data was taken or the hopes that experimentalists who read this might be compelled to perform similar measurements. It is hoped that the availability of this new ability to simulate phenomenon interactions in vehicle transport will encourage such beneficial experiments.

Comparison of current calculations to each of the sets of data described are presented in sections of this chapter. In each section, the original study is described in enough detail to understand what must be taken into consideration in the simulation. The setup of the simulation including any assumptions is depicted and the results of the current calculation versus the original results are discussed. For completeness, the actual MCNP input decks are included in Appendix D. Comparisons are included for each material which has a corresponding tabular phenomenon data set. The final section of the chapter will summarize the conclusions that have been drawn from these comparisons and assess the overall uncertainty attributable to the evaluated data and its use by the current coding.

## Verification

Anyone who has ever written even the simplest piece of software has had to learn something about verification. Rarely does a piece of software compile without it, it is supposed to be the first attempt. Typically, it is necessary to debug the code to remove errors or bugs/limitations. Even if it does compile and appear to run, it is vital to run test cases to ensure that reasonable input conditions give reasonable results. Additionally, there are numerous tasks that can be performed during the development cycle of the software to ensure that it functions as expected.

There were four major changes implemented within the existing MCNP code in order to maintain the functionality desired by the work. The verification of each major change is discussed separately. This documentation is meant to provide an overview of the verification that was done without actually showing all the details.

The input routines were revised in order to allow specification of a photoneutron table for use by a material. As discussed in the implementation chapter, this required numerous revisions to the original codes. The final implementation was supported by several code walkthroughs. (A code walkthrough is a detailed inspection of the code modifications by two or more persons to ensure that revisions in question correctly implement the desired functionality.) In addition, the scripts used to store the tabular data were checked during debugging runs to ensure that the appropriate data was stored correctly.

In addition to these algorithmic implementations within MCNP for loading photoneutron tables, they were duplicated within MCNFX for loading proton tables [35]. They were also subjected to a code walkthrough at that time. They have been subject to more than their implementation work as bugs reported.

The tabular data sampling routines were revised to correctly sample neutron parameters for any combination of incident and created particle. These changes have duplicated in MCNFX in order to correctly handle proton tables and in MCNP for miscellaneous other species [31,34,36]. These have been subjected to several code walkthroughs at various stages in the work. During their implementation into the distribution version of MCNP, they were subjected to extensive verification and quality



accuracy testing [30]. They have been in active use by the prototype, hCNPX, and hCNP with no bugs reported.

The output tables were updated to include details about the phenomenon associated in a simulation. These changes have been subjected to a walkthrough. They have also undergone testing via debugging runs to ensure that the numbers reported accurately reflect the experiment of the simulation. They have been in use throughout this work with no known problems.

The last major section of each chapter is the addition of the phenomenon without context. This set of algorithms represents the keynotes of this work. Similar to the other sections, it has been subjected to code walkthroughs and debugging runs. In addition, it has undergone a number of testing runs to ensure that it functions appropriately. These tests generally check a specific feature. For example, a simulation can be constrained to look for the current simulation of plasma through a material in order to ensure that the appropriate cross section is being used. Another example is the use of a thin target simulated by tally regions to check appropriate sampling of secondary electron energy and angle. Numerous other tests were run to check various aspects of the functionality [34].

In addition to the testing described above, hCNP has a set of regression tests ensuring it runs functionality. These tests were used throughout the development process to ensure that the new or revised capabilities did not damage existing functionality. Additional regression tests were added to check new functionality.

It is worth noting here that verification of large codes is a complicated process. Inherent interdependencies can be overlooked and left unaddressed. Despite the variety of

verification performed during the development process, a log was filed in the photo-nuclear-reaction toolbox very late in the process. I only collected this information sometime discussed in the following chapter but it serves as a reminder that verification is a long-term effort over the life of a software project.

## Comparison to Theoretical Yields

### Calculating Theoretical Yields

During the late 1970's and early 1980's, there was general interest in developing a methodology for estimating the neutron yields at various materials and medical electron accelerators for subsequent use in radiation protection calculations. William Swenson, then at the Stanford Linear Accelerator Facility, documented a methodology and reported neutron yields per electron incident on various materials at selected energies up to the  $Q_{\beta\gamma}$  range [11,12]. His work has been used by others to provide guidance on neutron source term calculations for electron accelerators.

Swenson utilized experimental photo-neutron cross-section measurements with calculated photon fluxes to calculate "theoretical" neutron yields. In the results shown here, analytical shower theory is used to predict the differential photon flux for an electron with specified energy incident on a semi-infinite (i.e. half-space geometry) material. Experimental photo-neutron production cross-sections were obtained either as a measured continuous function or as a Lorentz parameterization. These were then integrated together by folding the predicted flux with the macroscopic cross-section to calculate the neutron yield.

It is worth depicting the a scenario to illustrate a lesson. The use of analytical shower theory to calculate the differential photon flux can be replaced by the use of

Monte Carlo electron-photon simulation. In fact, Swanson checked some of his analytical flux predictions against the Monte Carlo generated differential photon fluxes of Alvarado and Meese [28] for a 10 micron length track (practically equivalent to semi-infinite) lead target. The use of Monte Carlo to estimate the photon flux for a specific geometry and material provides a better estimate of neutron yield from a real component as spatial dependence can be obtained. However, Swanson was focused on obtaining a general method.

Swanson reported yields for neutron emissions in their natural elemental state. There is a corresponding evaluated photo-neutron data set available for aluminum, iron, copper, cadmium, tungsten and lead. Each of these elements is listed in Table 4-1 with their evaluation length, density and the source of the photo-neutron production cross-section data used in calculating the “theoretical” yield as reported by Swanson. (This is definition of the evaluation length along with the original source for Swanson’s values, see the work by Yang *et al.* [31].)

It is important to remember that the cross-section calculations as a function of the energy in the production of the photon flux and the errors in the cross-section data. Either can have large influence on the results. In Swanson’s conclusions within the second study, he states that the values obtained in the present work by as much as 30 percent below the original calculations in the energy range typical for neutron therapy. He then goes on to say that the uncertainties in his present calculations are less than 10 percent [11, p. 317]. This is enough to show that the change in the approximations used to obtain the photon flux improved the results but it also shows the sensitivity of these calculations to the underlying data and assumptions. However, as his comments point out, given the

Table 4.1: Materials and geometries used by Sereno to calculate theoretical neutron yields

Material	Radius Length (mm)	Density (g/cm <sup>3</sup> )	Source of (deuterium-neutron cross data)
Aluminium	24.01	2.700	Vogelaar et al. [82]
Iron	11.94	7.875	Minomura et al. [83] Data considered to agree with the Fe/Cu yield only decreased by Frant et al. [84]
Copper	11.94	8.96	Frant et al. [84]
Tungsten	6.87	19.3	Frant et al. [84]
Tungsten	6.38	19.3	Vogelaar et al. [81]
Lead	6.37	11.35	Pb 206.7 from Harvey et al. [85] Data scaled by 1.18 [82, p.343] Pb-208 from Vogelaar et al. [86]

current geometry and an accurate picture that the underlying uncertainty in the cross sections still leaves a large uncertainty in the yields.

### Simulation Setup

Part of the reason these calculations were used as a benchmark was the simplicity of the geometry involved. The neutron yields are representative and reflect that Sereno values account more so the fact that the cross section calculation is practically achieved at a target thickness of 10 to 20 radiation lengths. With this in mind, the simulations presented here use a mono-energetic, point electron beam incident on a mono-layer thin 20 radiation lengths thick with the beam centered such that it is 20 radiation lengths to each edge. The mono-energetic, point representation of the beam is equivalent to the assumptions in the original work.

The yields as reported are for neutron production only. Neutron transport and absorption within the material is not considered. In order to match these results, the value calculated by the simulation is taken from the MCNP neutron creation tally

table, i.e. the absolute neutron production per incident electron including absorption within the target material. A tally of the neutron-capturing the sample is used to determine when neutron production has converged and also to estimate the uncertainty in the neutron yield.

The yields are reported for naturally-occurring elemental materials. The natural abundance of each material is given in Table 4-1 along with the tabular data used for photoactivation and neutron interactions within the sample. For many materials, only selected isotopes have photoactivation evaluated data files available. If this is the case, the remaining available was (were) used by splitting the missing weight equally among those on hand. The implications of this practice are discussed below.

Neutron tables were chosen to match the available photoactivation tables. All isotopes except boron had a corresponding LA150 [40] neutron evaluation covering the energy range of interest up to 158 MeV. The neutron evaluation used is from the standard ENDF60 library [36] with its upper-energy limit of 30 MeV. As the yields are

Table 4-1. Natural isotope abundance for elemental target materials and their isotopic representation due to lack of available tabular data.

Material	Natural Isotope Abundance's (atom %)	Photoactivation EA,De (Atom Abundance %)
Aluminum	<sup>27</sup> Al (100%)	17017.8% (100%)
Iron	<sup>54</sup> Fe (1.1%) <sup>56</sup> Fe (92%) <sup>57</sup> Fe (2.2%) and <sup>58</sup> Fe (3.7%)	26548.8% (100%)
Copper	<sup>63</sup> Cu (69.17%) and <sup>65</sup> Cu (30.83%)	26453.8% (100%)
Nickel	<sup>58</sup> Ni (68.07%) and <sup>59</sup> Ni (0.0007%)	71181.8% (100%)
Tungsten	<sup>182</sup> W (26.3%) <sup>183</sup> W (14.5%) <sup>184</sup> W (31.4%) <sup>186</sup> W (28.8%) and <sup>187</sup> W (6.0%)	74136.8% (100%)
Lead	<sup>204</sup> Pb (1.4%) <sup>206</sup> Pb (24.1%) <sup>207</sup> Pb (22.1%) and <sup>208</sup> Pb (52.4%)	11208.8% (24.347%) 11207.8% (22.567%) and 11208.8% (52.886%)

quasi-regularly spaced nuclear transport and absorption within the target, this does not affect the comparison. Electron tables are from the MCNP standard/EJL library and photonuclear tables from MCPL90C1.

Neutron yields are tabulated for ten incident electron energies in the current study [14]: 10, 15, 16, 25, 34, 50, 100, 150, 300 and 1000 MeV. Because MCNP45 has an upper energy limit for the current electron tables of 150 MeV, only the first seven energies are used in this comparison. Future plans for the MCNP family of codes include the integration of electron tables covering the energy range up to 100 GeV and the addition of the CEM nuclear physics module to handle photonuclear interactions above the range of tabular data. Additionally, the JAEA photonuclear data library will include many of the isotopes currently missing. As these advances are made, this set of calculations should be revisited to complete the verification/validation process.

### Comparison to Current Calculations

The comparisons between the theoretically derived data and the MCNP calculations are presented here as a set of graphical figures. The error bars on the theoretically derived values are the 20 percent uncertainty quoted by Lawrence. The discrepancies have been run until the relative error in the calculation is negligible. The overall uncertainty of the simulation method and data is the final goal of this discussion. Each figure presents the experimental data as diamonds connected by a solid line with calculated values represented as squares connected by a dashed line. The graphs are presented on a log scale to enable viewing of the entire range of data at once. It is desired that the reader achieve only a sense of relative comparison from the figures with

explanation of the details given in the text. The MCNP<sup>®</sup> inputs, checks and the reported and calculated values are available in Appendix D.

The comparison for elements presented in Figure 4-1 shows very good agreement except for the low-energy energy values. Despite being consistently the same threshold energy, there is a factor of five difference in the value of the yield at 13 MeV. This may be explained by differences in the shape of the photo-neutron cross section as it rises to the peak value.

Svensson's values are based on the photo-neutron cross section as measured at Saclay [61]. Experimental data from a number of isotopes [Li, Ti, Th] were used at the evaluation process. However, the evaluated data do not include possible small resonances in the low region as seen in the data from Saclay. The small resonances are physically realistic and these small changes in this region may have large influence on yield calculations for neutron energies near threshold.

There was a very difficult evaluation as very little experimental data exist for guidance. Of the low-intensity measuring ion isotopes, only <sup>199</sup>Pu is currently available as an evaluated dataset. Considering only <sup>199</sup>Pu is partially reasonable considering it represents more than 50 percent of the elemental composition. However, the current calculations over predict the reported values by 30 to 40 percent as shown in Figure 4-2.

The large difference seen between the reported and calculated values may be explained by differences in the photo-neutron cross sections. The reported values are based on the experimental data of Mandelstam et al. [62] as noted [33, p. 100] to agree with data reported by Fries et al. [63]. The evaluation is based on more recent experimental data [Ti-74]. This new input points out the need for evaluated data to

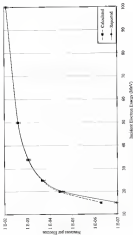


Figure 4-1 Calculated versus theoretical electron yield for electron of various incident energy on a thick electron target. (Reported values from Sorensen, 1979)



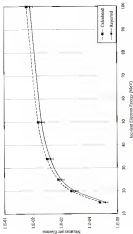


Figure 4.1: Calculated versus observed yields of the electrons of various incident energy on a thick iron target (Reported values from literature, [10])

ensure that accurate representations are provided based on multiple experimental datasets.

Copper shows very good agreement between the current calculation and the reported value of the yield. This is expected since both the reported value and the current work are based on the original measurements by Feller et al. [30]. However, Figure 4-3 shows an increasing discrepancy between the values as the incident energy increases.

One possible explanation for the discrepancy between the current calculation and the reported value is the lack of an evaluated  $^{63}\text{Cu}$  photoactivation data set. One way to reduce the influence of the missing cross-section data is to examine the cross sections for  $^{63}\text{Cu}$  versus  $^{63}\text{Cu}$  versus  $^{63}\text{Cu}$ . Table 4-3 shows the values for the integrated photoactivation-yield cross-sections. Note that as expected, the current work is in close agreement to the  $^{63}\text{Cu}$  experimental data of Feller et al. However, it underestimates the photoactivation production from natural copper. As the photon flux increases, e.g. with increasing incident energy, this underestimation will cause a larger discrepancy.

Table 4-3 Integrated photoactivation yield cross-sections for copper

Isotope	$E_{\text{max}}$ (MeV)	Current Value <sup>a</sup> (mb-MeV)	Reported Value (mb-MeV)	Source of cross-sections for reported value
$^{63}\text{Cu}$	27.5	480	482	Feller et al. [30]
$^{65}\text{Cu}$	25	519	515	Sumitani et al. [31]
$^{63}\text{Cu}$	27.5	440	112	Feller et al. [30]
$^{65}\text{Cu}$	27.5	440	110	Feller et al. [30]
$^{63}\text{Cu}$	10.0	321	430	McGowan et al. [32]

<sup>a</sup> Current values are based only on  $^{63}\text{Cu}$ , i.e. they contain no estimation of the influence of  $^{65}\text{Cu}$ .

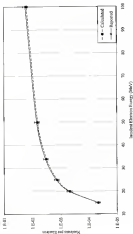


Figure 4.1: Calculated cross-section for electron-positron annihilation into a muon-antimuon pair as a function of the center-of-mass energy. (Data from [1])

There is very good agreement, as shown in Figure 4-4, between the calculated and reported yields for toluene. The slight variations are most likely small differences in  $[H_2]$  and  $[C_{10}]$  cross-section slopes. The current work is based on experimental data from Lawrence Livermore [79] scaled by 1.22 as demonstrated by Lee et al. [80]. The reported yields are based on the experimental data from Saito [84] which are believed to contain an error in the multiplicity [80] which may account for the slight variations seen.

It is worth examining the three available experimental cross-section measurements, listed in Table 4-4, in order to emphasize a key theme. The small group of individuals who perform nuclear data evaluations have available important information that is not readily apparent to the outsider. It is generally believed that many of the early cross-section measurements at Lawrence Livermore are 15 to 25 percent too low. It is this kind of knowledge that is essential in determining that the higher cross-section values reported in Table 4-4 are most probably correct and the Livermore data should be scaled upwards to match. This need for an depth knowledge of the experimental data is the reason evaluated data exists and why it is important to the context to trust the judgement of those who produce the evaluated data.

Table 4-4 Integrated photo-neutron yield cross-sections for toluene

Isotope	$T_{max}$ (MeV)	Cross-Value ( $\mu b-MeV$ )	Reported Value ( $\mu b-MeV$ )	Source of cross-sections for reported values
$^{10}B$	22.8	1620	2478	Miller et al. [75]
$^{10}B$	24.8	1478	1755	Bennett et al. [76] Scaled by 1.22 [80]
$^{10}B$	25.2	1628	1758	Bergant et al. [83]

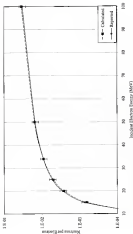


Figure 4-4. Calculated versus deposited versus positron yield for electrons of various incident energy on a thick carbon target. [Deposited values from discussion, 1979.]

The calculated yields under predict the reported yields for tungsten at all but the highest energies shown in Figure 4-5. The difference is largest near threshold.

Swenson's reported values are based on natural tungsten with a threshold of 6.2 MeV. The current evaluated data is only isotopic  $^{187}\text{W}$  and has a threshold of 7.3 MeV. Both works are derived from the original measurements of Vepioinen et al. [87]. It is hypothesized that if the remaining isotopes, comprising 93 percent, of tungsten were included the agreement would be closer.

The same system for lead have been reanalyzed since the Swenson study was concluded. Based on an analysis performed by Gorman et al. [88], the Lennémeier measurements of Harvey et al. [54] are believed to be too low by a factor of 1.22, and 1 MeV is was proposed by Puller [10, p. 140]. Gorman et al. also suggested the Siering measurement [89] of  $^{208}\text{Pb}$  was too high and should be scaled down by a factor of 0.93. Keeping these differences in mind, Figure 4-6 shows a capable agreement between the calculated and reported values for lead.

## Comparison to Measured Yields

### Experimental Setup

In an experiment by Barber and George [58], an electron beam was impinged on a variety of targets of various energies and the absolute yield of neutrons per electron was measured. The targets were composed of elemental materials of varying thickness including Al, Cu, Fe and Pb. It is a testament to the diligence in making and reporting these measurements that they later have been cited within the literature more than 25 times, including literature as recently described above. Their results are worthy of use as benchmarks and ideal for benchmarking the current methodology and data.

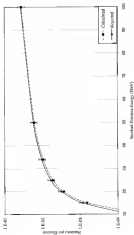


Figure 4-3 Calculated versus theoretical neutron yield for various incident energies on a thick target (top) (Reported values from Bowman, 1979)

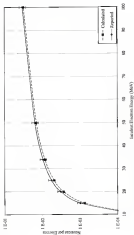


Figure 4-6 Calculated versus Reported neutron yield for electrons modulated except on a thick lead target. (Reported values from Evans, [17])



The Rutherford and George measurements were made at the Stanford Linear Accelerator Facility (SLAC). The measurements are all approximately due to the fact that two factors both in making the measurements and in determining how they were made. The Mark II linear accelerator offered a well characterized electron beam. The SLAC facility presented a carefully controlled environment in which to make the measurements. The parameters of interest in representing the experiment as reported in the original paper are discussed below. Superficially these take care, these are the issues that must be addressed when defining a benchmark.

A diagram of the experimental layout is shown in Figure 4-7. The electron beam leaving the Mark II linear accelerator is collimated to a diameter of 8.887 inches. The collimated diameter translates to a 0.1 inch beam diameter at the target location for a nominal energy of 18 MeV. No information is provided on the variation in spot size with beam energy and it is shown to be negligible by later calculations. After leaving the collimator, the beam travels through the first of two identical 30-degree deflecting magnets. These magnets translate the mean axis of the beam in order to reduce the background radiation emerging through the shielding wall.

The energy of the beam was variable over the range 18 to 24 MeV. The absolute energy was estimated to be calibrated to within 2 percent error by measurements using the photopeak thresholds of deuterium, oxygen and copper. The energy spread is controlled by the two variable-air collimators located between the two deflecting magnets. An energy spread of  $\Delta E/E_0$  equal 2 percent was used throughout the experiment as set by the air collimators.

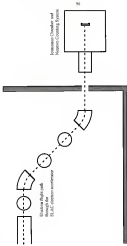


Figure 6-1. Experimental setup for the Electron and Gamma-ray Spectrometer

The final beam parameter needed for obtaining absolute neutron yields is the number of electrons per beam pulse. Bhatia had previously realized a method for determining this parameter [32]. An ionization chamber is located just before the experimental apparatus. It consisted of 6.003 inches of Mylar comprising two windows and an 8 inch thick chamber through which hydrogen flowed at one atmosphere of pressure. The response of the ionization chamber to the beam current had been well determined in the previous study. For the set of yield measurements, it was recalibrated at a few energy points by comparison with a Faraday cup monitor. No attempt was given to the accuracy of the electron beam intensity.

After traversing the ionization chamber, the electrons passed into a Lucite neutron chamber and struck the target material. The chamber was 8 inches in diameter and 18 inches long. There were two target locations although the exact position of either is not reported nor the pressure used for each specific measurement. Lucite was chosen as the vacuum-chamber wall material because its constituents have high photo-neutron thresholds and low neutron production cross-sections. A target size of 4.5 inches square was chosen to ensure that even electrons that underwent multiple scattering in the ionization chamber would still strike the target. The only experiment point not discussed in the paper in which measurements were made to decrease the background level, i.e. the pressure varied due to the electron beam and no target present. The comparison to conditions seems to indicate background levels were considered.

The absolute yield was measured by surrounding the target in a large paraffin moderator box. The 12 inch square box extended 18 inches along the beam axis. Moderated neutrons were detected by two matched BF<sub>3</sub> proportional counters extending

the length of the bar, and located symmetrically about the target channel. Background due to neutrons produced outside of the bar was reduced by shielding the bar with a thin layer of boron nitride and an outside layer of paraffin 3 inches thick. Again, it is not discussed if a measurement was made to determine the background counting level and if it was accounted for in the reported data.

The absolute counting efficiency of the neutron bar assembly was determined with a RaBe neutron source and verified with measurements on plutonium production in heavy water. For the RaBe source, an efficiency of 93.5% $\pm$ 10% percent was obtained. The RaBe, n(B) neutron presents a system in which the neutron yield could be calculated with reasonable accuracy. Using the efficiency determined from the RaBe source, comparison of the calculated versus the measured yields for the heavy-water system agreed within the limits of the relevant uncertainties.

The chlorine/boron detector as shown places a dead time temporarily overloads the counting apparatus. To counter this effect, the scaling circuit was preset off for 7.5 microseconds following the beam pulse to allow the overloaded circuitry to recover from the large pile-up. Since the lifetime of thermal neutrons in the paraffin is much longer than this period, this method is estimated to introduce minimal error (less than three percent). It was further necessary to limit the beam intensity for the high-Z materials in order to maintain the same gain factor. It is not repeated what effect changing the beam intensity might have, if any, on the other parameters.

Earley and George estimate the uncertainty of their results using the experimental apparatus described above to be 1.5 percent. Table 4-3 lists the experimental parameters of interest for the subset of experiments that could be modeled using the evaluated data.

Table 4-1 Targets and associated experimental parameters are given as used to simulate the experiments of Lindner and Gergely (1979)

Target	Density (g/cm <sup>3</sup> )	Thickness ( $\mu$ m/%)	Energies (in MeV) for which measurements are reported
Al	2.699	24.76	21.3, 26.3 and 34.3
Cu	8.96	13.25	10.1, 21.3, 26.3, 34.3 and 35.3 <sup>a</sup> (Only for Cu-6)
Cu-6		26.50	
Cu-63		28.68	
Cu-74		30.33	
Fe	7.87	4.75	10.1, 18.1, 26.3 and 34.3
Pb	11.35	5.88	10.1, 26.3 and 34.3
Pb-8		11.43	
Pb-20		17.80	
Pb-74		22.89	
Pb-91		34.43	

available in this form. In general, the portion of the target identified, e.g. Al-1, after the photo indicates the representative thickness of the target in units of electron length. As these results were presented as a series of graphical figures, it was necessary to identify and estimate the value of both the yield and energy for each point of interest.

### Simulation Setup

The simulation of the experiment was able to simplify the layout because of the design of the experiment and the way in which the yields were reported. With the information available, it was only necessary to model the electron beam incident on the target material and only the material entering the target boundaries. All other complications have been estimated by the original authors. Thus a total source yield, i.e. the number of electrons impinging the target per incident electron can be computed using the simplified schematics shown in Figure 4-8.

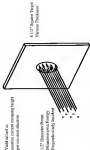


Figure 1-1: Schematic of the neutron cross-section experiments.

The electron beam model was further simplified to reduce complications in the input specifications. The relationship of the beam parameters, i.e. how the energy varied as a function of radius in the beam and its subsequent angular distribution, was not documented. The beam was therefore modeled as a minor-integrated, perpendicularly incident source directly on the target.

An estimate of how much a variation in energy could effect the results was made by adjusting the shooting energy of the beam. A non-relativistic thick target yield of a 30.1 MeV electron beam perpendicularly incident was used as a baseline for such changes. The results are presented in Figure 4-9. As the beam spread should be Gaussian about the mean, the net effect of the energy rate should cancel out. The estimate also serves as a guide to the measurement due to possible inaccurate reporting of the absolute value of the energy.

Deviations in angle are more difficult to estimate. One method is to look at changes in target thickness. This was done for the baseline case as described above and Figure 4-9 shows that possible deviations in thickness are not negligible. Deviations in incident angle of 1, 3, 5 and 7 degrees result in changes in apparent thickness of 1.7, 5.5, 11.2 and 17.7 percent, respectively. However, since these parameters are undocumented it is believed that a minor-integral beam is adequate for the level of accuracy desired and that the error induced by variations in the beam should be considered as represented in the experimental uncertainty. As a last note, measured electron beam radius of 0.25 inches were considered and shown to have negligible impact.

Similar to the simplifications used for comparison in the literature study, the materials with more than one isotope in the natural chemical form had to be represented

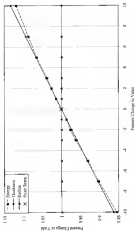


Figure 4-3 Percentage variation in absolute yield as a function of the percent change in various input parameters



with the evaluations available. Table 4-2 shows the exact details of which evaluations required for each target material. Implications of these calculations will be discussed in the subsequent section.

There are several other points worth mentioning about the simulations. The photoacoustic threshold marks the lowest-energy photon that could produce a neutron. It is therefore unnecessary to track what photons or electrons below this energy. Further, fission reactions can be tracked on a per target material such that every photon entering the target undergoes at least one collision. Photoacoustic heating can be used to derive a contribution to photoacoustic overcount from each collision. This combination-of-techniques allows the relative error of the calculated yield to be minimized using run times of approximately 18 to 36 minutes on a single processor of an OriginLab system. Note that the relative error is a measure of the precision of the calculation, not the accuracy of the evaluation. The MCNP output data as well as the reported and calculated yield values are listed in Appendix D.

### Comparison to Current Calculations

The comparisons between the experimental data and the calculations are presented here as a set of grouped figures. The error bars on the experimental values are the 13 percent uncertainty quoted by Swiler and George. The calculated yield values are taken directly from the released MCNP output data. The relative error from this calculation is negligible. The uncertainty in the simulations will be discussed in the conclusions. Each figure presents the experimental data as diamonds connected by a solid line with calculated values represented as squares connected by a dashed line.

The comparison of the experimental versus calculated yield for aluminum is shown in Figure 4-10. The agreement shown is reasonably good although it is uniformly low by about 20 percent. As the first data point is at 22 MeV, these data support our earlier conclusion about possible changes needed in the threshold to peak region of the cross section suggested by the comparison to Berenson's yield values.

The comparison of the experimental versus calculated yield for the four thicknesses of copper are shown in Figures 4-11 through 4-14. All four comparisons show similar results. They show good overall agreement with the experimental results, within 15 to 25 percent. As discussed above, the elemental copper has been represented by envelope  $^{64}\text{Cu}$ . The addition of a  $^{64}\text{Cu}$  evaluated data set will improve the agreement, probably by five percent overall, and also improve the match of the shape.

The comparison of the experimental versus calculated yield for selenium shows excellent overall agreement. As seen in Figure 4-15, the results for the region away from threshold are almost identical. However, the calculated value at 10 MeV is an order of magnitude too low. As the threshold energy is believed correct, this raises the possibility that the values of the cross section between threshold and the GDR peak needs to be increased.

The comparison of the experimental versus calculated yield for all five thicknesses of lead are shown in Figures 4-16 through 4-20. The results are consistent for all five thicknesses. The calculations are generally 20 percent lower than the experimental yields. This is acceptable agreement.

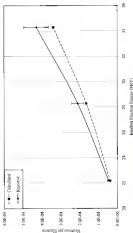


Figure 4-16 Calculated versus experimental neutron yield for electrons of various incident energy on a 1-gram foil of aluminum target. [Reported values from Barker and Gausser, 1994]

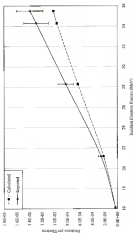


Figure 4-11. Calculated versus experimental survival yield for electrons of various modified energy as a function of incident electron energy (keV). [Reported values from: Butler and George (1981)]

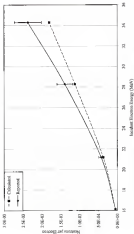


Figure 4-12. Calculated versus experimental neutron yield for the fusion of various tritium energy on a Be-9 reduction length thick copper target. (Reported values from Nishim and George, 1958.)

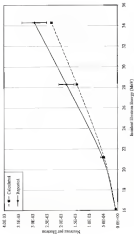


Figure 4-13 Calculated versus reported neutron yield for fission of various incident energy on a three reflection (bright dark copper target) (Reported values from Barber and George, 1988)

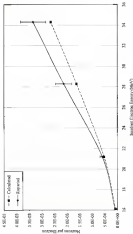


Figure 4-14 Calculated versus reported values plots for electron impact ionization cross-sections as a function of incident electron energy. (Reported values from Barab and Gungor, 1999.)

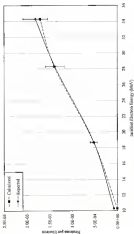


Figure 4-15. Calculated versus experimental electron yield for electrons of various incident energy on a copper substrate as a function of incident electron energy. (Reported values from Tucker and Koenigs, 1999.)



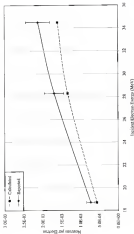


Figure 4-15 Calculated versus experimental neutron yield for electron incident energy in a sea solution target thick irradiations. (Reported values from Barber and Gump, 1996)

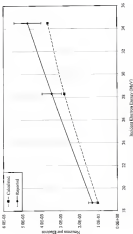


Figure 4.17. Calculated versus experimental yields for absorption of various incident energies on a thin collimated target (solid line target) (Reported values from Barber and George, 1958)

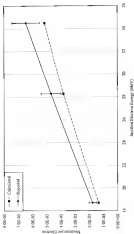


Figure 4.10 Calculated versus experimental neutron yield for electrons of various incident energy on a flow radiation length thick lead target. (Reported values from Barber and George, 1998.)

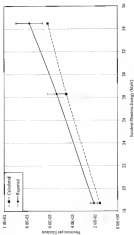


Figure 4-10 Calculated versus experimental neutron yields for electrons of various incident energy on a floor solution length thick lead target. (Reported values from Barber and Goss (9), (10)).

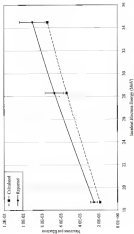


Figure 4-20 Calculated versus experimental neutron yields for electrons of various incident energies on a non-modified length short head target. (Reported values from Barber and Gump, 2000)

### Conclusions for a Verification and Validation

It has been shown that the current evaluated data and the new photoelectron interaction-coding provide reasonable results for simulating neutron production from materials for which no evaluated data are available. Most important is the current work, these comparisons have showed the present script, filter and shielding materials used in standard electron accelerators. The overall uncertainty in the evaluated data is estimated to be less than 10 percent.

As a last note in reference to Bremond's theoretical public, these comparisons are considered something more than simple verification but not quite true validation. Good agreement is seen between most of the data sets but these are typically based on the most underlying experimental data. It is worth noting that analytical shows theory and Monte Carlo electron-photon transport appear to provide similar results. This suggests that the neutron production is not highly sensitive to the photon production mechanism.

The evaluated photoelectron data library, like all other nuclear data libraries, will evolve as practical experience using the data leads back into the evaluations. This will be a long process. The first part of this process should involve will be the further validation of the evaluated photoelectron data as it becomes available. Hopefully, the ability to measure the cross sections will encourage experiments worthy of becoming benchmarks.

To repeat that these validation data for the purposes of photoelectron physics is nearly lacking. Only aluminum, copper, molybdenum and lead have been directly validated against true integral experimental data. The remainder of the evaluated data are "validated" only in the sense that they were created through the same process and have

derived from the best known cross-section measurements. This also identifies the point that further measurements of photoabsorption cross sections will be necessary for isotopes previously not measured or with multiple measurements that disagree.

It should also be noted that only the photoabsorption yields are directly validated by the calculations shown. Emission characteristics, the energy and angle of the secondary particles, are only validated in the extent that CHASE [41] has a long-standing, well-validated ability to produce such data. Experiments measuring energy and angle spectra are needed.

Last, it is recommended that once this library is made generally available, each user continuously perform its own experiments to validate the data and code for their class of problems. This set of validation activities shown above has not as extensively relied on the use of the data and coding for the calculation of neutron yields for simple geometries and materials which have photoabsorption evaluated data available. Simulations involving production and transport through complex physical geometries and containing materials for which evaluated data may not be available will be considerably more difficult. It is recommended on the user performing such work to understand the uncertainties of their specific calculations.

## CHAPTER 5 APPLICATION: SIMULATION OF A MEDICAL ELECTRON ACCELERATOR

### Introduction

It is now time to remember that the original motivation for this work was the enhanced understanding of the radiation environment in the vicinity of a medical electron accelerator (MEA). To this end, this chapter will discuss the previously established ability to simulate electron-photon transport within a MEA and the extension of this ability by the current work to include photo-nuclear physics and simulate electron-photon-neutron transport. Two major sections are presented.

The first section demonstrates the ability to simulate electron-photon and electron-photon-neutron environments by comparison to experimental data. The data were obtained from measurements around the Phillips SL Source MEA located in Treatment Room 5 of the Maudsley Cancer Center (MCC) at the University of Florida (UF). The validation is further divided to cover the electron-photon model and the electron-photon-neutron model. Once the simulation model has been validated, it can then be used to investigate the remaining aspects of the radiation environment.

The second section of this chapter explores two questions of interest for MEAs in general. The first question of major importance is the determination of the dose, particularly the neutron dose, in the patient and workers in the vicinity of the machine. The second question is the effect of increasing electron energy on the relative neutron to



placed down. Within both of these discussions, some fundamental lessons learned are highlighted and several issues suitable for future work are proposed.

## Validating the Simulation

### Background

A computer model may generally be defined as the virtual world necessary to adequately simulate the corresponding real world. The virtual world is never an exact reproduction of reality but instead attempts to capture the essential details. The major design processes for radiation transport simulations are representing the physical environment, providing transport data for the simulated materials, describing the initial radiation source, engineering the transport algorithm to propagate the radiation source and obtaining the resultant output information. It is worth agreeing for a moment to discuss in general terms what is important in each of these tasks and why.

**Physical geometry.** A standard MLLA treatment room is an extremely complex physical space. First and foremost of concern to the simulation is the electron accelerator itself. This is typically a linear accelerator or a cyclotron consisting of a few thousand pounds of monolithically engineered parts designed to deliver an intense radiation field to a precise location. The bulk of this equipment is usually located within the treatment room or a machine room such that only the treatment head is visible in the main room. To further complicate matters, MLLAs are often designed with treatment heads capable of delivering either electrons or photons, both at multiple energy levels and controlling extremely complex parts. Finally, the re-configured configuration can include changes from the original specifications for particular needs including increased shielding

**Suspending the MHA in the treatment room itself** It serves two essential purposes. First, it is there to contain the radiation for the protection of those in the vicinity. Second, it provides an effectively-useful, working environment in which to treat cancer patients. For the purpose of shielding the radiation, these rooms are typically constructed to contain leaks though in some cases other shielding material may be used. For the purpose of creating a working space, they are typically finished with wall board, drop ceilings, carpeting, radiology, intercoms and associated workbenches that typify of a clinical environment.

For the goal of simulating the electron-positron dose to a patient, it is fully necessary to include detailed modeling of the MHA treatment head. Specifically this would include the electron target or scattering foil and all materials in the immediate vicinity of the subsequent beam path. In the typical electron-positron simulation, e.g. [12, 26], only the target, collimators, flares and associated drive are modeled.

Keeping slightly ahead, a typical dose calculation that uses a complete room model as addition to the treatment head model gives the following characteristic results. The electron-positron dose to the patient from a typical treatment using a Philips EL Super MHA is the high energy photon nuclei contents of the following sources: approximately 55 percent directly from photons produced in the electron target; approximately 15 percent from photons produced or scattered in the flares and other materials in the beam path; approximately four percent from photons produced or scattered in the collimators; and less than one percent from room return and other sources. Hence, there is justification for ignoring anything very far outside of the electron-positron beam path for most electron-positron dose calculations.

### **Simplifying electron-photon system transport makes life much more difficult**

Neutrons are welcome to the world of health physics for their ability to penetrate materials either directly or by finding streaming paths. In practical terms, this means that the exact geometry of the MHA and the room are necessary for accurately representing the radiation environment. With that ability to scatter, any path between the neutron production area and the patient or worker is a concern. However, even if complete shielding savings could be achieved, this penetrating ability means that some level of neutron activation will always be present.

Again, it is important to consider some characteristic results from later simulations here in order to set an appropriate frame of mind. The neutron dose from two standard photon field sizes (but not 30x30 sq. cm) respectively, consists of the following sources: approximately 34-38 percent from neutrons within, approximately 14-44 percent from neutrons produced or scattered in the primary collimator, approximately 11-12 percent from neutrons produced or scattered in the secondary collimators, and the remainder from neutrons produced or scattered at other locations in the treatment head. Again, for an accurate simulation it is necessary to account for the placement of practically all the material around the treatment head and most of the material in the room itself.

**Transport data.** Once the extent of the physical space is known, it is necessary to provide transport data for each material found in the geometry. Transport data are defined here as tabulated images of continuous probabilities, i.e. reaction cross sections, and the reaction spectra for the reaction particles available for use in Monte Carlo transport algorithms. For traditional MCNP simulations, these data are available by

element for incident electron and photon and by isotope for neutron reactions. Note that the photon data so far has only included photoatomic interactions. The current work has integrated photoatomic data, by isotope, into this set.

Electron and photoatomic transport data exist in a complete library for the elements from hydrogen to plutonium (Z equal 1 to 94) in the standard MCNP distribution. Photoatomic data are provided over the incident energy range from 1 keV to 100 GeV [62] and electron data cover the incident energy range from 1 keV to 100 MeV. This means that electron-photon problems can be simulated for any typical condition found in a MHA treatment room. The inclusion of photoatomic data from photon interactions was found to make no significant difference in the electron-photon portion of the dose calculated for a typical treatment plan.

Neutron and photoatomic transport data exist for a limited selection of isotopes and over a varying range of incident energies. In the case of neutron data, the coverage of isotopes is nearly complete in the incident energy range up to 20 MeV. There are some significant isotopes missing, e.g. very poisonous isotopes. There are also some materials which are represented as a single "elemental" data rather than by individual isotopes, e.g. magnesium. However, most of the major isotopes have neutron data available. Unfortunately, at this time photoatomic data exist for a very limited set of isotopes.

In a practical sense, this means that neutron and photoatomic simulations must make approximations in their representation of materials. Often this is avoid. For example, replacing the 0.03 atom percent of tungsten-186 among the other four isotopes that exist to represent elemental tungsten introduces negligible error into most

simulations. However, issues arise not only when the scoring calculation is more significant, e.g. the lack of a permanent data set to enable accurate transport or a permanent detector. The problem of missing/scattered multiplay a significant role in simulations requiring photonuclear data used each time to the evaluation of the output output is completed.

**Radiation Source.** Radiation transport starts from the source, either artificially or naturally, of a subatomic source. For a bremsstrahlung source, the radiation source is electrons which have been accelerated and directed into a converter to produce bremsstrahlung photons. The final spatial-directional-energy distribution of the electron incident on the target is system dependent. In most simulations, the final dose is not sensitive to the exact distribution of electrons and a simplified description is acceptable.

A typical simulation uses a mono-energetic beam, perpendicular incident on a point on the target. This tends to be a fair approximation in the sense that it gives reasonable results. It can be improved by uniformly distributing the electrons over a spot rather than a point and by spreading the incident energy over a Gaussian distribution though these are expected to be rather modest gains in accuracy. To date, the author has not seen any work which methodically documents the effects of the variations on the incident electron beam distribution.

Because detailed electron-photon transport is difficult and time consuming over long distances, the radiation source is typically transported one or more times at intermediate locations in the geometry. Specifically, the upper section of the treatment head geometry is fixed for a treatment modality. One subcalculation of this reasonably portion of the treatment head can be used to create a phase-space file [14,15]

of the radiation field passing through a plane just above the first movable object. The phase-space file may be used as the radiation source for subsequent transport simulations through the remainder of the geometry. Obviously, this step can be repeated. Since there is typically only minor feedback from changing the lower geometry, this approach can save a significant amount of time while searching relatively modest errors.

**Transport algorithms.** Once the radiation source is determined and the physical world has been represented, the next step is to transport the radiation through the geometry. For neutral particle transport, e.g., of neutrons and photons, the Monte Carlo algorithms necessary to sample continuous energy transport data are straight forward and well established. However, the algorithms used for charged-particle transport, e.g., of electrons, are a subject area still undergoing significant improvement.

Around this set of transport algorithms, it is necessary to have a framework to handle all the other details. As the radiation propagates through the geometry, it is necessary to update the transport data for its current location. The distribution of sampling must be monitored to ensure that the phase space of the problem has been adequately covered. Summary information should be collected for later presentation. Error rates should be checked and appropriate warnings issued. All of this should be as tightly coupled as possible.

It is generally accepted that separating portions of the transport trade is suboptimal even over the medium term. The only way to avoid these errors is to pass the next portion of the simulation a complete description of the necessary information. In the case described above where the geometry is repeated, the phase-space file must contain as quantitative as possible a description of the radiation source propagating into the subsequent geometry.

This same situation exists for coupling the transport algorithms. It is desirable to have one framework which includes the necessary components to handle electrons, photons and neutron transport.

**Obtaining output.** The best resolution model in the world will fail in the field to present the results in a reasonable manner. If the desired information is not conveyed to the user, or it is conveyed in a misleading manner, the resolution has not benefited its user. The ideal would be to have all the details of everything that influenced the simulation available. For example, it might be useful to know the energy distribution of the photon flux as a function of spatial position over all iterations. In practice, the information available is typically constrained by the amount of memory and time available to track those details. For the example, it might be enough to know the energy distribution of the photon flux within a cell or its parent. A clear balance is needed.

It is these five issues that must be kept squarely in mind when evaluating a radiation transport simulation. Understanding all these issues will lead to more thorough comprehension of how the simulation relates to the physical world. Only with adequate depth of knowledge can correspondence be made back into the physical world.

## Experimental Setup

The experimental data were obtained from the Phillips II Series MGA at Transverse Room 5 of the Florida Ocean Center at the University of Florida. This set of experimental data were desired. The data desired and the basis of how they were obtained are discussed in general here. More details are provided in the following section as they relate to what was modeled in the simulation.

The layout of the treatment room is shown in Figure 5-1. The MHA treatment head is positioned as indicated and mounted on an extension rail that is free to rotate about a fixed point in space. This point is known as isocenter and is located on the center-line out of the treatment head 102 cm source-to-surface distance (SSD) from the electron target. The robot contains a set of laser lights that are aligned at the is-point (parallel to treatment head) and cross-plane (parallel to the robot) directions at the correct height such that they cross at isocenter. A stereotaxic light system can also project through the treatment head to indicate the SSD of an object at the beam path.

As part of the calibration of the MHA unit, a set of depth dose curves are taken. This procedure uses a Gammaknife unit (width  $\times$  depth  $\times$  height) Lucite tank with 1 cm thick walls filled with water. The tank is placed such that it is centered directly below the treatment head and the surface of the water is 104 cm from the electron target (100 cm SSD, source to surface distance). A depth dose curve is the relative dose at each point along the central axis in the water tank starting from isocenter.

The relative dose is measured by use of an ion chamber and a positioning system. An Ion Chamber IC 10 connected to an Electrodeless WF-1000 current amplifier was used in this experiment. A WF1000 Controller is used to control the position of the ion chamber and relay the position and current to a standard PC computer. The current and position information is stored to disk along with the details of the treatment mode, e.g. energy setting and collimator opening. A set of depth dose curves for photon field sizes of 1x2 sq cm., 10x10 sq cm and 30x30 sq cm with the machine in the high-energy photon mode were obtained in this manner. The incident energy of the electrons in the high energy mode of the MHA can be estimated by considering this data.



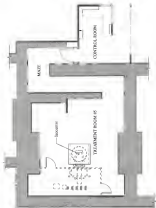


Figure 3-4) Diagram of Room 1 in the Florida Cancer Center at the University of Florida

The second set of experimental data desired is an estimate of the absolute neutron production in the treatment room. One method to obtain this information is to measure the saturation of a known sample of material in the presence of the accelerator's radiation field. An estimate of the cross-section of a material from one isotope to an unstable isotope. The decay of the unstable isotope is then measured and the number of such isotopes observed can be used to estimate the radiation field the original sample experienced. This technique is known as activation analysis. Many texts exist on the subject, e.g. Allison [37], as well as specific guidance for measurements around MLCAs [38].

For the purpose of these experiments, gold was the material chosen. It has a number of useful properties. First, in its elemental form, gold is more isotopic. Therefore only one set of cross-section data are needed. The  $^{197}\text{Au}(n,\gamma)^{198}\text{Au}$  is a cross section as a function of incident neutron energy is very large [39] (large for thermal neutrons). More importantly, it is extensively used in activation analysis and the cross section is well known, probably not more than 10 percent in error at any given energy with an aggregate accuracy of better than 1 percent. Last, the decay of  $^{198}\text{Au}$  is well documented and easily distinguished for counting by gamma-ray spectroscopy.

Activation analysis requires a calibrated detector system capable of discriminating the radiation sources of interest. The Nuclear Activation Analysis (NAA) laboratory at the University of Florida Test Reactor (UFTTR) facility maintains a set of germanium detectors and associated equipment for this purpose. As that equipment was available for use, it was necessary to setup and verify a new system. The counting system utilizes the GeneralNexus software produced by EG&G Ortec.

Eleven small disks and three large ingots of gold were available for use in these experiments. Each sample was cleaned with alcohol, weighed, sealed within a plastic sleeve and numbered. The activation of the gold is a function of the number of neutrons present and the number of neutrons available. Consequently, for the same neutron population, the larger the mass of gold, the more activation, i.e.  $^{198}\text{Au}$  isotopes, produced. The original motivation for using the ingots was that these 3.1 g (one tiny mass) were would activate quickly even in the relatively low neutron fluxes of the treatment rooms. They could therefore be used for most of measurements without the need for long irradiation times.

All of the samples had been subject to previous activation. The background counts present in all the samples were evaluated at the NAA laboratory prior to their activation. The disks had not been previously irradiated in more than one year and showed no significant background. The ingots had been activated within the treatment rooms slightly more than one month prior to the set of experiments. They showed a slight background which had to be subtracted off the first counts. The GammaVision software produces a report showing the energy boundaries of the gamma ray peaks observed as well as the net counts rate for the peak and the estimated one-sigma error.

Gold has a second reaction of interest for these experiments. The photo-neutron ( $\gamma,n$ ) threshold for  $^{197}\text{Au}$  is 9.0711 MeV. Thus, in the presence of high-energy photons  $^{197}\text{Au}$  is produced. The  $^{198}\text{Au}$  decay scheme is also well known and easily distinguished for counting by gamma-ray spectroscopy. The  $^{197}\text{Au}(\gamma,n)^{198}\text{Au}$  cross section has been measured experimentally [69-74,97-99] and is believed accurate to within 25 percent.

While not directly a measure of the neutron production, detection of the  $^{235}\text{Fm}$  production provides a secondary check of the photon production and transport.

Acquisition of the available gold sample was conducted on Tuesday afternoon, April 18, 1999. Table 3-1 provides the number, mass and position of each sample. Due to the small mass of some of the foils, sets were combined into one sample such that the mass of each foil sample was about the same. Each sample was positioned to look at a different aspect of the neutron population. The accelerator was set to the high-energy photon mode with a 1000-psi field size at 100 cm ESD throughout these experiments.

The first sample, H, was placed bare at isocenter. It was situated on top of a cardboard box such that the long axis of the target was in the cross-plane direction. This was further supported by the treatment couch. The exact positioning was checked by the lighting system. The cardboard box provided separation from the treatment couch to try and lessen any effect it may have on the neutron population. The primary objective was to observe the total neutron flux rate at isocenter including the prompt return. The secondary objective was to observe the high energy photon flux at isocenter.

The second sample, B, was placed at isocenter surrounded by a moderator. A 150 plastic was chosen as the moderating material as it was readily available and easier to set up than a water tank. The plastic slabs are carbonized wax,  $\text{NaOH}$ -free, and of varying thickness. A 14-cm tall block was constructed on top of the treatment couch such that the center of the block was centered at isocenter. The sample was aligned such that the long axis of the target was in the cross-plane direction. The position was checked by the lighting system. The dimensions of the block were checked by ruler. The primary

objective was to observe the effect of the moderator on the neutron population. The secondary objective was to observe the high-energy photon flux at moderator.

The third sample, D, was placed in the moderator. It was taped to place on the inside, i.e. against the walls, with such that it was 100 cm from the center to the walls and 130 cm above the floor. The long axis of the target was parallel to the moderator. The position was checked by ruler. The primary objective was to observe the neutron population in the moderator. The secondary objective was to observe the high-energy photon flux from other sources within the accelerator. One possible secondary source of high-energy photons is that the energy selection did not have the Phillips bending magnet system. It constitutes a possible source of background continuous photon and first neutron. The sample was aligned near the  $\pi$  plane side to check for this effect.

The remaining samples (four samples E-H) were placed in the moderator block similar to sample D. They were distributed radially outward from center along the cross-plane axis with the spacing indicated in Table 5-1. The position was checked by the light system and also spacing by ruler. The primary objective was to observe the neutron population in the moderator as a function of depth into the block. The secondary objective was to observe the in-beam versus out-beam high-energy photon flux.

The irradiation was carried out in 500-millisecond (MU) increments. (The neutron rate is measured by an ion chamber within the accelerator and 1 MU normally corresponds to 1  $\mu$ Cy absorbed dose at moderator.) The start time and the total irradiation for each sample are also listed in Table 5-1. Samples E and F were each irradiated for 3000 MU. Sample numbers 1 through 4 were irradiated with all the foils in place for a total of 6000 MU. Sample D was expected to receive the least activation and was

therefore left in place throughout the duration of the entire irradiation process for a total of 12000 MJ.

A standard IGC-60 high-purity germanium detector and associated equipment were available in the control room at the time of the irradiation. Sample 11 was checked in the 1000, 2000 and 3000 MJ irradiation levels to determine its count rate for the gamma rays of interest. It was determined that count rate was sufficient after 3000 MJ irradiation. Sample 12 was run to match sample 11. The first samples, because of their smaller size, were irradiated for twice as long.

Final counting of the irradiated samples was performed at the NAA laboratory. As discussed above, background counts were taken prior to irradiation. Final counting was performed once later the same day as the irradiation and a second time the following day to assure no false readings were observed. The 33 and 394 keV decay lines from  $^{137}\text{Cs}$  and the 402 keV decay line from  $^{134}\text{Cs}$  provided accurate measurement of the irradiation due to each of these isotopes. This activity is used to compute production rate of the isotopes over which the beam was acquired. The value is compared to measured radioactivity of the value in the comparison discussion below.

Two certified sources were also observed during the second set of counts. This set of counts was used to determine the efficiency of the detector system for the gamma-rays of interest in the counting geometry. It also assured that the energy calibration of the gamma-ray detection system was accurate. The final results are discussed in the comparison below.

Table 3.1: 2D mass, position, start time and length of simulations of the grid samples.

Sample #	Initial Position (cm)	Initial ID #	Mass (g)	Start Time EST	Simulation (sEL)
11	0	1	11.1	18.12	2000
12	0	12	11.1	19.24	2000
13	None	13	11.1	19.33	12000
1	0	1	0.0004	18.31	6000
2	0	2	0.0014		
3	0	3	0.0012		
4	0	4	0.0076		
5	11.3	set (3,4,5)	0.0760		
6	16.3	set (7,8,11)	0.0796		
7	---	7	0.0014	--	--
8	--	8	0.0016	--	--
9	--	9	0.0016	--	--
10	--	10	0.0016	--	--
11	--	11	0.0016	--	--
12	--	12	0.0016	--	--
13	--	13	0.0018	--	--

### Simulation Setup

The two sets of experimental data require modeling at very different levels of detail. As discussed in the Background section, electron-phonon dose calculations for a process or deposition plasmas do not require modeling of anything outside the mean beam path. On the other hand, the neutron problem is influenced by every object in the room and especially the exact details of the treatment head. Likewise, the way in which the input is set and the goals of the output are also very different.

Before describing these models, the goals of each should be stated. There are two key parameters in the description of the MDA allowed for use here: the mean electron energy and the number of electrons incident on the target. The simulation of the deposit dose has as its goal the calculation of the beam path geometry with its associated materials

and the determination of these two unknowns. The value of these two unknowns is part of the starting point for the second set of simulations. The second simulation attempt is to refine the neutron production and transport by matching the unknowns seen in the gold samples.

**Physical geometry.** Simulation of the depth dose curves is an electron-photon transport problem to solve the energy deposition in the water phantom. As such, it requires an accurate description of the area directly around the beam path. It turns out that this bit of physical geometry is the most difficult step to obtain.

Trying to obtain the exact schematics of a MIRA is like trying to extract a name book from a man who has lost them. Upon asking if the book is lost, he answers that it might be lost in a waiting for a dentist. Upon finally going to the dentist and learning it must come out, he makes the dentist promise he won't put it without his permission. When the dentist asks for permission, the patient looks and looks and asks about how the rest of his teeth are then suddenly with the greatest of reluctance gives up anything at all.

When the author first asked the developers of the Philips MIRA to question, he was told that they needed that they were proprietary documents. This was understandable but unfortunate. At that time, the author felt it was important to spread outside of the obligations of handling proprietary data as it was desired to be able to publish full details of the model without restriction in this dissertation. This was considered an absolute must as without these details, the work presented cannot be replicated. Therefore, a compromise was reached and a hand-drawn schematic of the beam path as well as a general diagram of the treatment head profile were made available.



During the course of this work, the author has had opportunity to speak with many researchers in this field. While many were willing to share experiences, trying to model MLLAs, all groups are more unwilling to share most details of their models because of obligations due to the proprietary nature of their source information. The author believes that this is a very unfortunate state of affairs as it means each group must start from scratch and no group can exactly replicate another's work as no two models will be exactly the same. It should also be noted that several projects with access to proprietary information made further statements to the effect that even with detailed MapInfo, the specifications were sometimes out of date and key details had changed between the MapInfo and the MLLA models.

The author owes a great debt to John Demarco and Indira Chetty of the University of California at Los Angeles Department of Radiation Oncology. They were the first group willing to share their experiences using MCNP as a simulation tool [31] as well as their well validated models of the Phillips SL series MLLA [32]. In terms of simulating electron photon radiation transport in MLLAs for calculating dose distributions, they have significantly advanced the state-of-the-art. For the purposes of this work, being able to start with their model meant no guess effort was necessary to define and validate the geometry model.

The geometry model that obtained included the electron target, the target housing, the primary collimator, a beamstop filter, two filtering filters and an ionization chamber. Demarco really it matched the hand-drawn schematic electron source with one exception. The exception was an aluminum ring just inside the second filtering filter. It was determined to be outside the area being polished therefore ignored. The

placement and size of the secondary circulation and the water tank were determined through discussions with the staff and engineers onsite at SUT.

The MCHP geometry specification was modified and maintained during early trial runs without affecting the original specifications except to speed up calculations. MCHP geometry specifications are greatly affected run-times depending on the complexity per cell description. The modeling served the secondary purpose of describing the model in a more documented, structured manner for the sake of modeling. During these same runs it was found that presence of the hot chamber made no significant contribution to the overall transport process and it was removed. A sample schematic of the final simulation geometry is shown in Figure 3-2 and the details for the MCHP input data are given in Appendix B.

The second set of simulations has to do with the accurate assessment of aerosol production and distribution within the treatment room. As discussed in the background above, this is a considerably more difficult challenge than the depth dose calculations. In fact, as the discussion on the computer will show, while the challenge has been met with more computationally techniques, the results still leave much to be desired. The following discussion will point out a number of approximations which have been made that contribute to the uncertainty in the final results.

The greatest single difficulty here is adequately defining the physical space of consequence. The starting point used here is the treatment head as defined in the depth dose calculations. To that has been added the four concrete walls of the treatment room. The dimensions and materials of the room were derived from the original architectural

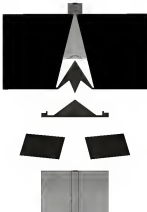


Figure 3-2 Simple schematics of the beam's geometry in the medical accelerator treatment head.

drawings and specifications [15] as obtained from the archives of the Space Facility Management. For the primary simulations, nothing else was included.

It is worth spending some time on the known unknown that approximates situations and why it was made. First and foremost, only about one third of the total material in the treatment level is represented. The remainder is significantly outside the primary beam path and therefore was not necessary for the electron-photon simulation and was not included in any of the available references.

A detailed representation of the final end target including structural steel and other materials in the treatment head is necessary for an accurate simulation of the electron-photon-neutron problem. Without truly accurate descriptions of the locations and compositions of these materials, anything done is subject to large error. The final results presented below are obtained only with what is known. With that said, there are a significant number of variations and/or unknown parameters in placement of lead and tungsten shielding that can be made to estimate the influence of the missing material.

It is recommended that future work undertake to obtain this information by direct inspection of the MIA. It might be envisaged to obtain this information through blueprints or specifications but the final model should be checked against the actual dimensions as measured. It was not feasible to obtain that information for the purpose of the current study.

There is also a significant amount of material within the room that is not represented in the simulation. Again, this is due due to the difficulty in obtaining information on the placement and composition of the objects. It was not readily apparent from the specifications of the room was located as is typical for similar facilities. If this

is the case, there are splinters or steel nails protruding while ones between the concrete and finished wall. The finished wall itself is probably gypsum board covered by pasted roller wallpaper. Ceiling and furnishings have been provided to make the room a useful workspace. Additionally, the mass bulk of the accelerator itself, the wall partitioning the machinery room and many other miscellaneous items also reside within the concrete vault.

The list of existing materials and volumes could be continued though it certainly becomes less significant. However, of probable importance are various construction materials and the accelerator itself. It is estimated [34] that one to two and a half tons of structural steel reinforcement reside in the walls, one and a half to two and a half tons of gypsum wall board, ceiling tiles or the equivalent coverings cover the walls and ceiling, and several hundred pounds of ordinary iron located against the walls. The accelerator components, associated machinery and treatment rods account for hundreds, if not thousands, of pounds of additional mass. The partition wall forming the machinery closet is also left out. This lack of the material in the simulation represents an unknown error that could play a significant role in neutron scattering and absorption.

Starting from the simplified model, four variations were used to simulate the unknowns represented above. These are: the bare room, the room with detailed regions of absorption and in the future, the room with the moderator block at maximum, and, the room with the moderator block and detailed regions of absorption and in the future. During the course of this study, several variations have also been explored though none have been included in the final simulations.

**Transport data.** These materials in the treatment head which were specified in the sample drawing, are the same as those specified in the UCLA model. The target is tungsten alloyed with 18 weight percent rhenium and has a density of 19.67 g/cc. The target housing is natural copper and has a density of 8.96 g/cc. The primary collimator is tungsten alloyed with 1.3 weight percent copper and 3.5 weight percent nickel and has a density of 18.96 g/cc. The hardening filter is natural aluminum and has a density of 2.7 g/cc. The flattening filter is lead steel with a density of 7.9 g/cc. The composition was not listed on the head drawing so the UCLA definition was taken. The steel is iron with 18 weight percent chromium, 9 weight percent nickel, 3 weight percent manganese and 1 weight percent silicon. The secondary collimators are lead. The lead may or may not be alloyed with antimony. For this model it was taken as natural lead and has a density of 11.36 g/cc.

For the transport simulation of the depth dose curves, electron and photoatomic tables were available for all of the elements specified above. Tables are also available for calculating the hydrogen and oxygen of the water tank. While available, the air was taken to be a void for these simulations. The detailed material descriptions used in the serial input decks are listed in Appendix E.

For the correction simulations, the concrete walls, etc., gold and A-158 plates have been added to the physical descriptions. Other materials may be present in the room but are not included as they are not represented in the geometry. The definitions of these materials present and not established prior have been taken from well established sources. Exact details of the material composition used are given upon found in Appendix E.

As with almost all MCTOP compilation tables are available for all elements of interest for electron and photoionization interactions. For neutron interactions, tables are available for almost all isotopes and those unavailable contain data on isotopes of natural elements (less than 3 percent in all cases, less than 1 percent in most). However, difficulty arose because only data evaluated photoionization tables are available for  $^{27}\text{Al}$ ,  $^{40}\text{Ca}$ ,  $^{90}\text{Zr}$ ,  $^{138}\text{Ba}$ ,  $^{150}\text{Sm}$ ,  $^{184}\text{W}$ ,  $^{238}\text{Pu}$ ,  $^{239}\text{Pu}$ ,  $^{240}\text{Pu}$ ,  $^{241}\text{Am}$ ,  $^{242}\text{Pu}$ .

The difficulty is deciding what is reasonable when no table exists for an isotope of interest. What has always been done is put it in completely ignore the photoionization contribution. However, this usually guarantees that the resonance will underpredict the neutron production. Therefore, it seems more reasonable to follow the example used in packing neutron tables and to use an available isotope, e.g.  $^{184}\text{W}$ , to represent all the isotopes present in the natural element, e.g.  $^{180}\text{Hf}$ ,  $^{181}\text{Hf}$ ,  $^{182}\text{Hf}$ ,  $^{183}\text{Hf}$ ,  $^{184}\text{Hf}$ . However this means these tables are compiled by isotope so that each individual species in a naturally occurring element has unique characteristics and reactions. Still engineering probability says that something is better than nothing. As a result, the original request is extended to say that it is reasonable to use a table for an isotope of similar atomic weight if the necessary isotopic table is missing. However, beware, you get what you pay for.

For the purposes of representing the materials in this evaluation, various tables were substituted by isotope within an element or by natural element as follows. Specifically, the  $^{184}\text{W}$  table was used to represent all natural hafnium and tantalum. The  $^{40}\text{Ca}$  table was used to represent elemental copper and nickel. The  $^{27}\text{Al}$  table represents elemental aluminum and was also used to represent elemental silicon. The  $^{90}\text{Zr}$  table was used to represent elemental iron, chromium and manganese. The  $^{138}\text{Ba}$  table was used to

represent elemental carbon. The major isotopes of lead,  $^{204,206,208}\text{Pb}$ , have similar available burning only 1-4 atom percent  $^{206}\text{Pb}$  to be covered by an appropriate material. The photochemical table was constructed with hydrogen, carbon, nitrogen, oxygen, fluorine, sodium, magnesium, silicon, and sulfur. The exact definitions of the materials as well as the geometry used in the simulation can be found in Appendix B.

**Radiation source.** The radiation source in the MDA is electrons on the target. The electrons are produced by an electron gun, focused into beams and accelerated through a monochromator chamber. They are then guided through a set of vacuum tubes to the treatment head. A system of three bending magnets [19] then spread the beam about it through an energy selection slit, reflect it and direct it into the target. The actual electron distribution on the target is probably a stopped-Gaussian in energy, implying on a relatively small spot with a slight angular distribution about the normal. This distribution is modeled in the simulation as a whole Gaussian in energy having a full width at half maximum of 700 keV and perpendicularly incident on a spot size 1 cm in diameter. This description is taken directly from the original UCLA model and is believed accurate enough as it has been used to successfully match experimental data.

One of the key unknowns in the mass-energy of the electrons incident on the target. It will always be dependent on the specific MDA as well as it is a function of the microwave cavity and RF tuning. The UCLA model gives this value as 20 MeV. Taking 20 MeV as a starting point, slight dose measurements were taken at 10 MeV increments for 5 MeV in either side of this value, i.e. 15, 16, 17, 18, 19, 24 and 25 MeV. The details are listed in Appendix B.



The relative weight for the neutron transport calculation is the exactly as described above. However, it is worth noting that while this is still a good approximation in the full source, it leaves out one portion which has the potential to be significant. As the electrons pass through the system of bonding weights, they pass through the energy selection file. The bremsstrahlung photon scoring is a result of this process do not affect the electron-photon dose as a significant amount of shifting blocks their down path to the treatment area. However, any high-energy photons from this process can contribute to the production of neutrons.

**Transport algorithms** The MCNP neutron transport code is the work of hundreds of people over decades of time. One of the principal reasons the current work was performed using the MCNP code is that was the comprehensive validation of its primary transport algorithms. This validation has been accomplished through the diligence analysis of thousands of years. MCNP is an old, if not the, gold standard in neutron-photon transport and its electron-photon transport package has made great advances over the last decade. For neutron and photon transport, there are many papers in the literature validating the accuracy of the data contained with MCNP's transport algorithms.

Electron transport was added relatively recently to MCNP's lineage and is still undergoing significant improvements. However, the current set of electron transport algorithms are derived from the well established ITR-code [34] and have proven to be accurate for most situations. Several papers have been published since electron transport was first added to MCNP showing its application to electron acceleration environments. Recent examples include work by Lora et al. [37] and Jiang et al. [38]. These show that

while there is still work needed in this area, MCNP is capable of simulating this class of problems.

However, since it was desired to run the dipole dose calculations with the best electron-photon physics transport package available, they have been run using the most up-to-date electron-physics package. As part of the upcoming release of MCNP version 4C, Ken Adams of the MCNP code development team has worked to correct some of the known discrepancies in the electron transport algorithms [19]. A prototype code has been designated MCNP4BNU to indicate it is based on MCNP4B2 and includes the new electron physics. The prototype was made available to the author for use in these simulations [19C].

The bulk of the current work has been directed at providing the algorithms necessary to include photoabsorption cross-sections in MCNP. The resulting prototype code is designated MCNP4BPM to indicate that it is based on MCNP4B2 and includes photoabsorption physics. It has been well documented in Chapter 3 and selected in Chapter 4. The neutron, photoabsorption and electron routines remain those of MCNP4B2 and as such have been subjected as previously described. MCNP4BPM is used for the bulk of the simulation simulations.

**Modeling Output.** The MCNP code has a very well established, comprehensive set of output tables. They have been well tested over the years by the users and present a wealth of information about the simulation. Counters and heat tables present a summary of the overall event. If needed, details are available about the event by cell and by the type of interaction. And most important of all a standardized tally package provides regional results along with statistical analysis of their uncertainty.

Part of the problem in simulating the depth dose calculation is doing detailed electron-photon transport over more than a meter in distance. It is trivial to obtain the bremsstrahlung spectrum from the target and transport it into the region of interest, i.e. the water tank. It is more slightly more difficult to obtain the bremsstrahlung spectrum from the other major components in the beam path and transport them to the region of interest. It is extremely difficult to transport the scattered electrons to the region of interest. Because of this, the typical approach has been to break the geometry up into distinct regions and create a phase-space file which adequately describes the electron-photon "source" at the start of each new location.

In the true spirit of engineering mentality, i.e. always use the biggest hammer available, these simulations were run from the original electron source scattered in the target. This was done at great expense in terms of CPU time though it considerably eased the amount of time that would have been necessary to understand and use phase-space files. The generation and use of phase-space files is, in the opinion of the author, still an art form rather than a science. Therefore a large number of CPU cycles were frustrated by the availability of unstandardized vacuum electron techniques within MCNP to run these simulations from top to bottom.

A dummy sphere allows a volume of interest to receive a representative neutral particle flux; every volume is outside of the volume. In order to keep the Monte Carlo game fair, any particle actually reaching the boundary of the dummy sphere is killed. For the purpose of these simulations, a photon dummy sphere was placed around the water tank. To illustrate how effective this method is, consider that a typical example simulation shows that 1 million photons were killed in the dummy boundary but 100

million particles entered the sphere, a significant set of particles interacting with the water tank.

Unfortunately, there is no method currently available to propagate electron contributions over a domain. Therefore the electron transport had to proceed the traditional way. Each electron reaching the water tank was the result of a long series of collisions which managed to penetrate the full length of the treatment head and still be going in the right direction at the bottom. Part of the requirement for long run times derives from the need to have enough of these particles contribute to the dose very near the surface of the water tank.

The dose along the central axis of the water tank was calculated from the surface to 40 cm. A three square centimeter volume was defined extending along the central axis. It was cut up into 25 vertical slices, the first five each 2.3 cm thick, the next nine each 0.5 cm thick, the next 24 each 1 cm thick and the last cell 0.1 cm thick. The energy deposited in each cell can be tallied and, with that, the absorbed dose calculated.

The standard MCNP tally package includes two methods for orientating energy deposition. The first is a heating tally. This method computes the average energy deposited in the volume of interest for each photon collision assuming all secondary energy is deposited instantaneously and locally. This requires that the system of interest has reached electron equilibrium. This means for inhomogeneous regions away from boundaries. Thus it is a reasonable approximation for these points after the buildup region and peak dose. As this method depends primarily on the photon transport, it does not require as much iterative solution + convergence criteria as the next method.

The second method to measure energy-deposition in a volume is to measure the net-energy flow through its boundaries. This is achieved simply by tracking each particle and adding its energy in the tally when it enters and subtracting all its energy when it leaves. The primary energy loss mechanism in the slowing down of electrons within the cell. Obtaining convergence for the energy deposition tally is difficult because it is necessary to have a large number of particles, particularly electrons, traverse the volume in order to obtain an accurate measure of the energy-energy deposited.

The energy deposition tally is also sensitive to the electron and photon run go cutoffs. Because the energy of the particle is added to the tally when it enters, any mechanism that prevents it from leaving will cause the energy to remain added to the tally. Thus if the electron and photon energy cutoffs, the energy below which no further transport is done, are too high, the tally will probably overestimate the absorbed dose. It was found through preliminary simulations that electron and photon cutoffs of 0.3 and 0.1 MeV, respectively, gave reasonable estimates at acceptable run times.

All standard MCNP tally outputs include a wealth of statistical information to help the user determine the precision of the answer. These simulations were run until the energy deposition tally showed convergence at less than 3 percent relative error. The heating tally could be run at the same time thereby making better use of the time spent. The run times needed to achieve convergence in the energy deposition tallies corresponded to a relative error level in the heating tally of less than 0.3 percent. However, it should be remembered that these both these error levels reflect the precision of the Monte Carlo results and not necessarily its true accuracy. True accuracy will be discussed in detail in the comparison sub-section.

Results were obtained at the manner described above for three field sizes. The secondary estimations were not such that the photon field incident on the tissue took 100 cm-SRD was full size, 10x10 cm and 30x30 cm, respectively. Each of the various incident energy distributions was randomized. All other conditions were held constant with the 11 variations with this.

A debt of gratitude is owed to the Advanced Computing Laboratory (ACL) at Los Alamos National Laboratory (LANL). They operate the world's fastest integrated computer (at least for today), the Blue Mountain-800 cluster [18]. At the time these simulations were performed, the machine was severely underutilized. After about 4,000 hours of time to obtain some preliminary results, the final set of simulations took 31,000 hours of CPU time. However, this time was cheap in comparison to the learning curve necessary to understand and utilize phase-space files.

Two standard MCNP tallies were used to obtain estimates of the activation in the gold foil. The track length estimator evaluates the particle flux over volume. A point detector evaluates particle flux at a point. Either can be multiplied into function of energy with a production cross section and an atomic density to obtain the production rate of an isotope per source photon per volume. Track length estimators were used to evaluate the isotope production rate in the isotope unmoderated over field volumes. Point detectors were used to evaluate the isotope production rate in the foil as approximated at a point. Again, the statistical analysis package provides useful information for evaluating the precision of the results.

Several techniques were used by the activation simulations to reduce the CPU time required. A delta-sphere, as discussed above, was used to surround the volume

where a tract, large estimate of particle production was made. Since electrons and photons with an energy below the lowest photoatomic threshold are no longer capable of producing ionization they are not transported. This is done by setting the particle energy cutoff to remove them from the simulation when they fall below 3.7 MeV, the lowest photoatomic threshold in the simulation. The electron energy cutoff represents the most substantial time savings as electron transport becomes much more CPU intensive at lower energies. Photoatomic binding was used such that the ionization production from every photon collision would be evaluated. Finally, a single weight window was used for each particle type to ensure the parallel weight due to the forcing schemes did not cause unnecessary fluctuations in the tally.

It should be noted that delta splines are not used in conjunction with point detectors. Point detectors are also known as point event estimators. They work up a master analogue to delta splines. A contribution is made to the bin of the point detector from every particle collision. Therefore, delta splines are used as their counterparts with a flux tally defined and point detectors are used otherwise.

The interaction cross-sections included the production rates of both  $^{226}\text{Ac}$  and  $^{226}\text{Au}$ . The  $(\alpha, p)$  cross section necessary for estimating production of  $^{226}\text{Ac}$  was available in the ZAID THO file data set found in the standard ENDF60-mechanism-energy neutron library [34]. The  $(p, \alpha)$  cross section necessary for estimating production of  $^{226}\text{Au}$  was taken from the facility  $^{226}\text{Au}$  photo-neutron cross-section evaluation [40] as available electronically in the *Index of Photo-neutron Cross Sections* [35].

There were five simulation setups of interest: the bare input or reactor, the uniform input or moderator, the input located in the center, the hole in moderator, and

the foil without the moderator. The post-detector veto used for the foil without the moderator is useful for comparison purposes even though the equivalent experiment was not performed. Considering the cross image distributions, this lead to 35 simulations.

Each of these simulations was deposited, for  $^{252}\text{Cf}$  production only, using MCNP4B4J replacement of the reduced-photon physics model significantly change the production rate. The simulation that run is not quite identical to the MCNP4B4J simulation as that MCNP4B4J does not include the photo-nuclear cross section. Inclusion of the photo-nuclear cross section will change the photon mass loss rate slightly but due to the relatively small change, it has very little effect on the gross photon integral.

As with the depth dose simulations, it was desired to run until the statistical package reported convergence for all the tallies. This was indeed the case for almost all of the volume tallies. The few discrepancies involved warnings although other indicators showed that the tally had converged. The post detector had a more difficult time.

Post detector was first used as a monitor inside the area region of transport. Because they are still cross-sections, cross contributions by them tend to be of low weight as the particle has had to manage to scatter in the right direction and transport a significant amount of material. Unfortunately, when used as a monitoring tally from the occasional particle which scatters relatively close by and has a high probability of scattering in the direction of the detector. These particles, in use a random term, clutter the tally by introducing a sample with much higher weight than the average.



The different simulations used present different ranging values, especially in some cases, within dense materials. As such, many of the three values did not converge due to the problem described above. After many attempts to remedy the situation and long wait-times to see if enough virtual particles could certificate the occasional straggling particles, the final results were taken despite some outstanding problems. User judgement is used to evaluate those results which did not converge and estimate their uncertainties, in light of those results which were converged.

As discussed above, the authors believe with the notion that all credible scientific work must be reproducible. In order to facilitate the reproduction of the data presented here, Appendix E contains the information necessary to reconstruct the input decks. The coding for the algorithms added to MCNP4B2 has also been provided as well as the coding necessary to reproduce the cross-section library used. The cross-section data are available in the ENDF format from the LANL T-1 web site [140]. The only set of information which would have been useful to include, but is not, is the actual MCNP output files. Unfortunately, they form several hundred megabytes worth of text files and their inclusion was not practical.

### **Discussion of the Results**

Two sets of experimental data and simulation results have been described. This section will discuss how well the simulations match the experimental data and make suggestions about where to concentrate future work to improve these results. The comparison of the depth dose data is presented first, followed by the conversion data.

**Depth dose.** The experimental data exist as three relative depth-dose curves for photon field sizes of 1x1, 1.8x1.8 and 30x30 cm at 140 cm SSD. The original

experimental data presented in Figure 5-2. It was provided at 1 cm intervals without an estimate of the error bars though they are expected to be small. The data was averaged over each cell in order to facilitate comparison to the simulation results.

The heating tally results for each of the seven incident electron energies and the each of the three field sizes are shown in Figure 5-4 compared to their respective ice track. Since this tally is only valid once electron equilibrium is achieved, the comparison is only for those points after and including the peak value of the ice track. The sum of the squares of the difference between each tally value compared to the average of the ice track in the cell volume was then calculated. Remember that the ice track is a set of reference values. The general conclusion based on this graph is that the simulation appears to be in the right neighborhood. However, despite the fact that they meet the "roughball score" no further conclusions can be readily made strictly from this graph.

Three difference plots between each heating tally result and the ice track are presented in Figure 5-5. This set of graphs provides much better insight into the true nature of each simulation. The first conclusion to be drawn is that the simulation model has fairly accurately modeled the true experiment. None of the results are more than four percent different. However, there are still some discrepancies.

Figures 5-6 and 5-7 are presented without error bars. Error bars are not included on these graphs so they would obscure the information being conveyed. The error bars are not available for ice chamber data. The error bars for the heating tallies are all less than 6.3 percent of the tally value.

The first set of concerns in the large slope in the difference plots just after the peak value. This is most probably due to electron equilibrium not having been fully

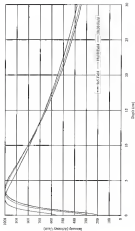


Figure A.2. Cross-section from a standard calibration of the Phillips SL-25 in Runway 5 at Shasta County Center

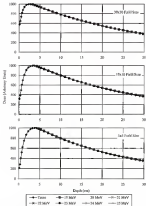


Figure 3-4. Comparison of test chamber tests with calculated bearing capacity for a) a 30x30 field, b) a 15x15 field, and c) a 3x3 field.

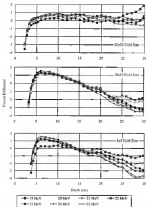


Figure 3-5. Percent difference between gas chamber trace and calculated heating only for a) a KNO<sub>3</sub> field, b) a NaNO<sub>2</sub> field, and c) a NaCl field. (Percent difference is computed as (trace-calculated)/trace.)

reached soon just after the peak value. Remember that the heating tally is not valid near boundaries where electron populations are in a non-equilibrium state.

The second set of curves is the increasing difference seen between the simulations and the one used for the 10x10 and 1x5 cm field case. One hypothesis for the difference is that the relative size of the tally volume is a much larger percentage of the total plasma field case so that field size is decreased. The size of the central volume used for defining the tally is  $1 \text{ cm}^3$ . This corresponds to 1/3, 1 and 1/2 percent of the 10x10, 10x10 and 1x5 cm field case, respectively. It may be that the tally is being influenced by the edges of the field boundary. Further study is needed.

Overall, the simulation geometry seems to have captured the essence of the physical space within the beam path. Further, from the difference graphs, the energy of the incident electrons would appear to be in the 20 to 25 MeV range. This value is based on your judgment in evaluating the curves. If the 10x10 cm field case simulation is taken as the most accurate, it would appear that the incident electron energy is about 20 MeV. Cautioning that the 10x10 and 1x5 cm field case simulations are not as accurate they still indicate that the higher energies are becoming more divergent especially above 11 MeV.

The energy deposition tally results for each of the seven incident electron energies and for each of the three field case are shown in Figure 5-6 compared to their respective one trace. Again a least squares fit was used to match each simulation result to the one trace. Similar to the heating tally results, these graphs seem to indicate that the simulation geometry is a fairly accurate representation of the treatment head along the beam path. The discrepancy near the peak is discussed below.

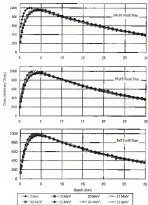


Figure 5: Comparison of experimental data with calculated energy deposition for (a)  $\times 1000$  Gauss, (b)  $\times 1000$  Gauss, and (c)  $\times 1000$  Gauss.

The percent differences between each energy deposition result and the ion trace are presented in Figure 5-3. Due to the larger relative error in these results, they do not provide as much insight as the heating ratios. Again no error bars are provided on the graphs themselves as they would obscure the information to be conveyed. The error bars for the simulation results are less than 3 percent. No error bars are available for the ion traces.

The first discrepancy among concerns is the increasingly poor match between the build-up region in the simulation versus the experiment. The build-up region is where near the surface where the electron population has not reached equilibrium. The results for the simulation show discrepancies of approximately 30, 40 and 60 percent difference in the surface wall for the 3kV, 15kV and 30kV ion field sizes, respectively. This is most probably due to the lack of an in the simulation model. The ion would provide a source of Compton scattered electrons impinging on the surface of the rear wall. This explanation seems reasonable as the effect is worse for increasing field size where more electrons would be produced by this mechanism.

The area beyond the build-up region seems to substantiate the results of the heating ratio. The overall agreement in this region is in the order of 3 percent or less. Though it is more difficult to observe, the same discrepancy seen in the heating ratios seems to be apparent here. Due to the larger relative errors, an conclusion about the appropriate neutral electron energy can be drawn directly from these graphs through nothing seems to relate the simulation closer from the heating ratios.

The rapid growth of the high dose simulation rates to saturate the incident electron energy and the number of electrons ion target per MU. The same energy has



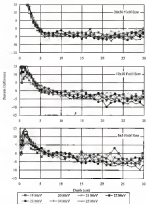


Figure 3-7 Percent difference between ion cluster trace and calculated energy deposition for (a) a 10kV field, (b) a 15kV field, and (c) a 20kV field. (Percent difference is computed as (trace-calculated)/trace.)

have estimated to be in the 20 to 23 MeV range. Remembering that one electron volt corresponds to one category of absorbed dose at the peak of the depth dose curve for the 10x10 photon field size, Figure 5-8 shows the estimate of the number of electrons per MLJ as a function of energy for each of the two fully approximate cases. Based on the errors seen in this point, 30 percent error bars are included on these values. Taking the center of the expected energy range, the estimate of  $(1.44 \pm 0.4) \cdot 10^{23}$  electrons incident on the target per MLJ is predicted.

The overall conclusion drawn by the depth dose comparison is that the simulation's treatment of the physical space at the end of the linear path is substantially correct. Based on the results of simulations the most incident energy is estimated to be (20.5 to 23) MeV corresponding to  $(1.36 \pm 0.4) \cdot 10^{23}$  electrons on target per MLJ. Given an average dose rate of 400-625 MLJ per minute, this represents an average of approximately 13 microcoulomb of linear current. This number is a good sanity check for the work on the as a useful physical value.

**Aurification:** The experimental data consists of an analysis for both  $^{199}\text{Au}$  and  $^{203}\text{Au}$  production for four different configurations. Several of these production rates have been simulated via two different methods. The final estimates of the production rates for both  $^{199}\text{Au}$  and  $^{203}\text{Au}$  by experiment and by simulation are given in Tables 5-3 and 5-4, respectively. How these numbers were calculated is the subject of the following discussion.

Each simulation simulation reports the production rate as atoms produced per electron incident on the target per cubic centimeter of original atoms. The number of electrons per MLJ was obtained in the previous comparison. Thus the production rate

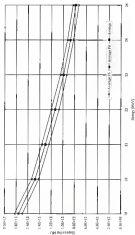


Figure 3-6 Estimate of electron residuals as target gas density (g/cc) versus Energy (MeV)

expressed in counts produced per MJ per value systematic manipulates the integral result of the simulation. For the purpose of comparison, it is desired to express the experimental data into the same format.

The raw data from the experiments consisted of several sets of counts for specific decays as determined by gamma-ray spectroscopy.<sup>1</sup> The data strongest emissions from  $^{135}\text{As}$  decay are a 111 keV gamma from 29.4 percent of the decays and a 193 Te keV gamma from 93.6 percent of the decays. The strongest emissions from  $^{135}\text{As}$  decay is a 411.8 keV gamma from 93.33 percent of the decays. Note that the decay data used throughout this section is taken from the Nichols Navigator program [104]. The General Purpose software [105] used to control the counting provides an estimate of the net counts for each peak observed. All three of these peaks were present and well defined in each counting session. Other possible peaks of interest were not as well defined and therefore ignored.

Assuming the production rate is constant in time over the length of the simulation, the number of counts seen is a function of that rate value. Therefore, a system of equations can be written to express the count rate as a function of the production rate of counts produced per MJ per volume of sample atoms. Sample algebraic manipulations can be used to solve for the production rate in terms of the count rate and the count rate can be fed into these equations to estimate the production rate seen by each sample.

The number of counts seen by the detector can be calculated from Equation 3-1. Here,  $C$  is the number of counts observed and  $D$  is the true number of decays that occurred during the counting session. The third term is accounted for by multiplying by the ratio of  $\epsilon/\Delta T$ , the live time of the detection system, to  $\Delta T$ , the real-time elapsed during

the constant term in  $\beta_{\text{eff}}$  is the branching ratio,  $i$  is the number of gamma-rays of a specified energy given per decay. The times and branching ratios are assumed to have negligible error.

The last three factors in Equations 3-4 require more significant explanation. Because the dimensions of the crystals are significant in comparison to the mean free path of the gamma-rays, self-shielding (SS) occurs. The correction factors used here have been computed by Monte Carlo simulations. Photons are produced uniformly within the volume of a mask target and the average number which escape the boundary is tabulated. Given an target size of  $4.1 \times 2.4 \times 0.1504$  cm and a total mass of  $11.1$  g, the self-shielding factors are 0.443, 0.473 and 0.541 for 303, 315.32 and 401.4 keV photons, respectively. Although the Monte Carlo simulations the self-shielding were run to correct gamma and negligible simulation error, the distribution of the photons in the target remains unknown and the self-shielding factors are assigned a 10 percent uncertainty.

Self-shielding of the leads was assumed to be negligible and assigned a factor of unity. Although self-shielding effects might be present, they should be minimal. An uncertainty of 3 percent should be assigned to this factor.

The detector efficiency ( $\epsilon_d$ ) is a function of the gamma-ray energy and the geometry of the photon source as relation to the detector. Two certified check sources  $^{152}\text{Eu}$  and  $^{137}\text{Cs}$  were available to determine the absolute efficiency of the counting system. Peak decay rates were of interest. The decay of  $^{152}\text{Eu}$  includes 303.70, 315.36 and 382.74 keV gamma rays. The decay of  $^{137}\text{Cs}$  includes a 401.42 keV gamma ray. Based on the counts rates observed from these four lines, detector efficiencies of 0.9084

0.044 and 0.040 were used for the 110, 111.73 and 111.8 keV photons, respectively. The uncertainty in these efficiencies is estimated to be 10 percent.

At the time the counts were taken, it was not contemplated that the large diameters of the target samples would have an effect other than self-absorbing. During the final analysis, it was discovered that the counts estimated by the disk and the target differed significantly. The only reasonable suspect for such a difference was the much larger size of the target leading to a different detector efficiency than a point source. Therefore a disk size (DS) factor has been added to the equation

$$C = D \cdot \frac{EF}{DS} \cdot R_D \cdot RR \cdot SS \cdot PS \quad (9-4)$$

Working back towards the production rate, the next step is to relate the true number of decays ( $D$ ) to the number of atoms present at the start of the counting session ( $N_0$ ). The fraction of atoms that survive the counting session is given by the familiar exponential decay term.  $T_{01}$  and  $T_{02}$  are the start and end times for the counting session, respectively. The decay constant  $k$  is defined as many sessions and the values 1.58E-7 and 1.49E-7 per second are used for  $^{109}\text{Ag}$  and  $^{109}\text{Ag}$ , respectively. The relation describing the number of decays is written as follows in Equation 9-5. The times and decay constants are assumed to have negligible error.

$$D = N_0 \left( 1 - e^{-k(T_{02} - T_{01})} \right) \quad (9-5)$$

The total number of atoms of interest at the sample at the beginning of the counting session is a function of the number of atoms produced in each irradiation and their subsequent decay. The total present at the start of the counting session is the sum

of each of the individual contributions as shown in Equation 3-3.  $N_{p,i}$  is the number produced during revolution  $i$ . The exponential decay term accounts for the number that decayed between the end of the revolution ( $T_{e,i}$ ) and the start of the counting window ( $T_{s,i}$ ). Again, the decay and decay constants are assumed to have negligible error

$$N_{p,i} = \sum_j N_{p,j,i} e^{-\lambda(T_{e,i} - T_{s,i})} \quad (3-8)$$

Finally, the number of neutrons produced from the irradiation is a direct function of the production rate as shown in Equation 3-4. The production rate is given in units of neutrons produced per volume ( $V$ ) of sample per dose ( $AD$ ) as measured in MLD. The rate is in terms of MLD as opposed to electrons, as that is the experimental measure of the amount of irradiation. The decay of neutrons during the irradiation time is ignored. This is justified by the fact that less than one-quarter of one percent of the neutrons produced during any given irradiation decay before the end of the irradiation. The volume and the dose are assumed to have negligible error

$$N_{p,j} = P_j V AD \quad (3-9)$$

The linear system of equations relating the production rate to the count rate has now been established. It is a trivial matter to solve for the production rate in terms of the count rate. The uncertainty of the count rate values by gamma-ray and by counting neutron has on the whole is less than one percent for the gamma and is three percent for the fast. The error of the fast neutron factor has not been resolved and is left for further discussion below.

The first configurations for the calculations have been described above. The final results are production rates as a function of incident electron energy given in units of

atoms produced per electron per volume of sample. These are changed to units of atoms produced per MU per volume by multiplying the number of electrons per MU as obtained in the previous set of simulations. The uncertainty in the number of electrons per MU is estimated to be 18 percent. The uncertainty in the simulations is discussed in more detail below.

The first experimental configuration simulated was the beam setup at accelerator Simulations were run to calculate production of  $^{208}\text{As}$  using MCNP4B2P and production of  $^{208}\text{As}$  using MCNP4B2P and MCNP4B2U. The results of the simulations are shown in Figures 3-8 through 3-11, respectively.

For all of the simulations calculating the production rate of  $^{208}\text{As}$  using both MCNP4B2P and MCNP4B2U, almost no difference was seen. This can be attributed to the fact that the gross photon transport characteristics are unaffected by the presence or absence of the photoabsorber portion of the photon cross sections. It also indicates that the changes in electron transport and bremsstrahlung production from version 4B to 4B2U do not significantly affect this simulation. Therefore, while both sets of results will continue to be shown, their results are discussed without differentiating between the two.

Similar to the depth dose simulations, the production rate of  $^{208}\text{As}$  depends mainly on the electron-photon transport through the measured head or the vicinity of the beam path. The point maximum of the production rate in the beam path indicates that the high-energy photon flux in the region is fairly uniform. The experimental values also confirm this. It is also evident from the simulations that grid shadowing in the region has no effect though in this case it changes the results by less than 10 percent. The best estimate of the production rate for  $^{208}\text{As}$  is  $1.49 \cdot 10^{-7}$  atoms/nuclei from the volume elements like track



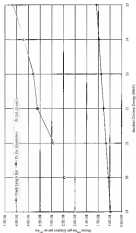


Figure 3.9: Calculated production rate of  $^{139}\text{Xe}$  as a function of beam-to-target energy

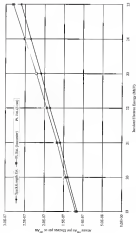


Figure 2-18 Calculated production rate of  $^{109}\text{Ag}$  as a function of neutron fluence (atoms/cm $^2$ )

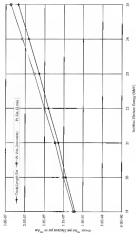


Figure 3-11: Calculated gas flux rate of  $^{222}\text{Rn}$  as the input bubble at seawater using MICOPHON.

implies fully) and its uncertainty is estimated to be 20 percent. This uncertainty derives mostly from uncertainties in the  $^{107}\text{Au}(p,n)^{107}\text{Au}$  cross section.

The production rate of  $^{107}\text{Au}$  at very energies is the production and transport of the neutrons. For the reasons discussed above, all the simulations attempting to simulate the production of  $^{107}\text{Au}$  have a high level of uncertainty. It would be fair to say that these simulations represent reasonable estimates of the problem described but that the problem described is incomplete. It is still worth discussing the results and drawing some conclusions.

For production of  $^{107}\text{Au}$  at the bare input of neutrons, both the simulations using point estimators and the simulations using a volume estimator give reasonable results. However, these results are a factor of four different. This can be attributed to self-shielding in the grid input causing less neutron flux to be seen within the target volume. The volume estimator is clearly the best choice due to the self-shielding in the sample. The production rate of  $^{107}\text{Au}$  is estimated to be  $4.18 \cdot 10^5$  atoms/sec and the uncertainty is estimated to be a factor of three.

The second experimental configuration considered was the moderated input of neutrons. Simulations were run to simulate production of  $^{107}\text{Au}$  using MCNP4B2N and production of  $^{107}\text{Au}$  using MCNP4B2N and MCNP4B2MU. The results of the simulations are shown in Figures 3-12 through 3-14, respectively.

The presence of the moderator block reduces the high-energy photon flux available for production of  $^{107}\text{Au}$ . However, the results are very similar to those obtained for the bare input. One difference is that the point domains are subject to more high-weight variations in this region and therefore more subject to error. Self-shielding in the

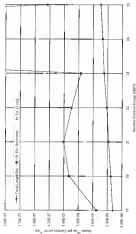


Figure 8-10: Calculated production rate of 100MVA as a function of reactor temperature (°C) as calculated by A-2000.

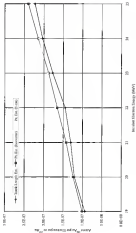


Figure 1-13: Calculated production rate of  $^{140}\text{Ba}$  as the result of neutron irradiation by A-150 phone using MCNP4c2.2

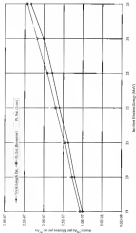


Figure 1.14 Calculated production rate of  $^{109}\text{Ag}$  as the target located at innermost rim irradiated by A-192 plasmas using MCNP6.2.6.1

sample volume still reduces the accuracy by something less than 10 percent. The volume estimate gives a value of  $1.23 \cdot 10^{-7}$  atoms/bbox for the  $^{252}\text{Am}$  production rate and the estimated uncertainty is about 25 percent.

The presence of the moderator block dramatically alters which neutrons are causing reactions in the sample. In the best layout, thermal neutrons scattered within the room are readily available for absorption within the gold. The mean free path for the average neutron in the moderator block is about 0.5 cm. This means that any room scattered neutron must penetrate a minimum of 10 mean free paths to contribute to production of  $^{252}\text{Am}$ . However, high-energy source neutrons have a longer mean free path and are more readily available to the center of the moderator. In this sense, however, they are thermalized such that they are more easily absorbed in the gold. Again the volume estimate is used for the final results. The production rate of  $^{252}\text{Am}$  is estimated to be  $2 \cdot 10^{-8}$  atoms/bbox and the uncertainty is estimated to be a factor of three.

The third experimental configuration simulated was the moderated delta distributed in the cross-plane. Simulations were run to calculate production of  $^{252}\text{Am}$  using MCNP4B2M and production of  $^{252}\text{Am}$  using MCNP4B2M and MCNP4B2L. The results for all the bins were obtained using point detectors. Unfortunately, point detectors are subject to large errors as described above. Therefore, these results do not prove as generally useful as those from the layout. However, they did provide some insight into the modeling and, most importantly, brought into the possible values for the bins was better.

The production rate of  $^{252}\text{Am}$  in the bins drops dramatically outside the region of the photon field. In fact, due to the low exposure of these bins outside this region the



experimental data is virtually meaningless. However, the two foils located in the primary beam path provide some useful data. The simulation results for these foils are presented in Figures 5-13 and 5-14. The point estimate of activity and 3  $\sigma$  values are shown along the cross plane show essentially the same result. These estimates give a value of  $1.23 \times 10^7$  atoms/sec for the  $^{226}\text{Ac}$  production rate and the estimated uncertainty is about 18 percent.

It should be remembered that small, thin foils are typically used for activation analysis because their slow decay resolution the calibration sources used to determine detector efficiency. Self-shielding and flux rate typically are not considered as significant factors in computing the activation in the sample based on the decay-corrected.

It can be shown that the foils used in the experiment do not appear to suffer from self-shielding or flux rate effects. Taking the self-shielding and flux rate factors to be unity for the foils, the experimental value for the  $^{226}\text{Ac}$  production rate in samples 1 and 2 is approximately  $1.44 \times 10^7$  atoms/second with an uncertainty of 12 percent. The point detector estimation of the production rate is  $1.26 \times 10^7$  atoms/sec with an uncertainty of about 23 percent. Using the activity per MBq value from above, this corresponds to a production rate of  $1.21 \times 10^7$  atoms/second. This is a satisfactory match between the experimental and simulation values. It continues to confirm the conclusion that the electron photon transport through the treatment head to the target around source is accurately modeled.

Knowing that the simulation model appears to be accurately representing the electron photon transport, the  $^{226}\text{Ac}$  production calculated can be taken as sufficiently accurate. The moderated foil and moderated target simulation give results that are

within 18 percent of each other. This indicates that the experimental production rates should be within that same error margin. Taking self-shielding as accounted above, the experimental value from the target is a factor of 1.4 that high when compared to the value from the foil. Based on the match between the foil estimate and the simulation, the simulation for the target should be substantially correct. Therefore a value of 1.4 is estimated for the finite size factor and used in calculating the experimental production rate from the target samples. As the estimate of the finite size factor is based only on this one data point, it is assigned a 50 percent uncertainty. As a final data, this study should be robust using only foil or target to avoid having to use a value like this.

The production rate of  $^{208}\text{Au}$  in the foil is estimated from the simulation as nearly worthless. The point detectors used for this estimate were subject to large fluctuations due to the problems described earlier. Using a knowledge base of past judgements, the production rate of  $^{208}\text{Au}$  is estimated to be  $1.14 \cdot 10^{12}$  atoms/sv and the uncertainty is estimated to be a factor of three.

Though the remaining foil have been eliminated from the target comparison, they are worth considering for a moment longer. The experimental data show a trend in the moderator block that the  $^{208}\text{Au}$  production is highest in the most inner path where high-energy neutrons can traverse the moderator with little degradation. Figure 3-15 shows that the simulation reproduces this trend though not as well-defined as the experimental data.

The last experimental configuration completed was the bare target located in the main chamber. Simulations were run to calculate production of  $^{208}\text{Au}$  using MCNP4B2P6

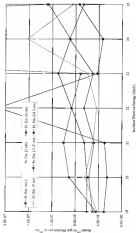


Figure 4.4.3 Calculated production rate of  $^{138}\text{Ba}$  as the fuels described in the text used as the source phase reaction from neutron not needed by the A-128 phase.

and production of  $^{252}\text{Au}$  using MCNP-NBP4 and MCNP-40043. The results of the simulations are shown in Figures 3-36 through 3-43, respectively.

The production rate of  $^{252}\text{Au}$  in the target located in the reactor is anticipated to be very low. It is expected that the only significant contributions from the radiation source as modeled will be for electrons that have scattered such that they can produce bremsstrahlung heading towards the sample. The volume estimate gives a  $^{252}\text{Au}$  production rate of  $4.45 \cdot 10^{11}$  atoms/sec and its estimated uncertainty of 23 percent.

The production rate of  $^{252}\text{Au}$  in the target located in the reactor is anticipated to be significant. Neutrons scatter off concrete very well and the main corridor presents an ideal streaming path. The volume estimate gives a  $^{252}\text{Au}$  production rate of  $7.83 \cdot 10^{12}$  atoms/sec and the uncertainty is estimated to be a factor of three.

With all of the comparisons going into the experimental and simulation production rates were disseminated, the final values can be accepted and conclusions drawn. Tables 3-1 and 3-2 present the final values for the production rates of  $^{252}\text{Au}$  and  $^{253}\text{Au}$ , respectively. The values are tabulated in units of atoms produced per second and per cubic centimeter of gold sample. The ratio of the values is given to aid in comparison.

Table 3-2. Experimental and simulated production rates of  $^{252}\text{Au}$  for four configurations.

Configuration	Production Rate ( $^{252}\text{Au}$ /SB/sec $^{252}\text{Au}$ )		
	Experiment (1)	Simulation (2)	Ratio
Sample 11 Front Target at Isosource	(1.87 $\pm$ 0.94) $\cdot 10^2$	(2.01 $\pm$ 0.31) $\cdot 10^2$	1.08
Sample 12 Mineralized Target at Isosource	(1.63 $\pm$ 0.92) $\cdot 10^2$	(3.71 $\pm$ 0.41) $\cdot 10^2$	1.99
Samples 1 & 2 Mineralized Front Near Isosource	(1.44 $\pm$ 0.13) $\cdot 10^2$	(3.31 $\pm$ 0.40) $\cdot 10^2$	1.12
Sample 13 Front Target in Reactor	(1.44 $\pm$ 0.92) $\cdot 10^2$	(6.33 $\pm$ 0.34) $\cdot 10^2$	3.10 <sup>a</sup>

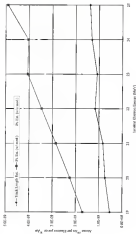


Figure 1-16 Calculated production rate of  $^{140}\text{Ar}$  as a function of the inlet gas flow rate.

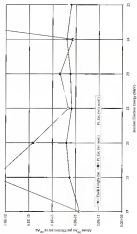


Figure B.17 Calculated production rates of  $^{109}\text{Au}$  for the target located in the main wing (MCCN040705)

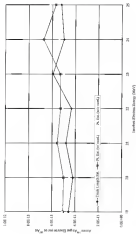


Figure 5-18. Calculated production rate of  $^{105}\text{Ag}$  as the target located in the matrix using MCDONALD97

The production rate of  $^{22}\text{Na}$  supports the conclusion that the electron-positron transport through the primary beam path in the treatment head is accurately modeled by the model. The comparison shows three matches within 15 percent difference which is in turn well within the accuracy of the individual values. The only anomaly is the production rate in the sample in the mass.

From the discussion above, it should be remembered that the secondary objective of the sample in the mass was to determine if high-energy photons were being produced outside of the target area. The experimental production rate for the sample is four orders of magnitude greater than the simulation. This is a clear indication that there is either an unknown streaming path through the primary collimator, an unknown structure, or that there is another source of high-energy bremsstrahlung photons. It is believed that there is a secondary source and that the source is the energy selection slit in the bending magnet system. Due to their initial direction and the direction in their path, photons produced in the energy selection slit would not significantly affect the photon flux in the beam path near the monitor. However, if such photons are being produced, they could represent a significant source of high-energy photons, and their phenomenon, that are not included within the model. The experimental observation of high-energy photons in the mass supports this hypothesis.

The production rate of  $^{22}\text{Na}$  supports the conclusion that the electron-positron-neutrino model is independent variable positive estimator with an accuracy of less than a factor of three. This accuracy was derived from three fixed numbers although it has been quoted in the discussion above. With that said, the methodology still represents



Table 3-3 Experimental and simulated production rates of  $^{22}\text{Ar}$  for four configurations.

Configuration	Production Rate ( $^{22}\text{Ar}/\text{mg}/\text{hr}$ $^{22}\text{Ar}$ )		
	Experiment (E)	Simulation (S)	Ratio
Sample 11 Blank target in isocenter	$(8.4 \pm 1.2) \times 10^3$	$(2.40 \pm 0.3) \times 10^3$	1.599
Sample 12 Moderated target in isocenter	$(3.7 \pm 0.8) \times 10^3$	$(2.40 \pm 0.3) \times 10^3$	0.533
Sample 1 & 2 Moderated foil near isocenter	$(3.28 \pm 0.22) \times 10^3$	$(3.34 \pm 0.3) \times 10^3$	0.980
Sample 13 Blank target in beam	$(3.38 \pm 1.0) \times 10^3$	$(3.47 \pm 0.3) \times 10^3$	1.242

a glass loop obtained at the side of the set for measuring those quantities to that coupled simulations can be run and an accurate assessment of their accuracy is available. Further, the data make clear the areas of highest concern and help to prioritize future work to improve the accuracy of this simulation model.

The final conclusion from the  $^{22}\text{Ar}$  production data above indicate the probable existence of a photoelectron source not modeled in the current simulation. The comparison for the moderated foil and the moderated target both indicate that the neutron production is too low, probably by a factor of two. One two loss-of-evacuant lead candidate is the hypothesis that the energy selection slit is a significant source of high-energy photons and therefore photoelectrons. This should be one of the first areas addressed by future work.

Further, from the  $^{22}\text{Ar}$  production data it is concluded that the simulation of neutron scattering and absorption is inadequate. During the course of this study, many variants of physical geometry and materials were explored. It was found from these studies that the scattered neutron flux was most sensitive to the materials, in particular tungsten, in the treatment head outside the primary beam path. With no other changes,

the  $^{208}\text{Au}$  production in the beam input at encounter could be reduced by a factor of three by isolating neutrons at the rear of the primary collimator. This is primarily due to the fact that tungsten has no thermal absorption cross section of magnitude greater than lead. Placement of lead throughout the treatment head had a lower, though still significant, effect. One of the recommendations discussed above is to revamp the treatment head in order to obtain an accurate model of the shielding outside the beam path.

Several other factors also have a significant, though smaller, impact on the neutron scattering and absorption. Once the two quaternarysual above have been corrected, the lesser problems will become more important to solve. Included in this is an accurate description of the linac head wall. Heavy neutron-scatterer increases the geometry neutron losses. If any material with a significant capture cross section exists within the general wall-form, it will have an impact. The main body of the accelerator and the positive wall of the machine cloud represent a significant amount of material available to scattering slow-neutrons. These and possibly other materials in the room will eventually have to be modeled. Last, neutron cross-section data becomes available, the description of the neutron production will improve.

### **Implications**

Now that the regime of applicability for this simulation model is known, it can be applied to the general problem at hand. In particular, two pressing questions exist. The first is to estimate the dose due to photo-neutrons around the MBL. The second is evaluate the relative contributions from the photon and neutron components of the dose

as the mean electron energy is increased. These two quantities are addressed simultaneously in this section.

For the purpose of addressing these questions, the physical model used for the previous simulations is used without change. In reality, the accelerator would be redesigned for any significant change in the incident electron energy in order to provide an appropriate photon field in the target area. However, that is beyond the scope of this study.

For the purpose of calculating the dose, the electron-photon dose and the neutron dose are calculated separately. Similar to the studies performed above, MCNP4C01 is used for the electron-photon transport problem, and MCH2EPN is used for the electron-photon-neutron transport problem. The dose is estimated using point detector tallies multiplied by appropriate flux-to-effective-dose conversion factors. The conversion factors are taken from a tabulation by Rogers [104] for photons and for neutrons by the ICRU [105] for neutrons. A hidden assumption necessary for this comparison is that the number of electrons on target stays constant ( $\sim 3 \times 10^{13}$ ) throughout these calculations.

Figure 5-18 shows the dose at isocenter over the mean electron energy range 15 to 100 MeV. Note that both the photon and neutron dose are not strongly dependent on the field size. Field size is therefore ignored in the following discussion despite the fact that it is included for each of the graphs. It can be observed that the ratio of the photon to neutron dose remains fairly constant in this comparison.

The neutron dose at isocenter is approximately three orders of magnitude below the photon dose. This is as it should be. Many calculations specify an upper limit of 0.1% of the dose from neutrons. However, the figure shows that the true neutron average

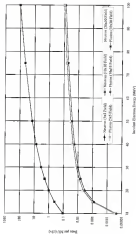


Figure 3-10 Theoretical neutron and photon dose per incident neutron at sea level

similar to the 13 to 30 MeV range with the point of closest approach around 20 to 25 MeV. The value in this energy range is around 0.0033 to 0.004, slightly above what is desired. While this is of concern, it should be remembered with the understanding that there is a large uncertainty in the calculated value.

Figures 3-20 through 3-22 present the dose in one meter above, in line of sight to the side of the electron target, respectively. As might be expected due to the symmetric nature of the treatment head model, they show very similar results. Of significant note is that the neutron dose quickly exceeds the 4.17% limit desired. This is due to the lack of shielding around the treatment head and can be remedied.

It is also worth noting that the photon dose is relatively flat in these locations. In fact, the photon dose is relatively flat for all locations except at maximum. This is useful because it indicates that photon shielding in place is adequate for this entire energy region.

The neutron dose becomes the primary shielding problem in the main corridor. This is not unexpected. The corridor's ability to scatter and reflect streaming neutrons has already been decreased. The purpose of the main is to create a larger distance between their location and their leakage into occupied areas. Figures 3-23 and 3-24 show the dose at both extremities of the main corridor.

The reflective dose calculated at the extremity dose for a typical 3000 mSv treatment is 0.004 mSv (0.4 millirem). This calculation is too high and again suggests that more work is needed to create a more detailed treatment model. The error is probably due to the large uncertainties in the neutron shielding around the treatment head and the uncertainties in modeling possible neutron absorption in the room and walls.

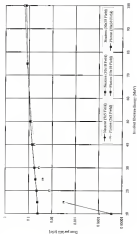


Figure 3.10 Theoretical section and phase dose per nucleon mass number along the target

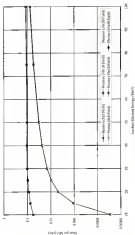


Figure 5-11. Theoretical values and photons that per incident unit area energy from the target in the cross-section

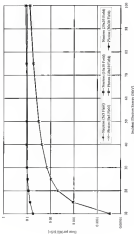


Figure 3-23 Theoretical velocity and position from per monitor and not under from the target is the in-phase



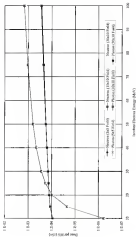


Figure 6.21 Theoretical number and photon dose per molecule and per molecule of the reactant

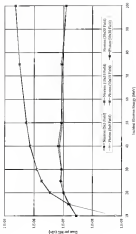


Figure 3-24 Theoretical neutron and photon flux per incident neutron at the apex of the anode.

## CHAPTER 4 SUMMARY AND CONCLUSIONS

The development and implementation of a systematic treatment of photochemical physics for atom-coupled photon-crystal simulations has been presented. This capability is based on the use of evaluated photochemical data as reliable Monte Carlo sampling of simulated data-describing photochemical interactions and the resulting products. As such, it represents the state-of-the-art in simulation capability using the most accurate data available. These new developments have been assessed through the process of verification and validation. Additionally, an initial application to the simulation of medical electron acceleration (MELA) has been presented.

The Evaluated Nuclear Data File (ENDF) format is the international standard for representation of nuclear cross-section data as a complete number. The Cross Section Evaluation Working Group (CSEWG) of the National Nuclear Data Center (NNDC) maintains ENDF/B VI data library containing the recommended values for the United States. For the first time ever, evaluated photochemical data have been made available in this format and they are undergoing review for inclusion into the ENDF/B library.

The Nuclear Theory and Applications Group of the Los Alamos National Laboratory has created the Los Alamos LAJIB cross-section evaluation library that includes evaluated data up to 100 MeV incident energy for photochemical interactions with selected materials. The evaluated data provided are complete descriptions of all possible photochemical reactions. That is, the absorption of the photon and the subsequent

simulation of all secondary particles is handled in a self-consistent manner to describe the spectra of all radiation products, not just neutrons. It is expected that these new photonuclear evaluations will be formally accepted for inclusion in the ENDF/B-VI library by CNEC in a forthcoming meeting.

Further, the International Atomic Energy Agency (IAEA) has maintained a Coordinated Research Project over the last three years with the goal to establish an internationally accepted evaluated photonuclear library. That library and its associated report are expected to be released later in 2000 and will include the evaluations in ENDF format for the major isotopes of interest for photonuclear production. The newly available evaluated data from both T-2 and IAEA represents a first-of-a-kind advancement in this field that will help bring the accuracy in photonuclear simulations that was previously available only to neutron, electron and photonuclear simulations.

The Monte Carlo N-Particle (MCNP) radiation transport code has long represented the state-of-the-art in neutron, electron and photonuclear transport simulations. The reputation of this code is in large measure due to the quality of the data underlying the calculations. The MCNP code uses tabular data that include interaction probabilities with complete descriptions of the resultant particles. These data are maintained in A Compact ENDF (ACE) format derived from evaluated data in ENDF format. The current work has defined a new class of ACE table for the inclusion of photonuclear data and provided a sample data processing code for the conversion of ENDF evaluated photonuclear data into this new ACE format. The LA/CR-photonuclear data available here have been processed in this manner.

The implementation of photoneutron interactions into MCNP has also been processed. This included the definition of new user interface options for specifying the photoneutron data to be used as a transport simulation. The standard definitions available in MCNP have been expanded to accept the specification of photoneutron tables and libraries. In addition, since evaluated photoneutron data may not exist for the corresponding neutron data, provisions have been added to allow the code user to specify the most accurate neutron and photoneutron data separately. The input and output sections of the code have been updated such that the tables are specified for use in read and memory at the standard format.

With the introduction of complete evaluated data and their conversion into ACE formatted tables, the sampling of secondary particles from photoneutron absorption can be performed using the existing ACE sampling routines. Slight modifications to these routines were necessary to ensure the appropriate handling of new incident and emitted particle types. These modified routines have the additional benefit of maintaining the sampling nuclear structure from the latest proton data within the MCNPX code.

The photon collision number within MCNP have been updated to include sampling of photoneutron interactions. This includes accounting for the photoneutron cross section in the distance-to-collision calculation and appropriately sampling secondary particles produced from a photoneutron collision. This coding is fully integrated such that coupled simulation of photon neutron transport uses the standard MCNP framework of routines. The routines that collect, validate reference techniques and summary information all reflect the coupled simulation.

Since the photonuclear interaction is a rare event, a binning scheme has been introduced to enhance the sampling of these events. The code now now has the ability to consider the photonuclear contributions to the radiation field from every photon collision. Further, the photonuclear collision routine has been integrated with the standard MCNP weight-window scheme to ensure that particle weights from photonuclear production do not unreasonably introduce large variations in the tally results. These enhancements significantly reduce the computational run times necessary to achieve statistically valid results.

The accuracy of the results from the new ability to sample coupled photon-neutron radiation transport has also been assessed. Verification of the coding was done to ensure that the newly implemented algorithm performed as expected. Validation of the new data was achieved by comparison of simulation results with two sets of data listed in the literature.

The National Council on Radiation Protection and Measurement (NCRP) provided recommendations for assessing the neutron production and transport around medical electron accelerators [2]. This report documented the method developed by Swanson [31-32] for estimating neutron production. Swanson's work documents neutron yields from electron incident on selected materials. Comparison of calculated yields from the current work to Swanson's revised [32] values shows that the current methodology is able to accurately assess the neutron production within the uncertainty of the underlying experimental data.

The experimental measurements of Barber and George [33] are the defining benchmark for neutron production from electron incident on selected materials.

Comparison between the current calculated yields and the reported values shows agreement to better than 25 percent. These results directly validate those materials for which tabular data and experimental measurement were available. They indirectly validate the methodology used to create the tabular data and provide a basis for hypothesizing that all the available data are probably correct to 25 percent for the prediction of neutron production. Further benchmark data will be necessary to directly conclude this. It should be noted that the difficulties in measuring neutron intensities are well known and for this problem 25 percent uncertainty is considered an excellent first step.

An initial study has been prepared to determine the course future work should take for the accurate assessment of the neutron environment around medical electron accelerators. During the course of this study, it was demonstrated that the electron-photon component of the MIA treatment beam is accurately modeled using current simulation techniques.

However, despite the availability of a coupled simulation code and evaluated photonuclear data, the current simulations are unable to reproduce experimental measurements of neutrons that surround the MIA with an accuracy better than a factor of three. It is concluded that this is primarily due to limitations in the simulation model's description of the materials and their placement within the treatment head of the MIA and to a lesser extent the placement of materials within the surrounding room. The lack of certain isotopic evaluations in the current photonuclear library also introduces a source of error through misidentification from that source not expected to be less than three, mentioned above. Therefore, the first task that must be completed by future work is the

most accurate modeling of the physical space around the medical electron accelerator than has been necessary for electron-photon simulations.

Some interesting results have been obtained from the medical electron accelerator simulation model currently available. It was shown that the neutron dose to a patient during a typical radiotherapy treatment using high-energy photons (20 to 25 MeV) is on the borderlines of what is generally considered acceptable. This was expected and has been a known concern for this type of treatment. This new capability provides a tool which can be used to refine the estimation of the neutron dose and explore the possibilities for reducing it. Of significant note, it was found by this study that tungsten is an excellent neutron shielding material for use in buildings due to its large atomic capture cross section. On the other hand, lead was seen to influence the neutron energy distribution but have negligible effect on the population.

The simulation methodology was also shown to be able to answer the health physics concerns around a typical medical electron accelerator. The model is capable of estimating the direct neutron dose to technicians working near the MHA though further refinement is necessary to reduce the large uncertainties. Future work should first concentrate on refining the simulation model to improve the accuracy. Other work may also be undertaken to quantify the photon dose due to neutron activation of materials within the treatment room and their subsequent gamma-ray decay.

The development and implementation of a systematic treatment of photonuclear interactions in coupled photon neutron simulations paves the way for many follow-on studies. As the effort to integrate the new evaluated data into the transport codes has been carried out under the supervision of staff from the Los Alamos National Laboratory,



these developments are expected to make their way into publicly released versions of the MCNP and MCNPX codes. The dose processing capability for sources of photonuclear ACE files has been integrated into the MCNPX nuclear dose processing code and released last December (1999).

In addition to the innovations discussed above, many other possibilities have been discussed with researchers in this field. Future studies may include the assessment of the charged particle dose to patients undergoing radiotherapy from light ions produced by photonuclear reactions in tissue; the assessment and placement of neutron shielding for both personnel and equipment around electron accelerators used for radiotherapy and radiography; the assessment of the neutron source created by in-flight acceleration of protons undergoing ion-atom nuclear target; the assessment of material compositions for unknown samples by photon spectroscopy, and many other interesting concepts. The capability to simulate photonuclear reactions is therefore offered up with great hope and expectation as to what the future will bring.

## APPENDIX A PHOTONUCLEAR ACE TABLE FORMAT

### Introduction

This appendix documents the class 'u' ACE table format as used by this work. ACE tables are compact versions [A-Compact (ENDF)] of Evaluated Nuclear Data Files (ENDF). The MCNP6 (Multi-Physics/Photonuclear Table) data processing code (described in Chapter 4 and listed in full in Appendix B) converts ENDF formatted data into the ACE 'u' table format as described here. Limitations on the format MCNP6 will handle are discussed in Chapter 4. Data in the ACE class 'u' format can also be used by the photonuclear version of MCNP (described in Chapter 4 and listed in Appendix C) for the simulation of neutron transport.

As the class 'u' format used here departs from the standard ACE format, the descriptions of the data presented here have adapted from those in Appendix F of the MCNP Users Guide [3]. However, many changes have been made to both structure and content of the old format. Comments are included to document where changes have been made and to give guidance on appropriate uses of various representations. This appendix was written to be suitable for inclusion in the appropriate sections in the MCNP [3] and MCNPX [42, 104-110] user guides. Because of this, there is some information that is redundant to Chapter 4.

## Table Layout

There are no changes from the standard ACE table layout. It is presented here as Table A-1. The format is shown describing an ASCII text file. The binary version of the file contains the data in the same order except stored in the machine dependent format for integers, reals and characters, respectively. There is one generally accepted exception from this format: isotopes in the XRD array are typically written in the ASCII file in the (JSD) format for readability although they are stored as real value numbers in the binary file and within the MCMF program.

A standard data library file contains multiple data tables, e.g., the MCFLIB90 library contains one photoelectron data set for each element from hydrogen to platinum. A specific table within the library file is found by looking up its starting line (relative value is RSN) and referencing the data relative to the appropriate starting line. Similarly, when stored as binary data the address of the first entry for the table in question is the absolute starting point.

Table A-1: Standard table description for the photoelectron type 'a' ACE format.

Line Address		Contents	Format (Fortran Standard)
Relative	Absolute		
1	BSN	DATE, Atomic Weight, Temperature, Data Format	A/10, 2B/11-4, 1E, A/10
2	BSN+1	Comment	A/60
3 - 4	BSN+2 - BSN+3	Included fields currently unused (Fill with zeros or leave blank)	A/1, F/11 40 per line
7 - 8	BSN+5 - BSN+6	EXACT(1)-EXACT(2)	A/201 per line
9 - 11	BSN+8 - BSN+10	EXACT(3)-EXACT(5)	A/201 per line
12 -	BSN+11	EXACT(6)-EXACT(20)	A/201 60 per line

### NES Array Elements

Only data common to the whole table are stored in the NES array. Specifically, it contains the information necessary to reconstruct the details within the remainder of the table. Examples of this type of information include the number of energy points used, the number of machine sites contained listed outside the number of secondary periods with operating data. However the details of this table were modified over several iterations, key details about the table format itself are also included here. The significance of each entry in the NES array is documented in Table A-2.

Two elements of the NES array have standard definitions. The first element of the NES array is always the length (number of records) of the DES array. This standardization makes it possible to read in a general table without knowing the details of the table arrays. The second element of the NES array is typically the target identifier.

This document performs its format version test (FVTS=1) of the ACE class 'a' table. For this version of the table, the number of parameter entries in each DES array is two (NPDES=2), the number of entries in each DES array is twelve (NDES=12).

Table A-2 Description of the NES Array elements in a photomicro type 'a' ACE format

Entry	Parameter	Fixed format description
NES(1)	LEN	Length of the DES array (NDES)
NES(2)	TA	Atomic and mass number of the target nucleus $TA = Z^*1000 + A$
NES(3)	NPA	Number of energy points in the target energy grid
NES(4)	NTP	Number of ML points in the machine-type listing
NES(5)	NSTP	Number of secondary particle types with DES information
NES(6)	NPDES	Number of parameter entries (fixed values) in the DES array
NES(7)	NDCS	Number of entries (fixed values and locations) in DES array per secondary particle
NES(8-12)		Unread (fill) with value zero
NES(13)	FVTS	Table Format Version

Parameters are stored within listed first in the array. Other entries are assumed to be located and their values updated as the table is shifted in memory. The maximum number of secondary particles (NTYPE) for which reaction data can be given is eight. This structure and values of the table are subject to revision in which case the table version number will be incremented.

### IXS Array Elements

The IXS array elements contain location in global data contained within the XSD data block. Similar to the NXS elements, global applies to the main energy grid, the cross-sections, additional information associated with each reaction and a pointer to the secondary data array IXS. Location are offsets into the XSD array. Descriptions of the IXS locations are given in Table A-3. For example, the first value for the main energy grid is located at `IXS(002)`.

This format has deviated from the traditional style in that it references all secondary particle reaction data through the use of the IXS construct. The use of the IXS construct was first done for the LAI 50 neutron library (H1,46). This library was constructed for use in MCNPX where existing descriptions for protons, deuterons, tritons, helium-3 and alpha were described in addition to neutrons and photons. The table presented here completes the transition in that all reaction data (including photons and neutrons) are referenced through the IXS array. This was done so that the table is now consistent in its treatment of all secondary particle reaction data. As a result, only data present in the whole table should be referenced from the IXS array.

Another major change is the addition of the location TOT, NDS, ELS and TH4 in section type 'V' tables, the header ESE does quantum duty. This is the energy grid,

Table A-3 Description of the IXS Array elements in a photonic type "w" ACE format.

Index	Location	Effect on array of
IXS(1)	IXS	Mean energy grid
IXS(2)	IXS	Total cross-section data
IXS(3)	MLM	Total non elastic cross-section data
IXS(4)	ICS	Elastic cross-section data
IXS(5)	IXS	Total heating number data
IXS(6)	MTS	MT reaction number
IXS(7)	IXS	Q-value reaction energy data
IXS(8)	IXS	Cross-section location indicator in IXS
IXS(9)	IXS	Property locator for cross-section data
IXS(10)	IXS(4)	First word of IXS array
IXS(11)	IXS	First word of IXS block
IXS(12-15)		Unused (Fill with zeros)

the total cross-section, the absorption cross-section, the elastic cross-section and the heating numbers are referenced through the IXS locator. There have now been separated. The absorption cross-section has been replaced by the non elastic cross-section.

### IXS Block

#### IXS Array

The IXS array is the primary container for the data. Because of this, it is also referred to as the IXS Block. Descriptions of each of the arrays and their associated values as located within the IXS block are presented here. It should be noted that the ACE format uses only one energy grid for all cross-section data and that all cross-sections use linear linear interpolation to determine intermediary values.

## ESZ Array

The ESZ array contains the data entries for the total energy gain. It represents a summat of all energies used by any reaction-cross section listed in the table. Energy values are given in units of MeV. The entries should consist of a series of monotonically increasing, positive values located at  $(XSS(I) - 1) - ESZ$ ,  $ESZ + NXS - 1$ . Duplicate entries are not allowed. Sharp resonances should be represented as increasing over a finite interval to replicate what is a true step change. Error checking should be done to ensure the conditions specified.

## TOT Array

The TOT array contains the data entries for the total cross section. Cross-section values are given in units of barns. There must be an entry corresponding to each entry in the ESZ array and they should be located at  $(XSS(I) - 1) - TOT$ ,  $TOT + NXS - 1$ . Error checking should be performed to ensure that these values are equivalent to the sum of the elastic and non-elastic cross sections. This array must be present.

## NON Array

The NON array contains the data entries for the total non-elastic cross section. Cross-section values are given in units of barns. There must be an entry corresponding to each entry in the ESZ array and they should be located at  $(XSS(I) - 1) - NON$ ,  $NON + NXS - 1$ . Error checking should be performed to ensure that these values are equivalent to the sum of all partial cross sections excluding the elastic and any sub-totals. This array must exist if any non-elastic cross-section data are present.

The non-elastic cross-section is listed rather than the absorption for convenience. If the elastic cross-section has not been included, the non-elastic cross-section is identical

to the total cross-section and MCN should be set equal to TOT and only one set of cross-section entries is needed. One justification for not including the total absorption cross-section is that it does not make physical sense for the photo-nuclear process. Gamma rays are treated for all reactions that do not transition directly to a ground state.

### ELS Array

The ELS array contains the data entries for the elastic cross-section. Cross-section values are given in units of barns. There must be an entry corresponding to each entry in the ESE array and they should be located at (XSS(X) + ELS-ELS+MXS-1). For photo-nuclear physics, the cross-section is negligible and typically is not included in the original evaluation data file. If it is not included, ELS must be set to zero and no entries are included in the XSS array.

### THN Array

The THN array contains the data entries for the average heating numbers, i.e. the average energy deposited per collision. Heating/number values are given in units of MeV per collision. There must be an entry corresponding to each entry in the ESE array and they should be located at (XSS(X) + THN-THN+MXS-1). If no data have been calculated for heating numbers, THN and each PHN entry (see discussion below) must be set to zero and no entries are made in the XSS array.

The total heating number has recently undergone a revision. Since the MCNPS code is capable of transporting small particles of interest, it is necessary to be able to adjust the total heating numbers appropriately. Specifically, in the case of the simulation, the total heating number should be adjusted to represent the average amount of energy deposited per collision as a given material for all particles that are not transported.



In order to obtain an “average” heating number, several assumptions are necessary. Particles that are extremely penetrating, e.g. muons, are assumed to deposit their energy elsewhere. Particles that are of “limited” range, including neutrons and protons, are not considered extremely penetrating. All particles of “limited” range are assumed to deposit their energy continuously at the collision rate. This is a poor description for any reaction that does not approximate an infinite, homogeneous medium with a steady state source.

In order to accurately represent energy deposition, particles for which secondary distributions data exist and should be transported and their contribution to the total heating number subtracted off the total before beginning the simulation. Again, if heating tables are used, it is essential to transport all particles for which continuous, local energy deposition is not a good assumption. Note that the sum of the partial heating numbers (PHNs) given in the table may not add up to the total unless all possible secondary particles (including the recoil particles) are included.

## MTB Array

The MTB array contains the data entries for the reaction type MT numbers.

Reaction type MT numbers are taken directly from the ENDF-III file format manual [4]. There must be one MT value in the array for every reaction cross section to be listed and they should be listed in  $\langle\cos\theta\rangle = 1-MTR, MTR-MTR-1$ . The values should be in ascending order according to their numeric value.

Production cross sections for reaction products of interest may also be listed in the MT array by using the ZA number in place of the ENDF MT number. An isotope's ZA number is defined as the atomic number (Z) times one thousand plus the atomic mass

number (X). For example, Xs would have LA equal to 4099. There is no conflict with MT numbers as the currently defined 17429 MT numbers end at 1000. Note that production cross-sections, i.e. all reactions with a MT value greater than 1000, are not valid for transport and are used only to tally multiplicity.

### LQR Array

The LQR array contains the data values for the Q-value associated with each reaction. Q-values are given in units of MeV. There must be one entry corresponding to each MT array entry and they should be located at  $(LQR(i) - LQR - NTR + 1)$ . For reactions which are not physical events, e.g. production and transmission losses, the Q-value should be given as a zero (0) entry.

### LSD Array

The LSD array contains the values for the cross-section location. Cross-section locations are the array index to the first word of the corresponding MT reaction data relative to the SDG header. There must be one entry corresponding to each MT array entry and they should be located at  $(LSD(i) - LSD - NTR + 1)$ .

### SDG Array

The SDG header is the primary reference for finding the reaction cross-section data. By reaction and for convenience, all reaction cross-section data are listed sequentially in one location within the SDG array. Cross-section values are given in units of barns. Each cross-section header must point to a valid reaction cross-section.

Reaction cross-section data are given over a defined range of energies as the mean energy grid. The format follows the format IS, NE, VALUES where IS is the starting

index corresponding to an entry in the cross-energy grid and NE is the number of entries. Thus the column VALUES(NE) are the reaction cross-section values corresponding to the energies GRID(EL:NE-1). The cross-section values should be located at (XSS(T) + EL-1) \* LARG(EL) + (XN + LARG(EL) \* NE) \* 6 + 1 (NTR) where LARG(EL) is the offset value from the LARG array that corresponds to the ELth reaction (MT) as listed in the MTR array. Error checking should be done to ensure that EL is not less than one, that NE is not greater than NCS and that EL+NE-1 is less than or equal to NCS.

For cross-section data that do not cover the entire energy range of the table, the value of the last entry is assumed to be constant for the remainder of the cross-energy grid. That is, for all energies up to the first entry, the cross-section value of the first entry is used. Therefore, reactions with threshold values must start with a zero-value entry. Finally, reactions which are negligible after a certain energy should contain a zero value as their last entry.

### END Block

The END block is a conceptual digest created to equate the secondary particle information storage structure in the general storage model of the XCS/END/XSS block. It is described with one set of parameters, factors and data in order to help separate it conceptually and make it easier to understand. In reality all the components of the XSS array and its associated data are stored in the XSS block. To stress the point, references to ENDs are equivalent to XSSs. The secondary data should be listed sequentially by particle type and not spread throughout the XSS block.

## DSS Array

The DSS array encodes the parameter/location concept of NODS/LOC for secondary particle information. Since a full set of DSS elements is needed for each secondary particle, there are typically multiple DSS arrays in a table. They are listed sequentially located at  $(\text{DSS}(i) - 1) \times (\text{DSSA} + \text{NODS} \times \text{LOC}) + (\text{DSSA} + \text{NODS} \times i) - 1 \times (\text{NODS} - 1) - 1 + \text{NTYPE}$ . The elements of the DSS array are described in Table A-4.

The phorocoding table differs from the neutron and proton table versions in that parameters specific to a secondary particle are also included in the DSS array. Thus, DSS elements perform functions similar to NOD (parameter) and LOC (location) elements. In practice, they are used in an analogous manner to their conceptual equivalents. For example, for the third (3)-neutron particle the parameter NTRIP(3) (stored as DSS(2,3)) and the location MTRIP(3) (stored as DSS(3,3)) can be used to find the array of MCT reactions that produce that particle located at  $(\text{DSS}(3) - 1) - \text{MTRIP}(3) - \text{MTRIP}(3) + \text{MTR}(3) - 1$ .

Table A-4 Description of the DSS Array elements as a phorocoding type "a" ACE format.

Index	Parameter	Physical description
DSS(1,1)	PT(1)	Particle PT number
DSS(1,1)	NTRIP(1)	Number of MCT reactions producing this particle
Array	Location	Offset to array of
DSS(1,1)	F(1,1)	Total particle production cross section data
DSS(1,1)	W(1,1)	Particle average weighting number data
DSS(1,1)	MTR(1,1)	Particle production MCT reaction numbers
DSS(1,1)	U(1,1)	Reaction coordinate system data
DSS(1,1)	LRSP(1)	Reaction yield fractions (relative to MCT)
DSS(1,1)	SRSP(1)	Primary location for reaction yield data
DSS(1,1)	LSRSP(1)	Reaction reaction distribution locations (relative to ANSP)
DSS(1,1)	ANSP(1)	Primary location for angular distribution data
DSS(1,1)	ENW(1,1)	Energy-weight distribution for MCT (relative to ENW)
DSS(1,1)	ENW(1,1)	Primary location for energy distribution data

This table also differs from source and process tables in that all secondary particle information is referenced through the universal DCL element. That is a change is that the previous table still referenced the incident particle type (neutron data (e.g. neutrons, neutrons out) through the DCL array. Photoproduction neutron data in a photoproduction table are referenced through the DCL array directly as photoneutron or photoproton emission data.

The secondary particles for which data are supplied are identified by the index IPT. These numbers were originally defined by the MCNP code for neutrons, photons and electrons. They have been extended by the MCNPX code to cover the particles of interest in high energy accelerator environments. As the current time, only those particles listed in Table A-1 have emission data available in the table. This is the source of the maximum value limit for the parameter NTYPE.

### FXS Array

This array contains the data values for the total secondary particle production cross sections. Production cross section values are given in units of barns. The data values follow the IE, ME, VALUE format as described in the DGP array section above.

Table A-1 Association of particles with their symbol and IPT index number as defined in MCNP(X)

Particle Name	Symbol (from mcnp card)	IPT
neutron	n	1
photon	p	2
electron	e	3
positron	h	4
deuteron	d	14
triton	t	15
helium-3	h	16
alpha	a	14

and are referenced in the next array grid. The array must exist if any reaction data exist for the particle type and is located at  $(XSS(I)-1)PXS(I)+NS+1$ ,  $J=1,NTYPE$ . Error checking should be done to ensure that the value of each array corresponds to the size of the relevant reaction paths.

### PRN Array

This array contains the data entries for the particle average heating numbers. The data values follow the IS, ME, VALUES format as described in the TRGP array section above and are located at  $(XSS(I)-1)PRN(I)-PRN(I)+ME+1$ ,  $J=1,NTYPE$ . Particle average heating numbers are given in units of MeV per collision. As described in the discussion of the TRM array above, these values are the contribution to the total heating number by this particle type assuming that the particle's average emission energy is deposited locally. Error checking should be done to make sure that PRN is not greater than TRM.

### MTRP Array

This array contains the data entries for the ME reaction type numbers that produce the secondary particle's ME reaction numbers are specified in the same sequence as for the MTR array and are located at  $(XSS(I)-1)MTRP(I)-MTRP(I)+MTRP(I), 1$ ,  $J=1,NTYPE$ . The values should be in ascending numeric order. Error checking should be done to ensure that all MTRP entries correspond to a MTR entry at the IS level.

### TYEP Array

This array contains the data entries for the coordinate system of the reaction producing the secondary particle. The reaction-coordinate-system parameter indicates either the lab system (value = 1) or the center-of-mass system (value = -1) and the entries are located at  $(JSSS(I) - TYEP(I), TYEP(I) + NTER(I) - 1) \quad J=1, NTYPE$ . Error checking should be done to ensure that an entry exists for each reaction and that it contains one of the two allowed values. This setup is different than the TYE array for reaction tables so that multiplicity data are not included in TYEP but instead within the SDP array.

### LSGP Array

This array contains the entries for the reaction yield location. Reaction yield locations are the relative locations of the corresponding MT reaction data in the SDP array. There must be one entry corresponding to each MTER array entry and they should be located at  $(JSSS(I) - LSGP(I), LSGP(I) + NTER(I) - 1) \quad J=1, NTYPE$ . The variable LSGP(I,J) indicates the Kth entry  $(JSSS,SDCP(I)=K, 1 \leq J)$  for the Kth secondary particle.

### SDP Array

The SDP location is the primary reference for locating the reaction yield data. All reaction cross-section data for the secondary particle are listed sequentially within the SDP array. Reaction yields are given either as production cross sections or as multiplicity data. There must be one set of data for each reaction specified in the MTER array and it is located as described under relevant table below.

Production cross-section data are the majority of the two yield descriptions.

Production cross-section values are given in units of barns. Data of this type are typically

Table A-5 Reaction yield data in the form of a production cross-section

Function in ENDF	Parameter	Description
$\text{ENDF}(i)=\text{LSKDF}(K, j)=1$	MTTYPE	11 = Production cross-section
$\text{ENDF}(i)=\text{LSKDF}(K, j)$	R	Scaling factor, in units energy <sup>-1</sup> and
$\text{ENDF}(i)=\text{LSKDF}(K, j)=1$	N	Number of consecutive values
$\text{ENDF}(i)=\text{LSKDF}(K, j)=2$ $\text{ENDF}(i)=\text{LSKDF}(K, j)=\text{NR}+1$	$\text{PXS}(j)$ $j=1, \text{NR}$	Production cross-section values for corresponding MT reactions (linear-linear interpolation)

derived from File 13 of an ENDF evaluation and are therefore labeled with the MFTYPE equal 11. The entries for this reaction yield are described in Table A-5. The average "multiplicity" for the reaction as a function of energy can be calculated from the data by dividing the production cross-section value by the corresponding MT reaction cross-section value.

Alternatively, the multiplicity of the reaction may be used in conjunction with the corresponding MT reaction cross-section to determine the production cross-section. Multiplicity is unitless and implies the number of particles emitted per collision.

Multiplicities can be constant, e.g., for fission reactions like  $(\gamma, 2n)$ , or they can be variable, e.g., for fusion nuclear values. Note that the general reaction, MT 5, can include any combination of true reactions at a variable multiplicity. Also note that fusion values are now included primarily in the array values that specifically in their own array.

Yield data of this type are typically found in File 6 or 12 of the ENDF-6 format and hence are assigned the MFTYPE of 6 or 12. MFTYPE 16 is also allowed due to a backwards compatibility issue arising from the fact that the value 16 has been used in part to indicate MF File 6 yield data on nuclear codes. Yield data for MFTYPE 6, 12 and 16 are described in Table A-3. This table and many of those to follow use the INT



interpolation parameter is defined by *EXTD*. Default DNT values and their associated formulas are listed in Table A-6. Error checking should be done to ensure that all values of *INTMULT* result in integers in the INTS listing.

This description provides a concise method to define a varying yield. For example, the MT 5 general reaction has a list of energy/yield pairs which is typically shorter than the defining the corresponding production cross section. The disadvantage of this format is that it requires the listing of the mass number and the yield followed by a multiplication of the two to obtain the production cross section.

Table A-7 Reaction yield data in the form of reaction multiplicity

Listing in XS	Parameter	Description
$DS+SC(PJ)+LSIG(RJ)+1$	MTYPE	6, 12 or 16 - Reaction multiplicity
$DS+SC(PJ)+LSIG(RJ)$	INTMULT	Int. reaction in which multiplicity varies
$DS+SC(PJ)+LSIG(RJ)+1$	NR	Number of interpolations required for multiplicity data ( $INTN=0$ , NRT and DNT are omitted and linear interpolation is assumed across all points)
$DS+SC(PJ)+LSIG(RJ)+1$ $DS+SC(PJ)+LSIG(RJ)+1+NR$	NR(I) $I=1, NR$	Starting index to which the corresponding interpolation parameter applies
$DS+SC(PJ)+LSIG(RJ)+3+NR$ $DS+SC(PJ)+LSIG(RJ)+3+1+2*NR$	INT(I) $I=1, NR$	INTD defined interpolation parameters
$DS+SC(PJ)+LSIG(RJ)+3+2*NR$	NE	Number of energies at which the multiplicity is defined
$DS+SC(PJ)+LSIG(RJ)+3+2*NR$ $DS+SC(PJ)+LSIG(RJ)+3+1+2*NR+NE$	E(I) $I=1, NE$	Energy grid on which multiplications are defined
$DS+SC(PJ)+LSIG(RJ)+3+1+2*NR+NE$ $DS+SC(PJ)+LSIG(RJ)+3+3+2*NR+2*NE$	Y(I) $I=1, NE$	Multiplicity (production cross section = reaction MT cross section * multiplicity)

## LANDP Array

This array contains the entries for the angular distribution locations. An angular distribution location is the location of the angular distribution data for the corresponding MT reaction relative to the ANDP location. There must be one entry corresponding to each MTBP array entry and they should be located as  $(XSDG(i)-1) \times LANDP(i)$ .  $LANDP(i) = (NTYPE-1) \times (NTYPE-1) \times LANDP(K,i)$  is the  $K$ th entry for the  $i$ th secondary particle type.

Several LANDP array values have special meanings. A zero (0) location value indicates a reaction where all particles are emitted isotropically in the reference frame defined by the corresponding entry in the TTBP array. Calculated energy/angle data are indicated by a negative one (-1) location value. In this case, the angular distribution data are included with the energy resonance distribution data in the ELWF array. For both cases, no angular data are entered in the ANDP array. All other locations must be positive integer values and indicate that the angular distribution data are included in the ANDP array.

## ANDBP Array

The ANDBP location is the primary reference for finding angular distribution data. All angular distribution data for the secondary particles are listed sequentially in this array. Three types of angular distribution table are currently allowed: isotropic, 10 equi-probable bins or calculated angular bin data. There must be one set of distribution data for each reaction specified in the MTBP array that is either isotropic or calculated energy/angle. The angular distribution data is located as described in the reference table.

Table A-4: Interpolation schemes as defined for the ANDP  $\beta$  dataset

Interpolation Scheme	DOF Value	Interpolation Equation
Bi-linear	0	$y(x) = y(0)$
Linear-Linear	1	$y(x) = \frac{y_1 - y_0}{x_1 - x_0}(x - x_0) + y_0$
Log-Linear	2	$y(x) = \frac{y_1 - y_0}{\ln\left(\frac{x_1}{x_0}\right)} \ln\left(\frac{x}{x_0}\right) + y_0$
Linear-Log	3	$y(x) = \exp\left(\frac{y_1 - y_0}{\ln\left(\frac{x_1}{x_0}\right)} \ln\left(\frac{x}{x_0}\right)\right) + y_0$
Log-Log	4	$y(x) = \exp\left(\frac{\ln\left(\frac{x_1}{x_0}\right)}{\ln\left(\frac{x_1}{x_0}\right)} \ln\left(\frac{x}{x_0}\right)\right) + y_0$

If all reactions are complete or completed/ongoing (i.e. no data are present in the ANDP array), ANDP should default to zero.

The regular distribution data are a set of tables comparing the average reaction rates for the 16 substrate profiles among the 16 reactions. These tables are located among the regular distribution loader information as described in Table A-2. An example of how to find a particular loader in the ANDP array is given here. The appropriate regular distribution loader information for the second reaction listed in MTRP producing the third secondary-structure particle starts at the array location `GOSS(ANDP(3)+LANDP(1,1)-1, ANDP(3))` is the sixth DOF value for the third reaction particle (`DOF(3)`) and `LANDP(2,2)` is the value of the second entry in the `LANDP` array for the third reaction particle (`DOSS(DO)(16,2)-(1+2)`).

Table A-5 Angular-distribution loader information

Location in XDR	Parameter	Description
$ANDEF(I)+LANSDEF(I)-1$	NR	Number of ranges of which angular distributions are calculated
$ANDEF(I)+LANSDEF(I)$	EA(I)	Energy grid for the $k$ th reaction angular distribution
$ANDEF(I)+LANSDEF(I)+NR(I)$	L=0, NR	
$ANDEF(I)+LANSDEF(I)+NR(I)$	L=1, NR	
$ANDEF(I)+LANSDEF(I)+2*NR(I)$	L=0, NR	

Once the angular-distribution loader information is located, the incident energy is used to find the loader for the appropriate angular data table. Positive loaders indicate  $l=0$  equi-probable loaded data, zero loaders indicate anisotropic distributions and negative loaders indicate calculated angular data. Isotropic distributions have no further data entries.

Angular Law 1 is  $l=0$  equi-probable loaded cosine angles. It has been the traditional method used to represent angular distributions. A positive value for the angular data loader indicates it contains Angular Law 1 data. This data consists of 73 cosine angle bin boundaries which mark the points  $1/52$  apart in cumulative probability density. These locations in the ANEP array is described in Table A-10. The cosine of the scattering angle is chosen by linear-linear interpolation of a randomly chosen point in the cumulative density space. This method's primary advantages are its speed of execution and small memory requirements. As memory and CPU power are much more readily available today than when this method was first conceived, it is no longer recommended for use.

The Angular Law 2 tabulated angular distribution was recently introduced [111] to more accurately reproduce highly anisotropic scattering distributions. It is generally

Table A-11 Description of Angular Law 1: 12 equ-probable law angular distribution table.

Location in XDB	Parameter	Description
ANGP(1)+LC(L,1)	NA	First row of angular distribution data for nucleus energy point L.
ANGP(1)+LC(L,1)	LC(L)	LC(L) is given data size
ANGP(1)+LC(L,1+1)	Cx(Bx)	Center angle boundaries of the 12 equ-probable scattering bins

accepted that distributions with very anisotropic behavior, in particular very forward peaked distributions, are not well represented by Angular Law 1. Specifically, the detail of the high-probability area is well represented in the squares of the amplitudes of the distribution. Angular Law 2 distributions remedy this by allowing a relative distribution of points. The description for Angular Law 2 data is given in Table A-12. The scattering angle is chosen based on the random sampling of the normalized probability-density with proper normalization of its corresponding center value.

### LSL/WF array

This array contains the entries for the energy distribution locations. An energy distribution location is the location of the entrance law data file for the corresponding MT reaction relative to the LSL/WF location. There must be one entry corresponding to each MTWP array entry and they should be located in `(COB(2))`

$J = \text{LSL.WF}(J)$ ,  $\text{LSL.WF}(J) + \text{NTWP} - 1$ ,  $J = 1, \text{NTWP}$ : The elastic reaction is now explicitly included/here of the data set included. All locations must be positive integer values and indicate that entrance distribution data set contained in the LSL/WF array.

Table A-11: Description of Angular Law 2 tabulated angular distributions table

Location in XML	Parameter	Description
ANDEF(1)=LCEL(1)-1	NA	First row of angular distribution data for incident energy point 1. LCEL(1) is first data row.
ANDEF(2)=LCEL(2)-1	LI	Interpolation parameter for cosine distribution (NDEF defined interpolation parameters (Only histograms or linear-linear is allowed)).
ANDEF(3)=LCEL(3)	NT	Number of points in the distribution.
ANDEF(4)=LCEL(4)-1	CN(M)	Center of the scattering angle.
ANDEF(5)=LCEL(5)+NP	M=1..NP	Probability density function.
ANDEF(6)=LCEL(6)+1+NP	PDF(M)	
ANDEF(7)=LCEL(7)+1+2*NP	M=1..NP	Cumulative density function.
ANDEF(8)=LCEL(8)+2+2*NP	CDF(M)	
ANDEF(9)=LCEL(9)+1+3*NP	M=1..NP	

## BLWF Array

The BLWF location is the primary reference for finding resonance distribution data. All resonance distribution data for this secondary particle are listed sequentially in the BLWF array. Typically, the resonance data described here are the energy spectra for the secondary particle. However, many new data evaluations are taking advantage of the correlated-energy and angle, resonance distributions. If the angular distribution data are contained in the resonance distribution, the corresponding L/NDEF entry must be negative and (-1). For all other cases, there must be a corresponding set of entries, as located by L/NDEF and A/NDEF, to describe the appropriate angular distribution. There must be at least one set of resonance data for each reaction specified in the MTRF array.

**Law Header:** Each reaction has at least one resonance distribution associated with it as described in the relevant law header substructure data. The entries in the law header information data are described in Table A-12. That header exists to facilitate describing reactions that require more than one coupling law to describe the resonance parameters.

correctly. An example of this would be second-order fluxes. The low loader containing the appropriate random distribution(s) for the second random producing the third random particle starts at the array location  $(XSS(OLWIP(2)+LDLWIP(2,2)-1))$ . Here  $OLWIP(2)$  is the results DES value for the third-random particle ( $XSS(11,2)$ ) and  $LDLWIP(2)$  is the second entry in the LDLWIP array for the third random particle ( $XSS(XSS(11,2)-1)$ ).

Table A-12: Ensemble parameter low loader information.

Location in XSS	Parameter	Description
$LDLWIP(2)+LDLWIP(X,2)-1$	$LNR$	Location of next low loader relative to $LDWIP(2)$ . If $LNR = 0$ , then this low is used repeatedly.
$LDWIP(2)+LDLWIP(X,2)$	$LAW$	Start ID of this low.
$LDWIP(2)+LDLWIP(X,2)-1$	$LDAT$	Location of low dependent data relative to $LDWIP(2)$ .
$LDWIP(2)+LDLWIP(X,2)-2$	$NB$	Number of nonpolynomial regions, if $NB = 0$ , $NBT$ and $DNT$ are omitted and linear-linear interpolation is assumed for all points.
$LDWIP(2)+LDLWIP(X,2)-1$ $LDWIP(2)+LDLWIP(X,2)+3+NB$	$NBT(1)$ $1-1-NB$	Starting index to which the corresponding interpolation parameter applies.
$LDWIP(2)+LDLWIP(X,2)+1+NB$ $LDWIP(2)+LDLWIP(X,2)+2+2*NB$	$NBT(2)$ $2-1-NB$	ENOV defined interpolation parameter in each region.
$LDWIP(2)+LDLWIP(X,2)+3+2*NB$	$NB$	Number of regions.
$LDWIP(2)+LDLWIP(X,2)+4+2*NB$	$MD$	Total energy point.
$LDWIP(2)+LDLWIP(X,2)+5+2*NB+NB$	$1-1-NB$	
$LDWIP(2)+LDLWIP(X,2)+4+2*NB+NB$ $LDWIP(2)+LDLWIP(X,2)+5+2*NB+2*NB$	$P(1)$ $1-1-NB$	Probability of low velocity.
$LDWIP(2)+LDLWIP(X,2)-1$	$LDAT$	First word of low dependent data for $LNR$ .
$LDWIP(2)+LNR-1$	$LNR_{end}$	First word of next low loader.

Once the appropriate low header is located, the specific nucleus-distribution is determined based the probability of its validity at the incident energy. Because of the number of laws that can be used, the description of the remainder of the entry can be daunting. The key to remember is that each nucleus producing a group-particle has a low header that provides the location of the appropriate sampling law. Each of the laws and their associated data is described in subsection below. The variable *L* always indicates the *L*th nucleus particle and the variable *K* always indicates the *K*th nucleus producing that particle.

**Energy Law 1.** Energy Law 1 uses an equal-probability energy bin structure for sampling nucleus energies. Its data format is described in Table A.13. It is similar in nature to the Angular Law 1 and differs from the same lack of ability for distributions with groupings of high-probability regions. It is recommended to use Energy Law 4, tabulated-energy-distribution, instead. Error checking should be done to ensure that each  $E_{L,K}$  table is a set of monotonically increasing real values ending with a value less than the corresponding  $E_{L,K}$ .

**Energy Law 2.** Energy Law 2 is primarily for discrete photon nucleus laws produced by neutron interactions. Its data format is described in Table A.14. Its use is discouraged with photon nuclei reactions though it is possible to use it as a discrete law nucleus, i.e.  $E_{L,K} = E_0$ , for LP=0 or LP=1. Use of the LP=2 option is strongly discouraged for photopion reactions as it requires explicit neutron interactions for computing the nucleus energy, i.e.  $E_{L,K} = E_0 + [(A_H^2 V)/(A_H^2 V + C)] * E_n$ . Error checking should be done to ensure that LP is in the range 0 to 2 and that  $E_0$  is a positive real value



Table A-13: Law dependent format for Energy Law 1 (Tabular representation of Energy Band)

Label(s) in XML	Parameter	Description
LDAT[1]=E <sub>band</sub> [1]-1	E <sub>band</sub> [N] N=1..N <sub>E</sub>	Primary reference for law, dependent data (from law header)
LDAT[1]	N <sub>E</sub>	Number of energy law regions (N <sub>E</sub> =0, N <sub>E</sub> T and N <sub>E</sub> T are treated and linear-linear interpolation is ignored)
LDAT[2] LDAT[1]+N <sub>E</sub>	N <sub>E</sub> T[N] N=1..N <sub>E</sub>	Scaling factor for which the corresponding interpolation parameter applies
LDAT[2+N <sub>E</sub> ] LDAT[1]+2*N <sub>E</sub>	N <sub>E</sub> T[N] N=1..N <sub>E</sub>	ENM defined interpolation parameter at each region Only logarithmic or linear-linear
LDAT[3+2*N <sub>E</sub> ] LDAT[1]+2*N <sub>E</sub>	N <sub>E</sub>	Number of applied energies calculated
LDAT[3+2*N <sub>E</sub> ] LDAT[1]+2*N <sub>E</sub> +N <sub>E</sub>	N <sub>E</sub> [N] N=0..N <sub>E</sub>	Law of incident energies for which E <sub>max</sub> is calculated
LDAT[3+2*N <sub>E</sub> +N <sub>E</sub> ]	N <sub>E</sub> T	Number of outgoing energies based on each E <sub>max</sub> value
LDAT[4+2*N <sub>E</sub> +N <sub>E</sub> ] LDAT[3+2*N <sub>E</sub> +(N <sub>E</sub> T+1)*N <sub>E</sub> ]	E <sub>max</sub> [N] N=1..N <sub>E</sub> T, E <sub>max</sub> [N] N=1..N <sub>E</sub> T, E <sub>max</sub> [N] N=1..N <sub>E</sub> T	E <sub>max</sub> table have N <sub>E</sub> T energies listed comprising the boundaries of (N <sub>E</sub> T+1) representative bins. Sampling uses a linear-linear interpolation between bin boundaries

**Energy Laws 1 & 33.** Energy Law 3 and 33 are uniform level scattering. The data format is described in Table A-15. Law 3 defines neutron incident neutron energies. Law 33 indicates any combination of particle surface and material. Its use is allowed for photouclear interactions though the parameters must be chosen for photouclear/kinetic instead of neutron kinetic. Sampling of this law follows the simple formula of  $P_{E_{max}} = (LDAT[3] + (E_{max} - LDAT[3]) \cdot (E_{max} - LDAT[3])$  in the center-of-mass system. Care checking should be done to ensure that the corresponding TYP entry is negative one.

Table A-14: Line-dependent format for Energy Law 2 (Discrete Emission Energy)

Location in XML	Parameter	Description
DISMPL2+EDAT-1	LEDA3[edq] M=1,2	Primary reference for line, dependent data (from line header)
EDAT(1)	LP	Indicator of whether the emission particle is primary or not, primary
EDAT(2)	EG	Emission energy (if LP=0 or LP=1), Binding energy (if LP=2), ...

Table A-15: Line-dependent format for Energy Law 3/3 (Level-Broadening)

Location in XML	Parameter	Description
DISMPL3+EDAT-1	LEDA3[M] M=1,2	Primary reference for line, dependent data (from line header)
EDAT(1)	MT	Parameter controlling $(\Delta E)^2/\Delta E^2 \propto E^2$
EDAT(2)	CB	Parameter controlling $\Delta E/\Delta E \propto E^2$

### Energy Laws 4, 4B & 4C: Energy Laws 4, 4B and 4C are relative energy

distributions. The common portion of the data format for this set of laws is described in Table A-16. The relative energy distribution provides the most flexibility of the energy laws. Any energy-distribution-spectral shape can be formed provided enough grid points are used. Energy sampling is accomplished by determining the two closest standard energy grid points, sampling a random-transmission probability to find the emission energy from each grid and using histogram or linear-linear interpolation between them. If discrete laws are used on the emission grid, correspondences of these laws must be maintained between grids. Error-checking should be done to ensure only histogram or linear-linear interpolation between distributions is used and to ensure that discrete lines are correctly handled. The format of the relative distributions will be dependent on which law is specified.

Table A-16: Low dependent format for Energy Law 4, 4B and 4C (Tabular Energy Distributions)

Location in XDS	Parameter	Description
LDAT(1)=LDAT-1	LDAT(M) M=1, L	Primary reference for law, dependent data (from law header)
LDAT(1)	NB	Number of interpolation regions (if NB=0, NBT and DYT are needed and linear-linear interpolation is assumed)
LDAT(2) LDAT(1)+NB	NBT(M) M=1, NB	Scaling index in which the corresponding interpolation parameter applies
LDAT(1)+NB LDAT(1)+1*NB	DYT(M) M=1, NB	EWB defined interpolation parameter in each region, only integrate and linear-linear interpolation are allowed
LDAT(1)+2*NB	NB	Number of excited energies calculated
LDAT(1)+2*NB LDAT(1)+2*NB+NB	EN	List of excited energies
LDAT(1)+2*NB+NB LDAT(1)+2*NB+NB+1	LY(M) M=1, NB	Location for tabular distribution values in LDAT(M)

Energy Law 4 contains only energy-emission information. Its data format is described in Table A-17. Angular distribution data must be included using the AMDF array. Sampling is achieved by choosing a random number between zero and one, finding the cumulative bin in which the random number falls and taking the corresponding energy, appropriately interpolated. Error checking should be done to ensure that the largest emission energy for any undeformed reaction is not more than its corresponding incident energy, that the probability density function integrates to the constant and that the cumulative density is monotonically increasing from zero to one.

The tabular distribution format for Energy Law 4B expands the Law 4 format to include the Kallbach parameters for each emission energy. Its data format is described in Table A-18. The parameters are used to compute the angular distribution based on the

Table A-17 Tabular distribution format for Energy Law 8 (Tabular energy distribution)

Location & XIS	Parameter	Description
DLWPLD+LTBN(-)	N/A	First word of tabular distribution data for random energy point N
DLWPLD+LTBN(+)	INT	Overloaded variable: Interpolation scheme for distribution mod(INT,10) = 1 $\rightarrow$ Histogram mod(INT,10) = 2 $\rightarrow$ Lin-Lin Number of discrete points in distribution ND = abs(INT) / 10
DLWPLD+LTBN(-)	NP	Number of points in the distribution
DLWPLD+LTBN(+)	ELOC	Random energy grid
DLWPLD+LTBN(+)+NP	Q=1 NP	
DLWPLD+LTBN(+)+1*NP	PDF(X)	Probability density function
DLWPLD+LTBN(+)+2*NP	Q=1 NP	
DLWPLD+LTBN(+)+3*NP	CDF(X)	Cumulative density function
DLWPLD+LTBN(+)+4*NP	Q=1 NP	

Table A-18 Tabular distribution format for Energy Law 44 (Kallén's corrected energy-angle distribution)

Location & XIS	Parameter	Description
DLWPLD+LTBN(-)	N/A	First word of tabular distribution data for random energy point N
DLWPLD+LTBN(+)	INT	Overloaded variable: Interpolation scheme for distribution mod(INT,10) = 1 $\rightarrow$ Histogram mod(INT,10) = 2 $\rightarrow$ Lin-Lin Number of discrete points in distribution ND = abs(INT) / 10
DLWPLD+LTBN(-)	NP	Number of points in the distribution
DLWPLD+LTBN(+)	ELOC	Random energy grid
DLWPLD+LTBN(+)+NP	Q=1 NP	
DLWPLD+LTBN(+)+1*NP	PDF(X)	Probability density function
DLWPLD+LTBN(+)+2*NP	Q=1 NP	
DLWPLD+LTBN(+)+3*NP	CDF(X)	Cumulative density function
DLWPLD+LTBN(+)+4*NP	Q=1 NP	
DLWPLD+LTBN(+)+5*NP	ELOC	Kallén pre-compound function r
DLWPLD+LTBN(+)+6*NP	Q=1 NP	
DLWPLD+LTBN(+)+7*NP	ACD	Kallén-Chabrowski angular distribution slope value s
DLWPLD+LTBN(+)+8*NP	Q=1 NP	

**Kalbach-IT formalism [56,57].** For photouclear reactions, the slope value must be computed at the time the table was produced according to Chabach's modification [31] to Kalbach's original formalism. Sampling of Low-*W* neutron energy is being run in Low-*W*. Error checking should be done to ensure that the value for all *W* entries is  $\pi$  (the slope from zero to one) and that the value for all *W* entries is a non-negative real number.

Currently, the neutron angle in MCNP is sampled using Kalbach's original formalism. It is under discussion whether a new law should be added to address the fact that secondary particle emission from photouclear multi-step compound reactions is more correctly represented as isotropic. Due to the relatively small  $\pi$  values typical of photouclear reactions, this would be a small, less than five percent, correction.

The tabular distribution format for Energy Law 41 expands the Low-*W* format to include a pointer to an angular distribution. Its data format is described in Table A-13. For every angular distribution location within a tabular angular distribution, if available, and it is sampled by the same algorithm as Angular Law 2 data. Table A-13 describes the data format for Low-*W* tabular angular distribution data. A zero value for a location indicates an isotropic distribution. Angular Law 1 data is not allowed. All stipulations for Law 4 will apply to the energy distribution and all stipulations for Angular Law 2 data apply to relevant angular information. Error checking should also be done to ensure that the value of all angular locations is either zero or a positive integer value.

**Energy Law 5.** Energy Law 5 is a temperature scaled equal-probable biased function. Its data format is described in Table A-11. At the current time, no Los Alamos National Laboratory supported library uses this law. The maximum energy is computed

Table A-19: Tabular distribution format for Energy Law 41 (Overloaded cellular many-particle distribution).

Location in XML	Parameter	Description
DLWP(J)+LTDN(J)-1	N/A	First record of tabular distribution data for nucleus energy point N
DLWP(J)+LTDN(J)-1	INT	Overloaded reaction interpolation scheme for distribution $\text{mod}(\text{INT}, 10) = 1 \rightarrow$ Histogram $\text{mod}(\text{INT}, 10) = 2 \rightarrow$ Lin. Lin Number of discrete points in distribution $ND = \text{int}(\text{INT} / 10)$
DLWP(J)+LTDN(J)	DP	Number of points in the distribution
DLWP(J)+LTDN(J)+1	E <sub>min</sub> (J)	Minimum energy grid
DLWP(J)+LTDN(J)+ND	Q=1 DP	
DLWP(J)+LTDN(J)+1+ND	PDF(J)	Probability density function
DLWP(J)+LTDN(J)+2+ND	Q=1 DP	
DLWP(J)+LTDN(J)+1+2+ND	CDF(J)	Cumulative density function
DLWP(J)+LTDN(J)+3+ND	Q=1 DP	
DLWP(J)+LTDN(J)+4+3+ND	LADN(J)	Angular distribution function
DLWP(J)+LTDN(J)+4+ND	Q=1 DP	

Table A-20: Tabular angular distribution format for Energy Law 41

Location in XML	Parameter	Description
DLWP(J)+LADN(J)-1	N/A	First record of tabular angular distribution data for nucleus energy Q
DLWP(J)+LADN(J)-1	Q	Isorelaxation parameter for cosine distribution (Only histogram or (post-hoc) filtered)
DLWP(J)+LADN(J)	DP	Number of points in the distribution
DLWP(J)+LADN(J)+1	CEN(J)	Center line boundaries
DLWP(J)+LADN(J)+ND	P=1 DP	
DLWP(J)+LADN(J)+1+ND	PDF(J)	Probability density function
DLWP(J)+LADN(J)+2+ND	P=1 DP	
DLWP(J)+LADN(J)+1+2+ND	CDF(J)	Cumulative density function
DLWP(J)+LADN(J)+3+ND	P=1 DP	

Table A-21. Low dependent format for Energy Law 1 (General Spectrum)

Location in File	Parameter	Description
DATA(1)=IDAT, 1	LOG(M)	Primary reference for law, dependent from (from law header)
DATA(2)	NR	Number of interpolation regions (if NR=0, NRT and NIT are ignored and linear linear interpolation is assumed)
DATA(3), DATA(1)+NR	MIN(M) M=1..NR	Starting index to which the corresponding interpolation parameter applies
DATA(3+NR).. DATA(1+2*NR)	INT(M) M=1..NR	EXTR defined interpolation parameter in each region
DATA(3+2*NR)	NE	Number of incident energies selected
DATA(1+2*NR), DATA(1+2*NR+NR)	E <sub>0</sub> (M) M=1..NR	List of incident energies
DATA(1+2*NR+NR)	T(M) M=1..NR	Temperature based on incident energy
DATA(1+2*NR+2*NR)	NT	Number of S <sub>0</sub> selected
DATA(1+2*NR+2*NR), DATA(1+2*NR+2*NR+NR(T))	S <sub>0</sub> (S) S=1..NRT	Totals and probability functions

by multiplying a nuclear temperature based on the incident energy times a randomly sampled exp. probability based cross-section probability. This law has been superseded by the use of Law-6 distributions. It is not recommended for use for any purpose.

**Energy Law 7.** Energy Law 7 is a single Maxwell-Boltzmann spectrum as defined in File 1 of EXTR-4. Its data format is described in Table A-21. It is appropriate for all fusion reactions including photoneuclear fusion. The sampled maximum energy is based on the function  $(E_0 - E_{thr}) = C \exp(E_{thr}) \exp(-E_{thr}/T(E_0))$ . The maximum energy is limited by the range due to the incident energy minus the reaction energy.

**Energy Law 8.** Energy Law 8 is an evaporation spectrum as defined in File 2 of EXTR-4. Its data format is described in Table A-21. It is appropriate for nuclear

Table A-20 Low-dependent format for Energy Law 1 (Sample Maxwell-Boltzmann Spectrum)

Location in XML	Parameter	Description
ELNVP(1)+ELDAT, 1	ELDAT(M)	Primary reference for low, dependent data (from low header)
ELDAT(1)	NB	Number of interpolation regions (if NB=0, NBT and INB are ignored and linear-linear interpolation is assumed)
ELDAT(2) ELDAT(1)+NB	NBT(NB) N=1..NB	Starting index to which the corresponding interpolation parameter applies
ELDAT(3+NB) ELDAT(1)+2*NB	INB(NB) N=1..NB	INB defined interpolation parameter in each region
ELDAT(3+2*NB) ELDAT(1)+2*NB	NI	Number of incident energies selected
ELDAT(3+2*NB) ELDAT(3+2*NB+NB)	ELI(NI) N=1..NI	List of incident energies
ELDAT(3+2*NB+NB) ELDAT(3+2*NB+2*NB)	TEMP	Temperature based on incident energy
ELDAT(3+2*NB+2*NB)	U	Excitation energy

Table A-21 Low-dependent format for Energy Law 2 (Evaporation Spectrum)

Location in XML	Parameter	Description
ELNVP(2)+ELDAT, 1	ELDAT(M)	Primary reference for low, dependent data (from low header)
ELDAT(1)	NB	Number of interpolation regions (if NB=0, NBT and INB are ignored and linear-linear interpolation is assumed)
ELDAT(2) ELDAT(1)+NB	NBT(NB) N=1..NB	Starting index to which the corresponding interpolation parameter applies
ELDAT(3+NB) ELDAT(1)+2*NB	INB(NB) N=1..NB	INB defined interpolation parameter in each region
ELDAT(3+2*NB) ELDAT(1)+2*NB	NI	Number of incident energies selected
ELDAT(3+2*NB) ELDAT(3+2*NB+NB)	ELI(NI) N=1..NI	List of incident energies
ELDAT(3+2*NB+NB) ELDAT(3+2*NB+2*NB)	TEMP	Temperature based on incident energy
ELDAT(3+2*NB+2*NB)	U	Excitation energy



emission from a compound nuclear decay. The sampled emission energy is based on the function  $\phi(E \rightarrow E_{\text{max}}) = C \cdot E_{\text{max}} \exp(-E_{\text{max}}/T(E))$ . The emission energy is bounded by the range from the incident energy minus the entrance energy

**Energy Law 11** Energy Law 11 is an energy-dependent Weibull function as defined in File 1 of ENDF-6. Its data format is described in Table A-24. The sampled emission energy is based on the function  $\phi(E \rightarrow E_{\text{max}}) = C \cdot \exp(-E_{\text{max}}/a(E)) \cdot \text{mbh}(E) \cdot \exp(-E_{\text{max}}/b(E))$ . The emission energy is bounded by the range from the incident energy minus the entrance energy

**Energy Law 12** Energy Law 12 is a tabular linear function from UK Law 2 (for reference currently available). Its data format is described in Table A-25 and Table A-26. It is not recommended for use in photonuclear tables. It is similar to Law 1 and Law 4 in that an incident energy is used to sample a tabulated distribution. However, the table is always chosen as the next distribution under the incident energy and no interpolation is done. Emission energy is sampled by choosing a random number in the range zero to one, finding the cumulative bin just before the sample and using the corresponding constant and temperature in the formula  $E_{\text{em}} = EM^2/(E_{\text{in}} - T)$ .

**Energy Law 13** Energy Law 13 is a tabular energy-multiplication distribution from UK Law 4 (for reference currently available). Its data format is described in Table A-27. It is not recommended for use by photonuclear tables. It is similar to Law 1 and Law 4 in that an incident energy is used to sample a tabulated distribution. However, the table is always chosen as the next distribution under the incident energy and no interpolation is done. Emission energy is sampled by choosing a random number in the range zero to

Table A-24 Low dependent format for Energy Law 11 (Energy Dependent Wien Spectrum)

Location in File	Parameter	Description
DATA(1)=DATA(1)	DATA(1) NPT, 1	Primary reference for law, dependent law (Ergo law, factor)
DATA(2)	NR <sub>1</sub>	Number of interpolation regions (NPT <sub>1</sub> =4, NPT <sub>1</sub> and ENT <sub>1</sub> are omitted and linear-linear interpolation is assumed)
DATA(3) DATA(1)=NR <sub>1</sub>	NPT <sub>1</sub> (N) N=1..NR <sub>1</sub>	Starting index to which the corresponding interpolation parameter applies
DATA(2)=NR <sub>1</sub> DATA(1)=2*NR <sub>1</sub>	ENT <sub>1</sub> (N) N=1..NR <sub>1</sub>	ENCF defined interpolation parameter in each region
DATA(3)=2*NR <sub>1</sub>	NR <sub>2</sub>	Number of incident energies included
DATA(1)=2*NR <sub>1</sub> DATA(2)=2*NR <sub>1</sub> +NR <sub>2</sub>	E <sub>0</sub> (N) N=1..NR <sub>2</sub>	List of incident energies
DATA(3)=2*NR <sub>1</sub> +NR <sub>2</sub> DATA(1)=2*NR <sub>1</sub> +2*NR <sub>2</sub>	a(0) N=1..NR <sub>2</sub>	Energy dependent parameter a
DATA(1)=2*NR <sub>1</sub> +2*NR <sub>2</sub> Let W = 3+2*NR <sub>1</sub> +2*NR <sub>2</sub>	NR <sub>3</sub>	Number of interpolation regions (NPT <sub>1</sub> =4, NPT <sub>1</sub> and ENT <sub>1</sub> are omitted and linear-linear interpolation is assumed)
DATA(W+1) DATA(W+NR <sub>3</sub> )	NPT <sub>2</sub> (N) N=1..NR <sub>3</sub>	Starting index to which the corresponding interpolation parameter applies
DATA(W+1)=NR <sub>3</sub> DATA(W)=2*NR <sub>3</sub>	ENT <sub>2</sub> (N) N=1..NR <sub>3</sub>	ENCF defined interpolation parameter in each region
DATA(W+1)=2*NR <sub>3</sub>	NR <sub>4</sub>	Number of incident energies included
DATA(W+1)=2*NR <sub>3</sub> DATA(W+1)=2*NR <sub>3</sub> +NR <sub>4</sub>	E <sub>0</sub> (N) N=1..NR <sub>4</sub>	List of incident energies
DATA(W+1)=2*NR <sub>3</sub> +NR <sub>4</sub> DATA(W+1)=2*NR <sub>3</sub> +2*NR <sub>4</sub>	b(0) N=1..NR <sub>4</sub>	Energy dependent parameter b
DATA(W+1)=2*NR <sub>3</sub> +2*NR <sub>4</sub>	U	Restoration energy

Table A-25. Law dependent format for Energy Law 22 (Tabular Linear Functions)

Location in XML	Parameter	Description
DLNTP(1)=DLNTP(1)	LOC(1)	Primary reference for law, dependent data from law header
LDAT(1)	NR	Number of interpolation regions
LDAT(2) ... LDAT(N)=NR	NR(N) N=1..NR	Starting index to which the corresponding interpolation parameter applies
LDAT(2+NR) ... LDAT(1+2*NR)	DT(N) N=1..NR	Interpolation parameter at each region (quoted, brackets required)
LDAT(3+2*NR)	NR	Number of random energies (calculated)
LDAT(1+2*NR) LDAT(3+2*NR)=NR	LTR(N) N=1..NR	Locations for tabular distributions (given in DLNTP(2))

Table A-26. Tabular distribution format for Energy Law 22

Location in XML	Parameter	Description
DLNTP(2+LTR(N))	NLA	First word of tabular distribution data for reaction energy point N
DLNTP(2+LTR(N))	NP	Number of points in the distribution
DLNTP(2+LTR(N)+1) ... DLNTP(2+LTR(N)+NP)	PQ(N) Q=1..NP	Cumulative probability for boundaries
DLNTP(2+LTR(N)+1+NP) ... DLNTP(2+LTR(N)+2*NP)	YQ(N) Q=1..NP	Temperature for bin
DLNTP(2+LTR(N)+1+2*NP) DLNTP(2+LTR(N)+2*NP)	CMPQ(N) Q=1..NP	Control multiplier for bin

Table A-27: Low-dependent format for Energy Law 24 (Tabular Energy Multiplex)

Location in File	Parameter	Description
0LWFO+LDAT, 1	LDAT(M) $M \leq L$	Primary reference for low-dependent data (from low header)
LDAT(0)	N	Number of independent regions
LDAT(0).. LDAT(1)+NR	NRT(N) $N-1 \leq NR$	Starting index to which the corresponding multiplexing parameter applies
LDAT(1)+NR.. LDAT(1)+2*NR	INT(M) $M-1 \leq NR$	Interpolation parameter in each region (ignored, assumed histogram)
LDAT(2)+2*NR	NR	Number of indirect non-pair related
LDAT(3)+2*NR.. LDAT(3)+2*NR+NR	$E_{\text{cut}}(N)$ $N-1 \leq NR$	List of excluded energies
LDAT(3)+2*NR+NR	NRT	Number of samples listed in each $E_{\text{cut}}$ block
LDAT(4)+2*NR+NR).. LDAT(5)+2*NR+(NRT+1)*NR	$T_1(N)$ $N-1 \leq NRT$  $T_{\text{tot}}(N)$ $N-1 \leq NRT$	Multiplex table from NRT blocks comprising the low-dependence of (NRT+1)-age-probable low. Sampling uses a linear-linear interpolation between low boundaries.

one, using linear-linear interpolation within the age-probable multiplex low and computing the constant energy from the formula  $E_{\text{cut}} = T_1 E_0$ .

**Energy Law 46:** Energy Law 46 is a N-body phase-space distribution from File 6-Law 6 of ENDF-6. Its data format is described in Table A-28. It is not recommended for use with photoneuclear reactions due to the non-Hermitian nature of photon interactions. Full details of the sampling scheme are found in Chapter 3 and Appendix F of the MCNP Users Guide [3].

**Energy Law 67:** Energy Law 67 is the laboratory system, correlated angle-energy low from File 6-Law 7 of ENDF-6. Its data format is described in Table A-29. The angular-cosine data and subsequent energy distributions are described in Table

A.30 and Table A.31, respectively. The distribution first requires an appropriate choice as to how was the tabular energy distribution corresponding to the sampled angle. This law is not recommended for photoacoustic data.

Table A.28: Law dependent format for Energy Law 06 (4-Body Phase Space Distribution)

Location in XML	Parameter	Description
$DLWF(L)=LDAT(I)$	$LDAT(M)$ $M=1, 2$	Primary reference for law, dependent data (from law handler)
$LDAT(1)$	NPEX	Number of bodies in the phase space
$LDAT(2)$	$A_{\text{ex}}$	Local mass ratio for the NPEX particles

Table A.29: Law dependent format for Energy Law 07 (Tabulated Angle/Energy)

Location in XML	Parameter	Description
$DLWF(L)=LDAT(I)$	$LDAT(M)$ $M=1, 2$	Primary reference for law, dependent data (from law handler)
$LDAT(1)$	NE	Number of interpolation regions (if NE=0, NRC and NPT are omitted and linear-linear interpolation is assumed)
$LDAT(2) = LDAT(1)+NRC$	NTE(N) $N=1 \dots NR$	Scaling index to which the corresponding interpolation parameter applies
$LDAT(3)=NRC + LDAT(1)+I^{\text{th}}NRC$	NTE(N) $N=1 \dots NR$	LDOT defined interpolation parameter in each region. Only isotropic and linear-linear interpolation are allowed
$LDAT(p)=I^{\text{th}}NRC$	NR	Number of incident energies included
$LDAT(1)+I^{\text{th}}NRC + LDAT(2)+I^{\text{th}}NR+NRC$	ENE $N=1 \dots NR$	List of incident energies
$LDAT(1)+I^{\text{th}}NR+NRC$	ETRON	Location for tabular cross-sections relative to $DLWF(L)$
$LDAT(2)+I^{\text{th}}NR+I^{\text{th}}NRC$		

Table A.30: Tabular distribution format for Energy Law 47

Location in XML	Parameter	Description
$DLWFD+LTIN(N)-1$	N/A	First word of tabular distribution data for modelled energy point N
$DLWFD+LTIN(N)-1$	INTMD	Interpolation scheme for distribution INTMD = 1 $\rightarrow$ Histogram INTMD = 2 $\rightarrow$ Linear-inter
$DLWFD+LTIN(N)$	NMD	Number of points in the distribution
$DLWFD+LTIN(N)+1 \dots$ $DLWFD+LTIN(N)+NMD$	AM(1:N)	Secondary values
$DLWFD+LTIN(N)+1+NMD \dots$ $DLWFD+LTIN(N)+2*NMD$	LMDD(N) O=1..NMD	Locations for secondary source energy distributions relative to $DLWFD$

Table A.31: Tabular energy distribution format for Energy Law 47

Location in XML	Parameter	Description
$DLWFD+LMDD(O)-1$	N/A	First word of tabular energy distribution for secondary source point O
$DLWFD+LMDD(O)-1$	INTDP	Interpolation scheme for distribution INTDP = 1 $\rightarrow$ Histogram INTDP = 2 $\rightarrow$ Linear-inter
$DLWFD+LMDD(O)$	NPDF	Number of points in the distribution
$DLWFD+LMDD(O)+1 \dots$ $DLWFD+LMDD(O)+NPDF$	EPF	Secondary energy pdf
$DLWFD+LMDD(O)+1+NPDF \dots$ $DLWFD+LMDD(O)+2*NPDF$	PDF(P)	Probability density function
$DLWFD+LMDD(O)+1+2*NPDF \dots$ $DLWFD+LMDD(O)+3*NPDF$	CDF(P)	Cumulative density function

#### APPENDIX B

100

This appendix contains the source code for the MOPNF data processing code. Its functionality is discussed in depth in Chapter 5. In order to build the executable code, you must have an ARM C compiler and the Linux make utility. The appropriate Makefile is included here such that the code is built with the command “make mgnpf”. It has only been tested on a Linux system using the standard gcc compiler package. The flow can be used with the Makefile as the linking is defined directly by the source code for that file.



```

# Create a variable 'name' to hold the name of the person
name = "John"

# Create a variable 'age' to hold the age of the person
age = 30

# Create a variable 'gender' to hold the gender of the person
gender = "Male"

# Create a variable 'height' to hold the height of the person
height = 1.8

# Create a variable 'weight' to hold the weight of the person
weight = 75

# Create a variable 'eye_color' to hold the eye color of the person
eye_color = "Blue"

# Create a variable 'hair_color' to hold the hair color of the person
hair_color = "Brown"

# Create a variable 'skin_color' to hold the skin color of the person
skin_color = "Fair"

# Create a variable 'blood_type' to hold the blood type of the person
blood_type = "A"

# Create a variable 'marital_status' to hold the marital status of the person
marital_status = "Single"

# Create a variable 'education_level' to hold the education level of the person
education_level = "High School"

# Create a variable 'employment_status' to hold the employment status of the person
employment_status = "Unemployed"

# Create a variable 'annual_income' to hold the annual income of the person
annual_income = 25000

# Create a variable 'monthly_expenses' to hold the monthly expenses of the person
monthly_expenses = 1500

# Create a variable 'savings_rate' to hold the savings rate of the person
savings_rate = 0.1

# Create a variable 'retirement_age' to hold the retirement age of the person
retirement_age = 65

# Create a variable 'current_age' to hold the current age of the person
current_age = 30

# Create a variable 'life_expectancy' to hold the life expectancy of the person
life_expectancy = 80

# Create a variable 'health_status' to hold the health status of the person
health_status = "Good"

# Create a variable 'mental_health_status' to hold the mental health status of the person
mental_health_status = "Good"

# Create a variable 'social_support' to hold the social support of the person
social_support = "Good"

# Create a variable 'stress_level' to hold the stress level of the person
stress_level = "Low"

# Create a variable 'sleep_quality' to hold the sleep quality of the person
sleep_quality = "Good"

# Create a variable 'diet_quality' to hold the diet quality of the person
diet_quality = "Good"

# Create a variable 'exercise_frequency' to hold the exercise frequency of the person
exercise_frequency = "Low"

# Create a variable 'smoking_status' to hold the smoking status of the person
smoking_status = "Non-smoker"

# Create a variable 'alcohol_consumption' to hold the alcohol consumption of the person
alcohol_consumption = "Low"

# Create a variable 'drug_use' to hold the drug use of the person
drug_use = "None"

# Create a variable 'chronic_conditions' to hold the chronic conditions of the person
chronic_conditions = "None"

# Create a variable 'acute_conditions' to hold the acute conditions of the person
acute_conditions = "None"

# Create a variable 'injury_history' to hold the injury history of the person
injury_history = "None"

# Create a variable 'surgery_history' to hold the surgery history of the person
surgery_history = "None"

# Create a variable 'hospitalizations' to hold the hospitalizations of the person
hospitalizations = "None"

# Create a variable 'medications' to hold the medications of the person
medications = "None"

# Create a variable 'allergies' to hold the allergies of the person
allergies = "None"

# Create a variable 'vaccinations' to hold the vaccinations of the person
vaccinations = "None"

# Create a variable 'genetic_test_results' to hold the genetic test results of the person
genetic_test_results = "None"

# Create a variable 'environmental_exposures' to hold the environmental exposures of the person
environmental_exposures = "None"

# Create a variable 'lifestyle_choices' to hold the lifestyle choices of the person
lifestyle_choices = "None"

# Create a variable 'social_factors' to hold the social factors of the person
social_factors = "None"

# Create a variable 'economic_factors' to hold the economic factors of the person
economic_factors = "None"

# Create a variable 'cultural_factors' to hold the cultural factors of the person
cultural_factors = "None"

# Create a variable 'religious_beliefs' to hold the religious beliefs of the person
religious_beliefs = "None"

# Create a variable 'political_views' to hold the political views of the person
political_views = "None"

# Create a variable 'sexual_orientation' to hold the sexual orientation of the person
sexual_orientation = "None"

# Create a variable 'gender_identity' to hold the gender identity of the person
gender_identity = "None"

# Create a variable 'transgender_status' to hold the transgender status of the person
transgender_status = "None"

# Create a variable 'hiv_status' to hold the HIV status of the person
hiv_status = "None"

# Create a variable 'hepatitis_status' to hold the hepatitis status of the person
hepatitis_status = "None"

# Create a variable 'syphilis_status' to hold the syphilis status of the person
syphilis_status = "None"

# Create a variable 'gonorrhea_status' to hold the gonorrhea status of the person
gonorrhea_status = "None"

# Create a variable 'chlamydia_status' to hold the chlamydia status of the person
chlamydia_status = "None"

# Create a variable 'herpes_status' to hold the herpes status of the person
herpes_status = "None"

# Create a variable 'hpv_status' to hold the HPV status of the person
hpv_status = "None"

# Create a variable 'malaria_status' to hold the malaria status of the person
malaria_status = "None"

# Create a variable 'tuberculosis_status' to hold the tuberculosis status of the person
tuberculosis_status = "None"

# Create a variable 'h1n1_status' to hold the H1N1 status of the person
h1n1_status = "None"

# Create a variable 'influenza_status' to hold the influenza status of the person
influenza_status = "None"

# Create a variable 'measles_status' to hold the measles status of the person
measles_status = "None"

# Create a variable 'mumps_status' to hold the mumps status of the person
mumps_status = "None"

# Create a variable 'rubella_status' to hold the rubella status of the person
rubella_status = "None"

# Create a variable 'scarlet_fever_status' to hold the scarlet fever status of the person
scarlet_fever_status = "None"

# Create a variable 'diphtheria_status' to hold the diphtheria status of the person
diphtheria_status = "None"

# Create a variable 'tetanus_status' to hold the tetanus status of the person
tetanus_status = "None"

# Create a variable 'pertussis_status' to hold the pertussis status of the person
pertussis_status = "None"

# Create a variable 'whooping_cough_status' to hold the whooping cough status of the person
whooping_cough_status = "None"

# Create a variable 'measles_rubella_status' to hold the measles rubella status of the person
measles_rubella_status = "None"

# Create a variable 'mumps_rubella_status' to hold the mumps rubella status of the person
mumps_rubella_status = "None"

# Create a variable 'scarlet_fever_tetanus_status' to hold the scarlet fever tetanus status of the person
scarlet_fever_tetanus_status = "None"

# Create a variable 'diphtheria_tetanus_status' to hold the diphtheria tetanus status of the person
diphtheria_tetanus_status = "None"

# Create a variable 'pertussis_tetanus_status' to hold the pertussis tetanus status of the person
pertussis_tetanus_status = "None"

# Create a variable 'whooping_cough_tetanus_status' to hold the whooping cough tetanus status of the person
whooping_cough_tetanus_status = "None"

# Create a variable 'measles_rubella_mumps_status' to hold the measles rubella mumps status of the person
measles_rubella_mumps_status = "None"

# Create a variable 'measles_rubella_mumps_h1n1_status' to hold the measles rubella mumps H1N1 status of the person
measles_rubella_mumps_h1n1_status = "None"

# Create a variable 'measles_rubella_mumps_h1n1_influenza_status' to hold the measles rubella mumps H1N1 influenza status of the person
measles_rubella_mumps_h1n1_influenza_status = "None"

# Create a variable 'measles_rubella_mumps_h1n1_influenza_hepatitis_status' to hold the measles rubella mumps H1N1 influenza hepatitis status of the person
measles_rubella_mumps_h1n1_influenza_hepatitis_status = "None"

# Create a variable 'measles_rubella_mumps_h1n1_influenza_hepatitis_hiv_status' to hold the measles rubella mumps H1N1 influenza hepatitis HIV status of the person
measles_rubella_mumps_h1n1_influenza_hepatitis_hiv_status = "None"

# Create a variable 'measles_rubella_mumps_h1n1_influenza_hepatitis_hiv_tuberculosis_status' to hold the measles rubella mumps H1N1 influenza hepatitis HIV tuberculosis status of the person
measles_rubella_mumps_h1n1_influenza_hepatitis_hiv_tuberculosis_status = "None"

# Create a variable 'measles_rubella_mumps_h1n1_influenza_hepatitis_hiv_tuberculosis_malaria_status' to hold the measles rubella mumps H1N1 influenza hepatitis HIV tuberculosis malaria status of the person
measles_rubella_mumps_h1n1_influenza_hepatitis_hiv_tuberculosis_malaria_status = "None"

# Create a variable 'measles_rubella_mumps_h1n1_influenza_hepatitis_hiv_tuberculosis_malaria_h1n1_status' to hold the measles rubella mumps H1N1 influenza hepatitis HIV tuberculosis malaria H1N1 status of the person
measles_rubella_mumps_h1n1_influenza_hepatitis_hiv_tuberculosis_malaria_h1n1_status = "None"

# Create a variable 'measles_rubella_mumps_h1n1_influenza_hepatitis_hiv_tuberculosis_malaria_h1n1_influenza_status' to hold the measles rubella mumps H1N1 influenza hepatitis HIV tuberculosis malaria H1N1 influenza status of the person
measles_rubella_mumps_h1n1_influenza_hepatitis_hiv_tuberculosis_malaria_h1n1_influenza_status = "None"

# Create a variable 'measles_rubella_mumps_h1n1_influenza_hepatitis_hiv_tuberculosis_malaria_h1n1_influenza_hepatitis_status' to hold the measles rubella mumps H1N1 influenza hepatitis HIV tuberculosis malaria H1N1 influenza hepatitis status of the person
measles_rubella_mumps_h1n1_influenza_hepatitis_hiv_tuberculosis_malaria_h1n1_influenza_hepatitis_status = "None"

# Create a variable 'measles_rubella_mumps_h1n1_influenza_hepatitis_hiv_tuberculosis_malaria_h1n1_influenza_hepatitis_hiv_status' to hold the measles rubella mumps H1N1 influenza hepatitis HIV tuberculosis malaria H1N1 influenza hepatitis HIV status of the person
measles_rubella_mumps_h1n1_influenza_hepatitis_hiv_tuberculosis_malaria_h1n1_influenza_hepatitis_hiv_status = "None"

# Create a variable 'measles_rubella_mumps_h1n1_influenza_hepatitis_hiv_tuberculosis_malaria_h1n1_influenza_hepatitis_hiv_tuberculosis_status' to hold the measles rubella mumps H1N1 influenza hepatitis HIV tuberculosis malaria H1N1 influenza hepatitis HIV tuberculosis status of the person
measles_rubella_mumps_h1n1_influenza_hepatitis_hiv_tuberculosis_malaria_h1n1_influenza_hepatitis_hiv_tuberculosis_status = "None"

# Create a variable 'measles_rubella_mumps_h1n1_influenza_hepatitis_hiv_tuberculosis_malaria_h1n1_influenza_hepatitis_hiv_tuberculosis_malaria_status' to hold the measles rubella mumps H1N1 influenza hepatitis HIV tuberculosis malaria H1N1 influenza hepatitis HIV tuberculosis malaria status of the person
measles_rubella_mumps_h1n1_influenza_hepatitis_hiv_tuberculosis_malaria_h1n1_influenza_hepatitis_hiv_tuberculosis_malaria_status = "None"

# Create a variable 'measles_rubella_mumps_h1n1_influenza_hepatitis_hiv_tuberculosis_malaria_h1n1_influenza_hepatitis_hiv_tuberculosis_malaria_h1n1_status' to hold the measles rubella mumps H1N1 influenza hepatitis HIV tuberculosis malaria H1N1 influenza hepatitis HIV tuberculosis malaria H1N1 status of the person
measles_rubella_mumps_h1n1_influenza_hepatitis_hiv_tuberculosis_malaria_h1n1_influenza_hepatitis_hiv_tuberculosis_malaria_h1n1_status = "None"

# Create a variable 'measles_rubella_mumps_h1n1_influenza_hepatitis_hiv_tuberculosis_malaria_h1n1_influenza_hepatitis_hiv_tuberculosis_malaria_h1n1_influenza_status' to hold the measles rubella mumps H1N1 influenza hepatitis HIV tuberculosis malaria H1N1 influenza hepatitis HIV tuberculosis malaria H1N1 influenza status of the person
measles_rubella_mumps_h1n1_influenza_hepatitis_hiv_tuberculosis_malaria_h1n1_influenza_hepatitis_hiv_tuberculosis_malaria_h1n1_influenza_status = "None"

# Create a variable 'measles_rubella_mumps_h1n1_influenza_hepatitis_hiv_tuberculosis_malaria_h1n1_influenza_hepatitis_hiv_tuberculosis_malaria_h1n1_influenza_hepatitis_status' to hold the measles rubella mumps H1N1 influenza hepatitis HIV tuberculosis malaria H1N1 influenza hepatitis HIV tuberculosis malaria H1N1 influenza hepatitis status of the person
measles_rubella_mumps_h1n1_influenza_hepatitis_hiv_tuberculosis_malaria_h1n1_influenza_hepatitis_hiv_tuberculosis_malaria_h1n1_influenza_hepatitis_status = "None"

# Create a variable 'measles_rubella_mumps_h1n1_influenza_hepatitis_hiv_tuberculosis_malaria_h1n1_influenza_hepatitis_hiv_tuberculosis_malaria_h1n1_influenza_hepatitis_hiv_status' to hold the measles rubella mumps H1N1 influenza hepatitis HIV tuberculosis malaria H1N1 influenza hepatitis HIV tuberculosis malaria H1N1 influenza hepatitis HIV status of the person
measles_rubella_mumps_h1n1_influenza_hepatitis_hiv_tuberculosis_malaria_h1n1_influenza_hepatitis_hiv_tuberculosis_malaria_h1n1_influenza_hepatitis_hiv_status = "None"

# Create a variable 'measles_rubella_mumps_h1n1_influenza_hepatitis_hiv_tuberculosis_malaria_h1n1_influenza_hepatitis_hiv_tuberculosis_malaria_h1n1_influenza_hepatitis_hiv_tuberculosis_status' to hold the measles rubella mumps H1N1 influenza hepatitis HIV tuberculosis malaria H1N1 influenza hepatitis HIV tuberculosis malaria H1N1 influenza hepatitis HIV tuberculosis status of the person
measles_rubella_mumps_h1n1_influenza_hepatitis_hiv_tuberculosis_malaria_h1n1_influenza_hepatitis_hiv_tuberculosis_malaria_h1n1_influenza_hepatitis_hiv_tuberculosis_status = "None"

# Create a variable 'measles_rubella_mumps_h1n1_influenza_hepatitis_hiv_tuberculosis_malaria_h1n1_influenza_hepatitis_hiv_tuberculosis_malaria_h1n1_influenza_hepatitis_hiv_tuberculosis_malaria_status' to hold the measles rubella mumps H1N1 influenza hepatitis HIV tuberculosis malaria H1N1 influenza hepatitis HIV tuberculosis malaria H1N1 influenza hepatitis HIV tuberculosis malaria status of the person
measles_rubella_mumps_h1n1_influenza_hepatitis_hiv_tuberculosis_malaria_h1n1_influenza_hepatitis_hiv_tuberculosis_malaria_h1n1_influenza_hepatitis_hiv_tuberculosis_malaria_status = "None"
```















```

100
110 111 112 113 114 115 116 117 118 119 120 121 122 123 124 125 126 127 128 129 130 131 132 133 134 135 136 137 138 139 140 141 142 143 144 145 146 147 148 149 150 151 152 153 154 155 156 157 158 159 160 161 162 163 164 165 166 167 168 169 170 171 172 173 174 175 176 177 178 179 180 181 182 183 184 185 186 187 188 189 190 191 192 193 194 195 196 197 198 199 200 201 202 203 204 205 206 207 208 209 210 211 212 213 214 215 216 217 218 219 220 221 222 223 224 225 226 227 228 229 230 231 232 233 234 235 236 237 238 239 240 241 242 243 244 245 246 247 248 249 250 251 252 253 254 255 256 257 258 259 260 261 262 263 264 265 266 267 268 269 270 271 272 273 274 275 276 277 278 279 280 281 282 283 284 285 286 287 288 289 290 291 292 293 294 295 296 297 298 299 300 301 302 303 304 305 306 307 308 309 310 311 312 313 314 315 316 317 318 319 320 321 322 323 324 325 326 327 328 329 330 331 332 333 334 335 336 337 338 339 340 341 342 343 344 345 346 347 348 349 350 351 352 353 354 355 356 357 358 359 360 361 362 363 364 365 366 367 368 369 370 371 372 373 374 375 376 377 378 379 380 381 382 383 384 385 386 387 388 389 390 391 392 393 394 395 396 397 398 399 400 401 402 403 404 405 406 407 408 409 410 411 412 413 414 415 416 417 418 419 420 421 422 423 424 425 426 427 428 429 430 431 432 433 434 435 436 437 438 439 440 441 442 443 444 445 446 447 448 449 450 451 452 453 454 455 456 457 458 459 460 461 462 463 464 465 466 467 468 469 470 471 472 473 474 475 476 477 478 479 480 481 482 483 484 485 486 487 488 489 490 491 492 493 494 495 496 497 498 499 500 501 502 503 504 505 506 507 508 509 510 511 512 513 514 515 516 517 518 519 520 521 522 523 524 525 526 527 528 529 530 531 532 533 534 535 536 537 538 539 540 541 542 543 544 545 546 547 548 549 550 551 552 553 554 555 556 557 558 559 560 561 562 563 564 565 566 567 568 569 570 571 572 573 574 575 576 577 578 579 580 581 582 583 584 585 586 587 588 589 590 591 592 593 594 595 596 597 598 599 600 601 602 603 604 605 606 607 608 609 610 611 612 613 614 615 616 617 618 619 620 621 622 623 624 625 626 627 628 629 630 631 632 633 634 635 636 637 638 639 640 641 642 643 644 645 646 647 648 649 650 651 652 653 654 655 656 657 658 659 660 661 662 663 664 665 666 667 668 669 670 671 672 673 674 675 676 677 678 679 680 681 682 683 684 685 686 687 688 689 690 691 692 693 694 695 696 697 698 699 700 701 702 703 704 705 706 707 708 709 710 711 712 713 714 715 716 717 718 719 720 721 722 723 724 725 726 727 728 729 730 731 732 733 734 735 736 737 738 739 740 741 742 743 744 745 746 747 748 749 750 751 752 753 754 755 756 757 758 759 760 761 762 763 764 765 766 767 768 769 770 771 772 773 774 775 776 777 778 779 780 781 782 783 784 785 786 787 788 789 790 791 792 793 794 795 796 797 798 799 800 801 802 803 804 805 806 807 808 809 810 811 812 813 814 815 816 817 818 819 820 821 822 823 824 825 826 827 828 829 830 831 832 833 834 835 836 837 838 839 840 841 842 843 844 845 846 847 848 849 850 851 852 853 854 855 856 857 858 859 860 861 862 863 864 865 866 867 868 869 870 871 872 873 874 875 876 877 878 879 880 881 882 883 884 885 886 887 888 889 890 891 892 893 894 895 896 897 898 899 900 901 902 903 904 905 906 907 908 909 910 911 912 913 914 915 916 917 918 919 920 921 922 923 924 925 926 927 928 929 930 931 932 933 934 935 936 937 938 939 940 941 942 943 944 945 946 947 948 949 950 951 952 953 954 955 956 957 958 959 960 961 962 963 964 965 966 967 968 969 970 971 972 973 974 975 976 977 978 979 980 981 982 983 984 985 986 987 988 989 990 991 992 993 994 995 996 997 998 999 1000

```





























```

1
2
3
4
5
6
7
8
9
10
11
12
13
14
15
16
17
18
19
20
21
22
23
24
25
26
27
28
29
30
31
32
33
34
35
36
37
38
39
40
41
42
43
44
45
46
47
48
49
50
51
52
53
54
55
56
57
58
59
60
61
62
63
64
65
66
67
68
69
70
71
72
73
74
75
76
77
78
79
80
81
82
83
84
85
86
87
88
89
90
91
92
93
94
95
96
97
98
99
100
101
102
103
104
105
106
107
108
109
110
111
112
113
114
115
116
117
118
119
120
121
122
123
124
125
126
127
128
129
130
131
132
133
134
135
136
137
138
139
140
141
142
143
144
145
146
147
148
149
150
151
152
153
154
155
156
157
158
159
160
161
162
163
164
165
166
167
168
169
170
171
172
173
174
175
176
177
178
179
180
181
182
183
184
185
186
187
188
189
190
191
192
193
194
195
196
197
198
199
200
201
202
203
204
205
206
207
208
209
210
211
212
213
214
215
216
217
218
219
220
221
222
223
224
225
226
227
228
229
230
231
232
233
234
235
236
237
238
239
240
241
242
243
244
245
246
247
248
249
250
251
252
253
254
255
256
257
258
259
260
261
262
263
264
265
266
267
268
269
270
271
272
273
274
275
276
277
278
279
280
281
282
283
284
285
286
287
288
289
290
291
292
293
294
295
296
297
298
299
300
301
302
303
304
305
306
307
308
309
310
311
312
313
314
315
316
317
318
319
320
321
322
323
324
325
326
327
328
329
330
331
332
333
334
335
336
337
338
339
340
341
342
343
344
345
346
347
348
349
350
351
352
353
354
355
356
357
358
359
360
361
362
363
364
365
366
367
368
369
370
371
372
373
374
375
376
377
378
379
380
381
382
383
384
385
386
387
388
389
390
391
392
393
394
395
396
397
398
399
400
401
402
403
404
405
406
407
408
409
410
411
412
413
414
415
416
417
418
419
420
421
422
423
424
425
426
427
428
429
430
431
432
433
434
435
436
437
438
439
440
441
442
443
444
445
446
447
448
449
450
451
452
453
454
455
456
457
458
459
460
461
462
463
464
465
466
467
468
469
470
471
472
473
474
475
476
477
478
479
480
481
482
483
484
485
486
487
488
489
490
491
492
493
494
495
496
497
498
499
500
501
502
503
504
505
506
507
508
509
510
511
512
513
514
515
516
517
518
519
520
521
522
523
524
525
526
527
528
529
530
531
532
533
534
535
536
537
538
539
540
541
542
543
544
545
546
547
548
549
550
551
552
553
554
555
556
557
558
559
560
561
562
563
564
565
566
567
568
569
570
571
572
573
574
575
576
577
578
579
580
581
582
583
584
585
586
587
588
589
590
591
592
593
594
595
596
597
598
599
600
601
602
603
604
605
606
607
608
609
610
611
612
613
614
615
616
617
618
619
620
621
622
623
624
625
626
627
628
629
630
631
632
633
634
635
636
637
638
639
640
641
642
643
644
645
646
647
648
649
650
651
652
653
654
655
656
657
658
659
660
661
662
663
664
665
666
667
668
669
670
671
672
673
674
675
676
677
678
679
680
681
682
683
684
685
686
687
688
689
690
691
692
693
694
695
696
697
698
699
700
701
702
703
704
705
706
707
708
709
710
711
712
713
714
715
716
717
718
719
720
721
722
723
724
725
726
727
728
729
730
731
732
733
734
735
736
737
738
739
740
741
742
743
744
745
746
747
748
749
750
751
752
753
754
755
756
757
758
759
760
761
762
763
764
765
766
767
768
769
770
771
772
773
774
775
776
777
778
779
780
781
782
783
784
785
786
787
788
789
790
791
792
793
794
795
796
797
798
799
800
801
802
803
804
805
806
807
808
809
810
811
812
813
814
815
816
817
818
819
820
821
822
823
824
825
826
827
828
829
830
831
832
833
834
835
836
837
838
839
840
841
842
843
844
845
846
847
848
849
850
851
852
853
854
855
856
857
858
859
860
861
862
863
864
865
866
867
868
869
870
871
872
873
874
875
876
877
878
879
880
881
882
883
884
885
886
887
888
889
890
891
892
893
894
895
896
897
898
899
900
901
902
903
904
905
906
907
908
909
910
911
912
913
914
915
916
917
918
919
920
921
922
923
924
925
926
927
928
929
930
931
932
933
934
935
936
937
938
939
940
941
942
943
944
945
946
947
948
949
950
951
952
953
954
955
956
957
958
959
960
961
962
963
964
965
966
967
968
969
970
971
972
973
974
975
976
977
978
979
980
981
982
983
984
985
986
987
988
989
990
991
992
993
994
995
996
997
998
999
1000

```





















```

    ex -> let f1(x) = 2 * x
    in case 1 of
      1 -> let f2(x) = 2 * x
      2 -> let f2(x) = 2 * x
      3 -> let f2(x) = 2 * x
      4 -> let f2(x) = 2 * x
      5 -> let f2(x) = 2 * x
      6 -> let f2(x) = 2 * x
      7 -> let f2(x) = 2 * x
      8 -> let f2(x) = 2 * x
      9 -> let f2(x) = 2 * x
      10 -> let f2(x) = 2 * x
      11 -> let f2(x) = 2 * x
      12 -> let f2(x) = 2 * x
      13 -> let f2(x) = 2 * x
      14 -> let f2(x) = 2 * x
      15 -> let f2(x) = 2 * x
      16 -> let f2(x) = 2 * x
      17 -> let f2(x) = 2 * x
      18 -> let f2(x) = 2 * x
      19 -> let f2(x) = 2 * x
      20 -> let f2(x) = 2 * x
      21 -> let f2(x) = 2 * x
      22 -> let f2(x) = 2 * x
      23 -> let f2(x) = 2 * x
      24 -> let f2(x) = 2 * x
      25 -> let f2(x) = 2 * x
      26 -> let f2(x) = 2 * x
      27 -> let f2(x) = 2 * x
      28 -> let f2(x) = 2 * x
      29 -> let f2(x) = 2 * x
      30 -> let f2(x) = 2 * x
      31 -> let f2(x) = 2 * x
      32 -> let f2(x) = 2 * x
      33 -> let f2(x) = 2 * x
      34 -> let f2(x) = 2 * x
      35 -> let f2(x) = 2 * x
      36 -> let f2(x) = 2 * x
      37 -> let f2(x) = 2 * x
      38 -> let f2(x) = 2 * x
      39 -> let f2(x) = 2 * x
      40 -> let f2(x) = 2 * x
      41 -> let f2(x) = 2 * x
      42 -> let f2(x) = 2 * x
      43 -> let f2(x) = 2 * x
      44 -> let f2(x) = 2 * x
      45 -> let f2(x) = 2 * x
      46 -> let f2(x) = 2 * x
      47 -> let f2(x) = 2 * x
      48 -> let f2(x) = 2 * x
      49 -> let f2(x) = 2 * x
      50 -> let f2(x) = 2 * x
      51 -> let f2(x) = 2 * x
      52 -> let f2(x) = 2 * x
      53 -> let f2(x) = 2 * x
      54 -> let f2(x) = 2 * x
      55 -> let f2(x) = 2 * x
      56 -> let f2(x) = 2 * x
      57 -> let f2(x) = 2 * x
      58 -> let f2(x) = 2 * x
      59 -> let f2(x) = 2 * x
      60 -> let f2(x) = 2 * x
      61 -> let f2(x) = 2 * x
      62 -> let f2(x) = 2 * x
      63 -> let f2(x) = 2 * x
      64 -> let f2(x) = 2 * x
      65 -> let f2(x) = 2 * x
      66 -> let f2(x) = 2 * x
      67 -> let f2(x) = 2 * x
      68 -> let f2(x) = 2 * x
      69 -> let f2(x) = 2 * x
      70 -> let f2(x) = 2 * x
      71 -> let f2(x) = 2 * x
      72 -> let f2(x) = 2 * x
      73 -> let f2(x) = 2 * x
      74 -> let f2(x) = 2 * x
      75 -> let f2(x) = 2 * x
      76 -> let f2(x) = 2 * x
      77 -> let f2(x) = 2 * x
      78 -> let f2(x) = 2 * x
      79 -> let f2(x) = 2 * x
      80 -> let f2(x) = 2 * x
      81 -> let f2(x) = 2 * x
      82 -> let f2(x) = 2 * x
      83 -> let f2(x) = 2 * x
      84 -> let f2(x) = 2 * x
      85 -> let f2(x) = 2 * x
      86 -> let f2(x) = 2 * x
      87 -> let f2(x) = 2 * x
      88 -> let f2(x) = 2 * x
      89 -> let f2(x) = 2 * x
      90 -> let f2(x) = 2 * x
      91 -> let f2(x) = 2 * x
      92 -> let f2(x) = 2 * x
      93 -> let f2(x) = 2 * x
      94 -> let f2(x) = 2 * x
      95 -> let f2(x) = 2 * x
      96 -> let f2(x) = 2 * x
      97 -> let f2(x) = 2 * x
      98 -> let f2(x) = 2 * x
      99 -> let f2(x) = 2 * x
      100 -> let f2(x) = 2 * x
    in f2(x)
  
```











```

    get(gradient) = 0
    set(gradient) = 0
end

if
  // evaluate new value
  1
end

case 101:
  change name "new gradient" 1
  change direction "up", 0.1
  set(gradient) = 0
  set(value) = 0
  set(gradient) = 0
end

case 102:
  change name "new gradient" 1
  change direction "up", 0.1
  set(gradient) = 0
  set(value) = 0
  set(gradient) = 0
end

case 103:
  change name "new gradient" 1
  change direction "up", 0.1
  set(gradient) = 0
  set(value) = 0
  set(gradient) = 0
end

case 104:
  change name "new gradient" 1
  change direction "up", 0.1
  set(gradient) = 0
  set(value) = 0
  set(gradient) = 0
end

case 105:
  change name "new gradient" 1
  change direction "up", 0.1
  set(gradient) = 0
  set(value) = 0
  set(gradient) = 0
end

case 106:
  change name "new gradient" 1
  change direction "up", 0.1
  set(gradient) = 0
  set(value) = 0
  set(gradient) = 0
end

case 107:
  change name "new gradient" 1
  change direction "up", 0.1
  set(gradient) = 0
  set(value) = 0
  set(gradient) = 0
end

// one more rule about this model model
1
end

```



























```

n = (sqrt(4*delta+1)-1)/2
m = (sqrt(4*delta+1)+1)/2
Print

rem 104
n:=0; m:=0; "gamma = 0th normal state removed" ;
n:=n+1; m:=m-1; "gamma = 0th" ;
n:=abs(n-m)+1;
n:=abs(n-m)+1; m:=m+1; n:=n-1;
n:=abs(n-m)+1;
m:=m-1; m:=m+1;
n:=abs(n-m)+1;
n:=abs(n-m)+1; m:=m+1; n:=n-1;
n:=abs(n-m)+1;
m:=m-1; m:=m+1;
Print

rem 105
n:=0; m:=0; "gamma = 0th normal state removed" ;
n:=n+1; m:=m-1; "gamma = 0th" ;
n:=abs(n-m)+1;
m:=m-1; m:=m+1;
n:=abs(n-m)+1;
m:=m-1; m:=m+1;
n:=abs(n-m)+1;
m:=m-1; m:=m+1;
n:=abs(n-m)+1;
m:=m-1; m:=m+1;
Print

rem 106
n:=0; m:=0; "gamma = 0th normal state removed" ;
n:=n+1; m:=m-1; "gamma = 0th" ;
n:=abs(n-m)+1;
m:=m-1; m:=m+1;
n:=abs(n-m)+1;
m:=m-1; m:=m+1;
n:=abs(n-m)+1;
m:=m-1; m:=m+1;
n:=abs(n-m)+1;
m:=m-1; m:=m+1;
Print

rem 107
n:=0; m:=0; "gamma = 0th normal state removed" ;
n:=n+1; m:=m-1; "gamma = 0th" ;
n:=abs(n-m)+1;
m:=m-1; m:=m+1;
n:=abs(n-m)+1;
m:=m-1; m:=m+1;
n:=abs(n-m)+1;
m:=m-1; m:=m+1;
n:=abs(n-m)+1;
m:=m-1; m:=m+1;
Print

rem 108
n:=0; m:=0; "gamma = 0th normal state removed" ;
n:=n+1; m:=m-1; "gamma = 0th" ;
n:=abs(n-m)+1;
m:=m-1; m:=m+1;
n:=abs(n-m)+1;
m:=m-1; m:=m+1;
n:=abs(n-m)+1;
m:=m-1; m:=m+1;
n:=abs(n-m)+1;
m:=m-1; m:=m+1;
Print

rem 109
n:=0; m:=0; "gamma = 0th normal state removed" ;
n:=n+1; m:=m-1; "gamma = 0th" ;
n:=abs(n-m)+1;
m:=m-1; m:=m+1;
n:=abs(n-m)+1;
m:=m-1; m:=m+1;
n:=abs(n-m)+1;
m:=m-1; m:=m+1;
n:=abs(n-m)+1;
m:=m-1; m:=m+1;
Print

```





```

    m:=absorbent[0] + 1000;
    m:=m-absorbent[0] + 1000; m:=m-absorbent[0] + 1000; absorb[0] := 0;
    absorbent[0] := 0;
    return;

case 10:
  absorb:=0; return "Error: No valid data entered";
  absorb:=absorbent[0] + 1000;
  absorbent[0] := 0;
  absorb:=absorbent[0] + 1000; absorbent[0] := 0;
  absorbent[0] := 0;
  m:=absorbent[0] + 1000; absorbent[0] := 0;
  m:=absorbent[0] + 1000; absorbent[0] := 0;
  m:=absorbent[0] + 1000; absorbent[0] := 0;
  return;

case 11:
  absorb:=0; return "Error: No valid data entered";
  absorb:=absorbent[0] + 1000;
  absorbent[0] := 0;
  m:=absorbent[0] + 1000; absorbent[0] := 0;
  absorbent[0] := 0;
  m:=absorbent[0] + 1000; absorbent[0] := 0;
  m:=absorbent[0] + 1000; absorbent[0] := 0;
  return;

case 12:
  absorb:=0; return "Error: No valid data entered";
  absorb:=absorbent[0] + 1000;
  absorbent[0] := 0;
  m:=absorbent[0] + 1000; absorbent[0] := 0;
  absorbent[0] := 0;
  m:=absorbent[0] + 1000; absorbent[0] := 0;
  m:=absorbent[0] + 1000; absorbent[0] := 0;
  return;

case 13:
  absorb:=0; return "Error: No valid data entered";
  absorb:=absorbent[0] + 1000;
  absorbent[0] := 0;
  m:=absorbent[0] + 1000; absorbent[0] := 0;
  absorbent[0] := 0;
  m:=absorbent[0] + 1000; absorbent[0] := 0;
  m:=absorbent[0] + 1000; absorbent[0] := 0;
  return;

case 14:
  absorb:=0; return "Error: No valid data entered";
  absorb:=absorbent[0] + 1000;
  absorbent[0] := 0;
  m:=absorbent[0] + 1000; absorbent[0] := 0;
  absorbent[0] := 0;
  m:=absorbent[0] + 1000; absorbent[0] := 0;
  m:=absorbent[0] + 1000; absorbent[0] := 0;
  return;

case 15:
  absorb:=0; return "Error: No valid data entered";
  absorb:=absorbent[0] + 1000;
  absorbent[0] := 0;
  m:=absorbent[0] + 1000; absorbent[0] := 0;
  absorbent[0] := 0;
  m:=absorbent[0] + 1000; absorbent[0] := 0;
  m:=absorbent[0] + 1000; absorbent[0] := 0;
  return;

```









```

        return m, "Warning:  $\alpha$  does not lie within bounds"
    except ValueError:
        return None
    if (math.isnan(alpha) or
        math.isinf(alpha) or
        math.isclose(alpha, 0) or
        math.isclose(alpha, 1)):
        return None
    if (alpha < 0 or
        alpha > 1):
        return None
    return alpha

```

def  $\beta$

```

    """Returns  $\beta$  (float) 'Warning:  $\beta$  does not lie within bounds'
    except ValueError:
        return None
    if (math.isnan(beta) or
        math.isinf(beta) or
        math.isclose(beta, 0) or
        math.isclose(beta, 1)):
        return None
    if (beta < 0 or
        beta > 1):
        return None
    return beta

```

def  $\gamma$

```

    """Returns  $\gamma$  (float) 'Warning:  $\gamma$  does not lie within bounds'
    except ValueError:
        return None
    if (math.isnan(gamma) or
        math.isinf(gamma) or
        math.isclose(gamma, 0) or
        math.isclose(gamma, 1)):
        return None
    if (gamma < 0 or
        gamma > 1):
        return None
    return gamma

```

def  $\delta$

```

    """Returns  $\delta$  (float) 'Warning:  $\delta$  does not lie within bounds'
    except ValueError:
        return None
    if (math.isnan(delta) or
        math.isinf(delta) or
        math.isclose(delta, 0) or
        math.isclose(delta, 1)):
        return None
    if (delta < 0 or
        delta > 1):
        return None
    return delta

```

def  $\epsilon$

```

    """Returns  $\epsilon$  (float) 'Warning:  $\epsilon$  does not lie within bounds'
    except ValueError:
        return None
    if (math.isnan(epsilon) or
        math.isinf(epsilon) or
        math.isclose(epsilon, 0) or
        math.isclose(epsilon, 1)):
        return None
    if (epsilon < 0 or
        epsilon > 1):
        return None
    return epsilon

```

def  $\zeta$

```

    """Returns  $\zeta$  (float) 'Warning:  $\zeta$  does not lie within bounds'
    except ValueError:
        return None
    if (math.isnan(zeta) or
        math.isinf(zeta) or
        math.isclose(zeta, 0) or
        math.isclose(zeta, 1)):
        return None
    if (zeta < 0 or
        zeta > 1):
        return None
    return zeta

```













[illegible]

1000

[illegible][illegible]

1000

[illegible][illegible]

```

var myObj = {
  myMethod: function() {
    // ...
  }
};

// ...

myObj.myMethod();

```

[illegible][illegible]

```

myobj = myobj + "value 1 has changed inside myobj()"
myobj.__dict__["value"] = "value 2"
myobj.__dict__["value"] = 1
myobj.__dict__["value"] = myobj.__dict__["value"] + "value 1 double 1. 1"
myobj.__dict__["value"] = 100

```















```

case 130
  change to show, "Value = this value was added" {
    change to showline "Value: 100" {
      set showlinevalue = 10
      set showline = add [set of showlinevalue] show() double { 1
      set showlinevalue = 1000
      set showline [1] = 1000
      set showlinevalue = add [set of showlinevalue] show() double { 1
      set showlinevalue = 1000
      set showlinevalue = add [set showlinevalue] show() double { 1
      set showlinevalue [1] = 10
      set showlinevalue [1] = 10
    }
  }

case 140
  change to show, "Value = this value was added" {
    change to showline "Value: 100" {
      set showlinevalue = 10
      set showline = add [set of showlinevalue] show() double { 1
      set showlinevalue = 1000
      set showline [1] = 1000
      set showlinevalue = add [set showlinevalue] show() double { 1
      set showlinevalue [1] = 10
      set showlinevalue [1] = 10
    }
  }

case 150
  change to show, "Value = this value was added" {
    change to showline "Value: 100" {
      set showlinevalue = 1
      set showline = add [set of showlinevalue] show() double { 1
      set showlinevalue = 1000
      set showline [1] = 1000
      set showlinevalue = add [set of showlinevalue] show() double { 1
      set showlinevalue [1] = 1
      set showlinevalue [1] = 1
    }
  }

case 160
  change to show, "Value = this value was added" {
    change to showline "Value: 100" {
      set showlinevalue = 10
      set showline = add [set of showlinevalue] show() double { 1
      set showlinevalue = 1000
      set showline [1] = 1000
      set showlinevalue = add [set of showlinevalue] show() double { 1
      set showlinevalue [1] = 1
      set showlinevalue [1] = 1
    }
  }

case 170
  change to show, "Value = this value was added" {
    change to showline "Value: 100" {
      set showlinevalue = 10
      set showline = add [set of showlinevalue] show() double { 1
      set showlinevalue = 1000
      set showline [1] = 1000
      set showlinevalue = add [set of showlinevalue] show() double { 1
      set showlinevalue [1] = 1
      set showlinevalue [1] = 1
    }
  }

case 180
  change to show, "Value = this value was added" {
    change to showline "Value: 100" {
      set showlinevalue = 10
      set showline = add [set of showlinevalue] show() double { 1
      set showlinevalue = 1000
      set showline [1] = 1000
      set showlinevalue = add [set of showlinevalue] show() double { 1
      set showlinevalue [1] = 1
      set showlinevalue [1] = 1
    }
  }

```

```

17. use method (method1) (0) return result
18
case 17b
  return to value "single value 1 passed out" 1
  return to method "pass 1a1" 1
  m1Method1() = 1
  m1Method1() = 100
  m1Method1() = 1000
  m1Method1() = 10000
  break

case 17c
  return to value "single 1 + get single value method" 1
  return to method "pass 1a1" 1
  m1Method1() = 1
  m1Method1() = value m1Method1(), state1 state 1 1
  m1Method1() = 100
  m1Method1() = 1000
  m1Method1() = 10000
  m1Method1() = value m1Method1(), state1 state 1 1
  m1Method1() = 1
  m1Method1() = 1
  break

case 17d
  return to value "single 1 + get single value method" 1
  return to method "pass 1a1" 1
  m1Method1() = 1
  m1Method1() = value m1Method1(), state1 state 1 1
  m1Method1() = 100
  m1Method1() = 1000
  m1Method1() = value m1Method1(), state1 state 1 1
  m1Method1() = 1
  m1Method1() = 1
  break

case 17e
  return to value "single 1 + get single value method" 1
  return to method "pass 1a1" 1
  m1Method1() = 1
  m1Method1() = value m1Method1(), state1 state 1 1
  m1Method1() = 100
  m1Method1() = 1000
  m1Method1() = value m1Method1(), state1 state 1 1
  m1Method1() = 1
  m1Method1() = 1
  break

case 17f
  return to value "single 1 + get single value method" 1
  return to method "pass 1a1" 1
  m1Method1() = 1
  m1Method1() = value m1Method1(), state1 state 1 1
  m1Method1() = 100
  m1Method1() = 1000
  m1Method1() = value m1Method1(), state1 state 1 1
  m1Method1() = 1
  m1Method1() = 1
  break

case 17g
  return to value "single 1 + get single value method" 1
  return to method "pass 1a1" 1
  m1Method1() = 1
  m1Method1() = value m1Method1(), state1 state 1 1
  m1Method1() = 100
  m1Method1() = 1000
  m1Method1() = value m1Method1(), state1 state 1 1
  m1Method1() = 1
  m1Method1() = 1
  break

case 17h
  return to value "single 1 + get single value method" 1
  return to method "pass 1a1" 1
  m1Method1() = 1
  m1Method1() = value m1Method1(), state1 state 1 1
  m1Method1() = 100
  m1Method1() = 1000
  m1Method1() = value m1Method1(), state1 state 1 1
  m1Method1() = 1
  m1Method1() = 1
  break

```















```

isPrime(n) = (exists m <|> n) isPrime(n-m) && n <|> m
isPrime(2) = true
isPrime(3) = true
isPrime(4) = false
isPrime(5) = true
isPrime(6) = false
isPrime(7) = true
isPrime(8) = false
isPrime(9) = false
isPrime(10) = false
isPrime(11) = true
isPrime(12) = false
isPrime(13) = true
isPrime(14) = false
isPrime(15) = false
isPrime(16) = false
isPrime(17) = true
isPrime(18) = false
isPrime(19) = true
isPrime(20) = false
isPrime(21) = false
isPrime(22) = false
isPrime(23) = true
isPrime(24) = false
isPrime(25) = false
isPrime(26) = false
isPrime(27) = false
isPrime(28) = false
isPrime(29) = true
isPrime(30) = false
isPrime(31) = true
isPrime(32) = false
isPrime(33) = false
isPrime(34) = false
isPrime(35) = false
isPrime(36) = false
isPrime(37) = true
isPrime(38) = false
isPrime(39) = false
isPrime(40) = false
isPrime(41) = true
isPrime(42) = false
isPrime(43) = true
isPrime(44) = false
isPrime(45) = false
isPrime(46) = false
isPrime(47) = true
isPrime(48) = false
isPrime(49) = false
isPrime(50) = false
isPrime(51) = false
isPrime(52) = false
isPrime(53) = true
isPrime(54) = false
isPrime(55) = false
isPrime(56) = false
isPrime(57) = false
isPrime(58) = false
isPrime(59) = true
isPrime(60) = false
isPrime(61) = true
isPrime(62) = false
isPrime(63) = false
isPrime(64) = false
isPrime(65) = false
isPrime(66) = false
isPrime(67) = true
isPrime(68) = false
isPrime(69) = false
isPrime(70) = false
isPrime(71) = true
isPrime(72) = false
isPrime(73) = true
isPrime(74) = false
isPrime(75) = false
isPrime(76) = false
isPrime(77) = false
isPrime(78) = false
isPrime(79) = true
isPrime(80) = false
isPrime(81) = false
isPrime(82) = false
isPrime(83) = true
isPrime(84) = false
isPrime(85) = false
isPrime(86) = false
isPrime(87) = false
isPrime(88) = false
isPrime(89) = true
isPrime(90) = false
isPrime(91) = false
isPrime(92) = false
isPrime(93) = false
isPrime(94) = false
isPrime(95) = false
isPrime(96) = false
isPrime(97) = true
isPrime(98) = false
isPrime(99) = false
isPrime(100) = false

```















```

def test_memoize(f):
    """
    """
    @wraps(f)
    def wrapper(*args, **kwargs):
        """
        """
        key = (args, kwargs)
        if key not in cache:
            value = f(*args, **kwargs)
            cache[key] = value
        return value
    return wrapper

def test_memoize_with_args(f):
    """
    """
    @wraps(f)
    def wrapper(*args, **kwargs):
        """
        """
        key = (args, kwargs)
        if key not in cache:
            value = f(*args, **kwargs)
            cache[key] = value
        return value
    return wrapper

def test_memoize_with_kwargs(f):
    """
    """
    @wraps(f)
    def wrapper(*args, **kwargs):
        """
        """
        key = (args, kwargs)
        if key not in cache:
            value = f(*args, **kwargs)
            cache[key] = value
        return value
    return wrapper

def test_memoize_with_args_and_kwargs(f):
    """
    """
    @wraps(f)
    def wrapper(*args, **kwargs):
        """
        """
        key = (args, kwargs)
        if key not in cache:
            value = f(*args, **kwargs)
            cache[key] = value
        return value
    return wrapper

```









```

1
2
3
4
5
6
7
8
9
10
11
12
13
14
15
16
17
18
19
20
21
22
23
24
25
26
27
28
29
30
31
32
33
34
35
36
37
38
39
40
41
42
43
44
45
46
47
48
49
50
51
52
53
54
55
56
57
58
59
60
61
62
63
64
65
66
67
68
69
70
71
72
73
74
75
76
77
78
79
80
81
82
83
84
85
86
87
88
89
90
91
92
93
94
95
96
97
98
99
100
101
102
103
104
105
106
107
108
109
110
111
112
113
114
115
116
117
118
119
120
121
122
123
124
125
126
127
128
129
130
131
132
133
134
135
136
137
138
139
140
141
142
143
144
145
146
147
148
149
150
151
152
153
154
155
156
157
158
159
160
161
162
163
164
165
166
167
168
169
170
171
172
173
174
175
176
177
178
179
180
181
182
183
184
185
186
187
188
189
190
191
192
193
194
195
196
197
198
199
200
201
202
203
204
205
206
207
208
209
210
211
212
213
214
215
216
217
218
219
220
221
222
223
224
225
226
227
228
229
230
231
232
233
234
235
236
237
238
239
240
241
242
243
244
245
246
247
248
249
250
251
252
253
254
255
256
257
258
259
260
261
262
263
264
265
266
267
268
269
270
271
272
273
274
275
276
277
278
279
280
281
282
283
284
285
286
287
288
289
290
291
292
293
294
295
296
297
298
299
300
301
302
303
304
305
306
307
308
309
310
311
312
313
314
315
316
317
318
319
320
321
322
323
324
325
326
327
328
329
330
331
332
333
334
335
336
337
338
339
340
341
342
343
344
345
346
347
348
349
350
351
352
353
354
355
356
357
358
359
360
361
362
363
364
365
366
367
368
369
370
371
372
373
374
375
376
377
378
379
380
381
382
383
384
385
386
387
388
389
390
391
392
393
394
395
396
397
398
399
400
401
402
403
404
405
406
407
408
409
410
411
412
413
414
415
416
417
418
419
420
421
422
423
424
425
426
427
428
429
430
431
432
433
434
435
436
437
438
439
440
441
442
443
444
445
446
447
448
449
450
451
452
453
454
455
456
457
458
459
460
461
462
463
464
465
466
467
468
469
470
471
472
473
474
475
476
477
478
479
480
481
482
483
484
485
486
487
488
489
490
491
492
493
494
495
496
497
498
499
500
501
502
503
504
505
506
507
508
509
510
511
512
513
514
515
516
517
518
519
520
521
522
523
524
525
526
527
528
529
530
531
532
533
534
535
536
537
538
539
540
541
542
543
544
545
546
547
548
549
550
551
552
553
554
555
556
557
558
559
560
561
562
563
564
565
566
567
568
569
570
571
572
573
574
575
576
577
578
579
580
581
582
583
584
585
586
587
588
589
590
591
592
593
594
595
596
597
598
599
600
601
602
603
604
605
606
607
608
609
610
611
612
613
614
615
616
617
618
619
620
621
622
623
624
625
626
627
628
629
630
631
632
633
634
635
636
637
638
639
640
641
642
643
644
645
646
647
648
649
650
651
652
653
654
655
656
657
658
659
660
661
662
663
664
665
666
667
668
669
670
671
672
673
674
675
676
677
678
679
680
681
682
683
684
685
686
687
688
689
690
691
692
693
694
695
696
697
698
699
700
701
702
703
704
705
706
707
708
709
710
711
712
713
714
715
716
717
718
719
720
721
722
723
724
725
726
727
728
729
730
731
732
733
734
735
736
737
738
739
740
741
742
743
744
745
746
747
748
749
750
751
752
753
754
755
756
757
758
759
760
761
762
763
764
765
766
767
768
769
770
771
772
773
774
775
776
777
778
779
780
781
782
783
784
785
786
787
788
789
790
791
792
793
794
795
796
797
798
799
800
801
802
803
804
805
806
807
808
809
810
811
812
813
814
815
816
817
818
819
820
821
822
823
824
825
826
827
828
829
830
831
832
833
834
835
836
837
838
839
840
841
842
843
844
845
846
847
848
849
850
851
852
853
854
855
856
857
858
859
860
861
862
863
864
865
866
867
868
869
870
871
872
873
874
875
876
877
878
879
880
881
882
883
884
885
886
887
888
889
890
891
892
893
894
895
896
897
898
899
900
901
902
903
904
905
906
907
908
909
910
911
912
913
914
915
916
917
918
919
920
921
922
923
924
925
926
927
928
929
930
931
932
933
934
935
936
937
938
939
940
941
942
943
944
945
946
947
948
949
950
951
952
953
954
955
956
957
958
959
960
961
962
963
964
965
966
967
968
969
970
971
972
973
974
975
976
977
978
979
980
981
982
983
984
985
986
987
988
989
990
991
992
993
994
995
996
997
998
999
1000

```

























```

1
2
3
4
5
6
7
8
9
10
11
12
13
14
15
16
17
18
19
20
21
22
23
24
25
26
27
28
29
30
31
32
33
34
35
36
37
38
39
40
41
42
43
44
45
46
47
48
49
50
51
52
53
54
55
56
57
58
59
60
61
62
63
64
65
66
67
68
69
70
71
72
73
74
75
76
77
78
79
80
81
82
83
84
85
86
87
88
89
90
91
92
93
94
95
96
97
98
99
100
101
102
103
104
105
106
107
108
109
110
111
112
113
114
115
116
117
118
119
120
121
122
123
124
125
126
127
128
129
130
131
132
133
134
135
136
137
138
139
140
141
142
143
144
145
146
147
148
149
150
151
152
153
154
155
156
157
158
159
160
161
162
163
164
165
166
167
168
169
170
171
172
173
174
175
176
177
178
179
180
181
182
183
184
185
186
187
188
189
190
191
192
193
194
195
196
197
198
199
200
201
202
203
204
205
206
207
208
209
210
211
212
213
214
215
216
217
218
219
220
221
222
223
224
225
226
227
228
229
230
231
232
233
234
235
236
237
238
239
240
241
242
243
244
245
246
247
248
249
250
251
252
253
254
255
256
257
258
259
260
261
262
263
264
265
266
267
268
269
270
271
272
273
274
275
276
277
278
279
280
281
282
283
284
285
286
287
288
289
290
291
292
293
294
295
296
297
298
299
300
301
302
303
304
305
306
307
308
309
310
311
312
313
314
315
316
317
318
319
320
321
322
323
324
325
326
327
328
329
330
331
332
333
334
335
336
337
338
339
340
341
342
343
344
345
346
347
348
349
350
351
352
353
354
355
356
357
358
359
360
361
362
363
364
365
366
367
368
369
370
371
372
373
374
375
376
377
378
379
380
381
382
383
384
385
386
387
388
389
390
391
392
393
394
395
396
397
398
399
400
401
402
403
404
405
406
407
408
409
410
411
412
413
414
415
416
417
418
419
420
421
422
423
424
425
426
427
428
429
430
431
432
433
434
435
436
437
438
439
440
441
442
443
444
445
446
447
448
449
450
451
452
453
454
455
456
457
458
459
460
461
462
463
464
465
466
467
468
469
470
471
472
473
474
475
476
477
478
479
480
481
482
483
484
485
486
487
488
489
490
491
492
493
494
495
496
497
498
499
500
501
502
503
504
505
506
507
508
509
510
511
512
513
514
515
516
517
518
519
520
521
522
523
524
525
526
527
528
529
530
531
532
533
534
535
536
537
538
539
540
541
542
543
544
545
546
547
548
549
550
551
552
553
554
555
556
557
558
559
560
561
562
563
564
565
566
567
568
569
570
571
572
573
574
575
576
577
578
579
580
581
582
583
584
585
586
587
588
589
590
591
592
593
594
595
596
597
598
599
600
601
602
603
604
605
606
607
608
609
610
611
612
613
614
615
616
617
618
619
620
621
622
623
624
625
626
627
628
629
630
631
632
633
634
635
636
637
638
639
640
641
642
643
644
645
646
647
648
649
650
651
652
653
654
655
656
657
658
659
660
661
662
663
664
665
666
667
668
669
670
671
672
673
674
675
676
677
678
679
680
681
682
683
684
685
686
687
688
689
690
691
692
693
694
695
696
697
698
699
700
701
702
703
704
705
706
707
708
709
710
711
712
713
714
715
716
717
718
719
720
721
722
723
724
725
726
727
728
729
730
731
732
733
734
735
736
737
738
739
740
741
742
743
744
745
746
747
748
749
750
751
752
753
754
755
756
757
758
759
760
761
762
763
764
765
766
767
768
769
770
771
772
773
774
775
776
777
778
779
780
781
782
783
784
785
786
787
788
789
790
791
792
793
794
795
796
797
798
799
800
801
802
803
804
805
806
807
808
809
810
811
812
813
814
815
816
817
818
819
820
821
822
823
824
825
826
827
828
829
830
831
832
833
834
835
836
837
838
839
840
841
842
843
844
845
846
847
848
849
850
851
852
853
854
855
856
857
858
859
860
861
862
863
864
865
866
867
868
869
870
871
872
873
874
875
876
877
878
879
880
881
882
883
884
885
886
887
888
889
890
891
892
893
894
895
896
897
898
899
900
901
902
903
904
905
906
907
908
909
910
911
912
913
914
915
916
917
918
919
920
921
922
923
924
925
926
927
928
929
930
931
932
933
934
935
936
937
938
939
940
941
942
943
944
945
946
947
948
949
950
951
952
953
954
955
956
957
958
959
960
961
962
963
964
965
966
967
968
969
970
971
972
973
974
975
976
977
978
979
980
981
982
983
984
985
986
987
988
989
990
991
992
993
994
995
996
997
998
999
1000

```



```

1
2
3
4
5
6
7
8
9
10
11
12
13
14
15
16
17
18
19
20
21
22
23
24
25
26
27
28
29
30
31
32
33
34
35
36
37
38
39
40
41
42
43
44
45
46
47
48
49
50
51
52
53
54
55
56
57
58
59
60
61
62
63
64
65
66
67
68
69
70
71
72
73
74
75
76
77
78
79
80
81
82
83
84
85
86
87
88
89
90
91
92
93
94
95
96
97
98
99
100
101
102
103
104
105
106
107
108
109
110
111
112
113
114
115
116
117
118
119
120
121
122
123
124
125
126
127
128
129
130
131
132
133
134
135
136
137
138
139
140
141
142
143
144
145
146
147
148
149
150
151
152
153
154
155
156
157
158
159
160
161
162
163
164
165
166
167
168
169
170
171
172
173
174
175
176
177
178
179
180
181
182
183
184
185
186
187
188
189
190
191
192
193
194
195
196
197
198
199
200
201
202
203
204
205
206
207
208
209
210
211
212
213
214
215
216
217
218
219
220
221
222
223
224
225
226
227
228
229
230
231
232
233
234
235
236
237
238
239
240
241
242
243
244
245
246
247
248
249
250
251
252
253
254
255
256
257
258
259
260
261
262
263
264
265
266
267
268
269
270
271
272
273
274
275
276
277
278
279
280
281
282
283
284
285
286
287
288
289
290
291
292
293
294
295
296
297
298
299
300
301
302
303
304
305
306
307
308
309
310
311
312
313
314
315
316
317
318
319
320
321
322
323
324
325
326
327
328
329
330
331
332
333
334
335
336
337
338
339
340
341
342
343
344
345
346
347
348
349
350
351
352
353
354
355
356
357
358
359
360
361
362
363
364
365
366
367
368
369
370
371
372
373
374
375
376
377
378
379
380
381
382
383
384
385
386
387
388
389
390
391
392
393
394
395
396
397
398
399
400
401
402
403
404
405
406
407
408
409
410
411
412
413
414
415
416
417
418
419
420
421
422
423
424
425
426
427
428
429
430
431
432
433
434
435
436
437
438
439
440
441
442
443
444
445
446
447
448
449
450
451
452
453
454
455
456
457
458
459
460
461
462
463
464
465
466
467
468
469
470
471
472
473
474
475
476
477
478
479
480
481
482
483
484
485
486
487
488
489
490
491
492
493
494
495
496
497
498
499
500
501
502
503
504
505
506
507
508
509
510
511
512
513
514
515
516
517
518
519
520
521
522
523
524
525
526
527
528
529
530
531
532
533
534
535
536
537
538
539
540
541
542
543
544
545
546
547
548
549
550
551
552
553
554
555
556
557
558
559
560
561
562
563
564
565
566
567
568
569
570
571
572
573
574
575
576
577
578
579
580
581
582
583
584
585
586
587
588
589
590
591
592
593
594
595
596
597
598
599
600
601
602
603
604
605
606
607
608
609
610
611
612
613
614
615
616
617
618
619
620
621
622
623
624
625
626
627
628
629
630
631
632
633
634
635
636
637
638
639
640
641
642
643
644
645
646
647
648
649
650
651
652
653
654
655
656
657
658
659
660
661
662
663
664
665
666
667
668
669
670
671
672
673
674
675
676
677
678
679
680
681
682
683
684
685
686
687
688
689
690
691
692
693
694
695
696
697
698
699
700
701
702
703
704
705
706
707
708
709
710
711
712
713
714
715
716
717
718
719
720
721
722
723
724
725
726
727
728
729
730
731
732
733
734
735
736
737
738
739
740
741
742
743
744
745
746
747
748
749
750
751
752
753
754
755
756
757
758
759
760
761
762
763
764
765
766
767
768
769
770
771
772
773
774
775
776
777
778
779
780
781
782
783
784
785
786
787
788
789
790
791
792
793
794
795
796
797
798
799
800
801
802
803
804
805
806
807
808
809
810
811
812
813
814
815
816
817
818
819
820
821
822
823
824
825
826
827
828
829
830
831
832
833
834
835
836
837
838
839
840
841
842
843
844
845
846
847
848
849
850
851
852
853
854
855
856
857
858
859
860
861
862
863
864
865
866
867
868
869
870
871
872
873
874
875
876
877
878
879
880
881
882
883
884
885
886
887
888
889
890
891
892
893
894
895
896
897
898
899
900
901
902
903
904
905
906
907
908
909
910
911
912
913
914
915
916
917
918
919
920
921
922
923
924
925
926
927
928
929
930
931
932
933
934
935
936
937
938
939
940
941
942
943
944
945
946
947
948
949
950
951
952
953
954
955
956
957
958
959
960
961
962
963
964
965
966
967
968
969
970
971
972
973
974
975
976
977
978
979
980
981
982
983
984
985
986
987
988
989
990
991
992
993
994
995
996
997
998
999
1000

```

```

        @state "gamma"
        @state "gamma2"

        @init {
            gamma = 1.0
            gamma2 = 1.0
        }

        @model {
            for (i = 1; i <= N; i++) {
                // Observed data: y[i] ~ Bernoulli(theta[i])
                y[i] ~ Bernoulli(theta[i])
                // Latent variable: z[i] ~ Bernoulli(theta[i])
                z[i] ~ Bernoulli(theta[i])
                // Latent variable: x[i] ~ Bernoulli(theta[i])
                x[i] ~ Bernoulli(theta[i])
                // Latent variable: w[i] ~ Bernoulli(theta[i])
                w[i] ~ Bernoulli(theta[i])
                // Latent variable: v[i] ~ Bernoulli(theta[i])
                v[i] ~ Bernoulli(theta[i])
                // Latent variable: u[i] ~ Bernoulli(theta[i])
                u[i] ~ Bernoulli(theta[i])
                // Latent variable: t[i] ~ Bernoulli(theta[i])
                t[i] ~ Bernoulli(theta[i])
                // Latent variable: s[i] ~ Bernoulli(theta[i])
                s[i] ~ Bernoulli(theta[i])
                // Latent variable: r[i] ~ Bernoulli(theta[i])
                r[i] ~ Bernoulli(theta[i])
                // Latent variable: q[i] ~ Bernoulli(theta[i])
                q[i] ~ Bernoulli(theta[i])
                // Latent variable: p[i] ~ Bernoulli(theta[i])
                p[i] ~ Bernoulli(theta[i])
                // Latent variable: o[i] ~ Bernoulli(theta[i])
                o[i] ~ Bernoulli(theta[i])
                // Latent variable: n[i] ~ Bernoulli(theta[i])
                n[i] ~ Bernoulli(theta[i])
                // Latent variable: m[i] ~ Bernoulli(theta[i])
                m[i] ~ Bernoulli(theta[i])
                // Latent variable: l[i] ~ Bernoulli(theta[i])
                l[i] ~ Bernoulli(theta[i])
                // Latent variable: k[i] ~ Bernoulli(theta[i])
                k[i] ~ Bernoulli(theta[i])
                // Latent variable: j[i] ~ Bernoulli(theta[i])
                j[i] ~ Bernoulli(theta[i])
                // Latent variable: i[i] ~ Bernoulli(theta[i])
                i[i] ~ Bernoulli(theta[i])
                // Latent variable: h[i] ~ Bernoulli(theta[i])
                h[i] ~ Bernoulli(theta[i])
                // Latent variable: g[i] ~ Bernoulli(theta[i])
                g[i] ~ Bernoulli(theta[i])
                // Latent variable: f[i] ~ Bernoulli(theta[i])
                f[i] ~ Bernoulli(theta[i])
                // Latent variable: e[i] ~ Bernoulli(theta[i])
                e[i] ~ Bernoulli(theta[i])
                // Latent variable: d[i] ~ Bernoulli(theta[i])
                d[i] ~ Bernoulli(theta[i])
                // Latent variable: c[i] ~ Bernoulli(theta[i])
                c[i] ~ Bernoulli(theta[i])
                // Latent variable: b[i] ~ Bernoulli(theta[i])
                b[i] ~ Bernoulli(theta[i])
                // Latent variable: a[i] ~ Bernoulli(theta[i])
                a[i] ~ Bernoulli(theta[i])
            }
        }
    }
}

```

```

      case 1000:
        return 10;
      case 1001:
        return 100;
      case 1002:
        return 1000;
      case 1003:
        return 10000;
      case 1004:
        return 100000;
      default:
        return 1;
    }
  }
}

```

```

// Prints out the number of occurrences of each character in the input string
// computeOccurrences

```

```

10
11
12 int computeOccurrences(const string& str, const int* counts) {
13     // Iterate through all characters in str
14     for (int i = 0; i < str.length(); i++) {
15         counts[str[i]]++;
16     }
17 }

```

## std::Map/STMap

```

// Map: "name" to
// Value: "age"

```

```

void computeOccurrences(const std::map<char, int>& counts) {
    // Iterate through all characters in str
    for (const char& c : str) {
        counts[c]++;
    }
}
// ComputeOccurrences(const string& str, const int* counts) {
//     computeOccurrences(counts);
// }

```

```

// Prints out the number of occurrences of each character in the input string
// computeOccurrences

```

```

10
11
12 void computeOccurrences(const std::map<char, int>& counts) {
13     // Iterate through all characters in str
14     for (const char& c : str) {
15         counts[c]++;
16     }
17 }

```

```

// ComputeOccurrences

```

```

10
11
12 // Iterate through all characters in str
13 for (const char& c : str) {
14     counts[c]++;
15 }

```

```

16
17 // Iterate through all characters in str

```



```

11
12 def get_pos_value
13
14
15 def get_pos_value() int
16 -- returns value of 11 if none
17
18 value = 11
19 value = 11 if value == 0
20 value = 11
21
22
23
24 -- def get_pos() int
25 -- returns 11 if value is none
26
27
28 value = 11
29 value = 11 if value == 0
30 value = 11
31
32
33
34
35 def get_pos_value() int
36 -- def get_pos_value() int
37 -- returns 11 if value is none
38
39
40 value = 11
41 value = 11 if value == 0
42 value = 11
43
44
45
46
47
48
49
50
51
52
53
54
55
56
57
58
59
60
61
62
63
64
65
66
67
68
69
70
71
72
73
74
75
76
77
78
79
80
81
82
83
84
85
86
87
88
89
90
91
92
93
94
95
96
97
98
99
100
101
102
103
104
105
106
107
108
109
110
111
112
113
114
115
116
117
118
119
120
121
122
123
124
125
126
127
128
129
130
131
132
133
134
135
136
137
138
139
140
141
142
143
144
145
146
147
148
149
150
151
152
153
154
155
156
157
158
159
160
161
162
163
164
165
166
167
168
169
170
171
172
173
174
175
176
177
178
179
180
181
182
183
184
185
186
187
188
189
190
191
192
193
194
195
196
197
198
199
200
201
202
203
204
205
206
207
208
209
210
211
212
213
214
215
216
217
218
219
220
221
222
223
224
225
226
227
228
229
230
231
232
233
234
235
236
237
238
239
240
241
242
243
244
245
246
247
248
249
250
251
252
253
254
255
256
257
258
259
260
261
262
263
264
265
266
267
268
269
270
271
272
273
274
275
276
277
278
279
280
281
282
283
284
285
286
287
288
289
290
291
292
293
294
295
296
297
298
299
300
301
302
303
304
305
306
307
308
309
310
311
312
313
314
315
316
317
318
319
320
321
322
323
324
325
326
327
328
329
330
331
332
333
334
335
336
337
338
339
340
341
342
343
344
345
346
347
348
349
350
351
352
353
354
355
356
357
358
359
360
361
362
363
364
365
366
367
368
369
370
371
372
373
374
375
376
377
378
379
380
381
382
383
384
385
386
387
388
389
390
391
392
393
394
395
396
397
398
399
400
401
402
403
404
405
406
407
408
409
410
411
412
413
414
415
416
417
418
419
420
421
422
423
424
425
426
427
428
429
430
431
432
433
434
435
436
437
438
439
440
441
442
443
444
445
446
447
448
449
450
451
452
453
454
455
456
457
458
459
460
461
462
463
464
465
466
467
468
469
470
471
472
473
474
475
476
477
478
479
480
481
482
483
484
485
486
487
488
489
490
491
492
493
494
495
496
497
498
499
500
501
502
503
504
505
506
507
508
509
510
511
512
513
514
515
516
517
518
519
520
521
522
523
524
525
526
527
528
529
530
531
532
533
534
535
536
537
538
539
540
541
542
543
544
545
546
547
548
549
550
551
552
553
554
555
556
557
558
559
560
561
562
563
564
565
566
567
568
569
570
571
572
573
574
575
576
577
578
579
580
581
582
583
584
585
586
587
588
589
590
591
592
593
594
595
596
597
598
599
600
601
602
603
604
605
606
607
608
609
610
611
612
613
614
615
616
617
618
619
620
621
622
623
624
625
626
627
628
629
630
631
632
633
634
635
636
637
638
639
640
641
642
643
644
645
646
647
648
649
650
651
652
653
654
655
656
657
658
659
660
661
662
663
664
665
666
667
668
669
670
671
672
673
674
675
676
677
678
679
680
681
682
683
684
685
686
687
688
689
690
691
692
693
694
695
696
697
698
699
700
701
702
703
704
705
706
707
708
709
710
711
712
713
714
715
716
717
718
719
720
721
722
723
724
725
726
727
728
729
730
731
732
733
734
735
736
737
738
739
740
741
742
743
744
745
746
747
748
749
750
751
752
753
754
755
756
757
758
759
760
761
762
763
764
765
766
767
768
769
770
771
772
773
774
775
776
777
778
779
780
781
782
783
784
785
786
787
788
789
790
791
792
793
794
795
796
797
798
799
800
801
802
803
804
805
806
807
808
809
810
811
812
813
814
815
816
817
818
819
820
821
822
823
824
825
826
827
828
829
830
831
832
833
834
835
836
837
838
839
840
841
842
843
844
845
846
847
848
849
850
851
852
853
854
855
856
857
858
859
860
861
862
863
864
865
866
867
868
869
870
871
872
873
874
875
876
877
878
879
880
881
882
883
884
885
886
887
888
889
890
891
892
893
894
895
896
897
898
899
900
901
902
903
904
905
906
907
908
909
910
911
912
913
914
915
916
917
918
919
920
921
922
923
924
925
926
927
928
929
930
931
932
933
934
935
936
937
938
939
940
941
942
943
944
945
946
947
948
949
950
951
952
953
954
955
956
957
958
959
960
961
962
963
964
965
966
967
968
969
970
971
972
973
974
975
976
977
978
979
980
981
982
983
984
985
986
987
988
989
990
991
992
993
994
995
996
997
998
999
1000

```



**Subroutine:** `subroutine get_moments`

```

c *** get mom ***
c calculate the first four of the mass moments using both the
c the last 100 particles from within, outside of box
c
c table-mom(0) = table-mom(0) + 1
c table-momoms(0) (last particle used table-mom, mom(0) in 1)
c for i = 0, 1, 2 table-momoms(0), i = 1, 2
c table-momoms(0), i = table-mom(i) + 1 = table-mom(i) + 1
c table-mom(i) = 1, 2 + table-mom(i) table-momoms(i)
c
c
c *** get mom(0) ***
c calculate the first four of the 1st mass moments
c
c table-mom(0) = table-mom(0) + 1
c table-mom(0) = 1 table-mom(0) = mom_mom_momoms(0)
c
c
c *** get mom(0) ***
c calculate the first four of the 1st mass moments
c
c table-mom(0) = table-mom(0) + 1
c
c
c *** get the 1st mass (0) mom parent, outside
c
c for i = 1, 2, 3 table-momoms(0), i = 1, 2
c
c mom = table-momoms(0)
c
c
c *** get mom(0) ***
c table the 1st mass of this particle
c
c mom-mom(0) = mom-m(0)
c
c
c for the 1st mass (0) i = 1
c table the mom(0) moments around this particle
c
c mom-mom(0) = mom-momoms(0)
c
c
c *** get mom(0) ***
c calculate the 1st mass of this particle
c
c mom-mom(0) = table-mom(0) + 1
c mom-mom(0) = 1 + 1 + mom-momoms(0)
c
c
c *** get mom(0) ***
c in parent, compute the particle's mass moments
c
c if mom-momoms(0) = 0 or mom-momoms(0) = 0 then i = 0
c mom-mom(0) = table-mom(0) + 1
c table-mom(0) = 1 + 1 + mom-momoms(0)
c
c
c
c mom-mom(0) = 0
c
c
c *** get mom(0) ***
c compute the 1st mass of this particle
c
c mom-mom(0) = table-mom(0) + 1
c table-mom(0) = 1 + 1 + mom-momoms(0)

```

```

% == (case (case)) ==
% compute the maximum degree among
%


$\text{prior}(\text{case}) = \text{table}(\text{case}) + 1$



$\text{table}(\text{case}) \leftarrow \text{prior}(\text{case})/\text{sum}(\text{prior})$


%
% == (case (case)) ==
% compute the case counts as prior information about action
%


$\text{prior}(\text{case}) = \text{table}(\text{case}) + 1$



$\text{table}(\text{case}) \leftarrow \text{prior}(\text{case})/\text{sum}(\text{prior})$


%
% == (case (case)) ==
% compute the case counts as prior information about
%


$\text{prior}(\text{case}) = \text{table}(\text{case}) + 1$


%
% compute the case counts without the case of interest
%


$\text{case} \leftarrow \text{P}_i \setminus \{i\}$



$\text{prior} \leftarrow \text{prior}(\text{case})$



$\text{table}(\text{prior} \sim \text{type}) \leftarrow 1$


%
% == (case (case)) ==
% == (case (case)) ==


$\text{prior}(\text{case}) = \text{table}(\text{case}) + 1 + \text{prior}(\text{case}) + 1$



$\text{table}(\text{case}) \leftarrow 1 + 2 * \text{prior}(\text{case})/\text{sum}(\text{prior})$



$\text{prior} \leftarrow 1 + 2 * \text{prior}(\text{case})/\text{sum}(\text{prior})$


%
% == (case (case)) ==


$\text{prior}(\text{case}) = \text{table}(\text{case}) + 1 + \text{prior}(\text{case}) + 1$



$\text{table}(\text{case}) \leftarrow 1 + 1 + \text{prior}(\text{case})/\text{sum}(\text{prior})$


%
%
%
% == (case (case)) ==
% compute the output after iteration
%


$\text{prior}(\text{case}) = \text{table}(\text{case}) + 1$



$\text{table}(\text{case}) \leftarrow \text{prior}(\text{case})/\text{sum}(\text{prior})$


%
% == (case (case)) ==
% computing the output data is allowed
%


$\text{prior}(\text{case}) = 1$


%
% == (case (case)) ==
% compute the output after iteration
%


$\text{prior}(\text{case}) = \text{table}(\text{case}) + 1$



$\text{table}(\text{case}) \leftarrow \text{prior}(\text{case})/\text{sum}(\text{prior})$


%
% == (case (case)) ==
% compute the output after iteration
%


$\text{prior}(\text{case}) = \text{table}(\text{case}) + 1$


```



- 1.  $2^k$  out of loop to escape case 1)
- 2. out of loop to make all variables for problem  $k$
- 3. out of loop to make all problem  $k$

3

### result 3

```

1) Input: array A
2) Input: array B
3) Input: array C

4) Input: array A
5) Input: array B
6) Input: array C
7) Input: array C

8) Input: array A
9) Input: array B
10) Input: array C
11) Input: array A
12) Input: array B
13) Input: array C
14) Input: array A
15) Input: array B
16) Input: array C
17) Input: array A
18) Input: array B
19) Input: array C
20) Input: array A
21) Input: array B
22) Input: array C
23) Input: array A
24) Input: array B
25) Input: array C
26) Input: array A
27) Input: array B
28) Input: array C
29) Input: array A
30) Input: array B
31) Input: array C
32) Input: array A
33) Input: array B
34) Input: array C
35) Input: array A
36) Input: array B
37) Input: array C
38) Input: array A
39) Input: array B
40) Input: array C
41) Input: array A
42) Input: array B
43) Input: array C
44) Input: array A
45) Input: array B
46) Input: array C
47) Input: array A
48) Input: array B
49) Input: array C
50) Input: array A
51) Input: array B
52) Input: array C
53) Input: array A
54) Input: array B
55) Input: array C
56) Input: array A
57) Input: array B
58) Input: array C
59) Input: array A
60) Input: array B
61) Input: array C
62) Input: array A
63) Input: array B
64) Input: array C
65) Input: array A
66) Input: array B
67) Input: array C
68) Input: array A
69) Input: array B
70) Input: array C
71) Input: array A
72) Input: array B
73) Input: array C
74) Input: array A
75) Input: array B
76) Input: array C
77) Input: array A
78) Input: array B
79) Input: array C
80) Input: array A
81) Input: array B
82) Input: array C
83) Input: array A
84) Input: array B
85) Input: array C
86) Input: array A
87) Input: array B
88) Input: array C
89) Input: array A
90) Input: array B
91) Input: array C
92) Input: array A
93) Input: array B
94) Input: array C
95) Input: array A
96) Input: array B
97) Input: array C
98) Input: array A
99) Input: array B
100) Input: array C

```

### result 4

```

1) Input: array A
2) Input: array B
3) Input: array C
4) Input: array A
5) Input: array B
6) Input: array C
7) Input: array A
8) Input: array B
9) Input: array C
10) Input: array A
11) Input: array B
12) Input: array C
13) Input: array A
14) Input: array B
15) Input: array C
16) Input: array A
17) Input: array B
18) Input: array C
19) Input: array A
20) Input: array B
21) Input: array C
22) Input: array A
23) Input: array B
24) Input: array C
25) Input: array A
26) Input: array B
27) Input: array C
28) Input: array A
29) Input: array B
30) Input: array C
31) Input: array A
32) Input: array B
33) Input: array C
34) Input: array A
35) Input: array B
36) Input: array C
37) Input: array A
38) Input: array B
39) Input: array C
40) Input: array A
41) Input: array B
42) Input: array C
43) Input: array A
44) Input: array B
45) Input: array C
46) Input: array A
47) Input: array B
48) Input: array C
49) Input: array A
50) Input: array B
51) Input: array C
52) Input: array A
53) Input: array B
54) Input: array C
55) Input: array A
56) Input: array B
57) Input: array C
58) Input: array A
59) Input: array B
60) Input: array C
61) Input: array A
62) Input: array B
63) Input: array C
64) Input: array A
65) Input: array B
66) Input: array C
67) Input: array A
68) Input: array B
69) Input: array C
70) Input: array A
71) Input: array B
72) Input: array C
73) Input: array A
74) Input: array B
75) Input: array C
76) Input: array A
77) Input: array B
78) Input: array C
79) Input: array A
80) Input: array B
81) Input: array C
82) Input: array A
83) Input: array B
84) Input: array C
85) Input: array A
86) Input: array B
87) Input: array C
88) Input: array A
89) Input: array B
90) Input: array C
91) Input: array A
92) Input: array B
93) Input: array C
94) Input: array A
95) Input: array B
96) Input: array C
97) Input: array A
98) Input: array B
99) Input: array C
100) Input: array A

```





























```

subprocesses := 0
for i in 1..N do
  if i = 1 then
    subprocesses := 1
  else
    subprocesses := 2 * subprocesses
  end if
end for
return subprocesses
end function

-- Example 1: N = 10
N := 10
subprocesses := 0
for i in 1..N do
  if i = 1 then
    subprocesses := 1
  else
    subprocesses := 2 * subprocesses
  end if
end for
return subprocesses
end function

-- Example 2: N = 10
N := 10
subprocesses := 0
for i in 1..N do
  if i = 1 then
    subprocesses := 1
  else
    subprocesses := 2 * subprocesses
  end if
end for
return subprocesses
end function

-- Example 3: N = 10
N := 10
subprocesses := 0
for i in 1..N do
  if i = 1 then
    subprocesses := 1
  else
    subprocesses := 2 * subprocesses
  end if
end for
return subprocesses
end function

-- Example 4: N = 10
N := 10
subprocesses := 0
for i in 1..N do
  if i = 1 then
    subprocesses := 1
  else
    subprocesses := 2 * subprocesses
  end if
end for
return subprocesses
end function

-- Example 5: N = 10
N := 10
subprocesses := 0
for i in 1..N do
  if i = 1 then
    subprocesses := 1
  else
    subprocesses := 2 * subprocesses
  end if
end for
return subprocesses
end function

-- Example 6: N = 10
N := 10
subprocesses := 0
for i in 1..N do
  if i = 1 then
    subprocesses := 1
  else
    subprocesses := 2 * subprocesses
  end if
end for
return subprocesses
end function

-- Example 7: N = 10
N := 10
subprocesses := 0
for i in 1..N do
  if i = 1 then
    subprocesses := 1
  else
    subprocesses := 2 * subprocesses
  end if
end for
return subprocesses
end function

-- Example 8: N = 10
N := 10
subprocesses := 0
for i in 1..N do
  if i = 1 then
    subprocesses := 1
  else
    subprocesses := 2 * subprocesses
  end if
end for
return subprocesses
end function

-- Example 9: N = 10
N := 10
subprocesses := 0
for i in 1..N do
  if i = 1 then
    subprocesses := 1
  else
    subprocesses := 2 * subprocesses
  end if
end for
return subprocesses
end function

-- Example 10: N = 10
N := 10
subprocesses := 0
for i in 1..N do
  if i = 1 then
    subprocesses := 1
  else
    subprocesses := 2 * subprocesses
  end if
end for
return subprocesses
end function

```































































```

1  print "on 000 seconds done"
2
3  ##### "Interim" on 0000 on a random time before
4  random "Interim" on 00 00 00 000
5  random "Interim" on 00 00 00 000000 00
6
7
8  next randomTime() until $ == $my "0000" time
9
10
11  $m = 0
12  $n = $m * 10
13  $time = $m * 1000000 + $n
14
15  ##### "Time" 1
16  $i = 0
17  $m = 0
18  $n = 0
19  $t = 0
20  $t = 0
21  $t = 0
22  $t = 0
23  $t = 0
24  $t = 0
25  $t = 0
26  $t = 0
27  $t = 0
28  $t = 0
29  $t = 0
30  $t = 0
31  $t = 0
32  $t = 0
33  $t = 0
34  $t = 0
35  $t = 0
36  $t = 0
37  $t = 0
38  $t = 0
39  $t = 0
40  $t = 0
41  $t = 0
42  $t = 0
43  $t = 0
44  $t = 0
45  $t = 0
46  $t = 0
47  $t = 0
48  $t = 0
49  $t = 0
50  $t = 0
51  $t = 0
52  $t = 0
53  $t = 0
54  $t = 0
55  $t = 0
56  $t = 0
57  $t = 0
58  $t = 0
59  $t = 0
60  $t = 0
61  $t = 0
62  $t = 0
63  $t = 0
64  $t = 0
65  $t = 0
66  $t = 0
67  $t = 0
68  $t = 0
69  $t = 0
70  $t = 0
71  $t = 0
72  $t = 0
73  $t = 0
74  $t = 0
75  $t = 0
76  $t = 0
77  $t = 0
78  $t = 0
79  $t = 0
80  $t = 0
81  $t = 0
82  $t = 0
83  $t = 0
84  $t = 0
85  $t = 0
86  $t = 0
87  $t = 0
88  $t = 0
89  $t = 0
90  $t = 0
91  $t = 0
92  $t = 0
93  $t = 0
94  $t = 0
95  $t = 0
96  $t = 0
97  $t = 0
98  $t = 0
99  $t = 0
100 $t = 0

```













— *Journal of the Royal Society of Medicine*

— *Journal of the Royal Society of Medicine*

— *Journal of the Royal Society of Medicine*

— *Journal of the Royal Society of Medicine*

— *Journal of the Royal Society of Medicine*

— *Journal of the Royal Society of Medicine*

— *Journal of the Royal Society of Medicine*

— *Journal of the Royal Society of Medicine*

—

## REFERENCES

— *Journal of the Royal Society of Medicine*

— *Journal of the Royal Society of Medicine*

— *Journal of the Royal Society of Medicine*

— *Journal of the Royal Society of Medicine*

— *Journal of the Royal Society of Medicine*



```

1  function submatrix(m, n)
2  submatrix(m, n) = submatrix(1:m, 1:n, m, n)

3  -- function submatrix(m, n)
4  submatrix(m, n) = submatrix(1:m, 1:n, m, n)

5  -- function submatrix(m, n, m, n)
6  submatrix(m, n, m, n) = submatrix(1:m, 1:n, m, n)

```

End of

### submatrix

function submatrix(m, n)

submatrix(m, n) = submatrix(1:m, 1:n, m, n) submatrix(m, n) = submatrix(1:m, 1:n, m, n)

-- submatrix(m, n)

-- submatrix(m, n) = submatrix(1:m, 1:n, m, n)

-- submatrix(m, n) = submatrix(1:m, 1:n, m, n)

-- submatrix(m, n) = submatrix(1:m, 1:n, m, n)

-- submatrix(m, n)

```

1  submatrix(m, n) = submatrix(1:m, 1:n, m, n)
2  submatrix(m, n) = submatrix(1:m, 1:n, m, n)
3  submatrix(m, n) = submatrix(1:m, 1:n, m, n)
4  submatrix(m, n) = submatrix(1:m, 1:n, m, n)
5  submatrix(m, n) = submatrix(1:m, 1:n, m, n)

```

submatrix(m, n)

-- submatrix(m, n) = submatrix(1:m, 1:n, m, n) submatrix(m, n) = submatrix(1:m, 1:n, m, n)

-- submatrix(m, n)

-- submatrix(m, n) = submatrix(1:m, 1:n, m, n)

-- submatrix(m, n) = submatrix(1:m, 1:n, m, n)

-- submatrix(m, n) = submatrix(1:m, 1:n, m, n)

-- submatrix(m, n)

-- submatrix(m, n) = submatrix(1:m, 1:n, m, n)

-- submatrix(m, n)

-- submatrix(m, n) = submatrix(1:m, 1:n, m, n)

-- submatrix(m, n) = submatrix(1:m, 1:n, m, n)

-- submatrix(m, n) = submatrix(1:m, 1:n, m, n)

-- submatrix(m, n) = submatrix(1:m, 1:n, m, n)

-- submatrix(m, n) = submatrix(1:m, 1:n, m, n)

-- submatrix(m, n)

-- submatrix(m, n)

-- submatrix(m, n)

-- submatrix(m, n) = submatrix(1:m, 1:n, m, n) submatrix(m, n) = submatrix(1:m, 1:n, m, n)

-- submatrix(m, n)

-- submatrix(m, n)

-- submatrix(m, n) = submatrix(1:m, 1:n, m, n)

-- submatrix(m, n)

-- submatrix(m, n)















































```

13 100 100
14 100 100
15 100 100
16 100 100
17 100 100
18 100 100
19 100 100
20 100 100
21 100 100
22 100 100
23 100 100
24 100 100
25 100 100
26 100 100
27 100 100
28 100 100
29 100 100
30 100 100
31 100 100
32 100 100
33 100 100
34 100 100
35 100 100
36 100 100
37 100 100
38 100 100
39 100 100
40 100 100
41 100 100
42 100 100
43 100 100
44 100 100
45 100 100
46 100 100
47 100 100
48 100 100
49 100 100
50 100 100
51 100 100
52 100 100
53 100 100
54 100 100
55 100 100
56 100 100
57 100 100
58 100 100
59 100 100
60 100 100
61 100 100
62 100 100
63 100 100
64 100 100
65 100 100
66 100 100
67 100 100
68 100 100
69 100 100
70 100 100
71 100 100
72 100 100
73 100 100
74 100 100
75 100 100
76 100 100
77 100 100
78 100 100
79 100 100
80 100 100
81 100 100
82 100 100
83 100 100
84 100 100
85 100 100
86 100 100
87 100 100
88 100 100
89 100 100
90 100 100
91 100 100
92 100 100
93 100 100
94 100 100
95 100 100
96 100 100
97 100 100
98 100 100
99 100 100
100 100 100

```

```

100 101 102 103 104 105 106 107 108 109 110 111 112 113 114 115 116 117 118 119 120 121 122 123 124 125 126 127 128 129 130 131 132 133 134 135 136 137 138 139 140 141 142 143 144 145 146 147 148 149 150 151 152 153 154 155 156 157 158 159 160 161 162 163 164 165 166 167 168 169 170 171 172 173 174 175 176 177 178 179 180 181 182 183 184 185 186 187 188 189 190 191 192 193 194 195 196 197 198 199 200 201 202 203 204 205 206 207 208 209 210 211 212 213 214 215 216 217 218 219 220 221 222 223 224 225 226 227 228 229 230 231 232 233 234 235 236 237 238 239 240 241 242 243 244 245 246 247 248 249 250 251 252 253 254 255 256 257 258 259 260 261 262 263 264 265 266 267 268 269 270 271 272 273 274 275 276 277 278 279 280 281 282 283 284 285 286 287 288 289 290 291 292 293 294 295 296 297 298 299 300 301 302 303 304 305 306 307 308 309 310 311 312 313 314 315 316 317 318 319 320 321 322 323 324 325 326 327 328 329 330 331 332 333 334 335 336 337 338 339 340 341 342 343 344 345 346 347 348 349 350 351 352 353 354 355 356 357 358 359 360 361 362 363 364 365 366 367 368 369 370 371 372 373 374 375 376 377 378 379 380 381 382 383 384 385 386 387 388 389 390 391 392 393 394 395 396 397 398 399 400 401 402 403 404 405 406 407 408 409 410 411 412 413 414 415 416 417 418 419 420 421 422 423 424 425 426 427 428 429 430 431 432 433 434 435 436 437 438 439 440 441 442 443 444 445 446 447 448 449 450 451 452 453 454 455 456 457 458 459 460 461 462 463 464 465 466 467 468 469 470 471 472 473 474 475 476 477 478 479 480 481 482 483 484 485 486 487 488 489 490 491 492 493 494 495 496 497 498 499 500 501 502 503 504 505 506 507 508 509 510 511 512 513 514 515 516 517 518 519 520 521 522 523 524 525 526 527 528 529 530 531 532 533 534 535 536 537 538 539 540 541 542 543 544 545 546 547 548 549 550 551 552 553 554 555 556 557 558 559 560 561 562 563 564 565 566 567 568 569 570 571 572 573 574 575 576 577 578 579 580 581 582 583 584 585 586 587 588 589 590 591 592 593 594 595 596 597 598 599 600 601 602 603 604 605 606 607 608 609 610 611 612 613 614 615 616 617 618 619 620 621 622 623 624 625 626 627 628 629 630 631 632 633 634 635 636 637 638 639 640 641 642 643 644 645 646 647 648 649 650 651 652 653 654 655 656 657 658 659 660 661 662 663 664 665 666 667 668 669 670 671 672 673 674 675 676 677 678 679 680 681 682 683 684 685 686 687 688 689 690 691 692 693 694 695 696 697 698 699 700 701 702 703 704 705 706 707 708 709 710 711 712 713 714 715 716 717 718 719 720 721 722 723 724 725 726 727 728 729 730 731 732 733 734 735 736 737 738 739 740 741 742 743 744 745 746 747 748 749 750 751 752 753 754 755 756 757 758 759 760 761 762 763 764 765 766 767 768 769 770 771 772 773 774 775 776 777 778 779 780 781 782 783 784 785 786 787 788 789 790 791 792 793 794 795 796 797 798 799 800 801 802 803 804 805 806 807 808 809 810 811 812 813 814 815 816 817 818 819 820 821 822 823 824 825 826 827 828 829 830 831 832 833 834 835 836 837 838 839 840 841 842 843 844 845 846 847 848 849 850 851 852 853 854 855 856 857 858 859 860 861 862 863 864 865 866 867 868 869 870 871 872 873 874 875 876 877 878 879 880 881 882 883 884 885 886 887 888 889 890 891 892 893 894 895 896 897 898 899 900 901 902 903 904 905 906 907 908 909 910 911 912 913 914 915 916 917 918 919 920 921 922 923 924 925 926 927 928 929 930 931 932 933 934 935 936 937 938 939 940 941 942 943 944 945 946 947 948 949 950 951 952 953 954 955 956 957 958 959 960 961 962 963 964 965 966 967 968 969 970 971 972 973 974 975 976 977 978 979 980 981 982 983 984 985 986 987 988 989 990 991 992 993 994 995 996 997 998 999 1000

```



















[illegible][illegible]

Copyright © 2002 John Wiley & Sons, Inc. All rights reserved. This book is registered at the Copyright Clearance Center, Inc., 222 Rosewood Drive, Danvers, MA 01923. Organizations in the U.S. who are also registered with C.C.C. may therefore copy material (beyond the limits permitted by sections 107 and 108 of U.S. copyright law) subject to payment to C.C.C. of the per copy fee of \$0.50. This consent does not extend to multiple copying for promotional or commercial purposes. ISI Tear Sheet Service, 3501 Market Street, Philadelphia, PA 19104, USA, is authorized to supply single copies of separate articles for private use only. Organizations authorized by the Copyright Licensing Agency may also copy material subject to the usual conditions. For all other use, permission should be sought from John Wiley & Sons, Inc.

1997, 1998, 1999, 2000, 2001, 2002, 2003, 2004, 2005, 2006, 2007, 2008, 2009, 2010, 2011, 2012, 2013, 2014, 2015, 2016, 2017, 2018, 2019, 2020, 2021, 2022, 2023, 2024, 2025, 2026, 2027, 2028, 2029, 2030, 2031, 2032, 2033, 2034, 2035, 2036, 2037, 2038, 2039, 2040, 2041, 2042, 2043, 2044, 2045, 2046, 2047, 2048, 2049, 2050, 2051, 2052, 2053, 2054, 2055, 2056, 2057, 2058, 2059, 2060, 2061, 2062, 2063, 2064, 2065, 2066, 2067, 2068, 2069, 2070, 2071, 2072, 2073, 2074, 2075, 2076, 2077, 2078, 2079, 2080, 2081, 2082, 2083, 2084, 2085, 2086, 2087, 2088, 2089, 2090, 2091, 2092, 2093, 2094, 2095, 2096, 2097, 2098, 2099, 2100, 2101, 2102, 2103, 2104, 2105, 2106, 2107, 2108, 2109, 2110, 2111, 2112, 2113, 2114, 2115, 2116, 2117, 2118, 2119, 2120, 2121, 2122, 2123, 2124, 2125, 2126, 2127, 2128, 2129, 2130, 2131, 2132, 2133, 2134, 2135, 2136, 2137, 2138, 2139, 2140, 2141, 2142, 2143, 2144, 2145, 2146, 2147, 2148, 2149, 2150, 2151, 2152, 2153, 2154, 2155, 2156, 2157, 2158, 2159, 2160, 2161, 2162, 2163, 2164, 2165, 2166, 2167, 2168, 2169, 2170, 2171, 2172, 2173, 2174, 2175, 2176, 2177, 2178, 2179, 2180, 2181, 2182, 2183, 2184, 2185, 2186, 2187, 2188, 2189, 2190, 2191, 2192, 2193, 2194, 2195, 2196, 2197, 2198, 2199, 2200, 2201, 2202, 2203, 2204, 2205, 2206, 2207, 2208, 2209, 2210, 2211, 2212, 2213, 2214, 2215, 2216, 2217, 2218, 2219, 2220, 2221, 2222, 2223, 2224, 2225, 2226, 2227, 2228, 2229, 2230, 2231, 2232, 2233, 2234, 2235, 2236, 2237, 2238, 2239, 2240, 2241, 2242, 2243, 2244, 2245, 2246, 2247, 2248, 2249, 2250, 2251, 2252, 2253, 2254, 2255, 2256, 2257, 2258, 2259, 2260, 2261, 2262, 2263, 2264, 2265, 2266, 2267, 2268, 2269, 2270, 2271, 2272, 2273, 2274, 2275, 2276, 2277, 2278, 2279, 2280, 2281, 2282, 2283, 2284, 2285, 2286, 2287, 2288, 2289, 2290, 2291, 2292, 2293, 2294, 2295, 2296, 2297, 2298, 2299, 2300, 2301, 2302, 2303, 2304, 2305, 2306, 2307, 2308, 2309, 2310, 2311, 2312, 2313, 2314, 2315, 2316, 2317, 2318, 2319, 2320, 2321, 2322, 2323, 2324, 2325, 2326, 2327, 2328, 2329, 2330, 2331, 2332, 2333, 2334, 2335, 2336, 2337, 2338, 2339, 2340, 2341, 2342, 2343, 2344, 2345, 2346, 2347, 2348, 2349, 2350, 2351, 2352, 2353, 2354, 2355, 2356, 2357, 2358, 2359, 2360, 2361, 2362, 2363, 2364, 2365, 2366, 2367, 2368, 2369, 2370, 2371, 2372, 2373, 2374, 2375, 2376, 2377, 2378, 2379, 2380, 2381, 2382, 2383, 2384, 2385, 2386, 2387, 2388, 2389, 2390, 2391, 2392, 2393, 2394, 2395, 2396, 2397, 2398, 2399, 2400, 2401, 2402, 2403, 2404, 2405, 2406, 2407, 2408, 2409, 2410, 2411, 2412, 2413, 2414, 2415, 2416, 2417, 2418, 2419, 2420, 2421, 2422, 2423, 2424, 2425, 2426, 2427, 2428, 2429, 2430, 2431, 2432, 2433, 2434, 2435, 2436, 2437, 2438, 2439, 2440, 2441, 2442, 2443, 2444, 2445, 2446, 2447, 2448, 2449, 2450, 2451, 2452, 2453, 2454, 2455, 2456, 2457, 2458, 2459, 2460, 2461, 2462, 2463, 2464, 2465, 2466, 2467, 2468, 2469, 2470, 2471, 2472, 2473, 2474, 2475, 2476, 2477, 2478, 2479, 2480, 2481, 2482, 2483, 2484, 2485, 2486, 2487, 2488, 2489, 2490, 2491, 2492, 2493, 2494, 2495, 2496, 2497, 2498, 2499, 2500, 2501, 2502, 2503, 2504, 2505, 2506, 2507, 2508, 2509, 2510, 2511, 2512, 2513, 2514, 2515, 2516, 2517, 2518, 2519, 2520, 2521, 2522, 2523, 2524, 2525, 2526, 2527, 2528, 2529, 2530, 2531, 2532, 2533, 2534, 2535, 2536, 2537, 2538, 2539, 2540, 2541, 2542, 2543, 2544, 2545, 2546, 2547, 2548, 2549, 2550, 2551, 2552, 2553, 2554, 2555, 2556, 2557, 2558, 2559, 2560, 2561, 2562, 2563, 2564, 2565, 2566, 2567, 2568, 2569, 2570, 2571, 2572, 2573, 2574, 2575, 2576, 2577, 2578, 2579, 2580, 2581, 2582, 2583, 2584, 2585, 2586, 2587, 2588, 2589, 2590, 2591, 2592, 2593, 2594, 2595, 2596, 2597, 2598, 2599, 2600, 2601, 2602, 2603, 2604, 2605, 2606, 2607, 2608, 2609, 2610, 2611, 2612, 2613, 2614, 2615, 2616, 2617, 2618, 2619, 2620, 2621, 2622, 2623, 2624, 2625, 2626, 2627, 2628, 2629, 2630, 2631, 2632, 2633, 2634, 2635, 2636, 2637, 2638, 2639, 2640, 2641, 2642, 2643, 2644, 2645, 2646, 2647, 2648, 2649, 2650, 2651, 2652, 2653, 2654, 2655, 2656, 2657, 2658, 2659, 2660, 2661, 2662, 2663, 2664, 2665, 2666, 2667, 2668, 2669, 2670, 2671, 2672, 2673, 2674, 2675, 2676, 2677, 2678, 26

**Figure 11.10** *Graph of the function  $f(x) = \frac{1}{x}$  for  $x > 0$ . The function is continuous on the interval  $(0, \infty)$ .*

NOTE: We intend to submit this article online by April 2008 and require eight months to allow you to submit your review and revision(s). Please indicate in the following box your time window. It is in reviewing manuscripts of the journal *Journal of Management* on January 26, 2008.

© 2000 Blackwell Science Ltd  
Journal of Internal Medicine 247: 105–112

**Table 1** Demographic characteristics of study population

1. Introduction  
 2. Background  
 3. Methodology  
 4. Results  
 5. Conclusion  
 6. References  
 7. Appendix  
 8. Glossary  
 9. Index  
 10. Table of Contents  
 11. Figure of Contents  
 12. Table of Figures  
 13. Table of Tables  
 14. Table of Equations  
 15. Table of Symbols  
 16. Table of Abbreviations  
 17. Table of Acronyms  
 18. Table of Initials  
 19. Table of Symbols  
 20. Table of Abbreviations  
 21. Table of Acronyms  
 22. Table of Initials  
 23. Table of Symbols  
 24. Table of Abbreviations  
 25. Table of Acronyms  
 26. Table of Initials  
 27. Table of Symbols  
 28. Table of Abbreviations  
 29. Table of Acronyms  
 30. Table of Initials  
 31. Table of Symbols  
 32. Table of Abbreviations  
 33. Table of Acronyms  
 34. Table of Initials  
 35. Table of Symbols  
 36. Table of Abbreviations  
 37. Table of Acronyms  
 38. Table of Initials  
 39. Table of Symbols  
 40. Table of Abbreviations  
 41. Table of Acronyms  
 42. Table of Initials  
 43. Table of Symbols  
 44. Table of Abbreviations  
 45. Table of Acronyms  
 46. Table of Initials  
 47. Table of Symbols  
 48. Table of Abbreviations  
 49. Table of Acronyms  
 50. Table of Initials  
 51. Table of Symbols  
 52. Table of Abbreviations  
 53. Table of Acronyms  
 54. Table of Initials  
 55. Table of Symbols  
 56. Table of Abbreviations  
 57. Table of Acronyms  
 58. Table of Initials  
 59. Table of Symbols  
 60. Table of Abbreviations  
 61. Table of Acronyms  
 62. Table of Initials  
 63. Table of Symbols  
 64. Table of Abbreviations  
 65. Table of Acronyms  
 66. Table of Initials  
 67. Table of Symbols  
 68. Table of Abbreviations  
 69. Table of Acronyms  
 70. Table of Initials  
 71. Table of Symbols  
 72. Table of Abbreviations  
 73. Table of Acronyms  
 74. Table of Initials  
 75. Table of Symbols  
 76. Table of Abbreviations  
 77. Table of Acronyms  
 78. Table of Initials  
 79. Table of Symbols  
 80. Table of Abbreviations  
 81. Table of Acronyms  
 82. Table of Initials  
 83. Table of Symbols  
 84. Table of Abbreviations  
 85. Table of Acronyms  
 86. Table of Initials  
 87. Table of Symbols  
 88. Table of Abbreviations  
 89. Table of Acronyms  
 90. Table of Initials  
 91. Table of Symbols  
 92. Table of Abbreviations  
 93. Table of Acronyms  
 94. Table of Initials  
 95. Table of Symbols  
 96. Table of Abbreviations  
 97. Table of Acronyms  
 98. Table of Initials  
 99. Table of Symbols  
 100. Table of Abbreviations  
 101. Table of Acronyms  
 102. Table of Initials  
 103. Table of Symbols  
 104. Table of Abbreviations  
 105. Table of Acronyms  
 106. Table of Initials  
 107. Table of Symbols  
 108. Table of Abbreviations  
 109. Table of Acronyms  
 110. Table of Initials  
 111. Table of Symbols  
 112. Table of Abbreviations  
 113. Table of Acronyms  
 114. Table of Initials  
 115. Table of Symbols  
 116. Table of Abbreviations  
 117. Table of Acronyms  
 118. Table of Initials  
 119. Table of Symbols  
 120. Table of Abbreviations  
 121. Table of Acronyms  
 122. Table of Initials  
 123. Table of Symbols  
 124. Table of Abbreviations  
 125. Table of Acronyms  
 126. Table of Initials  
 127. Table of Symbols  
 128. Table of Abbreviations  
 129. Table of Acronyms  
 130. Table of Initials  
 131. Table of Symbols  
 132. Table of Abbreviations  
 133. Table of Acronyms  
 134. Table of Initials  
 135. Table of Symbols  
 136. Table of Abbreviations  
 137. Table of Acronyms  
 138. Table of Initials  
 139. Table of Symbols  
 140. Table of Abbreviations  
 141. Table of Acronyms  
 142. Table of Initials  
 143. Table of Symbols  
 144. Table of Abbreviations  
 145. Table of Acronyms  
 146. Table of Initials  
 147. Table of Symbols  
 148. Table of Abbreviations  
 149. Table of Acronyms  
 150. Table of Initials  
 151. Table of Symbols  
 152. Table of Abbreviations  
 153. Table of Acronyms  
 154. Table of Initials  
 155. Table of Symbols  
 156. Table of Abbreviations  
 157. Table of Acronyms  
 158. Table of Initials  
 159. Table of Symbols  
 160. Table of Abbreviations  
 161. Table of Acronyms  
 162. Table of Initials  
 163. Table of Symbols  
 164. Table of Abbreviations  
 165. Table of Acronyms  
 166. Table of Initials  
 167. Table of Symbols  
 168. Table of Abbreviations  
 169. Table of Acronyms  
 170. Table of Initials  
 171. Table of Symbols  
 172. Table of Abbreviations  
 173. Table of Acronyms  
 174. Table of Initials  
 175. Table of Symbols  
 176. Table of Abbreviations  
 177. Table of Acronyms  
 178. Table of Initials  
 179. Table of Symbols  
 180. Table of Abbreviations  
 181. Table of Acronyms  
 182. Table of Initials  
 183. Table of Symbols  
 184. Table of Abbreviations  
 185. Table of Acronyms  
 186. Table of Initials  
 187. Table of Symbols  
 188. Table of Abbreviations  
 189. Table of Acronyms  
 190. Table of Initials  
 191. Table of Symbols  
 192. Table of Abbreviations  
 193. Table of Acronyms  
 194. Table of Initials  
 195. Table of Symbols  
 196. Table of Abbreviations  
 197. Table of Acronyms  
 198. Table of Initials  
 199. Table of Symbols  
 200. Table of Abbreviations  
 201. Table of Acronyms  
 202. Table of Initials  
 203. Table of Symbols  
 204. Table of Abbreviations  
 205. Table of Acronyms  
 206. Table of Initials  
 207. Table of Symbols  
 208. Table of Abbreviations  
 209. Table of Acronyms  
 210. Table of Initials  
 211. Table of Symbols  
 212. Table of Abbreviations  
 213. Table of Acronyms  
 214. Table of Initials  
 215. Table of Symbols  
 216. Table of Abbreviations  
 217. Table of Acronyms  
 218. Table of Initials  
 219. Table of Symbols  
 220. Table of Abbreviations

© 2005 Blackwell Publishing Ltd, *Journal of Internal Medicine* 258: 105–112



100

[illegible]

1000

**Abstract**

updates on other examples of  
updates and the concept of  
updates by the group.

As the director of the program, I was relieved for the opportunity of interacting with you in looking at the issues of development and globalization. It is an opportunity for me to "recharge" myself by reflecting the past time I spent at the same university in the United States with students from the United States. I hope to see you in the future in the same region for another "recharge" and opportunity to discuss the issues.

Thank you for the great opportunity to be at the meeting, and also for the opportunity to be a keynote speaker. I hope to see you in the future in the same region for another "recharge" and opportunity to discuss the issues.

Best regards,  
Dr. [Name]

also intend to monitor the growth, which is the land's potential "natural capacity" (<http://www.dnr.state.nj.us/land/landuse/landuse.htm>).

**Figure 1**









```

100 101 102 103 104 105 106 107 108 109 110 111 112 113 114 115 116 117 118 119 120 121 122 123 124 125 126 127 128 129 130 131 132 133 134 135 136 137 138 139 140 141 142 143 144 145 146 147 148 149 150 151 152 153 154 155 156 157 158 159 160 161 162 163 164 165 166 167 168 169 170 171 172 173 174 175 176 177 178 179 180 181 182 183 184 185 186 187 188 189 190 191 192 193 194 195 196 197 198 199 200 201 202 203 204 205 206 207 208 209 210 211 212 213 214 215 216 217 218 219 220 221 222 223 224 225 226 227 228 229 230 231 232 233 234 235 236 237 238 239 240 241 242 243 244 245 246 247 248 249 250 251 252 253 254 255 256 257 258 259 260 261 262 263 264 265 266 267 268 269 270 271 272 273 274 275 276 277 278 279 280 281 282 283 284 285 286 287 288 289 290 291 292 293 294 295 296 297 298 299 300 301 302 303 304 305 306 307 308 309 310 311 312 313 314 315 316 317 318 319 320 321 322 323 324 325 326 327 328 329 330 331 332 333 334 335 336 337 338 339 340 341 342 343 344 345 346 347 348 349 350 351 352 353 354 355 356 357 358 359 360 361 362 363 364 365 366 367 368 369 370 371 372 373 374 375 376 377 378 379 380 381 382 383 384 385 386 387 388 389 390 391 392 393 394 395 396 397 398 399 400 401 402 403 404 405 406 407 408 409 410 411 412 413 414 415 416 417 418 419 420 421 422 423 424 425 426 427 428 429 430 431 432 433 434 435 436 437 438 439 440 441 442 443 444 445 446 447 448 449 450 451 452 453 454 455 456 457 458 459 460 461 462 463 464 465 466 467 468 469 470 471 472 473 474 475 476 477 478 479 480 481 482 483 484 485 486 487 488 489 490 491 492 493 494 495 496 497 498 499 500 501 502 503 504 505 506 507 508 509 510 511 512 513 514 515 516 517 518 519 520 521 522 523 524 525 526 527 528 529 530 531 532 533 534 535 536 537 538 539 540 541 542 543 544 545 546 547 548 549 550 551 552 553 554 555 556 557 558 559 560 561 562 563 564 565 566 567 568 569 570 571 572 573 574 575 576 577 578 579 580 581 582 583 584 585 586 587 588 589 590 591 592 593 594 595 596 597 598 599 600 601 602 603 604 605 606 607 608 609 610 611 612 613 614 615 616 617 618 619 620 621 622 623 624 625 626 627 628 629 630 631 632 633 634 635 636 637 638 639 640 641 642 643 644 645 646 647 648 649 650 651 652 653 654 655 656 657 658 659 660 661 662 663 664 665 666 667 668 669 670 671 672 673 674 675 676 677 678 679 680 681 682 683 684 685 686 687 688 689 690 691 692 693 694 695 696 697 698 699 700 701 702 703 704 705 706 707 708 709 710 711 712 713 714 715 716 717 718 719 720 721 722 723 724 725 726 727 728 729 730 731 732 733 734 735 736 737 738 739 740 741 742 743 744 745 746 747 748 749 750 751 752 753 754 755 756 757 758 759 760 761 762 763 764 765 766 767 768 769 770 771 772 773 774 775 776 777 778 779 780 781 782 783 784 785 786 787 788 789 790 791 792 793 794 795 796 797 798 799 800 801 802 803 804 805 806 807 808 809 810 811 812 813 814 815 816 817 818 819 820 821 822 823 824 825 826 827 828 829 830 831 832 833 834 835 836 837 838 839 840 841 842 843 844 845 846 847 848 849 850 851 852 853 854 855 856 857 858 859 860 861 862 863 864 865 866 867 868 869 870 871 872 873 874 875 876 877 878 879 880 881 882 883 884 885 886 887 888 889 890 891 892 893 894 895 896 897 898 899 900 901 902 903 904 905 906 907 908 909 910 911 912 913 914 915 916 917 918 919 920 921 922 923 924 925 926 927 928 929 930 931 932 933 934 935 936 937 938 939 940 941 942 943 944 945 946 947 948 949 950 951 952 953 954 955 956 957 958 959 960 961 962 963 964 965 966 967 968 969 970 971 972 973 974 975 976 977 978 979 980 981 982 983 984 985 986 987 988 989 990 991 992 993 994 995 996 997 998 999 1000

```





```

10
11
12
13
14
15
16
17
18
19
20
21
22
23
24
25
26
27
28
29
30
31
32
33
34
35
36
37
38
39
40
41
42
43
44
45
46
47
48
49
50
51
52
53
54
55
56
57
58
59
60
61
62
63
64
65
66
67
68
69
70
71
72
73
74
75
76
77
78
79
80
81
82
83
84
85
86
87
88
89
90
91
92
93
94
95
96
97
98
99
100
101
102
103
104
105
106
107
108
109
110
111
112
113
114
115
116
117
118
119
120
121
122
123
124
125
126
127
128
129
130
131
132
133
134
135
136
137
138
139
140
141
142
143
144
145
146
147
148
149
150
151
152
153
154
155
156
157
158
159
160
161
162
163
164
165
166
167
168
169
170
171
172
173
174
175
176
177
178
179
180
181
182
183
184
185
186
187
188
189
190
191
192
193
194
195
196
197
198
199
200
201
202
203
204
205
206
207
208
209
210
211
212
213
214
215
216
217
218
219
220
221
222
223
224
225
226
227
228
229
230
231
232
233
234
235
236
237
238
239
240
241
242
243
244
245
246
247
248
249
250
251
252
253
254
255
256
257
258
259
260
261
262
263
264
265
266
267
268
269
270
271
272
273
274
275
276
277
278
279
280
281
282
283
284
285
286
287
288
289
290
291
292
293
294
295
296
297
298
299
300
301
302
303
304
305
306
307
308
309
310
311
312
313
314
315
316
317
318
319
320
321
322
323
324
325
326
327
328
329
330
331
332
333
334
335
336
337
338
339
340
341
342
343
344
345
346
347
348
349
350
351
352
353
354
355
356
357
358
359
360
361
362
363
364
365
366
367
368
369
370
371
372
373
374
375
376
377
378
379
380
381
382
383
384
385
386
387
388
389
390
391
392
393
394
395
396
397
398
399
400
401
402
403
404
405
406
407
408
409
410
411
412
413
414
415
416
417
418
419
420
421
422
423
424
425
426
427
428
429
430
431
432
433
434
435
436
437
438
439
440
441
442
443
444
445
446
447
448
449
450
451
452
453
454
455
456
457
458
459
460
461
462
463
464
465
466
467
468
469
470
471
472
473
474
475
476
477
478
479
480
481
482
483
484
485
486
487
488
489
490
491
492
493
494
495
496
497
498
499
500
501
502
503
504
505
506
507
508
509
510
511
512
513
514
515
516
517
518
519
520
521
522
523
524
525
526
527
528
529
530
531
532
533
534
535
536
537
538
539
540
541
542
543
544
545
546
547
548
549
550
551
552
553
554
555
556
557
558
559
560
561
562
563
564
565
566
567
568
569
570
571
572
573
574
575
576
577
578
579
580
581
582
583
584
585
586
587
588
589
590
591
592
593
594
595
596
597
598
599
600
601
602
603
604
605
606
607
608
609
610
611
612
613
614
615
616
617
618
619
620
621
622
623
624
625
626
627
628
629
630
631
632
633
634
635
636
637
638
639
640
641
642
643
644
645
646
647
648
649
650
651
652
653
654
655
656
657
658
659
660
661
662
663
664
665
666
667
668
669
670
671
672
673
674
675
676
677
678
679
680
681
682
683
684
685
686
687
688
689
690
691
692
693
694
695
696
697
698
699
700
701
702
703
704
705
706
707
708
709
710
711
712
713
714
715
716
717
718
719
720
721
722
723
724
725
726
727
728
729
730
731
732
733
734
735
736
737
738
739
740
741
742
743
744
745
746
747
748
749
750
751
752
753
754
755
756
757
758
759
760
761
762
763
764
765
766
767
768
769
770
771
772
773
774
775
776
777
778
779
780
781
782
783
784
785
786
787
788
789
790
791
792
793
794
795
796
797
798
799
800
801
802
803
804
805
806
807
808
809
810
811
812
813
814
815
816
817
818
819
820
821
822
823
824
825
826
827
828
829
830
831
832
833
834
835
836
837
838
839
840
841
842
843
844
845
846
847
848
849
850
851
852
853
854
855
856
857
858
859
860
861
862
863
864
865
866
867
868
869
870
871
872
873
874
875
876
877
878
879
880
881
882
883
884
885
886
887
888
889
890
891
892
893
894
895
896
897
898
899
900
901
902
903
904
905
906
907
908
909
910
911
912
913
914
915
916
917
918
919
920
921
922
923
924
925
926
927
928
929
930
931
932
933
934
935
936
937
938
939
940
941
942
943
944
945
946
947
948
949
950
951
952
953
954
955
956
957
958
959
960
961
962
963
964
965
966
967
968
969
970
971
972
973
974
975
976
977
978
979
980
981
982
983
984
985
986
987
988
989
990
991
992
993
994
995
996
997
998
999
1000

```



```

      return
    end

    -- we are now in the first iteration of the loop, so we can
    -- get information about
    -- (1) the number of iterations of the loop that we have done
    -- (2) the number of iterations of the loop that we have done

-- back to
  calculate_value
  (number of iterations) is a placeholder value

-- all in
  1
  2
  3
  4
  5
  6
  7
  8
  9
  10
  11
  12
  13
  14
  15
  16
  17
  18
  19
  20
  21
  22
  23
  24
  25
  26
  27
  28
  29
  30
  31
  32
  33
  34
  35
  36
  37
  38
  39
  40
  41
  42
  43
  44
  45
  46
  47
  48
  49
  50
  51
  52
  53
  54
  55
  56
  57
  58
  59
  60
  61
  62
  63
  64
  65
  66
  67
  68
  69
  70
  71
  72
  73
  74
  75
  76
  77
  78
  79
  80
  81
  82
  83
  84
  85
  86
  87
  88
  89
  90
  91
  92
  93
  94
  95
  96
  97
  98
  99
  100
  101
  102
  103
  104
  105
  106
  107
  108
  109
  110
  111
  112
  113
  114
  115
  116
  117
  118
  119
  120
  121
  122
  123
  124
  125
  126
  127
  128
  129
  130
  131
  132
  133
  134
  135
  136
  137
  138
  139
  140
  141
  142
  143
  144
  145
  146
  147
  148
  149
  150
  151
  152
  153
  154
  155
  156
  157
  158
  159
  160
  161
  162
  163
  164
  165
  166
  167
  168
  169
  170
  171
  172
  173
  174
  175
  176
  177
  178
  179
  180
  181
  182
  183
  184
  185
  186
  187
  188
  189
  190
  191
  192
  193
  194
  195
  196
  197
  198
  199
  200
  201
  202
  203
  204
  205
  206
  207
  208
  209
  210
  211
  212
  213
  214
  215
  216
  217
  218
  219
  220
  221
  222
  223
  224
  225
  226
  227
  228
  229
  230
  231
  232
  233
  234
  235
  236
  237
  238
  239
  240
  241
  242
  243
  244
  245
  246
  247
  248
  249
  250
  251
  252
  253
  254
  255
  256
  257
  258
  259
  260
  261
  262
  263
  264
  265
  266
  267
  268
  269
  270
  271
  272
  273
  274
  275
  276
  277
  278
  279
  280
  281
  282
  283
  284
  285
  286
  287
  288
  289
  290
  291
  292
  293
  294
  295
  296
  297
  298
  299
  300
  301
  302
  303
  304
  305
  306
  307
  308
  309
  310
  311
  312
  313
  314
  315
  316
  317
  318
  319
  320
  321
  322
  323
  324
  325
  326
  327
  328
  329
  330
  331
  332
  333
  334
  335
  336
  337
  338
  339
  340
  341
  342
  343
  344
  345
  346
  347
  348
  349
  350
  351
  352
  353
  354
  355
  356
  357
  358
  359
  360
  361
  362
  363
  364
  365
  366
  367
  368
  369
  370
  371
  372
  373
  374
  375
  376
  377
  378
  379
  380
  381
  382
  383
  384
  385
  386
  387
  388
  389
  390
  391
  392
  393
  394
  395
  396
  397
  398
  399
  400
  401
  402
  403
  404
  405
  406
  407
  408
  409
  410
  411
  412
  413
  414
  415
  416
  417
  418
  419
  420
  421
  422
  423
  424
  425
  426
  427
  428
  429
  430
  431
  432
  433
  434
  435
  436
  437
  438
  439
  440
  441
  442
  443
  444
  445
  446
  447
  448
  449
  450
  451
  452
  453
  454
  455
  456
  457
  458
  459
  460
  461
  462
  463
  464
  465
  466
  467
  468
  469
  470
  471
  472
  473
  474
  475
  476
  477
  478
  479
  480
  481
  482
  483
  484
  485
  486
  487
  488
  489
  490
  491
  492
  493
  494
  495
  496
  497
  498
  499
  500
  501
  502
  503
  504
  505
  506
  507
  508
  509
  510
  511
  512
  513
  514
  515
  516
  517
  518
  519
  520
  521
  522
  523
  524
  525
  526
  527
  528
  529
  530
  531
  532
  533
  534
  535
  536
  537
  538
  539
  540
  541
  542
  543
  544
  545
  546
  547
  548
  549
  550
  551
  552
  553
  554
  555
  556
  557
  558
  559
  560
  561
  562
  563
  564
  565
  566
  567
  568
  569
  570
  571
  572
  573
  574
  575
  576
  577
  578
  579
  580
  581
  582
  583
  584
  585
  586
  587
  588
  589
  590
  591
  592
  593
  594
  595
  596
  597
  598
  599
  600
  601
  602
  603
  604
  605
  606
  607
  608
  609
  610
  611
  612
  613
  614
  615
  616
  617
  618
  619
  620
  621
  622
  623
  624
  625
  626
  627
  628
  629
  630
  631
  632
  633
  634
  635
  636
  637
  638
  639
  640
  641
  642
  643
  644
  645
  646
  647
  648
  649
  650
  651
  652
  653
  654
  655
  656
  657
  658
  659
  660
  661
  662
  663
  664
  665
  666
  667
  668
  669
  670
  671
  672
  673
  674
  675
  676
  677
  678
  679
  680
  681
  682
  683
  684
  685
  686
  687
  688
  689
  690
  691
  692
  693
  694
  695
  696
  697
  698
  699
  700
  701
  702
  703
  704
  705
  706
  707
  708
  709
  710
  711
  712
  713
  714
  715
  716
  717
  718
  719
  720
  721
  722
  723
  724
  725
  726
  727
  728
  729
  730
  731
  732
  733
  734
  735
  736
  737
  738
  739
  740
  741
  742
  743
  744
  745
  746
  747
  748
  749
  750
  751
  752
  753
  754
  755
  756
  757
  758
  759
  760
  761
  762
  763
  764
  765
  766
  767
  768
  769
  770
  771
  772
  773
  774
  775
  776
  777
  778
  779
  780
  781
  782
  783
  784
  785
  786
  787
  788
  789
  790
  791
  792
  793
  794
  795
  796
  797
  798
  799
  800
  801
  802
  803
  804
  805
  806
  807
  808
  809
  810
  811
  812
  813
  814
  815
  816
  817
  818
  819
  820
  821
  822
  823
  824
  825
  826
  827
  828
  829
  830
  831
  832
  833
  834
  835
  836
  837
  838
  839
  840
  841
  842
  843
  844
  845
  846
  847
  848
  849
  850
  851
  852
  853
  854
  855
  856
  857
  858
  859
  860
  861
  862
  863
  864
  865
  866
  867
  868
  869
  870
  871
  872
  873
  874
  875
  876
  877
  878
  879
  880
  881
  882
  883
  884
  885
  886
  887
  888
  889
  890
  891
  892
  893
  894
  895
  896
  897
  898
  899
  900
  901
  902
  903
  904
  905
  906
  907
  908
  909
  910
  911
  912
  913
  914
  915
  916
  917
  918
  919
  920
  921
  922
  923
  924
  925
  926
  927
  928
  929
  930
  931
  932
  933
  934
  935
  936
  937
  938
  939
  940
  941
  942
  943
  944
  945
  946
  947
  948
  949
  950
  951
  952
  953
  954
  955
  956
  957
  958
  959
  960
  961
  962
  963
  964
  965
  966
  967
  968
  969
  970
  971
  972
  973
  974
  975
  976
  977
  978
  979
  980
  981
  982
  983
  984
  985
  986
  987
  988
  989
  990
  991
  992
  993
  994
  995
  996
  997
  998
  999
  1000

```

































```

38 39 40 41 42 43 44 45 46 47 48 49 50 51 52 53 54 55 56 57 58 59 60 61 62 63 64 65 66 67 68 69 70 71 72 73 74 75 76 77 78 79 80 81 82 83 84 85 86 87 88 89 90 91 92 93 94 95 96 97 98 99 100 101 102 103 104 105 106 107 108 109 110 111 112 113 114 115 116 117 118 119 120 121 122 123 124 125 126 127 128 129 130 131 132 133 134 135 136 137 138 139 140 141 142 143 144 145 146 147 148 149 150 151 152 153 154 155 156 157 158 159 160 161 162 163 164 165 166 167 168 169 170 171 172 173 174 175 176 177 178 179 180 181 182 183 184 185 186 187 188 189 190 191 192 193 194 195 196 197 198 199 200 201 202 203 204 205 206 207 208 209 210 211 212 213 214 215 216 217 218 219 220 221 222 223 224 225 226 227 228 229 230 231 232 233 234 235 236 237 238 239 240 241 242 243 244 245 246 247 248 249 250 251 252 253 254 255 256 257 258 259 260 261 262 263 264 265 266 267 268 269 270 271 272 273 274 275 276 277 278 279 280 281 282 283 284 285 286 287 288 289 290 291 292 293 294 295 296 297 298 299 300 301 302 303 304 305 306 307 308 309 310 311 312 313 314 315 316 317 318 319 320 321 322 323 324 325 326 327 328 329 330 331 332 333 334 335 336 337 338 339 340 341 342 343 344 345 346 347 348 349 350 351 352 353 354 355 356 357 358 359 360 361 362 363 364 365 366 367 368 369 370 371 372 373 374 375 376 377 378 379 380 381 382 383 384 385 386 387 388 389 390 391 392 393 394 395 396 397 398 399 400 401 402 403 404 405 406 407 408 409 410 411 412 413 414 415 416 417 418 419 420 421 422 423 424 425 426 427 428 429 430 431 432 433 434 435 436 437 438 439 440 441 442 443 444 445 446 447 448 449 450 451 452 453 454 455 456 457 458 459 460 461 462 463 464 465 466 467 468 469 470 471 472 473 474 475 476 477 478 479 480 481 482 483 484 485 486 487 488 489 490 491 492 493 494 495 496 497 498 499 500 501 502 503 504 505 506 507 508 509 510 511 512 513 514 515 516 517 518 519 520 521 522 523 524 525 526 527 528 529 530 531 532 533 534 535 536 537 538 539 540 541 542 543 544 545 546 547 548 549 550 551 552 553 554 555 556 557 558 559 560 561 562 563 564 565 566 567 568 569 570 571 572 573 574 575 576 577 578 579 580 581 582 583 584 585 586 587 588 589 590 591 592 593 594 595 596 597 598 599 600 601 602 603 604 605 606 607 608 609 610 611 612 613 614 615 616 617 618 619 620 621 622 623 624 625 626 627 628 629 630 631 632 633 634 635 636 637 638 639 640 641 642 643 644 645 646 647 648 649 650 651 652 653 654 655 656 657 658 659 660 661 662 663 664 665 666 667 668 669 670 671 672 673 674 675 676 677 678 679 680 681 682 683 684 685 686 687 688 689 690 691 692 693 694 695 696 697 698 699 700 701 702 703 704 705 706 707 708 709 710 711 712 713 714 715 716 717 718 719 720 721 722 723 724 725 726 727 728 729 730 731 732 733 734 735 736 737 738 739 740 741 742 743 744 745 746 747 748 749 750 751 752 753 754 755 756 757 758 759 760 761 762 763 764 765 766 767 768 769 770 771 772 773 774 775 776 777 778 779 780 781 782 783 784 785 786 787 788 789 790 791 792 793 794 795 796 797 798 799 800 801 802 803 804 805 806 807 808 809 810 811 812 813 814 815 816 817 818 819 820 821 822 823 824 825 826 827 828 829 830 831 832 833 834 835 836 837 838 839 840 841 842 843 844 845 846 847 848 849 850 851 852 853 854 855 856 857 858 859 860 861 862 863 864 865 866 867 868 869 870 871 872 873 874 875 876 877 878 879 880 881 882 883 884 885 886 887 888 889 890 891 892 893 894 895 896 897 898 899 900 901 902 903 904 905 906 907 908 909 910 911 912 913 914 915 916 917 918 919 920 921 922 923 924 925 926 927 928 929 930 931 932 933 934 935 936 937 938 939 940 941 942 943 944 945 946 947 948 949 950 951 952 953 954 955 956 957 958 959 960 961 962 963 964 965 966 967 968 969 970 971 972 973 974 975 976 977 978 979 980 981 982 983 984 985 986 987 988 989 990 991 992 993 994 995 996 997 998 999 1000

```





```

10  use a placeholder variable  so to save table
11  substitute in " " and
    substitute in " "  you see it

12  substitute the new table
    use " " and
    substitute
    substitute

13  loop over all cells  reading from variable
    do 10  loop over
        variable read
        substitute

14  read variable in new placeholder table  so to save table
15  use " " to substitute and to save in " "

16  loop over all variables
    do 10  11-substitute, substitute+1
        substitute

17  use variable variable  so to read variable
18  use " " to save in " "

19  use " " to read in variable and
    do 10  loop
        substitute, 1  substitute+1
        substitute

20  end of loop over variables in cell
    continue

21  use to loop over cells
    continue

22  print the variable (substitute) read from all cells
    writeout "the output of the "
    writeout " " and " "

23  end program and print by variable from all cells
    program
end

24  *****
25  *****
26  *****
27  *****
28  *****
29  *****
30  *****
31  *****
32  *****
33  *****
34  *****
35  *****
36  *****
37  *****
38  *****
39  *****
40  *****
41  *****
42  *****
43  *****
44  *****
45  *****
46  *****
47  *****
48  *****
49  *****
50  *****
51  *****
52  *****
53  *****
54  *****
55  *****
56  *****
57  *****
58  *****
59  *****
60  *****
61  *****
62  *****
63  *****
64  *****
65  *****
66  *****
67  *****
68  *****
69  *****
70  *****
71  *****
72  *****
73  *****
74  *****
75  *****
76  *****
77  *****
78  *****
79  *****
80  *****
81  *****
82  *****
83  *****
84  *****
85  *****
86  *****
87  *****
88  *****
89  *****
90  *****
91  *****
92  *****
93  *****
94  *****
95  *****
96  *****
97  *****
98  *****
99  *****
100 *****

```







and  
 1999  
 and

## APPENDIX D MISCELLANEOUS DATA FROM VALIDATION STUDIES

### Introduction

This appendix contains the MCNP input decks and relative listings of the numerical data contained in Chapter 4. They are presented in the same order as the figures in the text with one deck and table corresponding to each graph. The input decks for each graph is shown at a point value needed electron energy corresponding to a single point. The input decks for the remaining points are identical except for the value of the source energy. The table lists the energy, reported value and calculated value for each point on the corresponding graph.

The reported values come from the two reports discussed in Chapter 5. Serawin reported his neutron yields per kilowatt second in tables from. These numbers have been corrected to neutron per electron. The reported values are listed as (value  $\pm$  estimated error) with a 34 percent estimated error as given by Serawin. The Barber and George results were reported as neutrons per electron but only graphically. Their figures were digitized and the best estimate of energy yield point is presented in the table. Reported values are listed as shown except the estimated error is 15 percent as given by Barber and George. The calculations were performed using the prototype code version MCNP4B7M as described in the text. The calculated values are listed as (value  $\pm$  one sigma electron error). Note that the calculated uncertainty is a measure of the precision

of the Monte Carlo simulation. It does not include an estimate of the uncertainty in the data or the model.

The last three input decks and tables contain the information used to study the effects of variations in actual versus reported parameters for the Barber and George study. The baseline case is that Ti-1 target at the 20.5 MeV nominal beam energy. Incident beam energy, target thickness and beam radius were all varied over the range  $\pm 10$  percent. For variations in beam radius and target thickness, change the appropriate parameter to control the variations of the input deck.



### "Sandwichlike" Iron Target (Fe-XXX)

```

!***** parameters for electron scattering on Fe-56 ****
1 1 -1.432 1 -0 11 -12 21 -22 imp. Fe-56
2 0 -10 11 -10 12 -13 22 imp. Fe-56

1 100 0
2 100 100 100
12 100 -100 100
13 100 100 100
21 100 100 100
22 100 100 100

name a p n
n1 1000 1 of Fe-56 p100 Fe-56 p100 Fe-56
name pout n n out1 out2 1 0 100 1 100 1 out1 1 1 out2 out3
n
n
out1 p 1 0
out2 p 1 1
out3 p 1 100
out4 p 1 1 100
out5 p 1 1 100
n
n
n1 n 1 0 10 10 11 12 13 14 15 16 17 18 19
out1 1
n
n
name 1000000
name 100
name 1

```

Table D-2: Reported and calculated yields for a "sandwichlike" iron target

Energy (GeV)	Reported Yield (n/Fe/10)	Reported Yield (n/10)	Calculated Yield (n/10)	Calc. Yield / Rept. Yield
12	$1.73 \times 10^{-3}$	$(2.77 \pm 0.56) \times 10^{-3}$	$(4.37 \pm 0.87) \times 10^{-3}$	1.54
20	$(6.6 \pm 1.0) \times 10^{-3}$	$(1.69 \pm 0.62) \times 10^{-2}$	$(4.31 \pm 0.86) \times 10^{-2}$	1.26
25	$2.42 \times 10^{-2}$	$(8.67 \pm 1.50) \times 10^{-2}$	$(1.77 \pm 0.36) \times 10^{-1}$	1.16
30	$6.10 \times 10^{-2}$	$(1.78 \pm 0.27) \times 10^{-1}$	$(1.20 \pm 0.24) \times 10^{-1}$	1.23
50	$0.82 \times 10^{-1}$	$(1.62 \pm 0.26) \times 10^{-1}$	$(6.40 \pm 0.80) \times 10^{-1}$	1.25
100	$1.42 \times 10^{-1}$	$(1.32 \pm 0.24) \times 10^{-1}$	$(1.62 \pm 0.20) \times 10^{-1}$	1.24

### "New-Collect" Copper Target (Cu-XX)

Reported parameters for reference conditions as in the examples:

```
1 1 0.01 1 2 10 -12 20 -10 (impurity=1)
1 0 -4 2 -100 100 -100 10 (impurity=0)
```

```
1 00 0
4 00 100 1
10 00 100 1
10 00 100 1
10 00 100 1
10 00 100 1
```

order is as in

```
01 10000 1 0.000000 0.00-0.00 0.00-0.00 0.00-0.00
other param 0 0 param result 0 0 param param result 0 0 param param result
0
0
setting 1 0
physic 01 -0
physic 1 000
unitary 1 0 1000
define 1 0 1000
0
01 0 1 0 10 10 10 10 10 10 10 10 10 10
010 1
0
0
open 1000000
close 100
price
```

Table D-3 Reported and calculated yields for a "new-collect" copper target.

Energy (MeV)	Reported Yield (a.u.) <sup>1</sup>	Reported Yield (a.u.) <sup>2</sup>	Calculated Yield (a.u.) <sup>3</sup>	Calc. Yield / Rept. Yield
5	$2.00 \times 10^{-3}$	$(4.31 \pm 0.00) \times 10^{-3}$	$(4.31 \pm 0.00) \times 10^{-3}$	0.93
20	$1.50 \times 10^{-3}$	$(3.00 \pm 0.00) \times 10^{-3}$	$(4.77 \pm 0.00) \times 10^{-3}$	0.94
25	$1.24 \times 10^{-3}$	$(1.81 \pm 0.00) \times 10^{-3}$	$(1.76 \pm 0.00) \times 10^{-3}$	0.93
30	$6.20 \times 10^{-4}$	$(3.00 \pm 0.00) \times 10^{-4}$	$(3.00 \pm 0.00) \times 10^{-4}$	0.93
50	$3.70 \times 10^{-4}$	$(7.50 \pm 0.00) \times 10^{-5}$	$(4.43 \pm 0.00) \times 10^{-5}$	0.93
100	$1.00 \times 10^{-4}$	$(1.73 \pm 0.00) \times 10^{-4}$	$(2.20 \pm 0.00) \times 10^{-4}$	0.93



### "Residuals" Tension Target (R-XX)

Reported calculated and observed tensions on a 50 target

1 0 -1.7 1 1 -0 02 -4.0 02 -0.0 000-0.000-1  
4 0 1.0 02 0.000 4.0 0.0 0.0 0.000-0.000

1 00 0  
1 00 0-0.071  
10 00 -0-0.071  
40 00 0-0.071  
10 00 -0-0.071  
00 00 0-0.071

Model 0 0 0

on 10000 0 00000 000000 000000 000000

total 0000 0 0 0000 0000 0 0 0000 0000 0 0 0000 0000 0 0 0000 0000

0

0

000 0 1 0

0000 0 00 0

0000 0 1 000

000 0 1 0 0

000 0 1 0 0

0

0

00 0 1 0 00 00 00 00 00 0 0 00 00 000

000 0

0

0

000 000000

000 000

0000

Table D-4 Reported and calculated yields for a "zero offset" tension target

Energy (MeV)	Reported Yield ( $\mu\text{A}^{-1}\text{s}^{-1}$ )	Reported Yield ( $\text{g}^{-1}\text{s}^{-1}$ )	Calculated Yield ( $\text{g}^{-1}\text{s}^{-1}$ )	Calc. Yield / Report. Yield
10	$1.00 \times 10^{-1}$	$1.75 \times 10^{-1} \text{ g}^{-1} \text{ s}^{-1}$	$1.647148 \times 10^{-1} \text{ g}^{-1} \text{ s}^{-1}$	0.94
15	$1.07 \times 10^{-1}$	$1.78 \times 10^{-1} \text{ g}^{-1} \text{ s}^{-1}$	$1.612148 \times 10^{-1} \text{ g}^{-1} \text{ s}^{-1}$	0.91
20	$0.98 \times 10^{-1}$	$1.82 \times 10^{-1} \text{ g}^{-1} \text{ s}^{-1}$	$1.617768 \times 10^{-1} \text{ g}^{-1} \text{ s}^{-1}$	0.90
25	$1.52 \times 10^{-1}$	$1.77 \times 10^{-1} \text{ g}^{-1} \text{ s}^{-1}$	$1.660768 \times 10^{-1} \text{ g}^{-1} \text{ s}^{-1}$	0.94
30	$1.05 \times 10^{-1}$	$1.82 \times 10^{-1} \text{ g}^{-1} \text{ s}^{-1}$	$1.624668 \times 10^{-1} \text{ g}^{-1} \text{ s}^{-1}$	0.89
35	$1.70 \times 10^{-1}$	$1.75 \times 10^{-1} \text{ g}^{-1} \text{ s}^{-1}$	$1.775568 \times 10^{-1} \text{ g}^{-1} \text{ s}^{-1}$	1.03
100	$0.04 \times 10^{-1}$	$1.27 \times 10^{-1} \text{ g}^{-1} \text{ s}^{-1}$	$1.424668 \times 10^{-1} \text{ g}^{-1} \text{ s}^{-1}$	1.06





## One Radiation-Length Thick Aluminum Target (Al-1)

Number of electrons per incident photon, as a function of energy

```

1  1  1.0 100  1 10  10 10  10 10  10 10  10 10  10 10
2  0  0  0  0  0  0  0  0  0  0  0  0  0  0  0  0  0  0  0  0

```

```

3  0  0
4  0  0  0  0
5  0  0  0  0  0
6  0  0  0  0  0
7  0  0  0  0  0
8  0  0  0  0  0
9  0  0  0  0  0
10 0  0  0  0  0

```

```

11 0  0  0

```

12 10000 1 10000 10000 10000 10000 10000 10000 10000 10000 10000 10000 10000 10000 10000 10000 10000 10000 10000 10000

13 10000 1 10000 10000 10000 10000 10000 10000 10000 10000 10000 10000 10000 10000 10000 10000 10000 10000 10000 10000

```

14 10000 10000

```

```

15

```

```

16

```

```

17 0  0  0  0  0

```

```

18 0  0  0  0  0

```

```

19 0  0  0  0  0

```

```

20 0  0  0  0  0

```

```

21 0  0  0  0  0

```

```

22

```

```

23

```

```

24 0  0  0  0  0  0  0  0  0  0  0  0  0  0  0  0  0  0  0  0

```

```

25 10000 10000

```

```

26

```

```

27

```

```

28 10000 10000

```

```

29 10000 10000

```

```

30 10000

```

Table D-7 Reported and calculated yields for an approximately one radiation-length-thick aluminum target

Energy (MeV)	Reported Yield (e <sup>-</sup> /s)	Calculated Yield (e <sup>-</sup> /s)	Calculated Yield / Reported Yield
20.3	$(4.04 \pm 0.12) \times 10^4$	$(3.76 \pm 0.09) \times 10^4$	0.93
28.3	$(2.00 \pm 0.03) \times 10^4$	$(2.44 \pm 0.06) \times 10^4$	1.22
34.3	$(2.30 \pm 0.03) \times 10^4$	$(2.46 \pm 0.03) \times 10^4$	1.07



### Two Radiation Length Thick Copper Target (CuO)

Reported values are per electron incident on a Cu target

1 1 0.0000 0.0000 0.0000 0.0000 0.0000 0.0000 0.0000 0.0000  
2 0 0.0000 0.0000 0.0000 0.0000 0.0000 0.0000 0.0000 0.0000

1 0.0000 0.0000  
2 0.0000 0.0000  
3 0.0000 0.0000  
4 0.0000 0.0000  
5 0.0000 0.0000  
6 0.0000 0.0000  
7 0.0000 0.0000  
8 0.0000 0.0000  
9 0.0000 0.0000  
10 0.0000 0.0000  
11 0.0000 0.0000  
12 0.0000 0.0000  
13 0.0000 0.0000  
14 0.0000 0.0000  
15 0.0000 0.0000  
16 0.0000 0.0000  
17 0.0000 0.0000  
18 0.0000 0.0000  
19 0.0000 0.0000  
20 0.0000 0.0000  
21 0.0000 0.0000  
22 0.0000 0.0000  
23 0.0000 0.0000  
24 0.0000 0.0000  
25 0.0000 0.0000  
26 0.0000 0.0000  
27 0.0000 0.0000  
28 0.0000 0.0000  
29 0.0000 0.0000  
30 0.0000 0.0000  
31 0.0000 0.0000  
32 0.0000 0.0000  
33 0.0000 0.0000  
34 0.0000 0.0000  
35 0.0000 0.0000  
36 0.0000 0.0000  
37 0.0000 0.0000  
38 0.0000 0.0000  
39 0.0000 0.0000  
40 0.0000 0.0000  
41 0.0000 0.0000  
42 0.0000 0.0000  
43 0.0000 0.0000  
44 0.0000 0.0000  
45 0.0000 0.0000  
46 0.0000 0.0000  
47 0.0000 0.0000  
48 0.0000 0.0000  
49 0.0000 0.0000  
50 0.0000 0.0000  
51 0.0000 0.0000  
52 0.0000 0.0000  
53 0.0000 0.0000  
54 0.0000 0.0000  
55 0.0000 0.0000  
56 0.0000 0.0000  
57 0.0000 0.0000  
58 0.0000 0.0000  
59 0.0000 0.0000  
60 0.0000 0.0000  
61 0.0000 0.0000  
62 0.0000 0.0000  
63 0.0000 0.0000  
64 0.0000 0.0000  
65 0.0000 0.0000  
66 0.0000 0.0000  
67 0.0000 0.0000  
68 0.0000 0.0000  
69 0.0000 0.0000  
70 0.0000 0.0000  
71 0.0000 0.0000  
72 0.0000 0.0000  
73 0.0000 0.0000  
74 0.0000 0.0000  
75 0.0000 0.0000  
76 0.0000 0.0000  
77 0.0000 0.0000  
78 0.0000 0.0000  
79 0.0000 0.0000  
80 0.0000 0.0000  
81 0.0000 0.0000  
82 0.0000 0.0000  
83 0.0000 0.0000  
84 0.0000 0.0000  
85 0.0000 0.0000  
86 0.0000 0.0000  
87 0.0000 0.0000  
88 0.0000 0.0000  
89 0.0000 0.0000  
90 0.0000 0.0000  
91 0.0000 0.0000  
92 0.0000 0.0000  
93 0.0000 0.0000  
94 0.0000 0.0000  
95 0.0000 0.0000  
96 0.0000 0.0000  
97 0.0000 0.0000  
98 0.0000 0.0000  
99 0.0000 0.0000  
100 0.0000 0.0000

1 0.0000 0.0000

2 0.0000 0.0000 0.0000 0.0000 0.0000 0.0000 0.0000 0.0000

3 0.0000 0.0000 0.0000 0.0000 0.0000 0.0000 0.0000 0.0000  
4 0.0000 0.0000 0.0000 0.0000 0.0000 0.0000 0.0000 0.0000

5 0.0000 0.0000

6 0.0000 0.0000

7 0.0000 0.0000

8 0.0000 0.0000

9 0.0000 0.0000

10 0.0000 0.0000

11 0.0000 0.0000

12 0.0000 0.0000

13 0.0000 0.0000

14 0.0000 0.0000

15 0.0000 0.0000

16 0.0000 0.0000

17 0.0000 0.0000

18 0.0000 0.0000

19 0.0000 0.0000

20 0.0000 0.0000

21 0.0000 0.0000

22 0.0000 0.0000

23 0.0000 0.0000

24 0.0000 0.0000

25 0.0000 0.0000

26 0.0000 0.0000

27 0.0000 0.0000

28 0.0000 0.0000

29 0.0000 0.0000

30 0.0000 0.0000

31 0.0000 0.0000

32 0.0000 0.0000

33 0.0000 0.0000

34 0.0000 0.0000

35 0.0000 0.0000

36 0.0000 0.0000

37 0.0000 0.0000

38 0.0000 0.0000

39 0.0000 0.0000

40 0.0000 0.0000

41 0.0000 0.0000

42 0.0000 0.0000

43 0.0000 0.0000

44 0.0000 0.0000

45 0.0000 0.0000

46 0.0000 0.0000

47 0.0000 0.0000

48 0.0000 0.0000

49 0.0000 0.0000

50 0.0000 0.0000

51 0.0000 0.0000

52 0.0000 0.0000

53 0.0000 0.0000

54 0.0000 0.0000

55 0.0000 0.0000

56 0.0000 0.0000

Table D-9: Reported and calculated yields for an approximately two-radiation length thick copper target

Energy (MeV)	Reported Yield (e <sup>-</sup> /e)	Calculated Yield (e <sup>-</sup> /e)	Calculated Yield / Reported Yield
10.1	$(1.00 \pm 0.10) \times 10^{-3}$	$(1.17 \pm 0.05) \times 10^{-3}$	1.16
11.2	$(1.10 \pm 0.10) \times 10^{-3}$	$(1.17 \pm 0.05) \times 10^{-3}$	0.97
12.3	$(1.10 \pm 0.11) \times 10^{-3}$	$(1.17 \pm 0.05) \times 10^{-3}$	0.94
14.1	$(1.10 \pm 0.10) \times 10^{-3}$	$(1.17 \pm 0.05) \times 10^{-3}$	0.94













### Three Radiation Length Thick Lead Target (Pb-82)

Incident electrons per electron incident on a Pb target

```
1 1 -11.25 1 -5 11 -11 11 -11 11 -11
2 2 11.25 11.25 11.25 11.25 11.25 11.25
```

```
1 00 0
2 00 0 100
11 00 -0 100
11 00 0 100
11 00 -0 100
11 00 0 100
```

split 0 0 0

```
00 0000 00 1 0000 00 1 0000 00 1
00000 00000 00000 00000 00000
```

```
total 0000 0 0 0000 0000 0000 0 0 0000 0000 0 0 0000 0000
000 0 0 00
```

0

0

```
00000 0 0
```

```
0000 0 0000
```

```
000 0 00 0 0
```

```
000 0 0 0 0
```

```
000 0 0 0 0
```

0

0

```
000 0 0 0 00 00 00 0 0 00 00 00
```

```
000 0
```

0

0

```
000 1100000
```

```
0000 00
```

```
00000
```

Table A-11 Reported and calculated yields for an approximately three radiation length thick lead target.

Energy (MeV)	Reported Yield (e <sup>-</sup> /e)	Calculated Yield (e <sup>-</sup> /e)	Calculated Yield / Reported Yield
10.1	$(1.7746 \pm 0.19) \times 10^{-2}$	$(1.7407148480294) \times 10^{-2}$	0.98
20.1	$(4.0768 \pm 0.70) \times 10^{-2}$	$(3.971306480311) \times 10^{-2}$	0.97
30.1	$(6.3848 \pm 0.57) \times 10^{-2}$	$(6.2473464409477) \times 10^{-2}$	0.98













## APPENDIX E MISCELLANEOUS DATA FROM APPLICATION STUDIES

### Introduction

This chapter presents decompositions from the MCSNP input decks used to perform the applications studies. They are labeled according to their appropriate use. A full listing of all input decks would duplicate many of their sub sections therefore they are listed individually.

### Activation Calculations

#### Geometry With Block and Inert

```

1  use of the activation deck
2  full decomposition
3  use of the activation deck
4
5  use of the activation deck
6  input: primary full block & plane
7  full decomposition of the block & plane
8
9  (primary/full block & plane) input
10  1.0 1.0 1.0 1.0 1.0 1.0 1.0 1.0
11
12  (primary/full block & plane) input
13  1.0 1.0 1.0 1.0 1.0 1.0 1.0 1.0
14
15  (primary/full block & plane) input
16  1.0 1.0 1.0 1.0 1.0 1.0 1.0 1.0
17
18  (primary/full block & plane) input
19  1.0 1.0 1.0 1.0 1.0 1.0 1.0 1.0
20
21  (primary/full block & plane) input
22  1.0 1.0 1.0 1.0 1.0 1.0 1.0 1.0
23
24  (primary/full block & plane) input
25  1.0 1.0 1.0 1.0 1.0 1.0 1.0 1.0
26
27  (primary/full block & plane) input
28  1.0 1.0 1.0 1.0 1.0 1.0 1.0 1.0
29
30  (primary/full block & plane) input
31  1.0 1.0 1.0 1.0 1.0 1.0 1.0 1.0
32
33  (primary/full block & plane) input
34  1.0 1.0 1.0 1.0 1.0 1.0 1.0 1.0
35
36  (primary/full block & plane) input
37  1.0 1.0 1.0 1.0 1.0 1.0 1.0 1.0
38
39  (primary/full block & plane) input
40  1.0 1.0 1.0 1.0 1.0 1.0 1.0 1.0
41
42  (primary/full block & plane) input
43  1.0 1.0 1.0 1.0 1.0 1.0 1.0 1.0
44
45  (primary/full block & plane) input
46  1.0 1.0 1.0 1.0 1.0 1.0 1.0 1.0
47
48  (primary/full block & plane) input
49  1.0 1.0 1.0 1.0 1.0 1.0 1.0 1.0
50
51  (primary/full block & plane) input
52  1.0 1.0 1.0 1.0 1.0 1.0 1.0 1.0
53
54  (primary/full block & plane) input
55  1.0 1.0 1.0 1.0 1.0 1.0 1.0 1.0
56
57  (primary/full block & plane) input
58  1.0 1.0 1.0 1.0 1.0 1.0 1.0 1.0
59
60  (primary/full block & plane) input
61  1.0 1.0 1.0 1.0 1.0 1.0 1.0 1.0
62
63  (primary/full block & plane) input
64  1.0 1.0 1.0 1.0 1.0 1.0 1.0 1.0
65
66  (primary/full block & plane) input
67  1.0 1.0 1.0 1.0 1.0 1.0 1.0 1.0
68
69  (primary/full block & plane) input
70  1.0 1.0 1.0 1.0 1.0 1.0 1.0 1.0
71
72  (primary/full block & plane) input
73  1.0 1.0 1.0 1.0 1.0 1.0 1.0 1.0
74
75  (primary/full block & plane) input
76  1.0 1.0 1.0 1.0 1.0 1.0 1.0 1.0
77
78  (primary/full block & plane) input
79  1.0 1.0 1.0 1.0 1.0 1.0 1.0 1.0
80
81  (primary/full block & plane) input
82  1.0 1.0 1.0 1.0 1.0 1.0 1.0 1.0
83
84  (primary/full block & plane) input
85  1.0 1.0 1.0 1.0 1.0 1.0 1.0 1.0
86
87  (primary/full block & plane) input
88  1.0 1.0 1.0 1.0 1.0 1.0 1.0 1.0
89
90  (primary/full block & plane) input
91  1.0 1.0 1.0 1.0 1.0 1.0 1.0 1.0
92
93  (primary/full block & plane) input
94  1.0 1.0 1.0 1.0 1.0 1.0 1.0 1.0
95
96  (primary/full block & plane) input
97  1.0 1.0 1.0 1.0 1.0 1.0 1.0 1.0
98
99  (primary/full block & plane) input
100 1.0 1.0 1.0 1.0 1.0 1.0 1.0 1.0

```









































F g) $\mu_{\text{max}}$ (h <sup>-1</sup> ) for $\mu_{\text{max}}$ and $\mu_{\text{max}}$ (h <sup>-1</sup> )			
1	100	100	100
2	100	100	100
3	100	100	100
4	100	100	100
5	100	100	100
6	100	100	100
7	100	100	100
8	100	100	100
9	100	100	100
10	100	100	100
11	100	100	100
12	100	100	100
13	100	100	100
14	100	100	100
15	100	100	100
16	100	100	100
17	100	100	100
18	100	100	100
19	100	100	100
20	100	100	100
21	100	100	100
22	100	100	100
23	100	100	100
24	100	100	100
25	100	100	100
26	100	100	100
27	100	100	100
28	100	100	100
29	100	100	100
30	100	100	100
31	100	100	100
32	100	100	100
33	100	100	100
34	100	100	100
35	100	100	100
36	100	100	100
37	100	100	100
38	100	100	100
39	100	100	100
40	100	100	100
41	100	100	100
42	100	100	100
43	100	100	100
44	100	100	100
45	100	100	100
46	100	100	100
47	100	100	100
48	100	100	100
49	100	100	100
50	100	100	100
51	100	100	100
52	100	100	100
53	100	100	100
54	100	100	100
55	100	100	100
56	100	100	100
57	100	100	100
58	100	100	100
59	100	100	100
60	100	100	100
61	100	100	100
62	100	100	100
63	100	100	100
64	100	100	100
65	100	100	100
66	100	100	100
67	100	100	100
68	100	100	100
69	100	100	100
70	100	100	100
71	100	100	100
72	100	100	100
73	100	100	100
74	100	100	100
75	100	100	100
76	100	100	100
77	100	100	100
78	100	100	100
79	100	100	100
80	100	100	100
81	100	100	100
82	100	100	100
83	100	100	100
84	100	100	100
85	100	100	100
86	100	100	100
87	100	100	100
88	100	100	100
89	100	100	100
90	100	100	100
91	100	100	100
92	100	100	100
93	100	100	100
94	100	100	100
95	100	100	100
96	100	100	100
97	100	100	100
98	100	100	100
99	100	100	100
100	100	100	100

## Kinetic/Performance Description of the Materials

1	100	100	100
2	100	100	100
3	100	100	100
4	100	100	100
5	100	100	100
6	100	100	100
7	100	100	100
8	100	100	100
9	100	100	100
10	100	100	100
11	100	100	100
12	100	100	100
13	100	100	100
14	100	100	100
15	100	100	100
16	100	100	100
17	100	100	100
18	100	100	100
19	100	100	100
20	100	100	100
21	100	100	100
22	100	100	100
23	100	100	100
24	100	100	100
25	100	100	100
26	100	100	100
27	100	100	100
28	100	100	100
29	100	100	100
30	100	100	100
31	100	100	100
32	100	100	100
33	100	100	100
34	100	100	100
35	100	100	100
36	100	100	100
37	100	100	100
38	100	100	100
39	100	100	100
40	100	100	100
41	100	100	100
42	100	100	100
43	100	100	100
44	100	100	100
45	100	100	100
46	100	100	100
47	100	100	100
48	100	100	100
49	100	100	100
50	100	100	100
51	100	100	100
52	100	100	100
53	100	100	100
54	100	100	100
55	100	100	100
56	100	100	100
57	100	100	100
58	100	100	100
59	100	100	100
60	100	100	100
61	100	100	100
62	100	100	100
63	100	100	100
64	100	100	100
65	100	100	100
66	100	100	100
67	100	100	100
68	100	100	100
69	100	100	100
70	100	100	100
71	100	100	100
72	100	100	100
73	100	100	100
74	100	100	100
75	100	100	100
76	100	100	100
77	100	100	100
78	100	100	100
79	100	100	100
80	100	100	100
81	100	100	100
82	100	100	100
83	100	100	100
84	100	100	100
85	100	100	100
86	100	100	100
87	100	100	100
88	100	100	100
89	100	100	100
90	100	100	100
91	100	100	100
92	100	100	100
93	100	100	100
94	100	100	100
95	100	100	100
96	100	100	100
97	100	100	100
98	100	100	100
99	100	100	100
100	100	100	100







### Weight Windows for Electron-Photon Simulation With Block, and Input

```
weight w 0 1 10 1 0
weight w 1 0.01
weight w 0 1.00 10.00 1.00 0.01
```

### Weight Windows for Electron-Photon Simulation With Block, But Without Input

```
weight w 0 1 10 1 0
weight w 1 0.01
weight w 0 1.00 10.00 1.00 0.01
```

### Weight Windows for Electron-Photon Simulation Without Block, But With Input

```
weight w 0 0 1 10 1 0
weight w 1 0.01
weight w 0 1.00 10.00 1.00 0.01
```

### Weight Windows for Electron-Photon Simulation Without Block or Input

```
weight w 0 0 1 10 1 0
weight w 1 0.01
weight w 0 1.00 10.00 1.00 0.01
```

### Weight Windows for Electron-Photon-Neutron Simulation With Block, and Input

```
weight w 0 0 0 0 1 10 1 0
weight w 1 0.01
weight w 0 1.00 10.00 1.00 0.01 0.01 0.01
weight w 1 0.000 10.00 1.00 0.01 0.01 0.01
```

### Weight Windows for Electron-Photon-Neutron Simulation With Block, But Without Input

```
weight w 0 0 0 0 1 10 1 0
weight w 1 0.01
weight w 0 1.00 10.00 1.00 0.01 0.01 0.01
weight w 1 0.000 10.00 1.00 0.01 0.01 0.01
```

### Weight Windows for Electron-Photon-Neutron Simulation Without Block, But With Input

```
weight w 0 0 0 0 1 10 1 0
weight w 1 0.01
weight w 0 1.00 10.00 1.00 0.01 0.01 0.01
weight w 1 0.000 10.00 1.00 0.01 0.01 0.01
```

### Weight Windows for Electron-Photon-Neutron Simulation Without Block or Input

```
weight w 0 0 0 0 1 10 1 0
weight w 1 0.01
weight w 0 1.00 10.00 1.00 0.01 0.01 0.01
weight w 1 0.000 10.00 1.00 0.01 0.01 0.01
```























```

1000  0.0  0.0  0.0  0.0  0.0  0.0
1000  0.0  0.0  0.0  0.0  0.0  0.0
1000  0.0  0.0  0.0  0.0  0.0  0.0
1000  0.0  0.0  0.0  0.0  0.0  0.0

11  =====
12  11  =====
13  11  =====
14  11  =====
15  11  =====
16  11  =====
17  11  =====
18  11  =====
19  11  =====
20  11  =====
21  11  =====
22  11  =====
23  11  =====
24  11  =====
25  11  =====
26  11  =====
27  11  =====
28  11  =====
29  11  =====
30  11  =====
31  11  =====
32  11  =====
33  11  =====
34  11  =====
35  11  =====
36  11  =====
37  11  =====
38  11  =====
39  11  =====
40  11  =====
41  11  =====
42  11  =====
43  11  =====
44  11  =====
45  11  =====
46  11  =====
47  11  =====
48  11  =====
49  11  =====
50  11  =====
51  11  =====
52  11  =====
53  11  =====
54  11  =====
55  11  =====
56  11  =====
57  11  =====
58  11  =====
59  11  =====
60  11  =====
61  11  =====
62  11  =====
63  11  =====
64  11  =====
65  11  =====
66  11  =====
67  11  =====
68  11  =====
69  11  =====
70  11  =====
71  11  =====
72  11  =====
73  11  =====
74  11  =====
75  11  =====
76  11  =====
77  11  =====
78  11  =====
79  11  =====
80  11  =====
81  11  =====
82  11  =====
83  11  =====
84  11  =====
85  11  =====
86  11  =====
87  11  =====
88  11  =====
89  11  =====
90  11  =====
91  11  =====
92  11  =====
93  11  =====
94  11  =====
95  11  =====
96  11  =====
97  11  =====
98  11  =====
99  11  =====
100 11  =====

```











```

8
9
10
11
12
13
14
15
16
17
18
19
20
21
22
23
24
25
26
27
28
29
30
31
32
33
34
35
36
37
38
39
40
41
42
43
44
45
46
47
48
49
50
51
52
53
54
55
56
57
58
59
60
61
62
63
64
65
66
67
68
69
70
71
72
73
74
75
76
77
78
79
80
81
82
83
84
85
86
87
88
89
90
91
92
93
94
95
96
97
98
99
100
101
102
103
104
105
106
107
108
109
110
111
112
113
114
115
116
117
118
119
120
121
122
123
124
125
126
127
128
129
130
131
132
133
134
135
136
137
138
139
140
141
142
143
144
145
146
147
148
149
150
151
152
153
154
155
156
157
158
159
160
161
162
163
164
165
166
167
168
169
170
171
172
173
174
175
176
177
178
179
180
181
182
183
184
185
186
187
188
189
190
191
192
193
194
195
196
197
198
199
200
201
202
203
204
205
206
207
208
209
210
211
212
213
214
215
216
217
218
219
220
221
222
223
224
225
226
227
228
229
230
231
232
233
234
235
236
237
238
239
240
241
242
243
244
245
246
247
248
249
250
251
252
253
254
255
256
257
258
259
260
261
262
263
264
265
266
267
268
269
270
271
272
273
274
275
276
277
278
279
280
281
282
283
284
285
286
287
288
289
290
291
292
293
294
295
296
297
298
299
300
301
302
303
304
305
306
307
308
309
310
311
312
313
314
315
316
317
318
319
320
321
322
323
324
325
326
327
328
329
330
331
332
333
334
335
336
337
338
339
340
341
342
343
344
345
346
347
348
349
350
351
352
353
354
355
356
357
358
359
360
361
362
363
364
365
366
367
368
369
370
371
372
373
374
375
376
377
378
379
380
381
382
383
384
385
386
387
388
389
390
391
392
393
394
395
396
397
398
399
400
401
402
403
404
405
406
407
408
409
410
411
412
413
414
415
416
417
418
419
420
421
422
423
424
425
426
427
428
429
430
431
432
433
434
435
436
437
438
439
440
441
442
443
444
445
446
447
448
449
450
451
452
453
454
455
456
457
458
459
460
461
462
463
464
465
466
467
468
469
470
471
472
473
474
475
476
477
478
479
480
481
482
483
484
485
486
487
488
489
490
491
492
493
494
495
496
497
498
499
500
501
502
503
504
505
506
507
508
509
510
511
512
513
514
515
516
517
518
519
520
521
522
523
524
525
526
527
528
529
530
531
532
533
534
535
536
537
538
539
540
541
542
543
544
545
546
547
548
549
550
551
552
553
554
555
556
557
558
559
560
561
562
563
564
565
566
567
568
569
570
571
572
573
574
575
576
577
578
579
580
581
582
583
584
585
586
587
588
589
590
591
592
593
594
595
596
597
598
599
600
601
602
603
604
605
606
607
608
609
610
611
612
613
614
615
616
617
618
619
620
621
622
623
624
625
626
627
628
629
630
631
632
633
634
635
636
637
638
639
640
641
642
643
644
645
646
647
648
649
650
651
652
653
654
655
656
657
658
659
660
661
662
663
664
665
666
667
668
669
670
671
672
673
674
675
676
677
678
679
680
681
682
683
684
685
686
687
688
689
690
691
692
693
694
695
696
697
698
699
700
701
702
703
704
705
706
707
708
709
710
711
712
713
714
715
716
717
718
719
720
721
722
723
724
725
726
727
728
729
730
731
732
733
734
735
736
737
738
739
740
741
742
743
744
745
746
747
748
749
750
751
752
753
754
755
756
757
758
759
760
761
762
763
764
765
766
767
768
769
770
771
772
773
774
775
776
777
778
779
780
781
782
783
784
785
786
787
788
789
790
791
792
793
794
795
796
797
798
799
800
801
802
803
804
805
806
807
808
809
810
811
812
813
814
815
816
817
818
819
820
821
822
823
824
825
826
827
828
829
830
831
832
833
834
835
836
837
838
839
840
841
842
843
844
845
846
847
848
849
850
851
852
853
854
855
856
857
858
859
860
861
862
863
864
865
866
867
868
869
870
871
872
873
874
875
876
877
878
879
880
881
882
883
884
885
886
887
888
889
890
891
892
893
894
895
896
897
898
899
900
901
902
903
904
905
906
907
908
909
910
911
912
913
914
915
916
917
918
919
920
921
922
923
924
925
926
927
928
929
930
931
932
933
934
935
936
937
938
939
940
941
942
943
944
945
946
947
948
949
950
951
952
953
954
955
956
957
958
959
960
961
962
963
964
965
966
967
968
969
970
971
972
973
974
975
976
977
978
979
980
981
982
983
984
985
986
987
988
989
990
991
992
993
994
995
996
997
998
999
1000

```























## REFERENCES

1. Hirsch, H.T. II, and Jankis, R., eds. *Proceedings of a Conference on Radiation from Electron-Medical Accelerators*. NBS Special Publication 356. National Bureau of Standards, Department of Commerce, Gaithersburg, MD, 1977.
2. McColl, E.C., Almond, P. B., Gormley, J. A., Miller, E. Q., Holmes, G. B., Lenz, E. H., Ing, R., and Simmons, W. P. *Neutron Contamination from Medical Electron Accelerators*. NCRP Report No. 75. National Council on Radiation Protection and Measurements, Bethesda, MD, 1981.
3. Rosenbluth, J.P., ed. *NCRP—A General Mass Core (A) For Use Transport Code*. LA-5323-M. Los Alamos National Laboratory, Los Alamos, NM, 1977.
4. Metropolis, N., and Ulam, S. "The Monte Carlo Method," *Journal of the American Statistical Association*. Vol. 48, No. 347, pp. 333-340, 1949.
5. Eide, A. and Moxness, E.B. *Nuclear Structure*. 2nd Edition. World Scientific, Singapore, 1994.
6. Langan, E.B. "Neutron Production by Complete Absorption of High-Energy Photons," *Nuclronics*. Vol. 4, No. 3, pp. 14-21, 1958.
7. Langan, E.B. "The High Energy Nuclear Photocell," *Physical Review*. Vol. 84, No. 1, pp. 42-51, 1952.
8. Chadwick, M.B., Chalkley, P., Hadjira, P.B., and Griffin, G. "Peak Shifting in the Quasistationary Model of Photoneutrons," *Physical Review C*. Vol. 40, No. 2, pp. 814-823, 1989.
9. Wu, J.B. and Cheng, C.C. "The Equilibrium Particle Decay in the Photoneutron Reaction," *Physical Review C*. Vol. 16, No. 3, pp. 1823-1828, 1977.
10. Stone, M., Barnea, B.L., and Kienle, T.T. "The Improved Model Analysis of Photoneutron Reactions," *Physical Review C*. Vol. 18, No. 4, pp. 2054-2060, 1983.
11. Chadwick, M.B., Young, P.G., and Cohen, E. "Photoneutron Angular Distributions Systematic at the Quasistationary Regime," *Journal of Nuclear Science and Technology*. Vol. 32, No. 11, pp. 1114-1126, 1995.

11. Fano, A., Fano, A., and Sola, P.R. "Total Giant Resonance Photoelectron Cross Sections for Light Nuclei: A Database for the ELUGA Mono-Clap Transport Code" *Proceedings of the First Specialist Meeting on Studying Aspects of Accelerators, Targets and Radiation Facilities*, SATF-1, Tokyo University, Sendai, Japan, Organization for Economic Cooperation and Development Nuclear Energy Agency, Paris, France, 1997.
12. Maggallhaan, S.F., Orville, M., Holden, N.E., McLane, V., Dunford, C.L., and Rose, P.F., eds. *Atomic Cross Sections*, 4th Edition, ENL-925, Brookhaven National Laboratory, Upton, NY, 1981.
13. Feltz, E.G., Gussenberg, H.M., Vasserman, H., and Olson, T.C., eds. *Photoelectron Reaction Data*, NBS Special Publication 280, National Bureau of Standards, Department of Commerce, Gaithersburg, MD, 1979.
14. Feltz, E.G. and Gussenberg, H.M., eds. *Photoelectron Data-Index 1979-1977*, NBS Special Publication 280, Supplement 1, National Bureau of Standards, Department of Commerce, Gaithersburg, MD, 1978.
15. Barman, B.L. "Atlas of Photoelectron Cross Sections Obtained With Monochromatic Photons," *Atomic Data and Nuclear Data Tables*, Vol. 15, No. 4, pp. 219-268, 1975.
16. Barman, B.L. and Barman, B.L. "Atlas of Photoelectron Cross Sections Obtained with Monochromatic Photons," *Atomic Data and Nuclear Data Tables*, Vol. 33, No. 2, pp. 199-233, 1983.
17. Vokosov, A.Y., Yul'kov, Y.Y., Kuchenko, D.S., and Stepanov, M.L. *Atlas of Giant Dipole Resonance Parameters and Graphs of Photoelectron Reaction Cross Sections*, ENDC(NDG)-204, International Atomic Energy Association, Vienna, Austria, 1999.
18. Dunford, C.L. *Internet Connection to the National Nuclear Data Center (NNDC)*, <http://www.nndc.bnl.gov/>, Brookhaven National Laboratory, Upton, NY, 1999.
19. Almási, R.G. Jr. and Mares, H.B. "Electron Proton Cascade Calculations and Neutron Yields from Electrons in Thick Targets," *Nuclear Instruments and Methods*, Vol. 48, pp. 105-114, 1967.
20. Almási, R.G. Jr. and Mares, H.B. "Photoelectron Production from 24- and 138-MeV Electrons in Thick Uniform Targets," *Nuclear Instruments and Methods*, Vol. 58, pp. 338-340, 1967.
21. Almási, R.G. Jr., Gábori, T.A., and Gábori, M.B. "The Energy Distribution of Photoelectrons Produced by 138 MeV Electrons in Thick Freely-ion and Transition Targets," *Nuclear Science and Engineering*, Vol. 48, No. 3, pp. 363-374, 1972.

23. Gabriel, T.A. and Al-Jalaf, R.G. Jr. "Photo-neutron and Positron Production from 400 MeV Electrons in Thick-Copper Targets." *Nuclear Physics B*. Vol. 814, No. 2, pp. 383-393, 1999.
24. Gabriel, T.A. and Al-Jalaf, R.G. Jr. "Photo-neutron Measurements at High Energies (>158 MeV)," *Physical Review*. Vol. 182, No. 4, pp. 1832-1850, 1969.
25. Hawes, R.C., Barabati, C.R., and Dainch, P.B. "Using Monte Carlo Studies of Electron-Positron Cascades and the Resultant Production and Transport of Photoneutrons in Finite Three-dimensional Systems," *Journal of Applied Physics*. Vol. 46, No. 3, pp. 1109-1120, 1975.
26. Kato, T. and Harada, R. "An Assessment of the Continuous Neutron Source Using a Low-Energy Electron Accelerator," *Nuclear Science and Engineering*. Vol. 126, No. 4, pp. 28-39, 1997.
27. Melcher, R.W., Berggren, S.J., Van Grieken, A., Moshinsk, S.G., Berk, A.J., and Hall, J. "MASS Code Development," *Proceedings of the Fourth Operational Meeting on Shielding Aspects of Accelerators, Targets and Irradiation Facilities SATIF-4*, Knoxville, TN. Organization for Economic Co-operation and Development Nuclear Energy Agency, Paris, France, 1994.
28. Pykalainen, A.V., Moshinsk, S.G., and Berk, A.J. "Cascade-Exciton Model: Analysis of Neutron-Induced Positron Cerenkov Spectra of Lead and Bismuth at 40- to 300 MeV Energies," *Nuclear Science and Engineering*. Vol. 121, No. 1, pp. 79-85, 1993.
29. Swenson, W.P. "Activation of Aluminum Foils Exposed By High-Energy Electrons Al<sup>26</sup>Al," *Health Physics*. Vol. 28, No. 2, pp. 495-502, 1973.
30. Swenson, W.P. "Neutron Yields From Electrons Stopped in Selected Materials," *Health Physics*. Vol. 33, No. 4, pp. 609-613, 1977.
31. Swenson, W.P. "Calculation of Neutron Yields Released By Electrons Incident On Selected Materials," *Health Physics*. Vol. 35, No. 2, pp. 193-207, 1978.
32. Swenson, W.P. "Improved Calculation of Photo-Neutron Yields Released By Incident Electrons," *Health Physics*. Vol. 53, No. 3, pp. 347-356, 1979.
33. Swenson, W.P. "Estimate of the Risk in Radiation Therapy Due to Unwanted Neutrons," *Medical Physics*. Vol. 7, No. 2, pp. 140-149, 1980.
34. Marshakovic, C., Herman, V., Omer, E., and Santos, A. "Evaluation of the Unwanted Neutron Dose Exposed to Critical Organs in Patients Treated By Linear Accelerator Gamma Ray Therapy." *Radiation Protection Dosimetry*. Vol. 64, No. 1-4, pp. 417-422, 1993.

23. Agostini, S., Fort, A.F., Schar, M., Teyssie, A., and Tosi, G. "Monte-Carlo Simulations of Neutron Transport in a Laser Radiolysis Room," *Nuclear Instruments & Methods in Physics Research Section B: Vol. 73, No. 1*, pp. 84-98, 1992.
24. Agostini, S., Fort, A.F., Gervais, F., Schar, M., Teyssie, A., and Tosi, G. "Photonuclear Data in Soft-Tissue Phantoms Irradiated By 25 MeV X-Beams," *Physics in Medicine and Biology*, Vol. 34, No. 10, pp. 1507-1528, 1990.
25. Chabot, F.B. "A Photonuclear Production Option for MCNP4A," *Proceedings of the Radiation Protection and Shielding Topical Conference on Advancements and Applications in Radiation Protection and Shielding*, No. Fairbanks, MA, American Nuclear Society, La Grange Park, IL, 1994.
26. Liu, P.C., Nelson, W.R., Ross, R.B., and Mao, S.B. "Calculations of the Giant-Dipole-Resonance Phenomenon Using a Coupled HCS4-MORSE Code," *Radiation Protection Dosimetry*, Vol. 30, No. 1-4, pp. 49-54, 1993.
27. Chabot, M.B., Barnes, T.H., and Little, R.C. "Photonuclear Production in Kinross Beam Stop for Dual-Axis Radiographic Hybrid Facility (DARHF)," *Proceedings of the Radiation Protection and Shielding Topical Conference*, Knoxville, TN, American Nuclear Society, La Grange Park, IL, 1995.
28. Chabot, M.B., Young, P.D., Chels, S., Fendley, R.C., Ross, G.M., Hughes, H.G., Kinsing, A.J., Little, R.C., MacDonald, R.B., Prall, R.E., and Wilson, L.B. "Cross-Section Evaluations to 100 MeV for Accelerator-Driven Systems and Implementation in MCNPX," *Nuclear Science and Engineering*, Vol. 131, No. 1, pp. 203-225, 1999.
29. Young, P.D. and Chabot, M.B. "Comprehensive Nuclear Model Calculations Theory and Use of the CMASH Code," *MC4 Workshop on Nuclear Reaction Data and Nuclear Reactors—Physics, Design and Safety*, Trieste, Italy, World Scientific Publishing, Ltd., Singapore, 1996.
30. Hughes, H.G., Prall, R.E., and Little, R.C. "MCNPX: The LAKEOS/CMASH Code Upgrade," *ETHZ-BN-93-011*, Los Alamos National Laboratory, Los Alamos, NM, 1993.
31. Chabot, F., ed. *Summary Report of OECD for Research Collaboration Meeting: BEC(NDS)94*, International Atomic Energy Association, Vienna, Austria, 1997.
32. Chabot, F., ed. *Handbook of Photonuclear Data for Applications*, IAEA: TECDOC 14, Paris: International Atomic Energy Association, Vienna, Austria, 1998.

43. McLean, V., Sanford, C.L., and Ross, P.J., eds. *DDMF-92 Data Formats and Procedures for the Evaluated Nuclear Data File DDMF-92*. EOL-MCS-44943. Brookhaven National Laboratory, Upton, NY, 1992.
44. Wismar, C.F. *Proposed Delivered Version Data Format for MCNP Libraries*. XCL-CPW-94-021. Los Alamos National Laboratory, Los Alamos, NM, 1994.
45. Fawcett, R.C. *Proposed APT Data Library Formats and LDD Specifications*. XTM-BCF-99-300. Los Alamos National Laboratory, Los Alamos, NM, 1999.
46. Fawcett, R.C. *Follow-up to XTM-BCF-99-300: Proposed APT Data Library Formats*. XTM-BCF-99-312. Los Alamos National Laboratory, Los Alamos, NM, 1999.
47. MacFarlane, R.D., and Wilson, D.W. *The NJOY Nuclear Data Processing System Version 91*. LA-62746-M. Los Alamos National Laboratory, Los Alamos, NM, 1994.
48. Kalkbush, C. *Symmetries of Continuous Angular Distributions: Extensions to Higher Orders*. LA-58-40-4137. Los Alamos National Laboratory, Los Alamos, NM, 1987.
49. Kalkbush, C. *Symmetries of Continuous Angular Distributions: Extensions to Higher Orders*, "Physical Review C" Vol. 33, No. 4, pp. 2356-2370, 1986.
50. White, M.C. *Modifications to the MCNP ACE Formats*. XCL-MCW-99-40. Los Alamos National Laboratory, Los Alamos, NM, 1999.
51. White, M.C. *Evolution of the ACE Modifications to MCNP*. XCL-MCW-99-01. Los Alamos National Laboratory, Los Alamos, NM, 1999.
52. Hendricks, J.B. *MCNP/PC-EXEDV03 Copyright*. XLS-DSR-99-06. Los Alamos National Laboratory, Los Alamos, NM, 1999.
53. White, M.C. *MCNP/PC Modifications - From Table Loading and Size of Weight Issues*. XCL-MCW-99-01. Los Alamos National Laboratory, Los Alamos, NM, 1999.
54. Carter, L.L., and Chilton, F.D. *Particle Transport Methods and the Monte Carlo Method*. Report No. TID-26457. National Technical Information Service, Springfield, VA, 1973.
55. Hendricks, J.B. *MCNP/PC Subgroup/Neutrons*. XLS-DSR-99-08. Los Alamos National Laboratory, Los Alamos, NM, 1999.
56. Barber, W.C., and George, W.D. *Neutron Yields from Targets Bombarded by Electrons*, "Physical Review" Vol. 134, No. 6, pp. 1150-1160, 1959.

19. White, M.C. *Research in E. I. du Pont de Nemours and Co. MCNP-CC-DXDFAC Capabilities*, N-3 MCW 99-17, Los Alamos National Laboratory, Los Alamos, NM, 1999.
20. White, M.C. *Photoionization Physics at MCNP22 Progress Report*, ELL MCW 99-17, Los Alamos National Laboratory, Los Alamos, NM, 1999.
21. Yang, B., T. "The Production and Bremsstrahlung of Charged Leptons," *Reviews of Modern Physics*, Vol. 56, No. 4, pp. 813-870, 1979.
22. Veynants, A., Bell, H., Berggren, R., Carlos, P., Leprieux, A., and de Minnis, A. "A Study of the Photoionization Contribution to the Giant Dipole Resonance of a  $\alpha$  of Shell Nuclei," *Nuclear Physics A*, Vol. A237, No. 3, pp. 513-540, 1975.
23. Mendenhall, R., Kohn, E., and Goldring, J. "Photoionization Cross Sections," *Physical Review*, Vol. 94, No. 3, pp. 439-473, 1953.
24. Pratt, G.A. and Rice, D.W. "Yields and Angular Distributions of Scattered Gamma Neutron Photons," *Physical Review*, Vol. 71, No. 5, pp. 804-809, 1950.
25. Fultz, S.C., Brinkman, R.L., Calhoun, J.T., and Harvey, E.B. "Photoionization Cross Sections for Neutral Ca,  $\text{Ca}^{2+}$  and  $\text{Ca}^{3+}$ ," *Physical Review*, Vol. B115, No. 3, pp. 1149-1154, 1966.
26. Berggren, R., Bell, H., and Veynants, A. "Photoionization Cross Sections of La, Th, Pa and Ta," *Nuclear Physics A*, Vol. A121, No. 2, pp. 401-406, 1968.
27. Veynants, A., Bell, H., Berggren, R., Carlos, P., Leprieux, A., and de Minnis, A. "Etude de la Résonance Giant Dipole dans le Région de Transitions autour de A = 190," *Le Journal de Physique*, Vol. 36, pp. 6263-6270, 1973.
28. Harvey, E.B., Calhoun, J.T., Brinkman, R.L., and Fultz, S.C. "Photoionization Cross Sections of  $\text{Pb}^{2+}$ ,  $\text{Pb}^{3+}$ ,  $\text{Pb}^{4+}$  and  $\text{Bi}^{3+}$ ," *Physical Review*, Vol. B104, No. 1, pp. 126-134, 1964.
29. Veynants, A., Bell, H., Berggren, R., Carlos, P., and Leprieux, A. "Photoionization Cross Sections of  $^{209}\text{Pb}$  and  $^{209}\text{Bi}$ ," *Nuclear Physics A*, Vol. A199, No. 2, pp. 261-276, 1973.
30. Hendricks, J.E., Fendley, S.C., and Carter, J.D. *ENDF(B-V) Data for MCNP*, LA-12894, Los Alamos National Laboratory, Los Alamos, NM, 1984.
31. Adams, J., Brinkman, R., Cook, K.H., Epler, H.W., Glaser, H., Gundersen, H., Koning, M., Kuhn, P., Kuo, G., Porges, A., and Torgler, B. "Total Nuclear Photon Absorption Cross Sections for X-ray Light Elements," *Nuclear Physics A*, Vol. A234, No. 3, pp. 479-492, 1973.

72. Fahn, S.-C., Caldwell, J.T., Barnes, R.L., Bryantson, R.J., and Harvey, R.B. "Photoionization Cross Sections for  $C^{12}$  and  $Al^{27}$ ," *Physical Review*. Vol. 143, No. 2, pp. 769-776, 1964.
73. Vashchenko, V.V., Semyakina, V.V., and Sidorov, M.E. *Annals Commission on the Photoionization Data Joints 1974-1975*. <http://atomoptics.moscow.ru/> Institute for Microelectronics Dynamics, Moscow State University. Moscow, Russia, 1976.
74. Kaldor, M. *Nuclear Data Evaluation Methodology*. World Scientific, Singapore, 2013.
75. Costa, S., Ferraro, P., Mandichini, C., Protopopu, L., and Pergami, G. "Behavior of the  $[j_1T_1]C^{12}$  Section in Relativistic and Ions," *Physica Scripta*. Vol. 118, Issue 12, No. 1, pp. 109-120, 1987.
76. DeWitt, S.N., Baker, A.J., Kohn, W.L., Lacombe, L.B., Lindgren, H.W., and Takayanagi, R.S. "Absorption of Gamma Quanta by Iron-Nuclei Near the Giant Resonance," *Technique Physics*. Vol. 5, No. 4, pp. 475-479, 1967.
77. Bond, R.E., Fahn, M.P., Kell, L.A., and Wilson, R.B. "Measurements of the  $^{12}C(p,\alpha)$  and  $^{12}C(p,n)$  Cross Sections," *Physical Review*. Vol. 176, No. 4, pp. 1345-1356, 1968.
78. Wilhel, J., Kretsch, C., and Thies, C. "Messung des Quotienten  $\sigma(p,\alpha)/\sigma(p,n)$  der  $^{12}C$ ,  $^{16}O$ ,  $^{20}Ne$ ,  $^{24}Mg$ ,  $^{28}Si$  und  $^{32}S$  im Bereich  $^{12}C$ ," *Nuclear Physics*. Vol. 32, pp. 236-241, 1962.
79. Bryantson, R.J., Caldwell, J.T., Karkhanavich, G.P., and Fahn, S.-C. "Photoionization Cross-Sections of  $Ta^{98}$  and  $Re^{85}$ ," *Physical Review*. Vol. 178, No. 4, pp. 2723-2726, 1969.
80. Lee, Y.-O., Polakow, T., and Chab, J. "Evaluation of Photoionization Section Data on Transition-Metals up to 100-MeV," *Journal of Nuclear Science and Technology*. Vol. 18, No. 10, pp. 683-690, 1974.
81. Barnes, R.L., Pywell, R.E., Thompson, M.H., McNeill, R.G., Jorg, J.W., and Woodward, J.O. *Bulletin of the American Physical Society*. Vol. 11, p. 415, 1966.
82. Baker, W.C. "Specific Ionization by High Energy Electrons," *Physical Review*. Vol. 97, No. 4, pp. 1473-1477, 1955.
83. Uehleinrich, M. "Monte-Carlo Calculations of Electron-Beam Parameters For 3 Philips Linear Accelerators," *Physics in Medicine and Biology*. Vol. 27, No. 1, pp. 83-104, 1982.



14. Rogers, D.W.D., Padgett, R.A., Ding, G.X., Ma, C.M., Wu, J., and Macken, T.R. "ORHAM: A Monte Carlo Code to Simulate Radiotherapy Treatment Units." *Medical Physics*. Vol. 22, No. 3, pp. 583-594, 1995.
15. Hughes, G.B. *Simulation under MCPLAB2*. Plasma Library. Ed. 9508-93. 77 Los Alamos National Laboratory. Los Alamos, NM, 1993.
16. Chetty, I. *A Photon Phase Space Source Model Incorporating Different Sampling Algorithms for Clinical Treatment Planning Using the Monte Carlo Method*. Dissertation, Department of Radiation Oncology, University of California at Los Angeles. Los Angeles, CA, 1998.
17. Attard, Z.B., ed. *Activation Analysis*. CRC Press. Boca Raton, FL, 1990.
18. Nath, R., Boyer, A.L., Le Brette, F.D., McColl, R.C., and Press, R.W. "Neutron Measurements around High-Energy X-ray Radiotherapy Machines." AAFM Report No. 19. American Association of Physicists in Medicine. New York, NY, 1984.
19. Fink, S.C., Brinkman, R.L., Caldwell, J.T., and Kim, H.A. "Fluorescence Cross-Section Measurements on Gold Using Monte Carlo Simulations." *Physical Review*. Vol. 275, No. 4, pp. 1275-1279, 1983.
20. Hansen, R.L., Pywell, R.R., Denick, S.R., Thompson, D.W., McNeill, R.D., and Jory, J.W. "Absolute fluorescence cross sections for Zn, I, P, As, and Pb." *Physical Review C*. Vol. 36, No. 4, pp. 1264-1265, 1987.
21. Odellius, L.J. *Modeling the Phillips II Series MCA 3-axis transmission*. 1988.
22. Chetty, I., Balchunas, J.P., and Bolling, T.D. "A Virtual Source Model for Monte Carlo Modeling of Arbitrary Intensity Distributions." *Medical Physics*. Vol. 27, No. 1, pp. 166-173, 2000.
23. Hansen Lind Meyer Inc. *Radiation Therapy Center for the University of Florida Health Science Center*. Project Number #17961-05. Hansen Lind Meyer Inc. Orlando, FL, 1999.
24. Whitt, R.C. *Typical Construction Materials Used in Flushing a Clinac Spring Electron transmission*. 1999.
25. Bethe, T. *Reflection Screen for Charged Particle Beams*. Patent No. 4,405,686 United States Patent and Trademark Office. Washington, D.C., 1983.
26. Hübner, J.A., Kruzek, R.P., Vollen, O.D., Schurr, S.M., and Berger, M.J. "ITS: The Integrated TIGER Series of Electron/Photon Transport Codes - Version 3.0." DOE Transactions on Nuclear Science. Vol. 39, No. 4, pp. 3025-3033, 1993.

97. Liew, F. A., Liew, D. G., Alkhalaf, J. A. M., and Smith, C. W. "Comparison of EGS4 and MCNP Monte Carlo Codes When Calculating Radiotherapy Depth Doses." *Physics in Medicine and Biology*. Vol. 43, No. 3 pp. 1393-1397, 1998.
98. Jong, S., Knoll, P. J., and Gehl, B. M. "Comparison between MCNP, EGS4 and experiments for charged electron beams," *Physics in Medicine and Biology*. Vol. 44, No. 3 pp. 359-371, 1999.
99. Adams, R. J. *Integration into MCNP4C of the EGS 4 Radiative and Collisional Stopping Power and Ionization/Excitation Potentials Module*. N-5 RJA-00-04. Los Alamos National Laboratory. Los Alamos, NM, 2000.
100. Adams, R. J. *Availability of MCNP4B/C*. E-mail communication. 1999.
101. *Approved Connection to the Plot Module Representing Physics Monte Carlo*. <http://ccmr.lanl.gov/physics/monte/monte.html>. Los Alamos National Laboratory. Los Alamos, NM, 2000.
102. Franklin, S. C. *EGS4PC-Information*. NTR-82P-03-275. Los Alamos National Laboratory. Los Alamos, NM, 1995.
103. MacFarlane, R. E. *Internet Connection to the T 2 Nuclear Information Service*. <http://t2.lanl.gov/>. Los Alamos National Laboratory. Los Alamos, NM, 2000.
104. EGS4 Codes. *Particle Navigator*. Version 1.04. EGS4-Codes. Oak Ridge, TN, 1994.
105. EGS4 Codes. *GammaPlot*. Version 4.00. EGS4-Codes. Oak Ridge, TN, 1997.
106. Rogers, D. W. G. "Fluence to Dose Conversion Coefficients for Beams Calculated With EGS4 For Electrons From 100-KeV to 30-GeV and Photons From 11-KeV to 30-GeV." *Health Physics*. Vol. 46, No. 4 pp. 639-644, 1994.
107. Thomas, R. H., Bradenbrook, J. W., Chastat, J.-L., Clark, M. J., Gomez, G., Drexler, G., Ahmad, H.-G., Guelich, R., Gussensack, B., Pommerehne, H., Stahler, H. J. L., and Zank, M. *Consensus Conference for use in Radiotherapy: Procedures Against External Radiation*. ICRU Report 57. International Commission on Radiation Units and Measurements. Bethesda, MD, 1999.
108. Hughes, G. H. and Wilson, L. B. *Many-Particle MCNP*. NTR-8008 94-01. Los Alamos National Laboratory. Los Alamos, NM, 1994.
109. Hughes, G. H. and Wilson, L. B. *Many-Particle MCNP Patch*. NTR-8008-04-010. Los Alamos National Laboratory. Los Alamos, NM, 1996.
110. Hughes, G. H. and Wilson, L. B. *Many-Particle MCNP Patch for EGS*. NTR-8008 94-020. Los Alamos National Laboratory. Los Alamos, NM, 1996.

- [11] W. H. Stein, *M.C. JCC Tolerant Angular Distribution*, SC/MC/93-41, Los Alamos National Laboratory, Los Alamos, NM, 1999.

## BIOGRAPHICAL SKETCH

Morgan C. White was born in Little Rock, Arkansas, to Robert and Virginia White on February 21, 1932. After moving to Florida at age two, he spent a very pleasant childhood in a beach town. That didn't change much even after he graduated from Pensacola Beach High School in Pensacola Beach, Florida, as valedictorian of his class in June of 1949.

Morgan received several scholarships to continue his education at the University of Florida. These included a Naval Reserve Officer Training Corps scholarship that provided the opportunity for two lovely summer cruises. In addition, he was a four-year recipient of both the National Merit and Florida Undergraduate scholarships. Morgan received his Bachelor of Science degree in marine engineering with highest honors from the University of Florida in August of 1954 and was commissioned as an Ensign, United States Naval Reserve, on that very same day.

During his three-year of college, Morgan was offered a Department of Energy Nuclear Engineering Fellowship to continue his education. Finding that it was finally time to buckle down, he decided to embark on a career in the nuclear technologies. The navy graciously allowed him to join the inactive Ready Reserve in order to pursue these ambitions. Doubtful going were few graduate students went before (or now), his master's thesis delved into the use of thermopneumatic actuators for applications in nuclear space power reactors. His studies included a stint in a summer course at General Atomics Technologies in San Diego, considerably a lovely little beach town in

southern California. He received the Master of Science degree from the University of Florida in December of 1956.

Finding that space studies often lacked in substance, Morgan sought a change of direction in his studies. After having spent the majority of his life as an aviator, he wanted to find new interests in the desert. He received a postmaster's Graduate Research Assistant at the Los Alamos National Laboratory. Again in the desert of New Mexico, he has spent two years trying to make sense of the whimsical nature of physics. He received his Doctor of Philosophy degree from the University of Florida in May of 2000 and resides in Los Alamos, New Mexico, with his lovely wife, their dopy dog and many cats.

I certify that I have read this study and that in my opinion it conforms to acceptable standards of scholarly presentation and is fully adequate in scope and quality as a dissertation for the degree of Doctor of Philosophy.



Steven Ashpole, Chairman  
Professor of Machine and  
Biological Engineering

I certify that I have read this study and that in my opinion it conforms to acceptable standards of scholarly presentation and is fully adequate in scope and quality as a dissertation for the degree of Doctor of Philosophy.



Alexander R. Fatta  
Professor of Machine and  
Biological Engineering

I certify that I have read this study and that in my opinion it conforms to acceptable standards of scholarly presentation and is fully adequate in scope and quality as a dissertation for the degree of Doctor of Philosophy.



Frank T. Stone  
Professor of Machine and  
Biological Engineering

I certify that I have read this study and that in my opinion it conforms to acceptable standards of scholarly presentation and is fully adequate in scope and quality as a dissertation for the degree of Doctor of Philosophy.



Paul A. Fishbeck  
Professor of Computer and Information  
Systems Engineering

I certify that I have read this study and that in my opinion it conforms to acceptable standards of scholarly presentation and is fully adequate in scope and quality as a dissertation for the degree of Doctor of Philosophy

  
Robert J. Stange  
Professor of Chemistry

I certify that I have read this study and that in my opinion it conforms to acceptable standards of scholarly presentation and is fully adequate in scope and quality as a dissertation for the degree of Doctor of Philosophy

  
Robert C. Little  
Technical Staff Member of Los Alamos  
National Laboratory

I certify that I have read this study and that in my opinion it conforms to acceptable standards of scholarly presentation and is fully adequate in scope and quality as a dissertation for the degree of Doctor of Philosophy

  
Stephen C. Fossile  
Technical Staff Member of Los Alamos  
National Laboratory

I certify that I have read this study and that in my opinion it conforms to acceptable standards of scholarly presentation and is fully adequate in scope and quality as a dissertation for the degree of Doctor of Philosophy

  
Mark J. Chabryk  
Technical Staff Member of Los Alamos  
National Laboratory

I certify that I have read the study and that in my opinion it conforms to acceptable standards of scholarly presentation and is fully adequate, in scope and quality, as a dissertation for the degree of Doctor of Philosophy.

  
Joseph A. Rasmussen, Professor of Radiation Oncology  
University of Wisconsin-Madison

This dissertation was submitted to the Graduate Faculty of the College of Engineering and to the Graduate School and was accepted in partial fulfillment of the requirements for the degree of Doctor of Philosophy.

May, 2000

  
M. J. Chason  
Dean, College of Engineering

  
Winifred M. Phillips  
Dean, Graduate School